BUBBLE BEHAVIOUR IN SUBCOOLED FLOW BOILING AT LOW PRESSURES AND FLOW RATES

by

Vladan Prodanovic

B.Sc. The University of Belgrade, Yugoslavia, 1988

M.A.Sc. The University of Belgrade, Yugoslavia, 1994

A THESIS SUBMITTED IN PARTIAL FULFILMENT OF
THE REQUIREMENTS FOR THE DEGREE OF

DOCTOR OF PHILOSOPHY

in

THE FACULTY OF GRADUATE STUDIES

Department of Mechanical Engineering

We accept this thesis as conforming
to the required standard

THE UNIVERSITY OF BRITISH COLUMBIA

February 2001

In presenting this thesis in partial fulfilment of the requirements for an advanced degree at the University of British Columbia, I agree that the Library shall make it freely available for reference and study. I further agree that permission for extensive copying of this thesis for scholarly purposes may be granted by the head of my department or by his or her representatives. It is understood that copying or publication of this thesis for financial gain shall not be allowed without my written permission.

Department of Mechanical Engineering

The University of British Columbia
Vancouver, Canada

Date April 12, 2001

ABSTRACT

Bubble behaviour in subcooled flow boiling of water at pressures ranging from 1.05 to 3 bar, bulk liquid velocities from 0.08 to 0.8 m/s, heat fluxes from 0.2 to 1 MW/m^2 and subcoolings from 10 to 30 K was investigated experimentally and analytically. Experiments were carried out on a vertical, annular test section with an inner heating surface and upward flow.

High-speed photography at rates of 6000-8000 frames/s captured bubbles from inception to collapse, revealing variations of bubble shapes and sizes, as well as bubble sliding and detachment from the wall. Bubble growth and condensation rates, sliding velocities, variation of bubble lifetime and bubble size with flow rate, subcooling, heat flux and pressure were further examined. New correlations were proposed for maximum and detachment bubble diameters, bubble growth rate, bubble growth time, detachment time and condensation time.

High-speed photographic results showed changes in typical bubble behaviour with increasing heat flux, from the appearance of the first bubble toward the onset of significant void. In the low heat flux region nearly spherical bubbles slid long distances without changing significantly in size and shape, occasionally detaching from the surface and typically reattaching soon after. At higher heat fluxes sliding distances were reduced to about a couple of diameters, and detachments from the surface became typical bubble behaviour. After detachment, bubbles traveled in a direction normal to the heater into the subcooled liquid core, where they collapsed rapidly. Further increasing the heat flux resulted in significant bubble coalescence before the onset of significant void was reached. The abrupt change in bubble behaviour between the low and high heat flux regions indicated changes in the heat transfer mode. Based on these observations, a new model was proposed for the transition from partially developed to fully developed boiling.

It was observed that bubble shapes, particularly at detachment, deviated significantly from spherical. Therefore, a new ellipsoidal, rather than a spherical model, was used to describe bubble geometry. The analysis of forces acting on ellipsoidal bubbles led to a new bubble detachment model. The model suggests that the role of surface tension is to promote bubble detachment instead of opposing it.

Table of Contents

Abstract ii
List of Tables v
List of Figures vi
Nomenclature x
Acknowledgments xvi
Dedication xvii
1. INTRODUCTION 1
1.1 Removal of Heat by Controlled Boiling Processes – Some Industrial Applications 1
1.2 Subcooled Flow Boiling 2
1.2.1 Initiation of Boiling and ONB Models 3
1.2.2 Void Fraction and OSV Models 4
1.2.3 Axial Void Growth Models 6
1.3 Bubble Dynamics and Heat Transfer 8
1.3.1 Dynamics of a Spherical Bubble 9
1.3.2 Inertially Controlled Bubble Growth and Collapse (Isothermal Bubble Growth) 12
1.3.3 Thermally Controlled Bubble Growth (Isobaric Bubble Brow th) 15
1.3.4 Microlayer Evaporation 19
1.4 Research Background 20
1.5 Research Objectives 21

2. EXPERIMENTAL APPARATUS, PROCEDURE AND DATA ANALYSIS 29
2.1 Experimental Apparatus 29
2.1.1 Equipment 29
2.1.2 Test Section 30
2.1.3 Instrumentation 31
2.1.4 High-speed Photography 33
2.2 Experimental Procedure 33
2.3 Measured and Calculated Parameters 34
2.4 Experimental Conditions 36
2.5 Data Processing 36
2.5.2 Selection of a Typical Bubble 38
2.6 Error Analysis 39

3. BUBBLE BEHAVIOUR IN SUBCOOLED FLOW BOILING 58
3.1 Background Information and Literature Review 58
3.2 Experimental Observations 60
3.2.1 Variations of Bubble Behaviour with Heat Flux 60
3.2.2 Bubble Size, Shape and Lifetime – Qualitative Observations 63
3.2.3 Parallel and Normal Displacement 64
3.3 Bubble Size and Lifetime – Parametric Trends 65
3.3.1 Effect of Subcooling 65
3.3.2 Effect of Heat Flux 65
3.3.3 Effect of Liquid Velocity 66
3.3.4 Effect of Pressure 66
3.3.5 Bubble Shapes and Active Nucleation Sites 67
3.4 Correlations 67
3.4.1 Correlations for Bubble Growth and Condensation Rates 67
3.4.2 Correlations for Maximum and Detachment Diameters, Bubble Growth, Detachment and Condensation Time 68
3.5 Concluding Remarks 71

4. HEAT TRANSFER IN SUBCOOLED FLOW BOILING 92
4.1 Background Information and Literature Review 92
4.1.1 Fully Developed Boiling 93
4.1.2 Partially Developed Boiling 96
4.1.3 Transition from Partially to Fully Developed Boiling 96
4.2 Analysis of the Applicability of Heat Transfer Models 97
4.3 Proposed Heat Transfer Correlation 98
4.4 Bubble Behaviour and Heat Transfer Modes 99
4.5 Model for the Transition from Partial to Fully Developed Boiling 101
4.5.1 Formulation of the Model 101
4.5.2 Comparison of the Proposed Model with Previous Models 104
4.6 Concluding Remarks 104

5. FORCES ACTING ON A SINGLE BUBBLE IN SUBCOOLED FLOW BOILING 116
5.1 Background Information and Literature Review 116
5.2 Identification of Forces 121
5.3 Bubble Detachment Model (Normal Detachment) 126
5.3.1 Formulation of the Model 126
5.3.2 Physical Modelling – Ellipsoidal Bubble 127
5.3.3 Modelling of Forces 129
Comparison of the Model with Experimental Data 131
5.5 Concluding Remarks 133

CONCLUSIONS AND RECOMMENDATIONS 141
6.1 Conclusions 141
6.1.1 Bubble Behaviour 141
6.1.2 Heat Transfer 143
6.1.3 Detachment Model 143
6.2 Recommendations 145

BIBLIOGRAPHY 147

Appendices

A. PROPAGATION OF LIGHT THROUGH THE TEST SECTION 155

B. BUBBLE DETACHMENT MODELS 158
B.1 Model of Unal 158
B.2. Model of Zuber 159
B.3. Model of Mikic 159
B.4 Model of Zeitoun and Shoukri 160
B.5 Model of Serizawa and Kenning 160

C. SAMPLE CALCULATION PROCEDURE (in MathCad) FOR PREDICTING HEAT TRANSFER COEFFICIENTS USING CHEN-TYPE HEAT TRANSFER MODELS 162

D. RADIAL VELOCITY AND TEMPERATURE DISTRIBUTION IN A VERTICAL ANNULUS WITH AN INNER HEATER 166
D.1. Velocity distribution 166
D.1.1. Von Karman (1939) 167
D.1.2. Deissler (1955) 168
D.1.3. Kays and Leung (1963) 170
D.2. Temperature distribution 170
D.2.1 Martinelli Analogy (1947) 171
D.2.2 Deissler (1954) 173

E. THE INERTIAL FORCE DURING GROWTH OF AN ELLIPSOIDAL BUBBLE 174

List of Tables

Page

Table 1.1 Models for the prediction of ONB....23

Table 1.2 Thermally controlled bubble growth models....24

Table 1.3 Bubble growth in non-uniform temperature field....24

Table 2.1 Characteristics of the test section....41

Table 2.2 Experimental conditions....41

Table 2.3 Measured geometrical parameters of the bubble- output from the image analysis software....41

Table 2.4 Experimental conditions (measured and calculated parameters) for experiments at p=2bar....42

Table 2.5 Experimental conditions (measured and calculated parameters) for experiments at p=3bar....43

Table 2.6 Estimated errors for experimental parameters....44

Table 3.1. Typical Bubbles p=2bar....73

Table 3.2. Typical Bubbles p=3bar....73

Table 3.3 Bubble growth and condensation correlations....74

Table 3.4 Coefficients in equation (3.7)....74

Table 4.1 Heat transfer correlations for fully developed subcooled flow boiling....106

Table 4.2 Heat transfer correlations for subcooled flow boiling based on dimensional analysis....106

Table 4.3 Heat transfer correlations for partially developed subcooled flow boiling....107

Table 4.4 Transition from partially to fully developed subcooled flow boiling....107

List of Figures

Page

Figure 1.1 Section through the SLOWPOKE reactor....25

Figure 1.2 Subcooled flow boiling – temperature and void curve....26

Figure 1.3 Force balance on the thin lamina at bubble interface....27

Figure 1.4 Liquid thermal layer that supplies heat to the growing bubble....27

Figure 1.5 The microlayer evaporation – model of Snyder (1956)....28

Figure 2.1 Schematic of the apparatus....45

Figure 2.2 Photograph of the portion of the apparatus....45

Figure 2.3 Drawing of the test section....46

Figure 2.4 Schematic of the test section and photographic setup....46

Figure 2.5 Photograph of the test section....46

Figure 2.6 Drawings of the upper and lower aluminum plates....47

Figure 2.7 Photograph of the test section with glass box....48

Figure 2.8 Size of the region filmed during experiments....48

Figure 2.9 Sequence of the film with time steps....49

Figure 2.10 Schematic of the image processing system....49

Figure 2.11 Experiments at p=2bar used for analysis....50

Figure 2.12 Experiments at p=3bar used for analysis....51

Figure 2.13 Example of the enlarged bubble and calibration procedure for measuring bubble geometrical parameters using MATROX INSPECTOR v2.1....52

Figure 2.14 The blob analysis setup and results from the blob analysis....53

Figure 2.15 Location of the origin and bubble centroid coordinates....54

Figure 2.16 Bubble geometrical parameters....55

Figure 2.17 Maximum, minimum and mean diameter of a typical bubble from experiment P2-22....55

Figure 2.18 Typical bubble growth and collapse curves.....55

Figure 2.19 Statistical distribution of detachment diameters from experiment P2-22.....56

Figure 2.20 Bubbles from inception to collapse from experiment P2-22.....56

Figure 2.21 Bubbles from inception to collapse from experiment P1-06.....57

Figure 2.22 Experiments P1-06 and P2-22: comparative analysis of normalized bubble lifetimes and maximum diameters.....57

Figure 3.1 Photograph of the low heat flux region.....75

Figure 3.2 Photograph of the isolated bubble region.....75

Figure 3.3 Photograph of the significant coalescence region.....75

Figure 3.4 Bubble behaviour in the low heat flux region.....76

Figure 3.5 Photographs of bubble reattachment.....77

Figure 3.6 Bubble behaviour in the isolated bubble region.....78

Figure 3.7 Bubble growth interrupted by coalescence with large bubble.....79

Figure 3.8 Bubble displacement at high bulk liquid velocity.....80

Figure 3.9 Bubble displacement at low bulk liquid velocity.....80

Figure 3.10 Maximum and detachment diameters – experimental data at 2 and 3 bar.....81

Figure 3.11 Lifetimes and ejection times – experimental data at 2 and 3 bar.....82

Figure 3.12 Diameters and lifetimes – from Bibeau and Salcudean, p=1bar.....83

Figure 3.13 Variation of the contact time with heat flux and pressure.....84

Figure 3.14 Variation of bubble diameters and lifetimes with heat flux and pressure.....84

Figure 3.15 Variation of detachment diameters with Bo.....85

Figure 3.16 Variation of bubble lifetimes with Bo.....85

Figure 3.17 Bubble growth and condensation comparison with the model of Zuber.....86

Figure 3.18 Correlations for bubble growth and condensation rates....86

Figure 3.19 Comparison of experimental data with models for predicting maximum and detachment diameters in subcooled flow boiling....87

Figure 3.20 Comparison of experimental data with models for predicting maximum and detachment diameters in subcooled flow boiling – low flow rates....88

Figure 3.21 Comparison of experimental data with models for predicting maximum and detachment diameters in subcooled flow boiling – high flow rates....88

Figure 3.22 Correlation for the normalized maximum bubble diameter....89

Figure 3.23 Correlation for the normalized bubble detachment diameter....89

Figure 3.24 Correlation for the normalized bubble growth time, bubble condensation time and bubble ejection time....90

Figure 3.25 Comparison of the proposed correlation with the model of Unal....91

Figure 3.26 Variation of bubble diameters with pressure....91

Figure 4.1 The flow boiling curve....108

Figure 4.2 Chen-type correlations compared with experiments at p=1bar....109

Figure 4.3 Chen-type correlations compared with experiments at p=2bar....109

Figure 4.4 Fully developed boiling (FDB) correlations....110
Experiment S2-30-02 (p=2bar, T_{in}=30°C, Q=0.02l/s) – high subcooling
Experiment S2-75-02 (p=2bar, T_{in}=75°C, Q=0.02l/s) – low subcooling

Figure 4.5. Correlations of Shah and Kandlikar in partial and fully developed boiling....110

Figure 4.6 Correlations based on dimensional analysis....111

Figure 4.7 Proposed heat transfer correlation compared with combined experimental data of Faraji et al. (1994) at p=1bar and from the present study at p=2bar and p=3bar....111

Figure 4.8 Normalized parallel displacement – experimental data....112

Figure 4.9 Normalized parallel displacement correlation shown with experimental data at p=3bar....112

Figure 4.10 Transition point prediction from Shah model compared with experimental data of Bibeau and Salcudean....113

Figure 4.11 Prediction of the transition point - comparison of the proposed model with models of Shah and Kandlikar for p=1bar....114

Figure 4.12 Prediction of the transition point - comparison of the proposed model with models of Shah and Kandlikar for p=3bar....115

Figure 5.1a Bubble modelled as spherical segment....135

Figure 5.1b Forces acting on a bubble....135

Figure 5.1c Bubble modelled as ellipsoidal segment....135

Figure 5.2 Forces for experiment P2-03....136

Figure 5.3 Forces for experiment P2-22....137

Figure 5.4 Forces for experiment P3-41....138

Figure 5.5 Forces for experiment P3-49....139

Figure 5.6 Comparison of the detachment criterion (transition of the surface tension force) with experiments p=2bar....140

Figure 5.7 Comparison of the detachment criterion (transition of the surface tension force) with experiments p=1bar....140

Figure A.1. Angles of incidence and refraction between two media....155

Figure A.2 Location of the tip of the bubble on the photograph and the real location....156

Figure A.3 The size of the bubble "seen" on the photograph and the real size....157

Nomenclature

a	half diameter of the ellipse parallel to the heater surface [m], also coefficient in equation (1.37);
Bo	Boiling number, equation (3.6);
b	half diameter of the ellipse normal to the heater surface [m], also coefficient in equation (1.37) and in equation (3.7);
c_p	specific heat [J/kgK];
D	mean (Feret) bubble diameter at any instant [m];
D_{ejc}	bubble diameter at normal detachment [m];
D_{ejc}^{+}	non-dimensional bubble diameter at normal detachment defined by equation (3.2);
D_{max}	maximum bubble diameter [m];
D_{max}^{+}	non-dimensional maximum bubble diameter defined by equation (3.2);
D_n	bubble diameter in direction normal to the surface of the heater [m];
D_p	bubble diameter in direction parallel to the surface of the heater [m];
D_s	sauter diameter [m], defined by equation (B.14);
d_{base}	diameter of the bubble base [m];
E_{ke}	kinetic energy associated with bubble expansion [J];
E_σ	surface tension potential energy [J];
F_{AM}	added-mass force [N];
F_b	buoyancy force [N];
F_{cp}	contact pressure force [N];

F_D drag force [N];

F_{FS} free stream acceleration [N];

F_g gravitational force [N];

F_H hydrodynamic force [N];

F_I inertial force [N];

F_L shear lift force [N];

F_σ surface tension force [N];

G mass flux [kg/m^2s];

g acceleration of gravity [m/s^2];

h convection heat transfer coefficient [W/m^2K];

h_{fc} single phase forced convection heat transfer coefficient [W/m^2K];

I electrical current [A];

i_{fg} latent heat of evaporation [J/kg];

Ja Jakob number, equation (3.4);

Ja* modified Jakob number $Ja^*=(cp\Delta T_{sub}/i_{fg})$;

k thermal conductivity [W/mK];

Lp_{ejc} parallel displacement from inception to normal detachment (sliding distance) [m];

L_n normal displacement [mm];

L_p parallel displacement [mm];

l heated length [m];

l_{film} distance of the filming location from the beginning of the heater [m];

M molecular weight [kg/kmol];

$\dot{m}$	mass flow rate [kg/s];
Nu	Nusselt number;
p	pressure [N/m^2];
P_h	heated perimeter [m];
p_{sat}	saturation pressure [N/m^2];
p_∞	liquid pressure at the infinite distance from the bubble [N/m^2];
Pe	Peclet number;
Ph	heated perimeter [m];
Pr	Prandtl number;
Q	heat transfer rate [W];
$\dot{Q}$	volumetric flow rate [m^3/s];
q	heat flux [W/m^2];
R	radius of a spherical bubble [m], also reaction force in equation (5.5);
R_m	maximum radius of a spherical bubble [m];
R_{cav}	radius of the cavity [m];
r	radial distance to the spherical element [m];
Re	Reynolds number;
Re_B	bubble Reynolds number, $Re_B=U_BD/\nu_l$
Sr	non-dimensional shear rate defined by equation (5.18);
St	Stanton number;
S	surface area of the bubble [m^2], S=S1+S2;
S1	vapour-liquid contact area of the bubble [m^2];
S2	surface area of the bubble base [m^2];

s	distance to the ellipse center from the wall [m];
T_b	bulk liquid temperature [K];
T_{cr}	critical temperature [K];
T_{sat}	saturation temperature [K];
ΔT_{sat}	superheat ($\Delta T_{sat}=T_w-T_{sat}$) [K];
ΔT_{sub}	subcooling ($\Delta T_{sat}=T_{sat}-T_b$) [K];
T_w	wall temperature [K];
T_∞	liquid temperature at the infinite distance from the bubble [K];
t	time [s];
t_{acc}	initial period of acceleration, defined by equation (1.25) [s];
t_b	bubble lifetime (from inception to collapse) [s];
t_c	bubble condensation time [s];
t_c^+	non-dimensional bubble condensation time defined by equation (3.3);
t_{ejc}	bubble ejection time (normal detachment) [s];
t_{ejc}^+	non-dimensional bubble ejection time defined by equation (3.3);
t_m	bubble growth time [s];
t_m^+	non-dimensional bubble growth time defined by equation (3.3);
U	bulk liquid (mean) velocity [m/s];
U_B	bubble velocity [m/s]
u	bubble radial velocity [m/s];
V	voltage [V];
V_B	bubble volume [m^3];
X_a	true mass quality;

X_{eq} equilibrium quality, defined by equation (2.4);

x, y coordinates;

z distance to the center of mass of the bubble from the wall [m];

Greek symbols:

α thermal diffusivity [m^2/s], also advancing contact angle in equation (5.3);

β receding contact angle;

ε nonsphericity, $\varepsilon = a/b$, also correction factor in equation (1.38) and coefficient in equation (5.19);

ϕ angle defined by equation (E.2);

μ viscosity [Pas];

ν kinematic viscosity [m^2/s];

θ dimensionless subcooling, defined by equation (3.5), also equilibrium contact angle in equations (5.1), (5.2) and (5.3);

ρ density [kg/m^3];

σ surface tension [N/m];

σ_{rr} normal stress at the vapour-liquid interface, defined by equation (1.9);

η, ξ transformed coordinates defined by equations (E.7) and (E.6);

Subscripts:

B bubble;

b, bulk bulk liquid;

FC forced convection;

FDB	fully developed boiling;
G	gas;
in	inlet of the test section;
l	liquid phase;
ONB	onset of nucleate boiling;
OSV	onset of significant void;
out	outlet of the test section;
PDB	partially developed boiling;
pool	pool boiling;
tp	two-phase;
TRANS	transition from partial to fully developed boiling;
v	vapour phase;
w	wall;

Acknowledgments

I would like to express my sincere gratitude to my supervisors, Dr. Martha Salcudean and Dr. Daniel Fraser for their trust, support and guidance. I am very thankful for the opportunity to be part of this interesting and challenging research.

My thanks are extended to Dr. Ian Gartshore, Dr. Bruce Bowen and Dr. Steven Rogak for their valuable advices and suggestions. Also, technical support at various stages of the experimental work, provided by Mr. Kegang Zhang, Mr. Mike Savage and Mr. Sean Bygrave is respectfully acknowledged.

I also wish to thank my family and friends for their continuous encouragement and my wife, Jelena Nestorovic-Prodanovic, for her love, patience and support.

To Konstantin, Marko and Vuk

Chapter 1

INTRODUCTION

Heterogeneous boiling, or boiling of a liquid adjacent to a hot solid surface, is known to be a highly efficient heat transfer process. The main advantage is that high heat fluxes can be obtained with small variations of the surface temperature. The boiling process, whether it happens in a stagnant (pool boiling) or flowing liquid (flow boiling), is very complex in nature. It encompasses thermodynamics, heat transfer and fluid dynamics. Hence, a multidisciplinary approach is needed for research and proper design of engineering applications of boiling.

1.1 Removal of Heat by Controlled Boiling Processes – Some Industrial Applications

Traditionally, boiling heat transfer is recognized as an important process and widely used in the chemical, petrochemical and nuclear industries. Industrial applications include steam generation in boilers, evaporators in process industry and nuclear reactors, among others. Nevertheless, the above mentioned advantage of removing large amounts of heat with small changes in surface temperatures has recently found engineering applications which, at first sight, do not have much in common with boiling. A good example is the cooling of electronic components. New applications, such as in electronics, redefine the importance of knowledge on bubble dynamics and heat transfer at the microscopic level. This is because of the small size of electronic equipment relative to the size of the bubble.

An important application of pool or flow boiling in the nuclear industry is to control the power output of small pool-type low pressure nuclear reactors, such as SLOWPOKE and MAPLE. These reactors, both designed by Atomic Energy of Canada Limited (AECL), have "an open chimney in a pool" arrangement. They operate at pressures ranging from100 to 300 kPa and use water as a working fluid. They belong to a class of reactors with negative void coefficient of reactivity [1], which means that an

increase in the amount of void results in decreasing reactivity of the system. As power increases in the reactor core, boiling occurs at the surface of fuel rods producing void space and, thus, decreasing the density of the mixture. A decrease in density of the water results in decreasing reactivity of the core, causing the reduction of power. The SLOWPOKE reactor (see Figure 1.1.) was designed to use natural convection of the subcooled water (subcooled pool boiling) for the removal of the heat from the core, while in the MAPLE reactor, the heat is removed by forced convection.

In order to define working conditions and, in particular, to carry out a safety analysis of these reactors, it is necessary to simulate the boiling process which occurs at the heated surface. Simulations for the SLOWPOKE reactor at low flow velocities (below 1 m/s) and low pressures have been carried out by Salcudean et al. [2,3], McLeod [4], Bibeau [5,6], Farajisarir [7] and Zeitoun [8]. Also, Kowalski and Harwel [9], and Bibeau [6] among others, have investigated void formation in MAPLE reactors using both circular and finned geometries.

This study was partly motivated by the need to provide a better understanding of bubble behaviour during boiling under working conditions such as those in the SLOWPOKE and MAPLE reactors. This was partly done in the above mentioned studies. However, a more thorough analysis, covering the complete operating pressure range was still needed.

This study also provides a general discussion and experimental analysis of heat transfer in partial and fully developed boiling regions as well as an investigation of the forces acting on a bubble and the bubble detachment mechanism.

1.2 Subcooled Flow Boiling

The boiling of a liquid flowing over a heated solid surface is essentially characterized by the appearance of the vapour phase on the heater surface. Bubbles are initiated from small pits and cavities called nucleation sites. In order to activate the nucleation sites, the surface temperature has to exceed the saturation temperature of the liquid at that pressure. If, at the same location, the temperature of the bulk liquid remains below saturation, the process is known as subcooled flow boiling [10].

The distinct regions and locations of subcooled flow boiling are shown in Figure 1.2. The graph shows the variations of the wall and bulk liquid temperatures along the heater surface. The location B is called the Onset of Nucleate Boiling (ONB). The heat transfer rate increases downstream of the ONB due to the boiling process. However, the amount of void (i.e. vapour) remains low and fairly constant. As shown, at a certain location B", the slope of the void growth curve changes significantly resulting in a dramatic increase in the amount of vapour. This location is known as the Onset of Significant Void (OSV). Kandlikar [11] has named the region between OSV and the onset of saturated flow boiling as the Significant Void Flow Region.

A number of papers deal with the heat transfer mechanism in flow boiling [25, 26, 27, 28], whether it is single-phase convection, latent heat, microconvection due to bubble agitation or transient conduction of cooler liquid replacing departing bubbles. These important heat transfer modes will be discussed in detail in Chapter 4.

1.2.1 Initiation of Boiling and ONB Models

The concept of nucleation sites, as cavities on the solid surface that contain trapped gas or vapour and act as nuclei for growing bubbles, was first introduced by Bankoff [12] and subsequently confirmed experimentally by Clark et al. [13]. The amount of gas/vapour trapped in a cavity and, hence, the number of potential nucleation sites, generally depends on the geometry of the cavity (shape, angles), surface tension, pressure and temperature of the liquid and temperature of the surface. Excess temperature of the surface is required for inception of a bubble. Boiling inception of well wetting fluids requires higher superheat. The reason is because such fluids displace the gas/vapour from larger cavities, thus reducing the number of active nucleation sites. This results in a hysteresis effect for ascending and descending surface temperatures during boiling.

A review of models for the prediction of ONB point is given by Butterworth and Shock [14], and by Spindler [15].

Most of these studies analyzed the relationship between heat flux and wall superheat at boiling incipience. Hsu [16] introduced the criterion for bubble growth. It is

based on the assumption that a bubble will grow from the nucleation site if the temperature of the liquid at the bubble tip is greater than the saturation vapour temperature. Following this criterion, Bergles and Rohsenow [17], Davis and Anderson [18] and Sato and Matsumura [19] developed the ONB models shown in Table 1.1. These models are generally not applicable to well wetting fluids. Therefore, a modification of the model of Davis and Anderson was proposed by Frost and Dzakowic (1967) for such fluids.

In another approach, Hino and Ueda [20] and Hahne et al. [21] used the critical cavity radius, r*, as a bubble growth criterion. According to [21] the value of $2\sigma/r^*$ is equal to the excess pressure in the vapour nucleus. It is taken to have the value of 1.54 bar within a margin of error of +/-20%. Those models are also listed in Table 1.1.

Unal [22] used high-speed photography to directly measure boiling inception in water. He correlated the data with the heat transfer equation previously developed for determining the initial point of net vapour generation (OSV). The total heat transfer consists of two terms: the heat flux due to boiling and the heat flux due to supressed forced convection. This approach has been discussed in detail in [23]. The correlation for the heat flux at ONB is shown in Table 1.1.

Serizawa [24] also used a heat balance to estimate the conditions at OSV except that he included the heat transfer at the liquid-vapour interface as well. His model requires predicting the interfacial heat transfer coefficient, h_c, as explained in [24]. The empirical correlation is also shown in Table 1.1.

1.2.2 Void Fraction and OSV Models

The void fraction starts from zero at ONB and remains at a low value until, at a certain point downstream, it increases rapidly. This point is known as the onset of significant void (OSV) and is characterized by a rapid increase in the slope of the void growth curve. The OSV point separates the void growth curve into two parts [29]. The boiling region upstream of the OSV is called the *highly subcooled region* while the region downstream of OSV is known as the *low subcooled region.* The highly subcooled region is defined as the attached void region where small, formed bubbles slide along the

heated surface or remain attached to the wall and condense very rapidly. In the low subcooled region the subcooling decreases and ejected bubbles can survive into the fluid core. Some authors, such as Spindler [15] and, Zeitoun and Shoukri [30] also state that OSV refers to the point where the vapor generation rate exceeds the condensation rate allowing significant void formation.

Bubbly flow is assumed to take place for most of the void growth profile. Slug flow begins for void fractions above approximately thirty percent, as reported by Kocamustafaogullari and Ishii [31] and Bibeau [6].

Models which predict the location of the onset of significant void can be divided into three groups. Some authors locate the OSV at the point where fully developed nucleate boiling begins. This concept was first proposed by Griffith et al. [29]. They assumed that, at OSV, the surface of the heater was fully covered with bubbles. Hence, the total heat flux at the wall was used to generate vapour and the total heat flux to the subcooled liquid was supplied by condensing bubbles. At OSV the vapour generation and condensation rates are assumed to be equal.

Other models which correlate the heat transfer rate at OSV include those of Ahmad [33], Saha and Zuber [34] and Unal [23]. Ahmad [33] related the OSV to bubble detachment and the initiation of fully developed boiling. Saha and Zuber [34] argued that OSV could be either thermally or hydrodynamically controlled. They defined that the transition between the two occurred at the Peclet number, Pe=70000. Unal [23] based his model on the idea that, at OSV, the forced convection contribution to the total heat transfer vanishes. Also, upon carrying out high-speed photography experiments, he concluded that the location of the OSV point was not related to first bubble detachment.

Another group of models are based on the assumption that OSV is defined as the location when the first bubbles depart the heater. Bowring [32] was the first to introduce this concept. Bubble detachment can be determined by balancing the forces acting on a bubble (Levy [35], Staub [36], Rogers et al. [37]). It can be shown that static forces used to estimate detachment diameters in these models do not give satisfactory results for cases of low pressure subcooled flow boiling.

The third group of models assume the existence of a bubble layer. Dix [38] introduced the idea of OSV as the point of bubble ejection from the bubble layer. Serizawa and Kenning [24] developed this idea further by relating the existence of the bubble layer to the action of thermocapillary forces. Bubbles become unstable in the bubble layer after a certain critical point and they are ejected into the fluid core.

Most of these models have been developed for high pressure applications. Recent bubble visualization studies [39, 40] have shown that these models are not generally applicable to subcooled boiling at low pressures and low flow rates. Bubbles were seen to detach long before OSV. In general, bubble behaviour at low pressures appeared to be different from that assumed in the above mentioned models. The need for investigating bubble behaviour at low pressures and for establishing a bubble detachment criterion was the driving force for the present study.

1.2.3 Axial void growth models

Models for predicting the axial void fraction profile in subcooled flow boiling are divided into two basic categories: profile-fitting models [35, 36, 37, 34] and mechanistic models [29, 33, 32, 41, 26].

In profile-fitting models, the void fraction is obtained from empirical correlations. First, the OSV is located by using the models described above. After calculating the equilibrium quality at the OSV, the void fraction is obtained using correlations from the literature. Most of these models use the correlation of Zuber and Findlay [42].

In mechanistic models, the true mass quality is calculated for the two phases from conservation equations (continuity and energy equations) which have to be solved simultaneously. This can be done by assuming different heat transfer mechanisms in the nucleate boiling region. Once the true mass quality is evaluated, the void growth is usually predicted by using correlations which relate the void fraction and the true mass quality. For example, the above mentioned correlation of Zuber and Findlay [42] is used in models like those of Rouhani and Axelsson [41] and Lahey [26].

The basic heat transfer concept is the division of heat removed from the surface by vapor and liquid phases. Many authors adopted the mechanism proposed by Bowring

[32] with some modification [41, 26]. It considers heat transferred through single-phase forced convection between bubbles, by latent heat and by agitation of departing bubbles (pumping action) causing added convection.

Most void fraction models were developed for high pressure subcooled nucleate boiling and are not applicable to low pressure and low velocity conditions. Experimental investigations of low pressure flow boiling in a test section with an annular cross-section were performed by Evangelisti and Lupoli [43] (p = 1 bar), Edelman and Elias [44] (p = 1 bar) and by Shoukri et al. [45] (p = 1-2 bar). These experiments have been compared with the models of Levy [35, 44] and Saha and Zuber [34]. Very detailed reviews of void growth models and their ranges of application can be found in Bibeau [6] and Zeitoun [8].

Recent experimental investigations were carried out by Bibeau and Salcudean [46] (p = 1-3 bar) and, Zeitoun and Shoukri [30] (p = 1-1.8 bar) under low pressure and low flow rate conditions. They also introduced new void growth models. Zeitoun and Shoukri [30] proposed a new OSV model based on a balance between vapor generation and condensation rates.

Bibeau [6] developed a phenomenological model which consists of parameters that could be analytically or experimentally evaluated. This is unlike most other models that are discussed above, all of which depend on *a priori* assumed parameters or parameters obtained from the void fraction experimental data. The model is based on a bubble ebullition cycle obtained from a high speed photographic study [7]. Correlations for bubble diameters and lifetimes were obtained for atmospheric pressure and, hence, this model has been validated only for a pressure of 1 bar. The present research is partially motivated by the possible extension of the bubble accounting model to subcooled nucleate boiling at pressures up to 3 bar. The aim is to provide correlations for maximum and detachment diameters and lifetimes needed for the bubble accounting model, which cover the experimental pressure range of 1–3 bar.

1.3 Bubble Dynamics and Heat Transfer

In exploring bubble dynamics, one has to distinguish between gas bubble dynamics and vapour bubble dynamics. Most studies of gas bubbles consider the case of a cavity filled with permanent, noncondensable gases. The amount of gas in the cavity is independent of the temperature and pressure of the surrounding liquid. Vapour bubble content, on the other hand, shows a strong dependence on thermodynamic conditions of the liquid at the boundary. Hence, vapour bubble dynamics have to include the liquid - vapour phase-equilibrium parameters.

Probably the most interesting topic, particularly in earlier gas bubble dynamics research, was investigation of bubbles as sources of sound and, in later research, sonoluminescence. Models of small-amplitude (linearized) oscillations and non-linear oscillations of gas bubbles have been thoroughly reviewed by Plesset and Prosperetti [47] and modern, non-linear techniques in bubble dynamics by Feng and Leal [48].

The focus of this study is on vapour bubble dynamics and the presence of noncondensable gases in the bubble content will be assumed negligible. A substantial number of papers were reviewed by Tong [49], Plesset and Prosperetti [47] and also by Brennen [50], among others. It was pointed out [51] that the investigation of vapour bubble dynamics includes processes of bubble growth and departure, and restitution of the thermal layer after bubble departure – also known as the waiting period.

Vapour bubble dynamics cannot be studied separately from the heat transfer process. They are interconnected and they affect each other. Given the temperature of the surrounding liquid, it is clear that one can further subdivide this topic into vapour bubble dynamics in a subcooled liquid and vapour bubble dynamics in a superheated liquid.

Flow boiling makes vapour bubble dynamics extremely complex. In addition to the already complicated model of a spherical bubble growing in the liquid with non-uniform temperatures and in the presence of a wall, one has to put the surrounding liquid in motion (again, non-uniform due to viscous effects) and let the bubble slide at speeds typically different from the bulk liquid velocity. Also, deformation and asymmetry of the bubble can contribute significantly as well as turbulence and local variations of the surface temperature and liquid temperature. As a result, one cannot expect to obtain an

analytical solution, which includes all relevant parameters. Good bubble growth or departure diameter correlations are still concerned with particular types of boiling that occur within a certain range of subcoolings, pressures and flow conditions. They are based on experimental data. It is to be expected that the rising number of numerical studies [52, 53, 54] will contribute significantly to solving more complex boiling problems.

In what follows, a review of studies on vapour bubble dynamics is given. Although each study introduces certain assumptions and simplifications (spherical bubble, uniformly superheated liquid, unbound liquid, etc.), they represent milestones in solving complex bubble dynamics problems.

1.3.1 Dynamics of a Spherical Bubble

The Rayleigh-Plesset Equation

For a spherical bubble growing symmetrically in an unbound stagnant liquid, it is convenient to write the conservation of mass and momentum in polar coordinates with the origin placed at the center of mass of the bubble. Given that changes occur only in the radial direction, the conservation of liquid mass is:

$$\frac{1}{r^2}\frac{\partial}{\partial r}\left(r^2 u\right)=0 \tag{1.1}$$

The Navier-Stokes equation in the radial direction is:

$$-\frac{1}{\rho_l}\frac{\partial p}{\partial r}=\frac{\partial u}{\partial t}+u\frac{\partial u}{\partial r}-\frac{\mu_l}{\rho_l}\left[\frac{1}{r^2}\frac{\partial}{\partial r}\left(r^2\frac{\partial u}{\partial r}\right)-\frac{2u}{r^2}\right] \tag{1.2}$$

where u represents the radial velocity.

One can introduce the following assumptions:

- Temperature (T_∞) and pressure (p_∞) of the liquid far from the bubble are known and constant (pressure regulates the growth and collapse of the bubble);
- Thermo-physical properties (density, viscosity) of the liquid are constant;
- Content of the bubble is homogeneous and the vapor temperature and pressure within the bubble are uniform;

- Zero mass transport across the vapor-liquid interface.

The last assumption leads to the equation that defines the velocity of the liquid at the interface (r = R):

$$u_{r=R} = \frac{dR}{dt} \tag{1.3}$$

From the conservation of mass one can obtain the equation for the radial velocity[1]:

$$u = \left(\frac{R}{r}\right)^2 \frac{dR}{dt} \tag{1.4}$$

The Navier-Stokes equation in the r-direction (1.2) yields[2]:

$$-\frac{1}{\rho_l}\frac{\partial p}{\partial r} = \frac{1}{r^2}\frac{\partial F}{\partial t} - \frac{2F^2}{r^5}; \quad F(t) = R^2\frac{dR}{dt} \tag{1.5}$$

which upon integration from r (with corresponding pressure p) to infinity, with $p \to p_\infty$ as $r \to \infty$ gives:

$$-\frac{p - p_\infty}{\rho_l} = \frac{1}{r}\frac{\partial F}{\partial t} - \frac{F^2}{2r^4} \tag{1.6}$$

The classical Rayleigh solution is based on defining the liquid pressure at the bubble interface from the Young-Laplace equation for the spherical bubble:

$$p_B - p_{r=R} = \frac{2\sigma}{R} \tag{1.7}$$

---

[1] The conservation of mass in polar coordinates can be solved to obtain: $u(r,t) = \frac{F(t)}{r^2}$ where F(t) represents the constant of integration. It is, therefore, a function of t only.

[2] One can derive the same equation by assuming inviscid fluid, that is, without the viscous term in equation (1.2). Indeed, upon substitution, the viscous term in the Navier-Stokes equation vanishes.

Substituting this pressure in equation (1.6) and replacing F with R^2dR/dt leads to the Rayleigh equation:

$$\frac{p_B - p_\infty}{\rho_l} = R\frac{d^2R}{dt^2} + \frac{3}{2}\left(\frac{dR}{dt}\right)^2 + \frac{2\sigma}{\rho_l R} \tag{1.8}$$

In a more advanced approach the liquid pressure on the interface can be replaced by the normal stress in the radial direction (see Figure 1.3):

$$\sigma_{rr} = -p + 2\mu_l\frac{\partial u}{\partial r} \tag{1.9}$$

The dynamic boundary condition on the bubble surface gives a force balance on the thin lamina, i.e.,

$$p_B - p_{r=R} - \frac{4\mu_l}{R}\frac{dR}{dt} - \frac{2\sigma}{R} = 0 \tag{1.10}$$

Substitution of the liquid pressure at the interface (1.10) into equation (1.6) gives the general form of the Rayleigh-Plesset equation, namely

$$\frac{p_B - p_\infty}{\rho_l} = R\frac{d^2R}{dt^2} + \frac{3}{2}\left(\frac{dR}{dt}\right)^2 + \frac{4\nu_l}{R}\frac{dR}{dt} + \frac{2\sigma}{\rho_l R} \tag{1.11}$$

Bubble Contents

In general, the pressure inside the bubble consists of the saturation pressure of the vapor at a given temperature and the partial pressure of a noncondensable gas[3]. Hence:

$$p_B = p_{sat}(T_B) + p_{Go}\left(\frac{T_B}{T_\infty}\right)\left(\frac{R_o}{R}\right)^3 \tag{1.12}$$

[3] This term can be obtained as follows:
The partial pressure of the noncondensable gas p_G can be expressed according to Dalton's law as: $p_G V_B = R_G T_B$ It can also be expressed as a pressure of the reference volume V_0 with radius R_0 at the liquid temperature T_∞: $p_{G0} V_0 = R_G T_\infty$. Upon dividing the left and right hand sides of the first equation by the left and right hand sides of the second equation, one can obtain the partial pressure of the contaminant gas as shown in equation (1.12)

Upon adding and subtracting $p_{sat}(T_\infty)$ in the above equation, one can rewrite the Rayleigh-Plesset equation in the following form:

$$\frac{p_{sat}(T_\infty)-p_\infty}{\rho_l}+\frac{p_{sat}(T_B)-p_{sat}(T_\infty)}{\rho_l}+p_{Go}\left(\frac{T_B}{T_\infty}\right)\left(\frac{R_o}{R}\right)^3 = R\frac{d^2R}{dt^2}+\frac{3}{2}\left(\frac{dR}{dt}\right)^2+\frac{4\nu_l}{R}\frac{dR}{dt}+\frac{2\sigma}{\rho_l R} \tag{1.13}$$

The first term on the left hand side does not include thermal effects as all parameters are defined at the liquid temperature T_∞. The second term is known as the thermal term. In the absence of significant thermal effects the bubble dynamics is "inertially controlled" and the second term is set to zero. The second term can be significant in various situations and, if its magnitude is much larger than that of the inertial terms, then the bubble growth is thermally controlled.

If the temperature difference is relatively small, the second term in equation (1.13) can be evaluated by using a Taylor expansion where derivatives of the second and higher orders are neglected, i.e.,

$$\frac{p_{sat}(T_B)-p_{sat}(T_\infty)}{\rho_l}=A(T_B-T_\infty) \tag{1.14}$$

The coefficient A can be obtained by using the Clausius-Clapeyron relation and is

$$A=\frac{1}{\rho_l}\frac{dp}{dt}=\frac{\rho_v i_{fg}}{\rho_l T_\infty} \tag{1.15}$$

In the text that follows, several characteristic solutions to the Rayleigh-Plesset equation are reviewed.

1.3.2 Inertially controlled bubble growth and collapse (isothermal bubble growth)

If the bubble growth is inertially controlled, the contribution of the second term on the left-hand side of equation (1.13) is small compared to the pressure difference, contained in the first term. Therefore, the second term can be excluded from equation

(1.13). Furthermore, if one assumes a pure vapour bubble without noncondensable gases and negligible viscous and surface tension effects, equation (1.13) becomes:

$$\frac{p_{sat}(T_\infty) - p_\infty}{\rho_l} = R\frac{d^2R}{dt^2} + \frac{3}{2}\left(\frac{dR}{dt}\right)^2 \tag{1.16}$$

Equation (1.16) can also be rearranged to obtain the following form:

$$\frac{d}{dt}\left[R^3\left(\frac{dR}{dt}\right)^2\right] = 2R^2\frac{dR}{dt}\frac{p_{sat}(T_\infty) - p_\infty}{\rho_l} \tag{1.17}$$

which, after integration, gives[4]:

$$R^3\left(\frac{dR}{dt}\right)^2 = \frac{2}{3}R^3\frac{p_{sat}(T_\infty) - p_\infty}{\rho_l} + K \tag{1.18}$$

where K is the constant of integration. Upon introducing the following boundary condition:

$$\frac{dR}{dt} = 0 \text{ at } R=R_0 \tag{1.19}$$

and assuming a step function change of the pressure at infinity: $p_\infty(t>0) = p_\infty^*$, one can determine the constant of integration K and obtain the analytical solution of equation (1.17) as:

$$\left(\frac{dR}{dt}\right)^2 = \frac{2}{3}\frac{p_{sat}(T_\infty) - p_\infty^*}{\rho_l}\left(\frac{R^3 - R_0^3}{R^3}\right) \tag{1.20}$$

Rayleigh [55] analyzed the collapse of spherical bubbles from a certain initial radius $R=R_0$ to $R=0$ by integrating equation (1.20) from $t=0$ to $t=t_C$, where t_C represents the total collapse time. Collapse is caused by a sudden increase in pressure $p_\infty(t=0) < p_\infty^*$. Writing $\xi = R/R_0$ one can integrate equation (1.20) and get:

---

[4] The same equation can be obtained from the conservation of mechanical energy which equates the kinetic energy of expansion with the work done to the liquid as follows:

$\frac{1}{2}\rho_l\int 4\pi r^2u^2dr = \Delta p\frac{4}{3}\pi R^3 + \text{const}$; $\Delta p = p_{SAT}(T_\infty) - p_\infty$ is assumed to be constant.

$$t_C = R_0\left[\frac{3\rho_l}{2\left(p_\infty^* - p_B\right)}\right]^{\frac{1}{2}} \int_0^1 \frac{\xi^{\frac{3}{2}} d\xi}{\left(1-\xi^3\right)^{\frac{1}{2}}} \tag{1.21}$$

This result can be expressed in terms of gamma functions:

$$t_C = R_0\left[\frac{\rho_l}{6\left(p_\infty^* - p_B\right)}\right]^{\frac{1}{2}} \frac{\Gamma\left(\frac{5}{6}\right)\Gamma\left(\frac{1}{2}\right)}{\Gamma\left(\frac{4}{3}\right)} = 0.915 R_0\left[\frac{\rho_l}{\left(p_\infty^* - p_B\right)}\right]^{\frac{1}{2}} \tag{1.22}$$

Brennen [50] pointed out that such an analysis of bubble collapse, although it is one of the most important theories in bubble dynamics, could be misleading for at least three reasons. The first is obviously the exclusion of thermal effects. There is also the fact that pressures at the boundary become very high near the final stages of collapse thus questioning the assumption of incompressibility. The assumption of spherical symmetry can also be violated during collapse.

Bubble collapse excluding thermal effects has been widely investigated in order to shed light on cavitation damage. Early theories suggested that cavitation damage was due to high pressures developed near a collapsed spherical cavity. Later investigations shifted the attention of scientists to the formation of liquid jets on collapsing bubbles near the wall.

Bankoff and Mikesell [56] compared the Rayleigh solution applied to bubble growth with experimental results of Gunther [57]. Upon analyzing bubble radius-time curves in highly subcooled nucleate boiling, they noticed the apparent symmetry of the growth and collapse curves. This suggests an approach to bubble growth that is similar to cavitation. They used equation (1.22) to calculate bubble growth time in high subcooling.

There is, indeed, experimental evidence that bubble growth is explosive in the early stages although it becomes considerably slower as the bubble approaches its maximum diameter. This is particularly evident at lower and moderate subcoolings. Plesset and Prosperetti [47] suggested that thermal effects become important at elevated temperature. The criterion for determining the relative importance of the thermal term will be discussed later in the text.

However, if inertially controlled bubble growth is assumed, equation (1.20) gives the asymptotic bubble growth rate ($R>>R_0$) as:

$$\frac{dR}{dt} = \left(\frac{2}{3} \frac{p_{sat}(T_\infty) - p_\infty^*}{\rho_l} \right)^{\frac{1}{2}} \tag{1.23}$$

The initial period of acceleration can be estimated from (1.23) with the initial value:

$$\left. \frac{d^2R}{dt^2} \right|_{t=0} = \frac{p_\infty(0) - p_\infty^*}{\rho_l R_0} \tag{1.24}$$

Hence:

$$t_{acc} = \left(\frac{2}{3} \frac{\rho_l R_0^2 \left(p_{sat}(T_\infty) - p_\infty^* \right)}{\left(p_\infty(0) - p_\infty^* \right)^2} \right)^{\frac{1}{2}} \tag{1.25}$$

1.3.3 Thermally controlled bubble growth (isobaric bubble growth)

The widely used Plesset-Zwick assumption states that the heat for bubble growth is supplied to the bubble interface through a thin thermal boundary layer surrounding the bubble. The thickness of the thermal boundary layer, δ_T, is considerably smaller than the bubble radius, i.e.,

$$R >> \delta_T \approx \frac{(T_B - T_\infty)}{\left(\frac{\partial T}{\partial r} \right)_{r=R}} \tag{1.26}$$

Thermally Controlled Bubble Growth in Uniformly Superheated Liquid

Bosnjakovic (1930) postulated three hypotheses for the growth of a spherical bubble in a slightly superheated liquid:

- All the heat supplied through the thin thermal boundary layer is used for the production of vapour (i.e. the additional heating or cooling of the bubble content is assumed to be negligible). The entire bulk liquid outside of the thermal boundary layer is slightly superheated;

- The heat is transmitted to the boundary by conduction only;
- Thermodynamic equilibrium is assumed at the bubble boundary (i.e. the vapour is at uniform saturation temperature T_{sat});

The thermal diffusion equation in polar coordinates is given by:

$$\frac{\partial T}{\partial t} + u\frac{\partial T}{\partial r} = \alpha_l \frac{1}{r^2}\frac{\partial}{\partial r}\left(r^2 \frac{\partial T}{\partial r}\right) \tag{1.27}$$

The temperature T is a function of the radial coordinate and time, T=T(r,t). In the case where Bosnjakovic's hypotheses hold, the corresponding set of boundary conditions is as follows:

$$\begin{aligned} &T(r,0) = T_\infty; \\ &T(R,t) = T_{sat}; \\ &T(\infty,t) = T_\infty; \end{aligned} \tag{1.28}$$

The velocity, u, in the diffusion equation (1.27) is defined by equation (1.4), and the energy balance is given by:

$$\frac{dR}{dt} = \frac{k_l}{i_{fg}\rho_v}\left(\frac{\partial T}{\partial r}\right)_{r=R} \tag{1.29}$$

As discussed in detail by van Stralen and Cole [58], Bosnjakovic's hypotheses have been justified by several investigators performing experiments on superheated liquids, namely Jakob and Fritz (1931), and Pruger (1941), among others. Given that the thickness of the thermal boundary layer is of the order of $(\pi\alpha_l t)^{1/2}$, the energy balance (1.29) becomes:

$$i_{fg}\cdot\rho_v \frac{dR}{dt} = k\frac{T_\infty - T_B}{\sqrt{\pi\alpha_l t}} \tag{1.30}$$

Integration over the time period, t, leads to the following relationship for the bubble radius as a function of time:

$$R = \frac{2}{\sqrt{\pi}}\left(\frac{\rho_l cp_l (T_\infty - T_B)}{\rho_v i_{fg}}\right)\sqrt{\alpha_l t} = \frac{2}{\sqrt{\pi}} Ja\sqrt{\alpha_l t} \tag{1.31}$$

The importance of equation (1.31) lies in the fact that bubble growth and collapse curves can be approximated by the relation:

$$R = C1\sqrt{\alpha_l t} \tag{1.32}$$

where C1 is a function of the Jacob number.

The second term in equation (1.13), determined with the aid of the Taylor expansion (1.14), can now be written in the form:

$$(T_B - T_\infty)\frac{\rho_v i_{fg}}{\rho_l T_\infty} = -\left(\frac{\rho_v{}^2 i_{fg}{}^2}{\rho_l{}^2 cp_l T_\infty \sqrt{\alpha_l}}\right)\frac{\sqrt{\pi}}{2} R \frac{1}{\sqrt{t}} \tag{1.33}$$

The parameter in brackets in equation (1.33) is crucial for determining bubble dynamic behaviour. One can conclude, by comparing the inertial term (1.23) and the thermal term in equation (1.13), that the second term will gain importance with respect to time, likely making initially inertia controlled bubbles thermally controlled as they grow. The *first critical time*, t_{c1}, which represents the time when the order of magnitude of the thermal term becomes equal to the order of magnitude of the inertial term, can be evaluated from equation (1.33):

$$t_{c1} = \frac{p_{SAT}(T_\infty) - p_\infty{}^*}{\rho_l}\left(\frac{\rho_v{}^2 i_{fg}{}^2}{\rho_l{}^2 cp_l T_\infty \sqrt{\alpha_l}}\right)^{-2} \tag{1.34}$$

The most important theories of thermally controlled growth of spherical bubbles, such as those of Forster and Zuber [59], Plesset and Zwick [60] and Scriven [61] are listed in Table 1.2. These theories used more developed calculation procedures, based on the procedure described in this section.

Mikic et al. [62] developed a model which spans both, hydrodynamically controlled growth and thermally controlled growth. After combining equations (1.14) and (1.20) (for R_0=0 and $\Delta p = p_B - p_\infty$) with the rate of bubble growth with vapour temperature (equation 1.35, from Plesset and Zwick [60]), one can obtain the following non-dimensional form of the bubble growth equation:

$$\frac{dR}{dt} = \frac{1}{2}\frac{b}{\sqrt{t}}\left(1 - \frac{T_B - T_{sat}}{T_\infty - T_{sat}}\right); \qquad b = \sqrt{\frac{12\alpha_l}{\pi}}Ja \tag{1.35}$$

$$R^+ = \frac{2}{3}\left[\left(t^+ + 1\right)^{\frac{3}{2}} - \left(t^+\right)^{\frac{3}{2}} - 1\right] \tag{1.36}$$

where:

$$R^+ = \frac{aR}{b^2}; \qquad t^+ = \frac{a^2 t}{b^2}; \qquad a = \left(\frac{2i_{fg}\rho_v\left(T_\infty - T_{sat}\right)}{3\rho_l T_{sat}}\right)^{\frac{1}{2}} \tag{1.37}$$

In case where $t^+ << 1$, equation (1.36) becomes Rayleigh's equation, whereas if $t^+ >> 1$ it becomes equal to the Plesset and Zwick solution.

Thermally Controlled Bubble Growth in a Non-uniform Temperature Field

Models shown in the previous section represent groundwork for the development of the theory of bubble dynamics. However, they are not applicable to subcooled boiling, because of the assumption of uniform heat transfer from a superheated liquid. More appropriate models should take into account temperature gradients in the liquid surrounding the growing bubble.

Zuber [63] modified the energy balance (1.30) by including an additional term, q_B, which accounts for the heat transfer from the bubble to the cooler bulk liquid:

$$i_{fg} \cdot \rho_g \frac{dR}{dt} = \varepsilon k \frac{T_\infty - T_B}{\sqrt{\pi \alpha_l t}} - q_B \tag{1.38}$$

where $\varepsilon = \pi/2$ is the correction factor for the sphericity of the bubble. Zuber assumed that the temperature gradient between vapour and liquid phases was equal to the gradient between the surface of the heater and the liquid preceding nucleation. In other words, the total heat flux to the bubble is less than the corresponding heat flux in the superheated liquid for an average heat flux from the heated surface. Following this idea, he obtained the bubble growth relation by expressing the bubble radius and time normalized with maximum radius and growth time. The relations for the bubble growth, bubble maximum diameter and bubble growth time, are shown in Table 1.3.

Other authors, such as Cole and Shulman, accounted for the existence of a temperature gradient by taking half of the actual wall superheat. Others multiplied the Plesset and Zwick [60] prediction for superheated boiling with a factor less than unity, e.g., Van Stralen [64].

Mikic and Rohsenow [65] expressed the temperature gradient as a function of waiting time, t_w. The waiting time denotes the time preceding bubble growth, during which the liquid, initially at uniform temperature, is in direct contact with the heated surface. The bubble subsequently grows in the non-uniform temperature field created during t_w. The energy balance is given by:

$$i_{fg} \cdot \rho_v \frac{dR}{dt} = \varepsilon k \left(\frac{\Delta T_{sat}}{\sqrt{\pi \alpha_l t}} - \frac{\Delta T_{sat} + \Delta T_{sub}}{\sqrt{\pi \alpha_l (t + t_w)}} \right); \quad \varepsilon = \sqrt{3} \tag{1.39}$$

The equations for the bubble diameter, maximum diameter and waiting time are shown in Table 1.3.

1.3.4 Microlayer Evaporation

Various heat transfer mechanisms in subcooled boiling are still the subject of arguments between researchers. It is, however, widely accepted that vapour content in the bubble is generated from the thin liquid layer, called the *microlayer*, which resides underneath the bubble. The concept of heat transfer through the liquid microlayer was introduced by Snyder and Edwards [66] and confirmed experimentally by Moore and Mesler [67]. Their research was followed by direct observation of the microlayer as in photographs by Sharp and in Ouwerkerk [68]. Cooper and Loyd [69] investigated the thickness of the microlayer by using a set of microthermometers located on the heating surface. They were able to observe a change in microlayer thickness with bubble size. They concluded that microlayer profiles were wedge shaped and that the initial thickness of the microlayer is directly proportional to the distance from the center of the bubble. The experimental approach to investigating the microlayer has been addressed in other studies, such as Jawurek [70] and Koffman and Plesset [71].

The microlayer can be described as a thin liquid layer (thickness in the order of 1μm), wedge-shaped, with a dry patch in the center. The size of the dry patch depends on

the size of bubble and the wettability of the liquid. The line which borders the vapour-solid interphase (dry patch) is called the three-phase line (TPL). A schematic of the bubble and liquid microlayer is shown in Figure 1.5. The figure is taken from Snyder and Robin [66] and shows the model as visualized by Snyder (1952).

In a recent study, Mitrovic [72] discussed the inner (non-evaporating) and outer (vapour generating) parts of the liquid film as well as the liquid velocity in the film and the shape and motion of the TPL. Several authors (e.g., Buyevich and Webbon [73]) recently questioned the existence of a dry spot that represents the vapour-solid interface.

Unal [74] used a microlayer evaporation model to predict bubble radius and bubble growth rates. He assumed that vapour for the growth of a spherical bubble is supplied from the microlayer (total heat input through the microlayer). He also assumed that condensation occurs on the upper half (heat output by condensation to the surrounding liquid). The model of Unal is given in detail in Appendix B.

1.4 Research Background

Void growth models have mainly been developed for moderate and high pressures and, in general, are not in accordance with void growth experimental data at low pressure conditions. Recent studies suggest that the physics and mechanisms of void growth are different at low pressures and low flow rates. The assumptions about the position of the OSV, the negligible value of void fraction in the highly subcooled region and bubble detachment studies based on force balances are usually not valid for low pressure conditions.

As discussed in the preceding text, OSV models can roughly be classified into three categories. The first category consists of models that relate OSV to transition from partial to fully developed boiling. In the second category are models that take detachment of the first bubble as a critical parameter for OSV. Finally, the models in the third category are based on the existence of a bubble layer and the assumption that OSV occurs when the first bubbles are ejected from the bubble layer into the fluid core. Several assumptions need clarification:

- Recent experimental observations show that, at low pressures and flow rates, bubbles behave in a different manner than that assumed in most void growth models. Bubbles are seen to detach from the surface long before OSV is reached. Also, bubble shapes appear to deviate from the typically assumed spherical shape;
- Transition from partially to fully developed boiling appears to occur before OSV is reached. At present, there is a significant lack of reliable studies that link the change in heat transfer rates to eventual changes in bubble behaviour, particularly for subcooled flow boiling;
- According to recent photographic studies, the existence of the bubble layer in low pressure and low flow rate subcooled flow boiling is questionable;
- Bubble detachment models based on a force balance fail to predict the detachment time and diameters of detaching bubbles. This is particularly evident when using models based on a static force balance. Several points, such as the deviation of bubble shape, or reduction of bubble size before detachment are not taken into account. Also, several recent studies challenge the assumption of the existence of a stable contact area between the bubble vapour phase and the solid phase. Force balances, based on whether the vapour-solid interface exists or not, will differ significantly. This point has to be further addressed.

1.5 Research Objectives

Given the existence of relevant void growth experimental data at low pressures (1 to 3 bar), it is important to perform a bubble visualization study, covering this pressure range, and for the subcooling and flow rate conditions that are relevant to the working conditions of SLOWPOKE and MAPLE nuclear reactors. These experimental results will allow development of correlations for bubble radius, bubble growth time and bubble condensation time, as well as a general understanding of bubble behaviour in low pressure subcooled flow boiling. As well it will help reveal the relation between the bubble beahviour and heat transfer. Measurements of bubble size and motion will be used for development of a force model for low pressure and low velocity subcooled boiling conditions which, at present, does not exist in the open literature.

The specific objectives of the proposed investigation are:

- To perform high speed photography experiments for subcooled nucleate boiling in vertical upward flow for pressures between 1 and 3 bar, flow rates between 0.02 and 0.2 kg/s and subcoolings between 10 and 30 °C, in order to investigate bubble behaviour;
- To analyze the effect of pressure, flow rates, subcooling and heat flux on bubble geometric parameters;
- To develop correlations for maximum diameter, detachment diameter, growth, detachment and condensation times, and bubble growth rates for the pressure range 1 - 3 bar;
- To investigate heat transfer, in particular the transition from partially to fully developed boiling, with respect to the observed bubble behaviour;
- To develop a model of forces acting on bubbles during low pressure subcooled boiling, to estimate the order of magnitude of parallel and normal forces by comparing the model with experimental data, and to determine the bubble detachment mechanism;

The structure of this text is such that the experiments, explained in detail in Chapter 2, have been further analyzed and discussed from the aspect of bubble behaviour in Chapter 3, heat transfer in Chapter 4 and detachment modelling in Chapter 5. Each of these three chapters contains a review of literature and concluding remarks relevant for the material described therein.

Table 1.1 Models for the prediction of ONB

Bergles and Rohsenow (1964)	$q_{ONB} = 1120 p^{1.156} \left(1.8\Delta T_{sat,ONB}\right)^{2.16} / p^{0.0234}$; (water)
Davis and Anderson (1966)	$q_{ONB} = \dfrac{i_{fg} k_l}{8\sigma T_{sat}\left(\dfrac{1}{\rho_v} - \dfrac{1}{\rho_l}\right)} \cdot \Delta T_{sat,ONB}^{\ 2}$; (water)
Frost and Dzakowic (1967)	$q_{ONB} = \dfrac{i_{fg} k_l}{8\sigma T_{sat}\left(\dfrac{1}{\rho_v} - \dfrac{1}{\rho_l}\right)} \cdot \Delta T_{sat,ONB}^{\ 2} \dfrac{1}{Pr^2}$;(refrigerants)
Hino and Ueda (1985)	$q_{ONB} = \dfrac{k_l}{r_{max}^{\ *}} \Delta T_{sat,ONB} - \dfrac{2\sigma k_l T_{sat}}{i_{fg}\rho_v \left(r_{max}^{\ *}\right)^2}$; $r_{max}^{\ *}$=0.22-0.34 μm (R11, R113,...)
Hahne et al. (1990)	$q_{ONB} = h_{FC}\left[\dfrac{2\sigma T_{sat}\left(\dfrac{1}{\rho_v} - \dfrac{1}{\rho_l}\right)}{r^* i_{fg}} + \Delta T_{sub}\right]$; $2\sigma/r^*$=1.54 bar $h_{FC} = \dfrac{(\xi/8)(Re-1000)Pr}{1+12.7(\xi/8)^{0.5}\left(Pr^{0.67}-1\right)} \dfrac{k_l}{D}$; $\xi = \left[1.82\log(Re) - 1.64\right]^{-2}$; (R12, water,...)
Unal (1977)	$q_{ONB} = \dfrac{h_{FC}\Delta T_{sub,ONB}}{0.665}$; h_{FC} from Dittus Boelter (water)
Serizawa (1979)	$\dfrac{q_{ONB}}{G c_p \Delta T_{sub,ONB}} = 0.0142\left(\dfrac{\rho_v}{\rho_l}\right)^{0.1}\left[\dfrac{h_c D_h}{k_l}\dfrac{\sigma T_{sat}\left(\dfrac{1}{\rho_v} - \dfrac{1}{\rho_l}\right)k_l}{i_{fg} q_{ONB} D_h^{\ 2}}\right]^{0.29}$ (water)

Table 1.2 Thermally controlled bubble growth models

Forster and Zuber (1954)	$R = \sqrt{\pi} Ja \sqrt{\alpha_l t}$
Plesset and Zwick (1954)	$R = \frac{\sqrt{12}}{\sqrt{\pi}} Ja \sqrt{\alpha_l t}$
Scriven (1959)	$R = \sqrt{2Ja} \sqrt{\alpha_l t}$; small Ja $R = \frac{\sqrt{12}}{\sqrt{\pi}} Ja \sqrt{\alpha_l t}$; large Ja

Table 1.3 Bubble growth in non-uniform temperature field

Zuber (1961)	$\frac{R}{R_m} = \sqrt{\frac{t}{t_m}} \left(2 - \sqrt{\frac{t}{t_m}} \right)$ $R_m = \frac{1}{2} Ja \sqrt{\pi \alpha_l t_m}$ $\sqrt{\pi \alpha_l t_m} = \frac{k_l \Delta T_{sat}}{q}$ Ja with ΔTsat (wall superheat) q – wall heat flux
Mikic and Rohsenow (1964)	$\frac{R}{R_m} = \frac{\left(\frac{t}{t_m}\right)^{\frac{1}{2}} \left\{ 1 - \theta \left\{ \left[1 + \left(\theta^2 - 1\right) \frac{t}{t_m} \right]^{\frac{1}{2}} - \left[\left(\theta^2 - 1\right) \frac{t}{t_m} \right]^{\frac{1}{2}} \right\} \right\}}{1 - \theta \left[\theta - \left(\theta^2 - 1\right)^{\frac{1}{2}} \right]}$ $R_m = \frac{2}{\pi} \sqrt{3} Ja \sqrt{\pi \alpha_l t_m} \left\{ 1 - \theta \left[\theta - \left(\theta^2 - 1\right)^{\frac{1}{2}} \right] \right\}$ $\theta = \frac{\Delta T_{SAT} + \Delta T_{sub}}{\Delta T_{SAT}}$ Ja with ΔTsat (wall superheat)

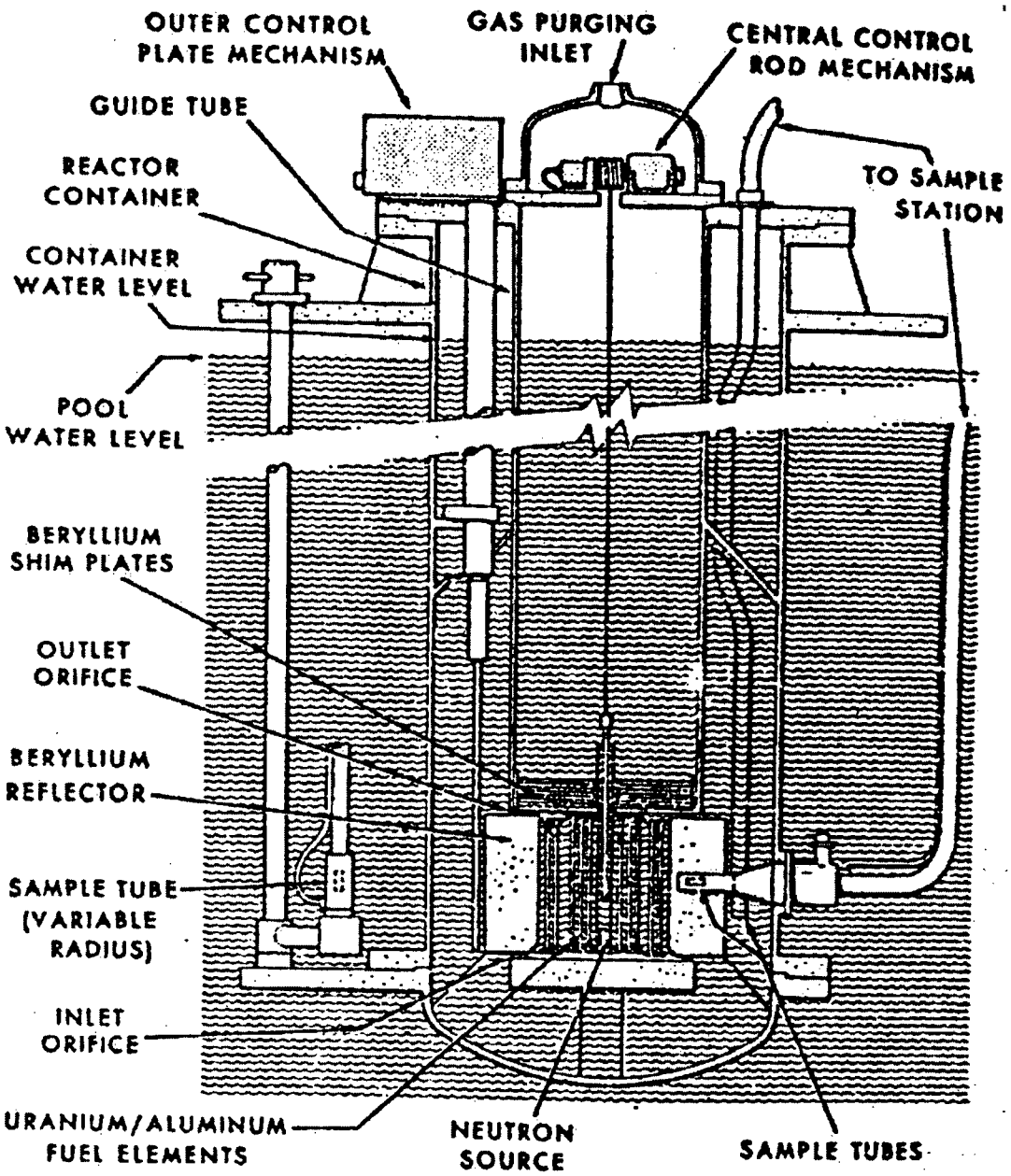

Figure 1.1 Section through the SLOWPOKE reactor [1]

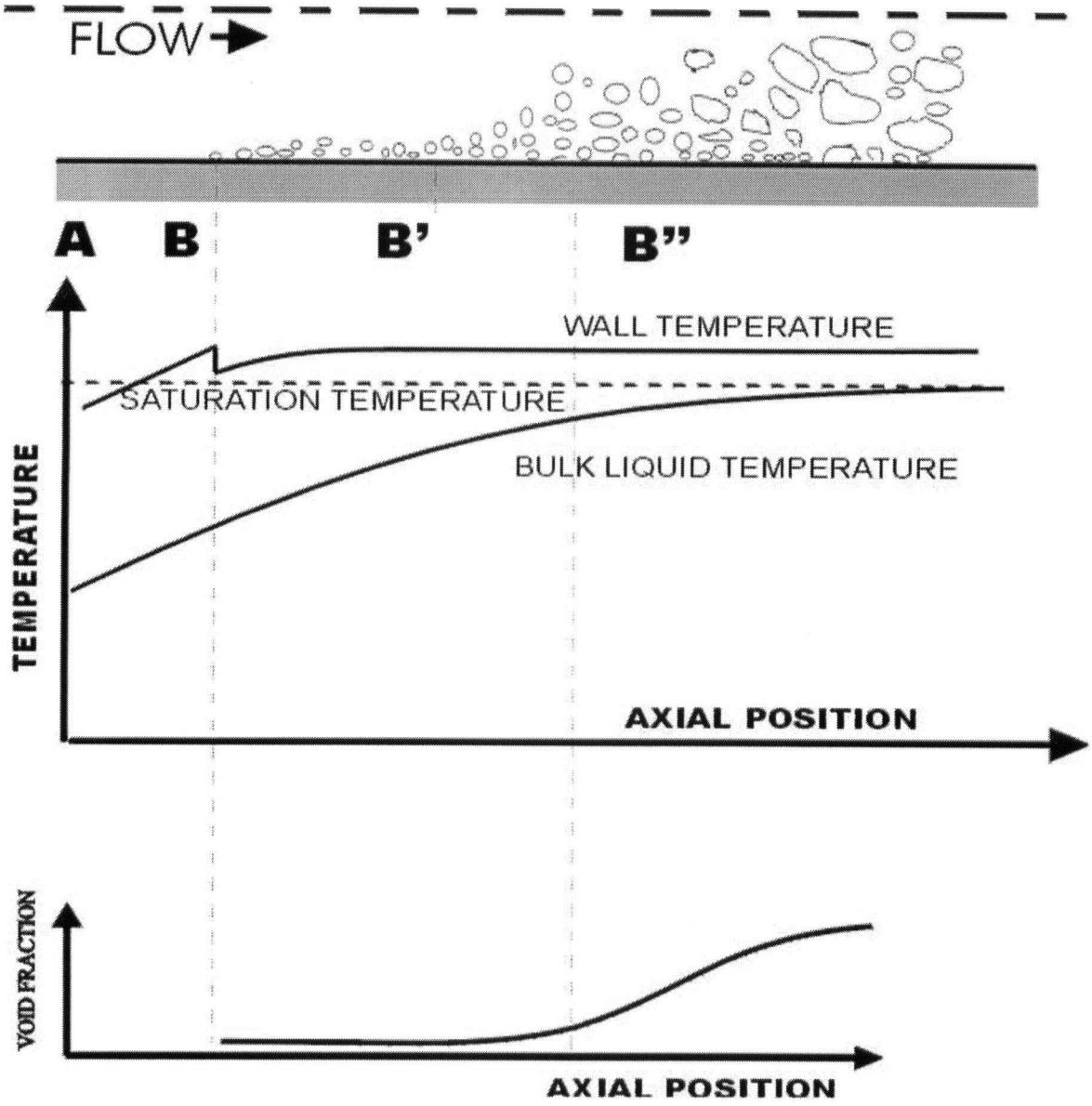

Figure 1.2 Subcooled flow boiling – temperature and void curve

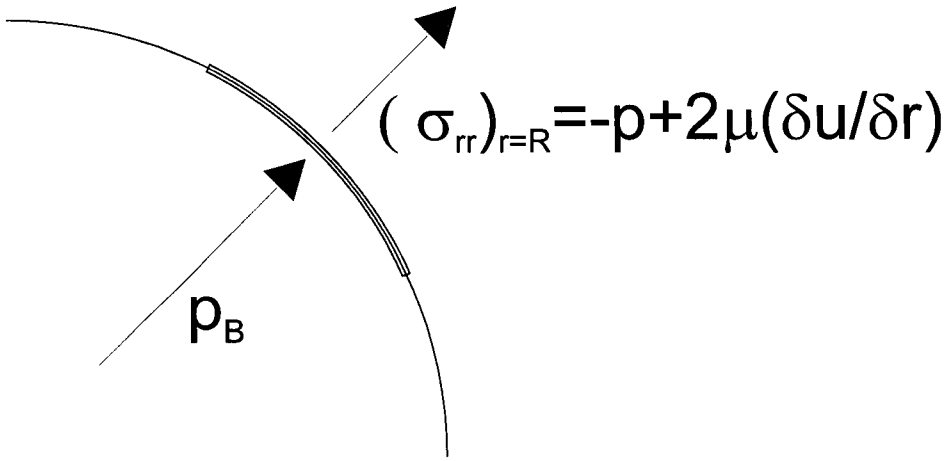

Figure 1.3 Force balance on the thin lamina at bubble interface

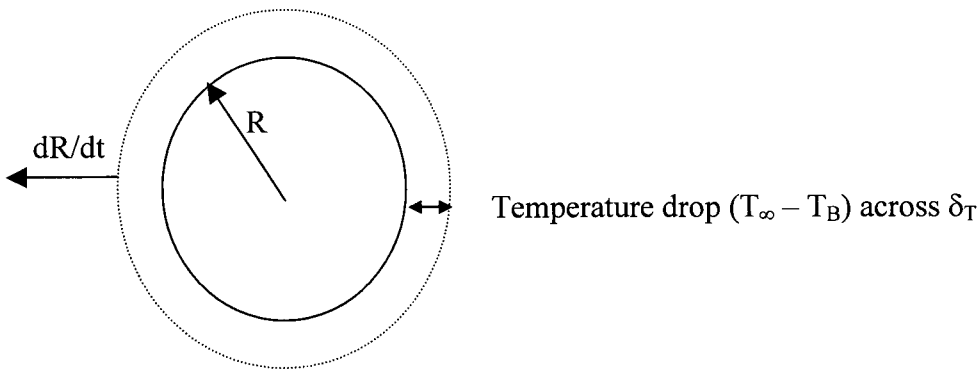

Figure 1.4 Liquid thermal layer that supplies heat to the growing bubble

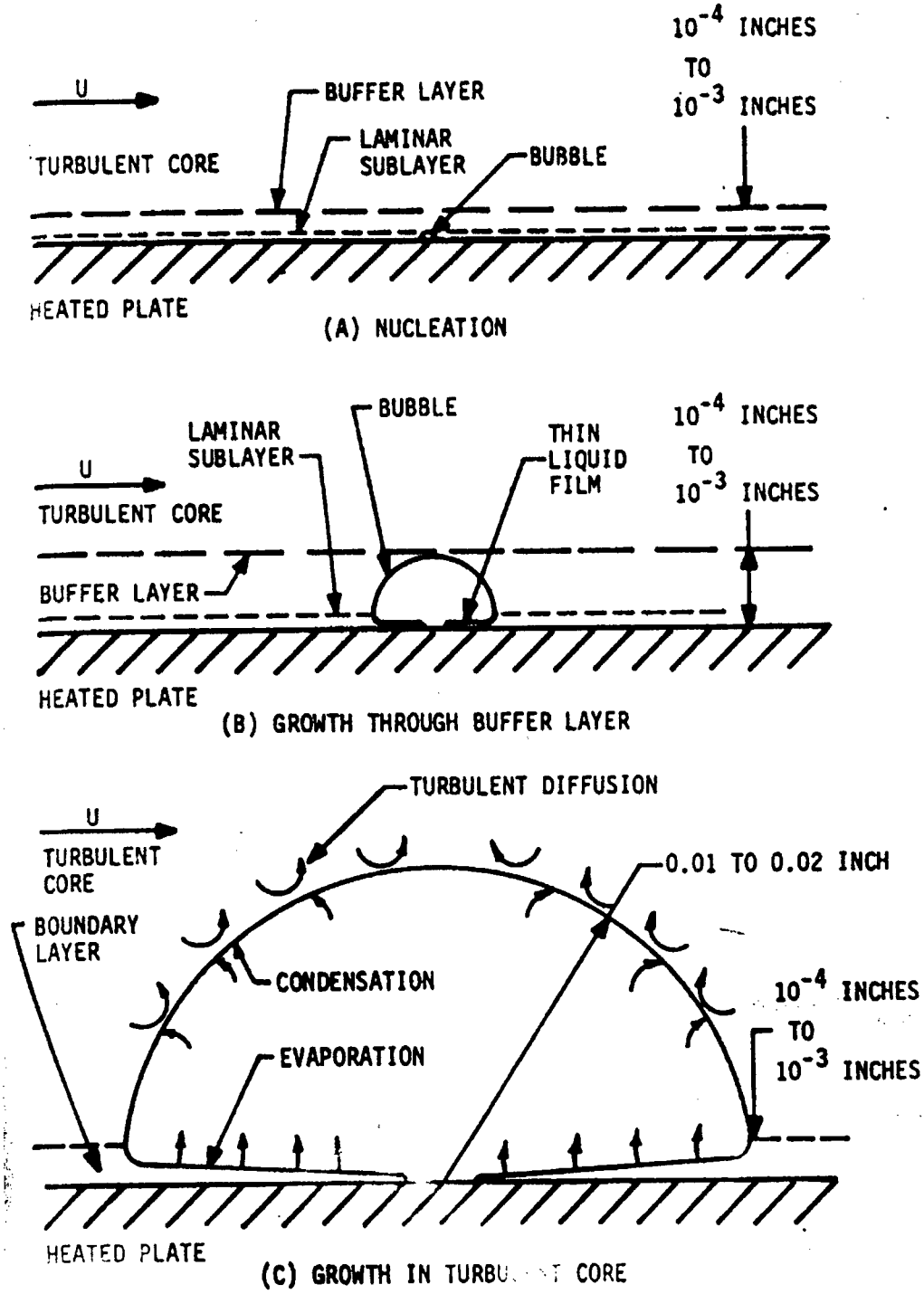

Figure 1.5 The microlayer evaporation – model of Snyder (1956)

From Snyder N.W. and Robin T.T.,"Mass Transfer Model in Subcooled Nucleate Boiling" Trans ASME (1969) Vol 91C, p.405

Chapter 2

EXPERIMENTAL APPARATUS, PROCEDURE AND DATA ANALYSIS

2.1 Experimental apparatus

The experimental facility is located at the University of British Columbia. It was originally built by Eric Bibeau in 1986-1987 and subsequently redesigned on several occasions to accommodate various experimental investigations (e.g. circular and finned test sections, upward and downward flow of coolant, void growth and/or high-speed photography experiments). During the course of the current investigation, the original data acquisition program, developed by Bibeau, has been replaced by commercial *LABTECH NOTEBOOK* software. The test section was modified to allow the use of high-speed photographic equipment. Part of the test section was redesigned to reduce light refraction, and security features were added to the apparatus.

2.1.1 Equipment

Shown in Figure 2.1 is a schematic of the apparatus. The closed loop facility has a capacity of 3 m^3 and is fitted with a vertical, electrically heated, annular test section. Prior to entering the test section the distilled water is circulated via a main pump from a storage reservoir through an immersion heater, filter and flow metering system. The liquid-vapour mixture exiting the test section passes through a vertical cross-flow condenser and heat exchanger before returning to the main pump.

The role of the pre-heater (immersion heater) is to adjust and maintain constant temperature of the liquid at the entrance of the test section. It is equipped with a temperature control device, heater on-off control switch and temperature display.

The filtering system consists of a *BARNSTEAD dual PCS* with a high capacity cartridge (separate bed resin, average purity 175000 ohm-cm) and an oxygen removal cartridge to eliminate dissolved gases and prevent internal corrosion.

The flow metering system consists of two turbine flow-meters, for high and low flow rates, and a by-pass line. After passing through the flow metering system, the water is fed into the test section through the inlet (lower) plenum. All connections between the test section and the rest of the two-phase flow loop are made of thick rubber in order to absorb vibrations and electrically isolate the test section.

The manually operated water-water heat exchanger located between the condenser and the main pump allows for the removal of excess heat and the adjustment of liquid temperature before re-circulation. The immersion heater, condenser and pumps are computer controlled. They are operated from a PC computer by using an interactive program written by Bibeau.

A separate loop is used for the pressurization of the apparatus. The pressure is maintained constant at the outlet of the test section by running a filling pump and controlling the re-circulation through a flow control valve located at the inlet of the storage tank.

The loop is equipped with several air bleed valves, located at high points along the apparatus, to remove the trapped air. All components of the apparatus are made of non-oxidizing metals. The immersion heater, condenser and pumps are made of stainless steel, heat exchanger and pipes made of copper, and plenums and fittings made of brass.

2.1.2 Test Section

The test section consists of a vertical annulus with two plenums (at the inlet and outlet), and pressure and temperature measurement instrumentation, all mounted together on a platform made of phenolic plastic. It has been designed to simulate the boiling process in SLOWPOKE and MAPLE nuclear reactors by matching the hydraulic diameters of single fuel pins. The flow can be diverted to feed the test section through the upper (downward flow) or lower (upward flow) plenum. For the purpose of this investigation, the water was circulated upward through the annulus with a circular heater (large circular FES) which corresponds to conditions in the SLOWPOKE reactor.

The test section is 0.78 m long. The annulus consists of an electrically heated rod and an outer quartz glass tube (22 mm ID). The heater is a 12.7 mm diameter hollow stainless steel rod welded to solid copper rods. The heated length of 0.48 m is located 0.22 m downstream of the inlet plenum thus allowing for the flow to develop fully. This is shown in Figure 2.3. The figure also shows the location of thermocouples.

The test section is equipped with a horizontal table, which spans the annular section and supports the high-speed camera. The light diffuser and two racks of reflector lamps with cooling fans are also mounted on the test section. The schematic of the test section with the photographic equipment is shown in Figure 2.4. The characteristics of the test section are given in Table 2.1. Presented in Figure 2.5 is a detail from the photograph in Figure 2.2, which shows the test section of the apparatus during experiment.

A square cross-section glass box filled with water surrounded the test section to correct distortion due to refraction. The glass box is made of thin plate glass with two aluminum plates at the top and bottom of the box. The two aluminum plates were carefully designed and built. Their function is to secure a tight connection between the box and the outer glass tube of the test section and to keep the glass plates parallel in order to minimize the distortion of light. The drawings of the two aluminum plates are shown in Figure 2.6. A photograph of the portion of the test section with the mounted glass box is shown in Figure 2.7. Details about the effects of the refracted light and calculations are given in Appendix A.

A large range of heat fluxes was supplied to the test section by means of a 64 kVA A.C. power supply. The 600 V input line steps down to the required 4 to 32 V (16 V for most experiments).

2.1.3 Instrumentation

The loop allows for varying power input, pressure, flow rate and inlet temperatures of the liquid. Thus, one can obtain a desired subcooling at the filming location along the test section for any given set of experimental parameters.

2.1.3.1 Volumetric Flow Rate

Two turbine flow meters are used to measure the volumetric flow rate. The low volumetric flow rate is measured using a *fti FLO-4* flow-meter which has a linear flow range of 0.006-0.06 l/s. The high volumetric flow rate is measured with a *Itt BARTON 7285* flow-meter, which has linear response within the flow range of 0.06-0.6 l/s. Frequency signals were fed to a high-speed analog/digital I/O expansion board (*Metrabyte DAS20*) and processed using *LABTECH NOTEBOOK* software.

2.1.3.2 Voltage and Current

The voltage across the heater rod was obtained using an *OMEGA DP18-AV2* voltmeter (range 19.99 V, resolution 10 mV, signal integration period 80 ms, read rate 3.12 Hz, accuracy 0.2%+/-1 count). Current was measured using an induction coil *HAMMOND Class H* which generates an A.C. signal proportional to the current and an *OMEGA DP18-AC4* milliammeter (range 1999 mA, resolution 1 mA, signal integration period 80 ms, read rate 3.12 Hz, accuracy 0.2%+/-1 count). The product of the voltage and current gives the power supplied to the heater. The detailed procedure for calibration of the induction coil using a shunt was described by Bibeau [5].

2.1.3.3 Pressure

Static pressure at the inlet and outlet of the test section was measured using Bourdon type pressure gauges (+/- 140 Pa). The pressure difference across the test section for typical experimental conditions is about 7 kPa.

2.1.3.4 Temperature

Temperatures of the water were measured at the test section inlet and outlet. The surface temperature of the heater was obtained at the filming location. An ungrounded, K-type, shielded thermocouple (*THERMOELECTRIC K-18-U*) was used to measure the temperature in the inlet (lower) plenum. In order to avoid inaccurate measurements in the two-phase flow leaving the test section, the outlet temperature was measured at a location one meter downstream from the outer plenum, also using an ungrounded, K-type, shielded thermocouple (*THERMOELECTRIC K-116-U*).

Six intrinsic thermocouples (K-type, 0.102 mm wire diameter encased in a stainless steel sheath 0.508 mm in diameter) were embedded in the surface of the heater. The locations of the thermocouples are shown in Figure 2.3. All six thermocouples were used for validation of heat balances used in the calculations. High-speed photography experiments require knowledge of the surface temperature only at the filming location. Hence, only the last thermocouple (440 mm downstream from the start of the heated section) was used in analyzing the visualization results. Temperatures were monitored using an *OMEGA* thermometer.

2.1.4 High-speed Photography

Bubbles were filmed with a 16mm High Speed Motion Picture Camera *HYCAM K20S4 E* fitted with a MACRO lens *(SIGMA zoom – α III* f=35-135mm) and a reversible ring (*YASHICA/CONTAX 55mm* + C-adapter), using *KODAK Eastman Ektachrome H-S 7250* films. Allowable film speeds are between 4000 and 8000 frames/s. The camera was located at about 440 mm from the start of the heated section and could capture a region of about 8 mm along the heater surface. The filmed region is illustrated in Figure 2.8. A single film could capture about 1 s of the boiling process. Time steps of 1 ms were marked on the film using a 1 kHz pulse generator. The sequence of the film with time steps is shown in Figure 2.9.

Developed films were digitized using a CCD camera (*TAMRON/FOTOVIX II*), and later studied using image analysis software (*MATROX INSPECTOR v2.0*). Each digitized image was enlarged 100 times to allow accurate measurements of bubble geometry. The schematic of the image processing system is shown in Figure 2.10.

Lighting consisted of twelve 300 W halogen projector lamps. A ground glass screen was used to diffuse the light source.

2.2 Experimental Procedure

The preparation of the apparatus for experiments included: cleaning the test section and heater surface with mild boric acid solution to remove oxides and possible fouling residue, filling the loop with distilled water and degassing the water. The

degassing process is necessary in order to decrease the level of dissolved air in the loop. Dissolved air can affect the boiling process and alter experimental results. The partial pressure of a dissolved gas changes the pressure of the system.

The time required for preparation is about 5 hours. The average experiment lasted approximately 30 minutes and included the time necessary to set and stabilize desired pressure, subcooling, flow rate and heat flux. The filming time was about 1 s.

The degassing procedure starts by pressurizing the loop to the maximum allowable pressure (p = 3 bar) and setting the maximum heat input which does not produce boiling. When the temperature of the water reached approximately 105 °C, the heat was shut off and the pressure was decreased to atmospheric. The air bleed valves have to be open. Sudden depressurization induces boiling and the released gases and vapour leave the loop through the air vents. The degassing procedure was repeated at least two or three times before each experiment. After the degassing was over, the experimental parameters were set and the experiments started.

2.3 Measured and Calculated Parameters

Important experimental parameters for this investigation include pressure, heat flux, subcooling and flow rate. The pressure and flow rates were measured directly during experiments. The heat flux was estimated by measuring the voltage across the test section and the current. The heat flux was obtained from:

$$q = \frac{V \cdot I}{P_h \cdot l} \tag{2.1}$$

In order to calculate the subcooling at the filming location, the local bulk liquid temperature at the same location was determined. It can be shown that a simple energy balance can be formulated as follows:

$$q = \frac{\dot{m} cp_l (T_{out} - T_{in})}{P_h l} = \frac{\dot{Q} \rho_l cp_l (T_{out} - T_{in})}{P_h l} \tag{2.2}$$

Equation (2.2) (i.e. predicted output temperature) agrees with experimental data within the accepted error of measurements. Thus, assuming a linear variation of bulk

temperature with distance along the heater, the subcooling at the filming location can be calculated from:

$$\Delta T_{sub} = T_{sat} - \left(T_{in} + \frac{qP_h l_{film}}{\dot{Q}\rho_l cp_l} \right) \tag{2.3}$$

Hence, the equilibrium quality is given by:

$$X_{eq} = \frac{cp_l}{i_{fg}} \left(T_{in} + \frac{qP_h l_{film}}{\dot{Q}\rho_l cp_l} - T_{sat} \right) \tag{2.4}$$

The experiments were planned to systematically cover the region between ONB and OSV. Hence, heat fluxes corresponding to the ONB and OSV have to be estimated for any given set of experimental conditions. The equation by Hahne et al. [21], is used to calculate the heat flux at ONB, i.e.,

$$q_{ONB} = h_{FC} \left[\frac{2\sigma T_{sat} \left(\frac{1}{\rho_v} - \frac{1}{\rho_l} \right)}{R_{cav} i_{fg}} + \Delta T_{sub} \right] \tag{2.5}$$

The single fluid forced convection heat transfer coefficient, h_{FC}, was calculated using the Dittus-Boelter equation. The coefficient R_{cav} is set equal to 4.5×10^{-6} m, as calculated previously by Bibeau [6] for the same experimental apparatus.

The heat flux at OSV was obtained from the following correlation by Bibeau and Salcudean [75].

$$St_{OSV} = 130 Pe^{-0.88} \tag{2.6}$$

Equation (2.6) represents a modification of Saha and Zuber's model, which accounts for the liquid velocity (i.e. variation of the Nusselt number at OSV). Equation (2.6) has been used previously to correlate void growth experimental data obtained on the same apparatus (Bibeau and Salcudean [46] ; Bibeau and Salcudean [75]). All fluid properties were evaluated at the saturation temperature.

2.4 Experimental Conditions

The experimental part of the present investigation includes 61 films taken at pressures of 2 and 3 bar (29 at 2 bar and 32 at 3 bar). Mass flow rates ranged from 0.02 to 0.2 kg/s, corresponding to mean liquid velocities from 0.08 to 0.8 m/s in the annular test section. Inlet temperatures were adjusted to obtain the desired subcooling (10, 20 and 30 K) at the filming location. Heat flux was varied systematically from 0.2 to 1 MW/m^2 while, for each test, local subcooling and flow rate were held constant. This range covers the boiling process from the appearance of the first bubble (ONB), to the higher heat fluxes beyond OSV. A summary of experimental conditions is given in Table 2.2. Figures 2.11 and 2.12 illustrate the location and codes of experiments with respect to ONB and OSV. The reason for the lower number of experiments performed at the mass flow rate of 0.02 kg/s compared to experiments at higher flow rates is that it was impossible to obtain inlet temperatures of water less than 10 °C and, therefore, attain higher heat fluxes (closer to OSV). Nevertheless, it will be shown that even at the attained heat fluxes, significant coalescence occurs for low flow rate experiments, thus preventing accurate quantitative analysis of bubble behaviour.

2.5 Data Processing

Important parameters for the investigation of bubble behaviour are:

- Bubble growth time, ejection time and collapse time;
- Maximum bubble diameter and diameter at ejection;
- Bubble diameters along principal axes, bubble elongation;
- Bubble displacement in directions parallel and normal to the surface of the heater;
- Bubble contact angles, inclination angle;

Approximately 100 bubbles from each film were used to obtain detachment diameters (normal detachment, ejection) and 10-30 bubbles were analyzed from inception to collapse. Bubble lifetimes were typically captured on 5-30 subsequent frames. Lifetimes of less than 5 frames were considered insufficient for an accurate analysis. The

ejection time and diameter were always measured from the frame preceding the frame on which the bubble is physically separated from the surface of the heater. It was found that applying techniques described in this study for contact angle measurements lead to rather inaccurate data. Therefore, contact angles are excluded from further analysis.

Digitized frames were analyzed one by one with the *MATROX INSPECTOR v2.1* image analysis software. Bubble photographs were enlarged and the bubble contour was traced manually for each bubble. It was possible to obtain enlargements of about 100 times the original bubble size. An example of an enlarged bubble and the calibration procedure is shown in Figure 2.13. Geometrical bubble parameters were measured using a standard subroutine ("blob analysis") provided in the software package. Manual tracing of the bubble contour and the blob analysis setup, as well as the look of the frame containing the blob analysis results are shown in Figure 2.14. Also, an example of the program output with the most important measured parameters is shown in Table 2.3. Shown in Figure 2.15 is the location of the bubble centroid (BCB) as well as the leftmost and bottommost positions of the bubble. Their coordinates, shown on the same figure, are relative to the bubble origin (point 1), which was set manually for each bubble. The origin was placed at the intersection of the cross-hair markers, which appear on each photograph (frame) and originate at the camera lens (same position on each photograph).

The mean diameters were calculated from measurements of 32 different Feret diameters (distances between opposing parallel tangents on the surface of the bubble – i.e., close to the bubble diameter). Also, the maximum and minimum Feret diameters were taken to represent two diameters along principal axes of the bubble (typically normal and parallel to the surface of the heater). Thus, their ratio represents the elongation of the bubble. Maximum and minimum Feret angles represent the angles that the maximum and minimum Feret diameters form with the horizontal axis. Negative values denote the inclination in the direction opposing the flow.

A projection of the bubble centroid on the surface of the heater on the first frame was assumed to be the location of the nucleation site. Distances from the nucleation site to the location of the bubble centroid on each subsequent frame showed the displacement of the bubble in the directions normal and parallel to the heater. These geometrical

parameters are shown in Figure 2.16. Shown in Figure 2.17 are the two diameters along the principal axes and the mean diameter from a typical experiment. Bubble growth time, ejection time, condensation time and lifetime were deduced from the mean diameter, D, vs. time graphs, as shown in Figure 2.18. In some experiments it was also possible to follow multiple bubbles growing from the same nucleation site which allowed for a determination of the bubble frequency and waiting time, t_w. However, in most experiments it was extremely difficult to follow bubbles rising from the same nucleation site and, hence, determination of the bubble frequency was excluded from the analysis.

2.5.2 Selection of a Typical Bubble

As mentioned before, over 100 bubbles from each film were used to determine the detachment diameter for a given set of experimental conditions. It was found that this number of bubbles represented a good statistical sample for the analysis. The arithmetic mean was calculated and used as a typical detachment diameter for each experiment. Shown in Figure 2.19 is a typical example, a statistical distribution of detachment diameters for experiment P2-22.

The density of active nucleation sites and the size of bubbles as well as distortion of light on the surface of the heater during experiments made impossible the isolation of one nucleation site from which data could be taken. Hence, the image analysis included all visible bubbles on the film regardless of the location of inception.

Upon analyzing bubbles from inception to collapse, a significant difference in bubble diameters and lifetimes for bubbles on the same film (same experimental conditions) has been observed. This has been attributed to the fact that bubbles were initiated from different nucleation sites and/or, experienced varying local temporal thermal and velocity fields.

It can be shown that the latter effects are dominant in creating scatter in experimental data. In fact, previous analysis of bubbles growing from the same nucleation site (Faraji et al. [76], p=1.05 bar experiments) had shown similar variations of bubble diameters and lifetimes. Figure 2.20 shows the bubble size and lifetime distribution from different nucleation sites at fixed conditions. Observations previously

made on a single active nucleation site are shown in Figure 2.21. It was concluded that, within the experimental range of this study, the same procedure for determining the average parameters can be applied to all bubbles regardless of whether they originate from the same or various nucleation sites. The conclusion about the relative insignificance of the advantage of having bubbles growing from the same nucleation site becomes more obvious if the same parameters from the previous two examples are normalized with corresponding parameters of the average bubbles. This is shown on Figure 2.22.

The mechanism for identifying typical bubbles from each film is similar with that of Faraji et al. [76] Typical bubbles in this study are, therefore, those whose lifetimes, detachment diameters and initial growth rates are closest to averages for a given set of experimental conditions.

2.6 Error Analysis

Experimental errors for quantities measured directly were obtained from manufacturer's specifications. Errors associated with calculated parameters were estimated using the error propagation method. The errors are listed in Table 2.6. The errors of calculated parameters, such as power, subcooling and bubble diameters and lifetimes were obtained as follows.

Power

The errors in the heat flux measurements were estimated using the error propagation method and errors in the measurements of voltage and current specified by the manufacturer. The obtained error in calculating heat flux was equal to +/-0.4%.

Subcooling

The error in calculating the subcooling can also be estimated using the error propagation method. The procedure is shown below. The bulk liquid temperature at the filming location is equal to:

$$T_{bulk} = T_{in} + \frac{qP_h l_{film}}{\dot{Q}\rho_l cp_l} \tag{2.7}$$

The differential with respect to inlet temperature, heat flux and volumetric flow rate is given by:

$$dT_{bulk} = \frac{\partial T_{bulk}}{\partial T_{in}} dT_{in} + \frac{\partial T_{bulk}}{\partial q} dq + \frac{\partial T_{bulk}}{\partial \dot{Q}} d\dot{Q} \tag{2.8}$$

Hence:

$$dT_{bulk} = dT_{in} + (T_{bulk} - T_{in})\left(\frac{dq}{q} - \frac{d\dot{Q}}{\dot{Q}}\right) \tag{2.9}$$

Using the error terms given in Table 2.6, and assuming that the maximum difference between the inlet and bulk temperature was about 110 K, the error associated with liquid subcooling becomes:

$$dT_{bulk} \cong (1K) + (110K)(0.004 - 0.003) = 1.1K \tag{2.10}$$

Time

The error in the time measurements consists of the error in the assumption of constant speed of the film (0.01 ms) and the accuracy of the pulse generator (+/-0.01 ms). One has to add the "zero time" error and the "detachment time" error for the accurate prediction of bubble lifetime. The "zero time" error is associated with the fact the real bubble inception does not occur exactly when the frame is photographed. Rather, it happens in the time interval between the first frame accounted for and the preceding frame. At a speed of 8000 frames per second, the "zero time" error equals to 0.125ms. In the same manner, the "detachment time" error corresponds to the time interval between the frame at which the bubble is first seen to be losing physical connection with the wall and the preceding frame. However, the "zero time" and "detachment time" errors do not affect the calculations of bubble sliding and normal velocities.

Diameter

The errors in measuring Feret diameters and the parallel and normal bubble displacements included uncertainty in locating the bubble centroid, nucleation site and bubble contour. The uncertainty was estimated at 2 pixels. Given the typical resolution of 0.025mm/pixel, the calculated error was 0.05 mm or about 5%.

TABLE 2.1 Characteristics of the test section

Cross-sectional area [mm^2]	246.56
Glass tube (outer) I.D. [mm]	21.80
Heater tube (inner) O.D. [mm]	12.70
Glass tube length [mm]	780
Heated length of the inner tube [mm]	480
Entrance length [mm]	220
Exit length [mm]	80
Hydraulic diameter [mm]	9.10
Heated perimeter [mm]	39.89
Wetted perimeter [mm]	108.39

TABLE 2.2 Experimental conditions

Pressure [bar]	2, 3
Mass Flow rate [kg/s] (bulk liquid velocity [m/s])	0.02 (0.08), 0.1 (0.41), 0.2 (0.82)
Heat Flux [MW/m^2]	0.2 – 1.2
Subcooling [K]	10, 20, 30

TABLE 2.3 Measured geometrical parameters of the bubble- output from the image analysis software

Values in [mm]

Label	Time [ms]	Area [mm^2]	Feret Min. Diam.	Feret Min. Angle	Feret Max. Diam.	Feret Max. Angle	Feret Mean Diam.	Convex Perim.	Centr X	Centr Y
4784-0	0	0	0	0	0	0	0	0	0	0
4784-1	0.286	0.07316	0.2016	90	0.4627	8.438	0.3544	1.114	2.089	2.846
4784-2	0.572	0.3811	0.5153	90	0.9301	8.438	0.7542	2.37	2.459	2.618
4784-3	0.858	0.6749	0.7038	-87.19	1.196	8.438	0.9952	3.127	2.613	2.5
4784-4	1.144	0.8343	0.8066	90	1.269	14.06	1.089	3.422	2.708	2.41
4784-5	1.43	0.9057	0.9074	90	1.231	11.25	1.106	3.475	2.817	2.375
4784-6	1.716	0.9594	0.9858	90	1.224	11.25	1.125	3.535	2.939	2.322
4784-7	2.002	0.9132	0.997	90	1.174	16.88	1.1	3.458	3.042	2.264
4784-8	**2.288**	**0.8398**	**1.001**	**-45**	**1.083**	**11.25**	**1.053**	**3.31**	**3.151**	**2.219**
4784-9	2.574	0.741	0.9485	-39.38	1.005	39.38	0.9856	3.097	3.279	2.117
4784-10	2.86	0.6018	0.8461	73.13	0.9553	-5.625	0.8943	2.81	3.397	2.007
4784-11	3.146	0.4382	0.6416	75.94	0.8898	-19.69	0.7759	2.438	3.536	1.92
4784-12	3.432	0.2882	0.4641	70.31	0.8514	-19.69	0.6668	2.095	3.694	1.822
4784-13	3.718	0.1751	0.3888	61.88	0.5991	-30.94	0.5	1.571	3.834	1.714
4784-14	4.037	0	0	0	0	0	0	0	0	0

partial output – coordinates of the box not included; bubble ejection marked

Table 2.4 Experimental conditions (measured and calculated parameters) for experiments at p = 2 bar

Experiment	Flow rate [l/s]	Inlet T. [°C]	Outlet T. [°C]	Surface T. [°C]	Voltage [V]	Current [A]	Heat Flux [MW/m2]	Equ.Quality	Bulk T [°C]	ΔTsub [°C]
Flow rate 0.1l/s										
P2-01	0.104	91.6	99.4	140.00	5.23	734	0.20	-3.95	100.06	20.44
P2-02	0.102	82.7	99.5	149.44	7.37	1019	0.39	-4.04	99.58	20.92
P2-03	0.106	46.7	88.4	175.00	11.05	1489	0.86	-7.38	82.29	38.21
P2-04	0.106	55.8	90	170.56	10.23	1388	0.74	-6.57	86.51	33.99
P2-05	0.108	63	92	164.44	9.05	1236	0.58	-6.52	86.75	33.75
P2-06	0.103	72.8	92.5	153.89	7.4	1022	0.39	-5.96	89.63	30.87
P2-07	0.109	82	91.4	141.11	5.24	734	0.20	-5.87	90.09	30.41
P2-08	0.106	70.9	98.9	163.89	9.26	1263	0.61	-4.69	96.20	24.30
P2-11	0.104	95.1	108.6	150.00	6.65	920	0.32	-2.30	108.59	11.91
P2-12	0.101	101	109.6	142.22	5.26	734	0.20	-2.07	109.76	10.74
Flow rate 0.02l/s										
P2-10	0.02	8.1	100.6	159.44	7.48	1038	0.41	-4.52	97.11	23.39
P2-13	0.02	11.3	97.5	158.89	8.09	1115	0.47	-1.12	114.71	5.79
P2-14	0.02	46.5	97.4	154.44	6.41	886	0.30	-1.72	111.61	8.89
P2-15	0.022	49.3	94.5	145.00	5.25	729	0.20	-6.05	89.19	31.31
Flow rate 0.2l/s										
P2-09	0.202	85.5	98.8	162.22	9.25	1261	0.61	-4.20	98.74	21.76
P2-16	0.2	104	108.6	138.33	5.27	733	0.20	-2.33	108.43	12.07
P2-17	0.2	102.9	110.5	141.67	6.45	890	0.30	-2.13	109.48	11.02
P2-18	0.2	101.9	110.5	144.44	7	961	0.35	-2.10	109.61	10.89
P2-19	0.2	97	101.2	136.67	5.21	729	0.20	-3.70	101.35	19.15
P2-20	0.2	91.9	101.4	147.22	7.52	1033	0.41	-3.80	100.81	19.69
P2-21	0.204	82.7	91.4	144.72	7.48	1031	0.40	-5.63	91.37	29.13
P2-22	0.2	74.7	91.7	153.33	9.2	1247	0.60	-6.31	87.85	32.65
P2-23	0.2	70.6	93.1	160.00	10.67	1436	0.80	-6.25	88.17	32.33

Grey area – calculated parameters

Table 2.5 Experimental conditions (measured and calculated parameters) for experiments at p = 3 bar

Experiment	Flow rate [l/s]	Inlet T. [°C]	Outlet T. [°C]	Surface T. [°C]	Voltage [V]	Current [A]	Heat Flux [MW/m2]	Equ.Quality	Bulk T [°C]	ΔTsub [°C]
Flow rate 0.1l/s										
P3-24	0.1	85.8	113.5	161.11	7.54	1023	0.40	-5.95	103.57	30.13
P3-28	0.1	105.5	112.2	150.00	5.28	726	0.20	-3.83	114.33	19.37
P3-29	0.1	97.1	114.1	158.89	7.53	1018	0.40	-3.74	114.76	18.94
P3-30	0.1	95.2	103.1	149.44	5.27	726	0.20	-5.87	104.02	29.68
P3-31	0.1	87.3	104	159.44	7.53	1019	0.40	-5.67	104.98	28.72
P3-32	0.1	77.5	103.1	168.89	9.24	1238	0.60	-5.90	103.86	29.84
P3-44	0.1	112.8	122.8	149.17	5.35	727	0.20	-2.36	121.76	11.94
P3-45	0.1	106.7	122.7	153.89	6.59	890	0.31	-2.66	120.21	13.49
P3-46	0.1	79.1	117.5	165.56	9.62	1279	0.64	-5.19	107.45	26.25
P3-47	0.1	78	104.8	165.00	9.26	1234	0.60	-5.80	104.33	29.37
P3-48	0.1	68	108	176.11	10.74	1427	0.80	-6.00	103.31	30.39
P3-49	0.1	57.7	108.7	183.33	12.09	1592	1.00	-6.25	102.05	31.65
Flow rate 0.02l/s										
P3-25	0.021	77	125.9	150.00	5.36	734	0.21	-2.67	120.17	13.53
P3-26	0.02	69.9	117.7	150.00	5.28	724	0.20	-3.90	113.94	19.76
P3-27	0.019	57.5	113	151.11	5.34	733	0.20	-5.68	104.97	28.73
P3-50	0.02	57.1	125.6	157.78	6.57	890	0.31	-1.82	124.46	9.24
P3-51	0.02	46.6	119.9	158.33	6.5	885	0.30	-4.12	112.87	20.83
P3-52	0.02	36.6	111.1	161.11	6.5	883	0.30	-6.12	102.72	30.98
Flow rate 0.2l/s										
P3-33	0.2	118.3	121.3	147.78	5.35	733	0.20	-2.15	122.82	10.88
P3-34	0.2	114.6	121.8	155.83	7.52	1017	0.40	-2.03	123.41	10.29
P3-35	0.2	108.3	113.3	151.67	6.52	887	0.30	-3.70	114.96	18.74
P3-36	0.2	104.1	111.5	155.56	7.53	1018	0.40	-4.10	112.93	20.77
P3-37	0.2	100.4	112.6	162.78	9.24	1234	0.60	-3.98	113.54	20.16
P3-38	0.2	97.8	104.7	152.22	6.52	889	0.30	-5.77	104.48	29.22
P3-39	0.2	96.9	117	170.00	10.78	1426	0.80	-3.77	114.61	19.09
P3-40	0.2	96.6	105	156.11	7.51	1015	0.40	-5.60	105.38	28.32
P3-41	0.2	90.6	104.9	163.89	9.25	1237	0.60	-5.91	103.78	29.92
P3-42	0.2	86.3	105.4	171.11	10.8	1431	0.81	-5.85	104.10	29.60
P3-43	0.2	82	106.2	177.78	12.1	1590	1.00	-5.84	104.16	29.54

Grey area – calculated parameters

TABLE 2.6 Estimated errors for experimental parameters

Measured parameters	Error (+/-)
Pressure	140 Pa
Temperature	1.0 K
Volumetric flow rate	0.3%
Voltage	0.2%
Current	0.2%
Heat flux	0.4%
Subcooling	1.1 K
Time	0.02 ms
Bubble diameter	0.05 mm

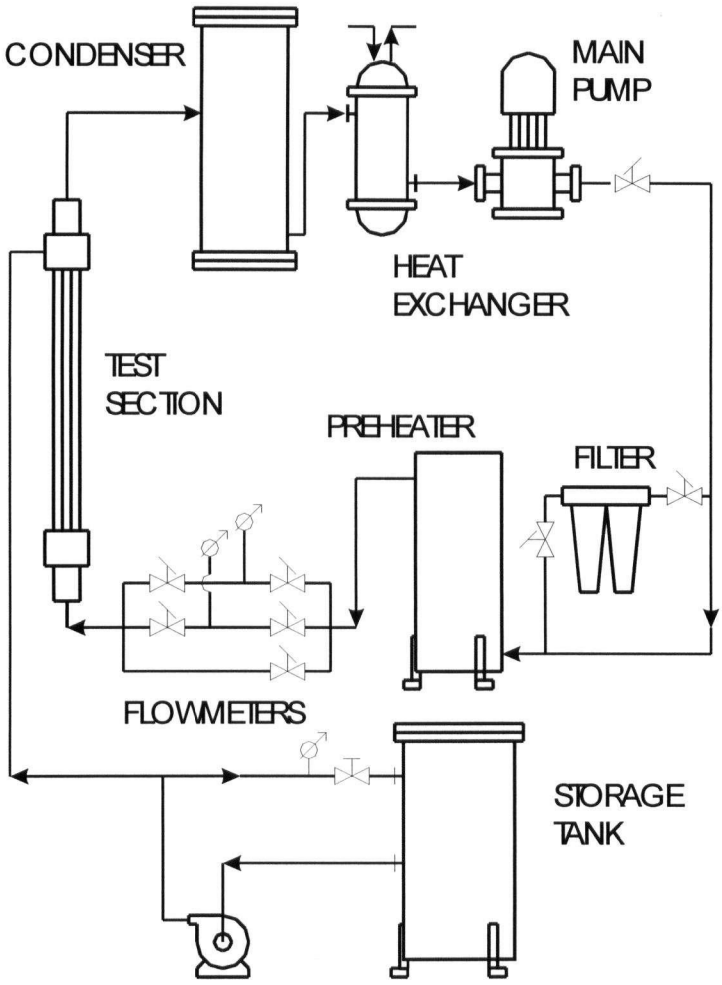

Figure 2.1 Schematic of the apparatus

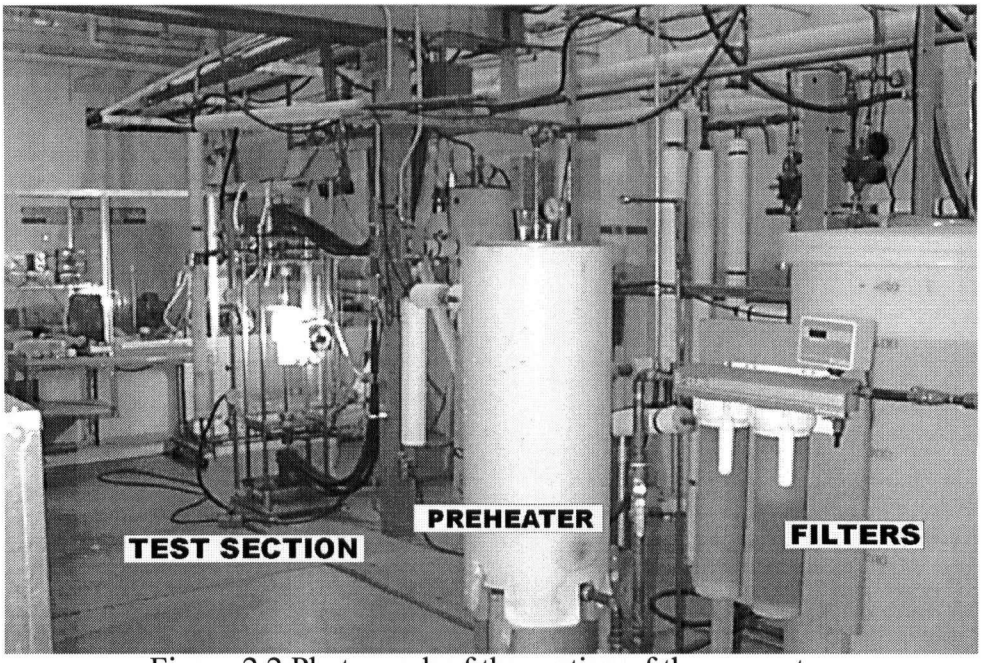

Figure 2.2 Photograph of the portion of the apparatus

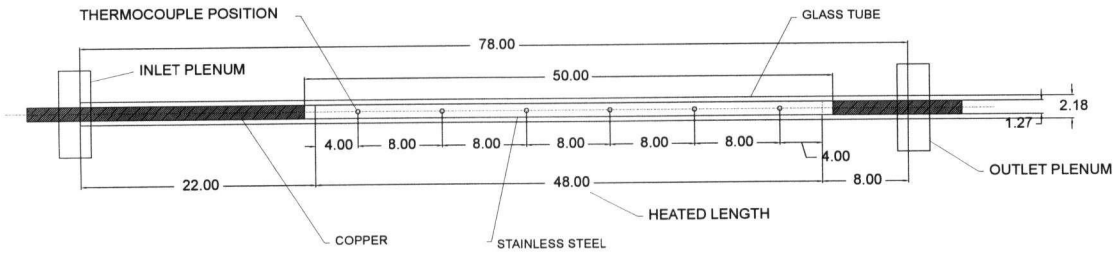

Figure 2.3 Drawing of the test section

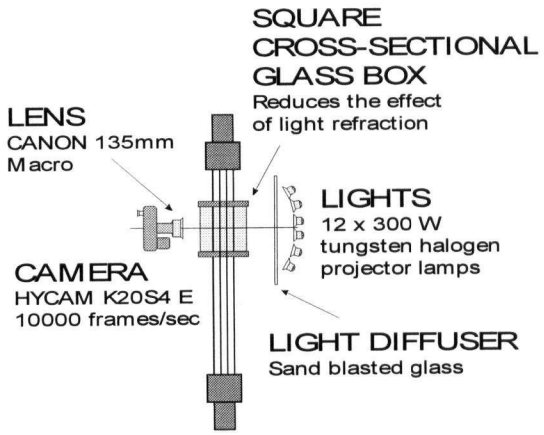

Figure 2.4 Schematic of the test section and photographic setup

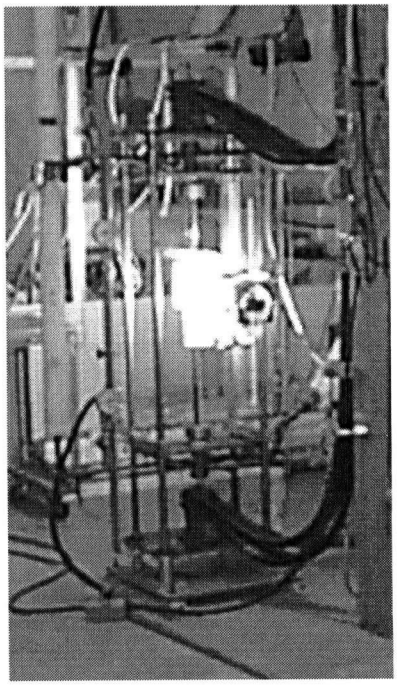

Figure 2.5 Photograph of the test section

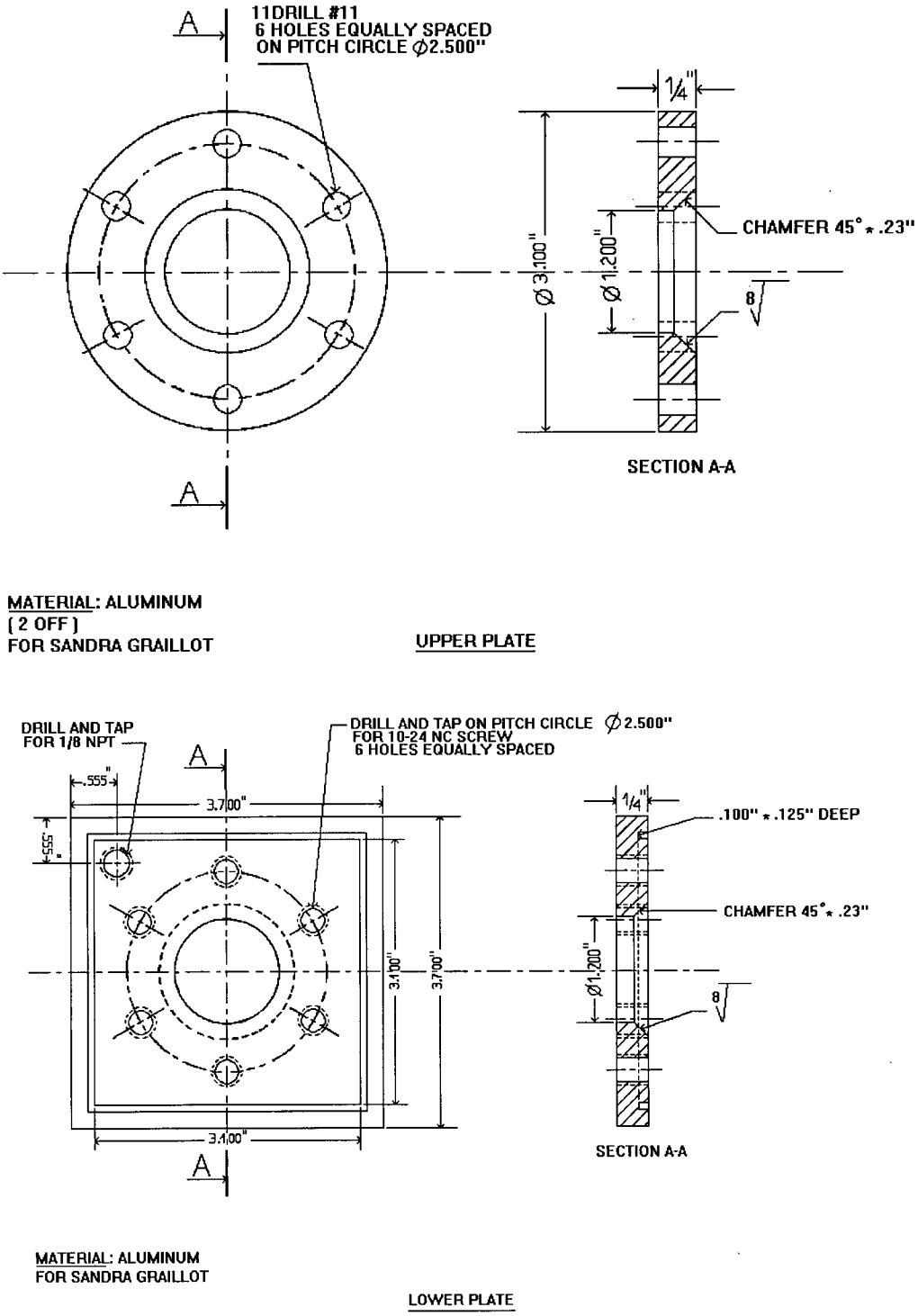

Figure 2.6 Drawings of the upper and lower aluminum plates

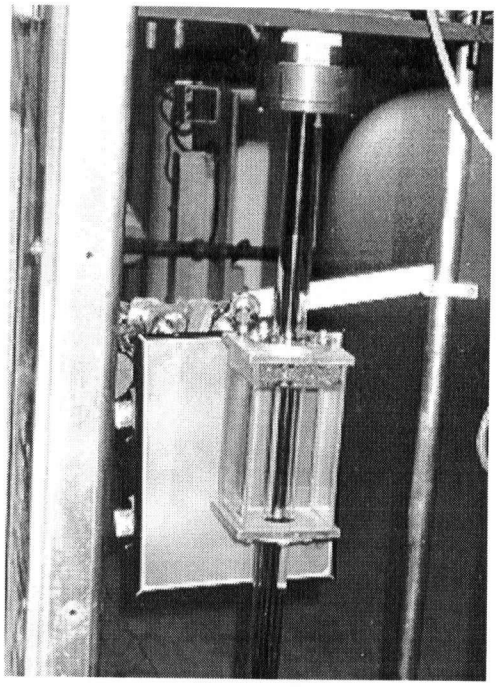

Figure 2.7 Photograph of the test section with glass box

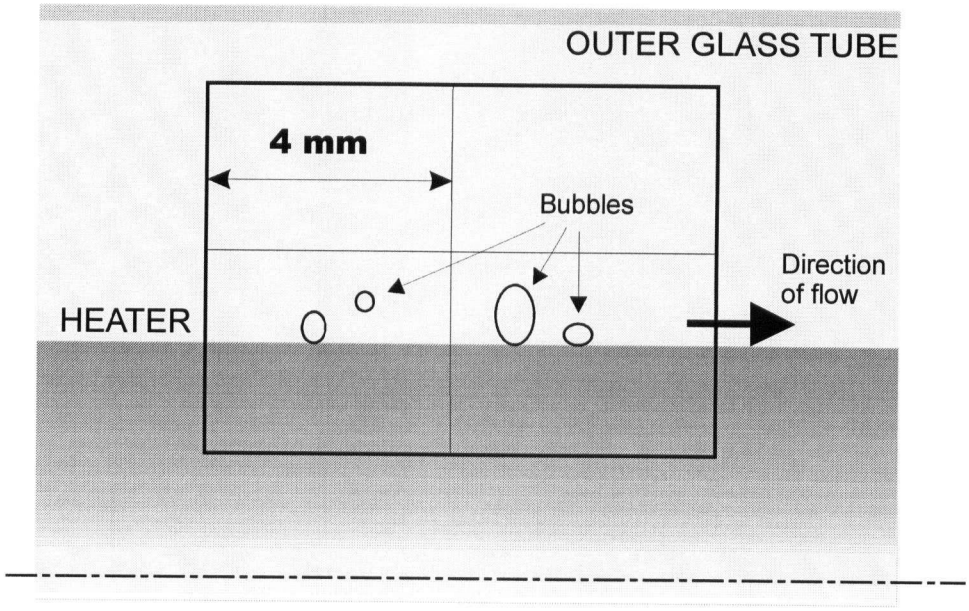

Figure 2.8 Size of the region filmed during experiments

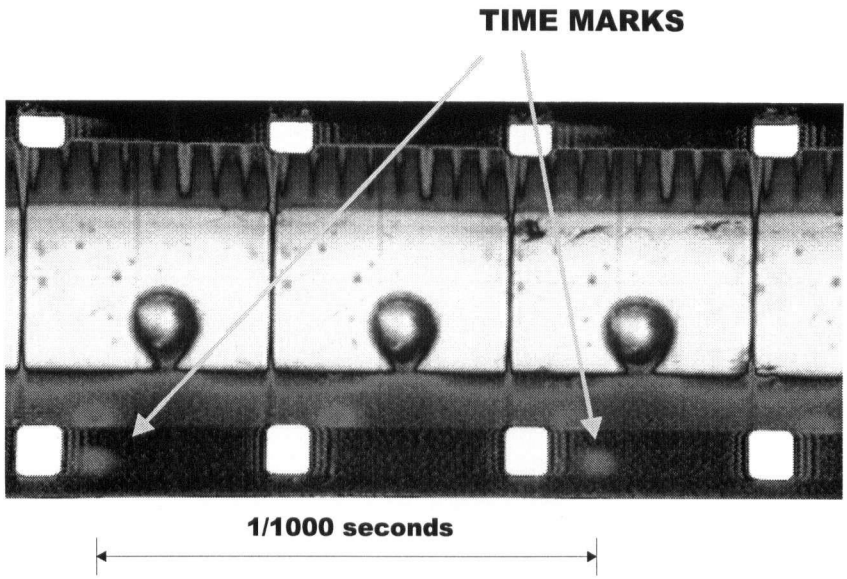

Figure 2.9 Sequence of the film with time steps

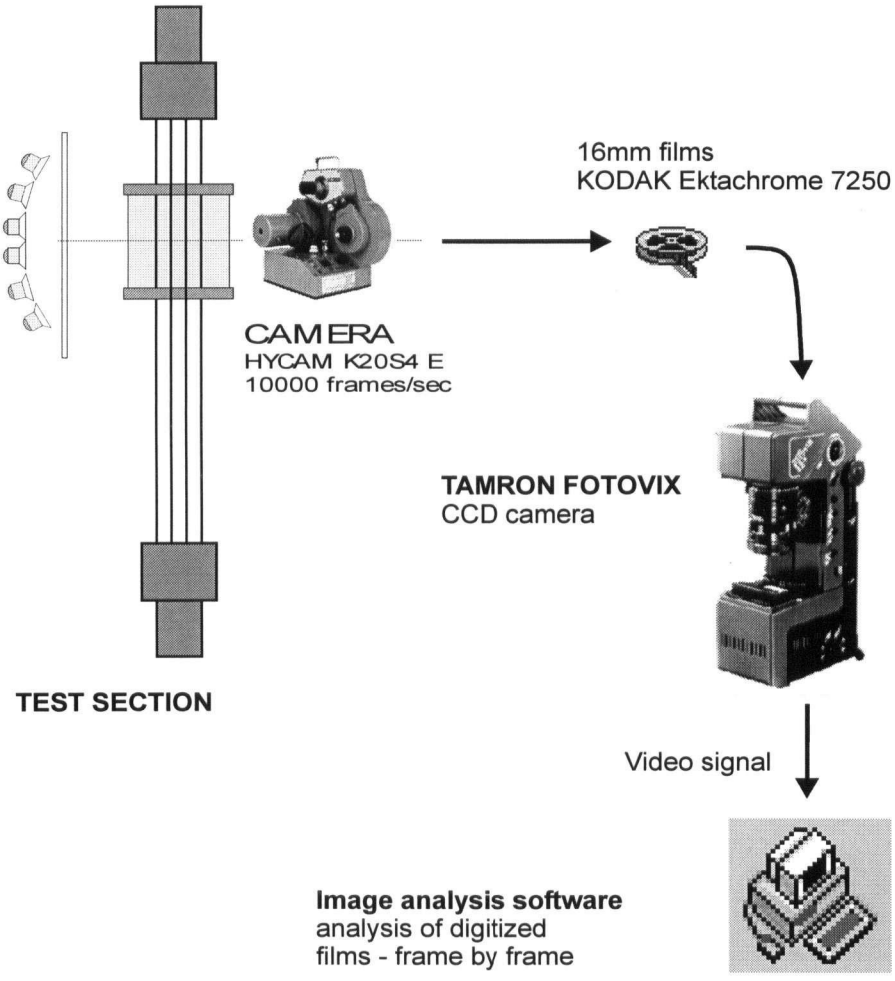

Figure 2.10 Schematic of the image processing system

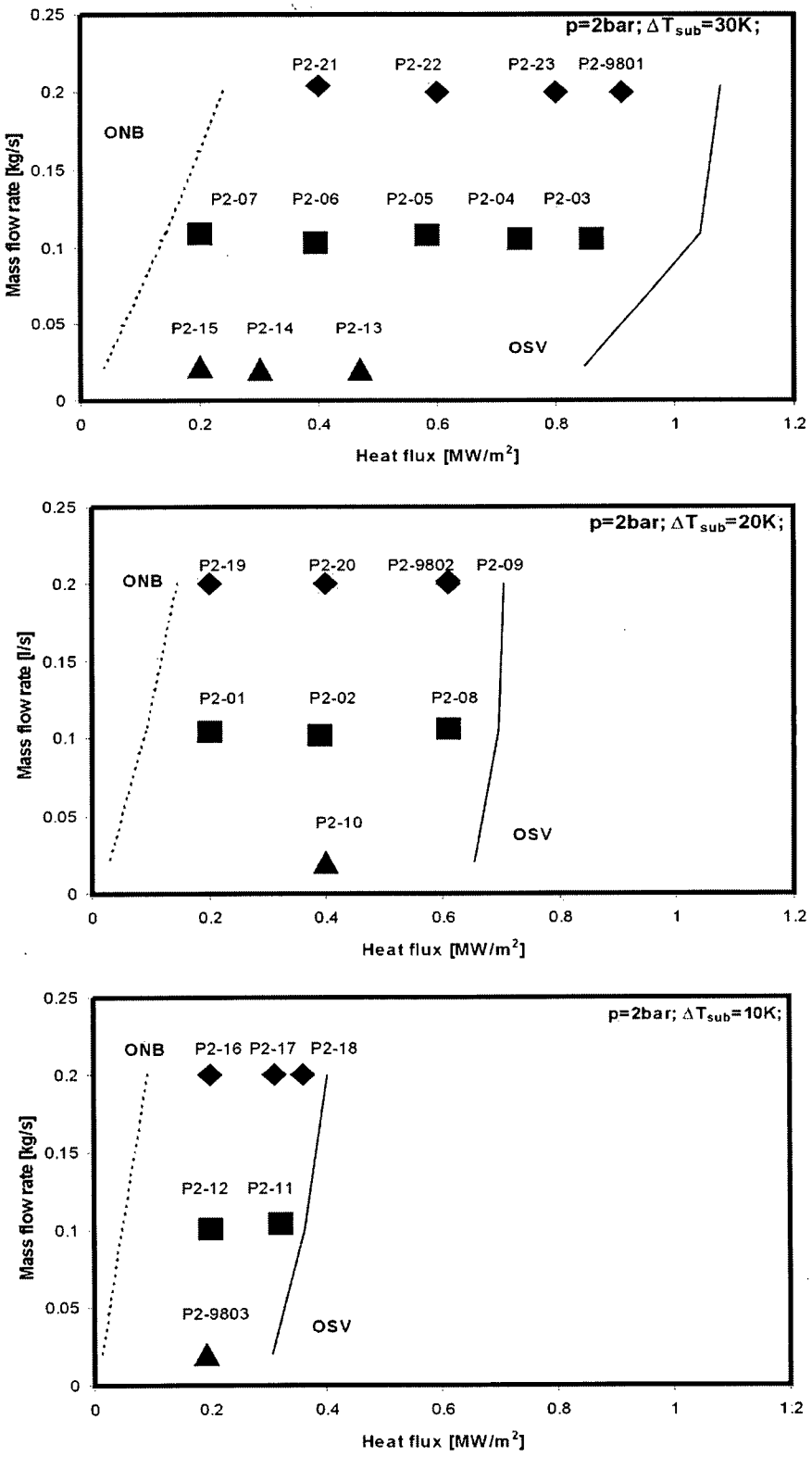

Figure 2.11 Experiments at p = 2 bar used for analysis

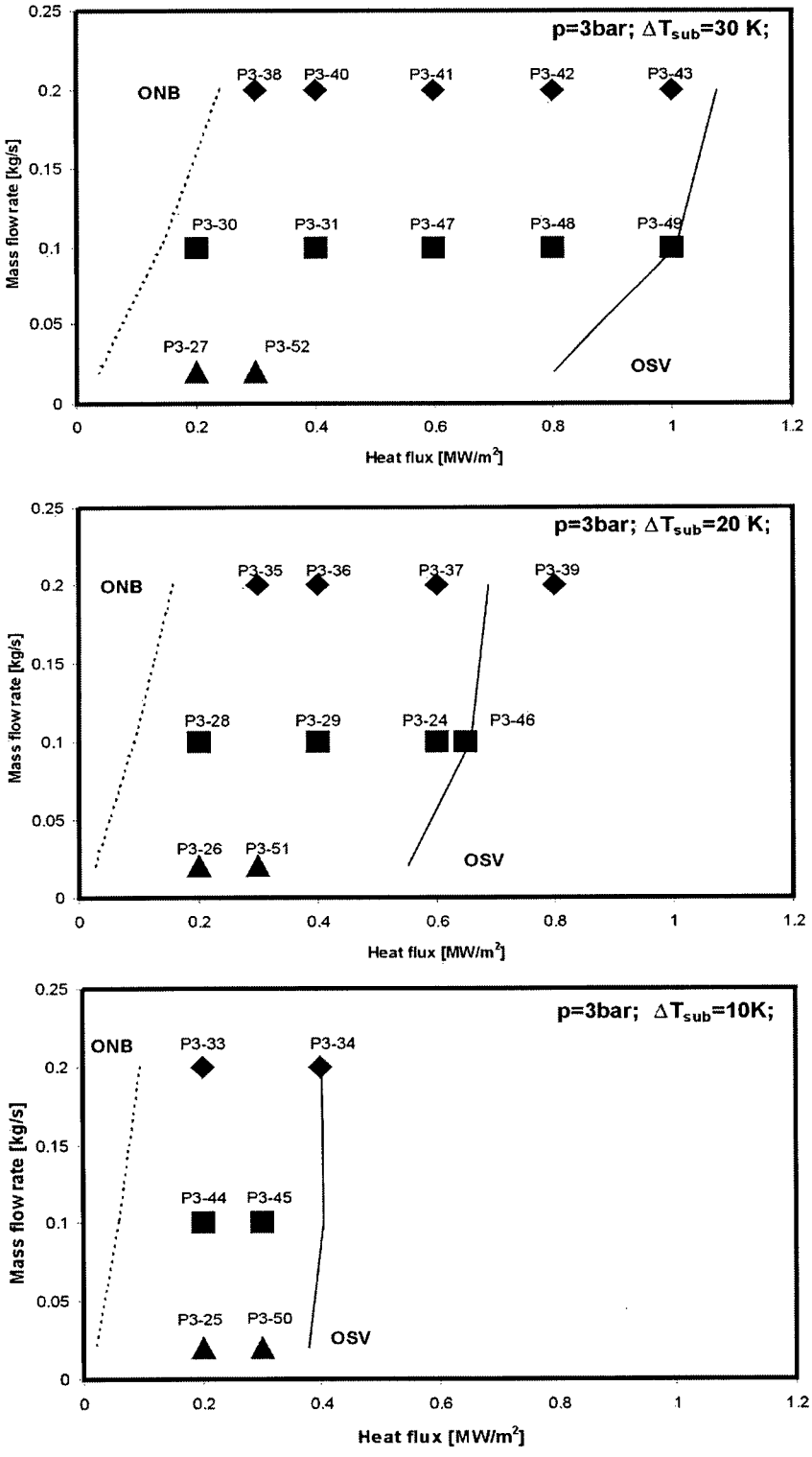

Figure 2.12 Experiments at p = 3 bar used for analysis

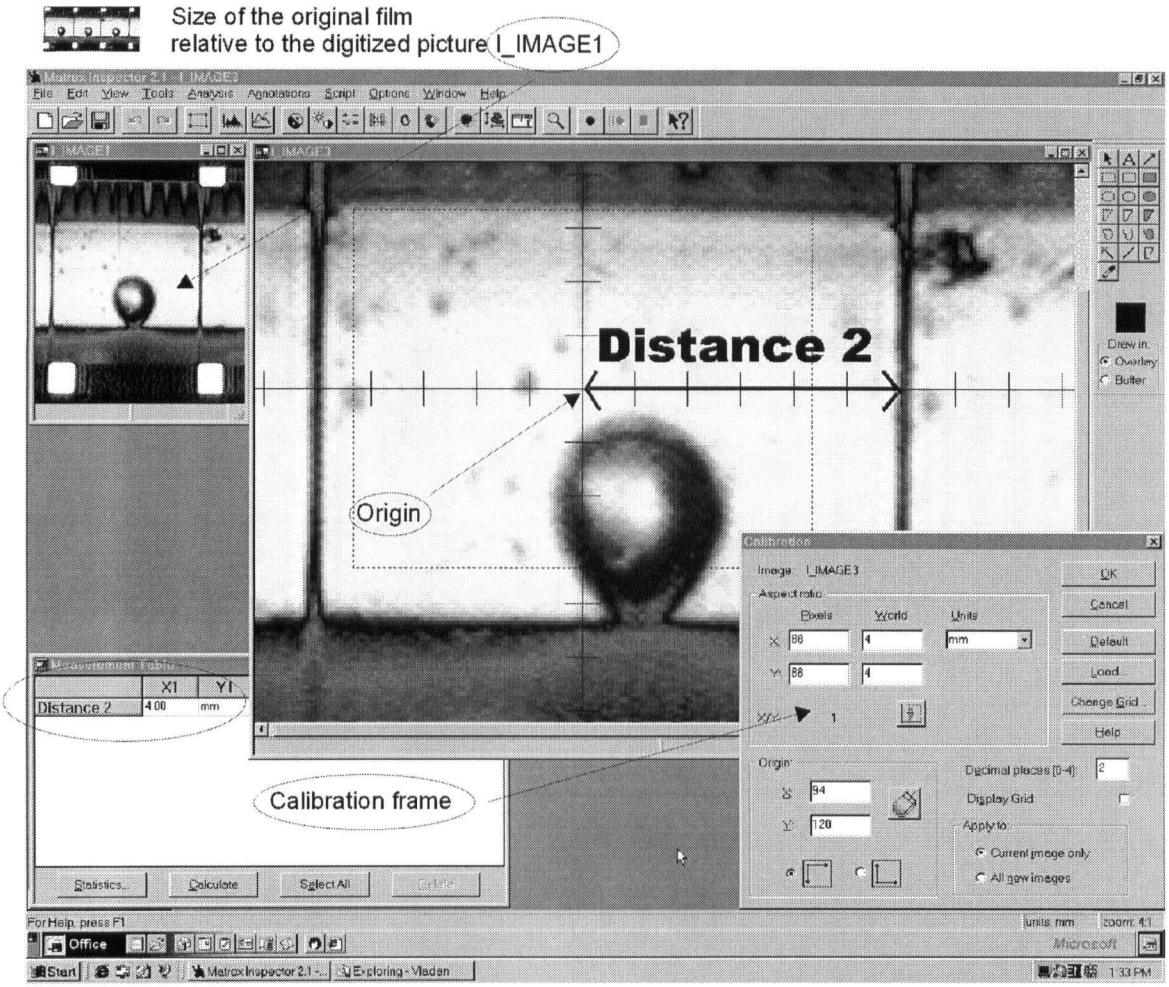

Figure 2.13 Example of the enlarged bubble and calibration procedure for measuring bubble geometrical parameters using MATROX INSPECTOR v2.1

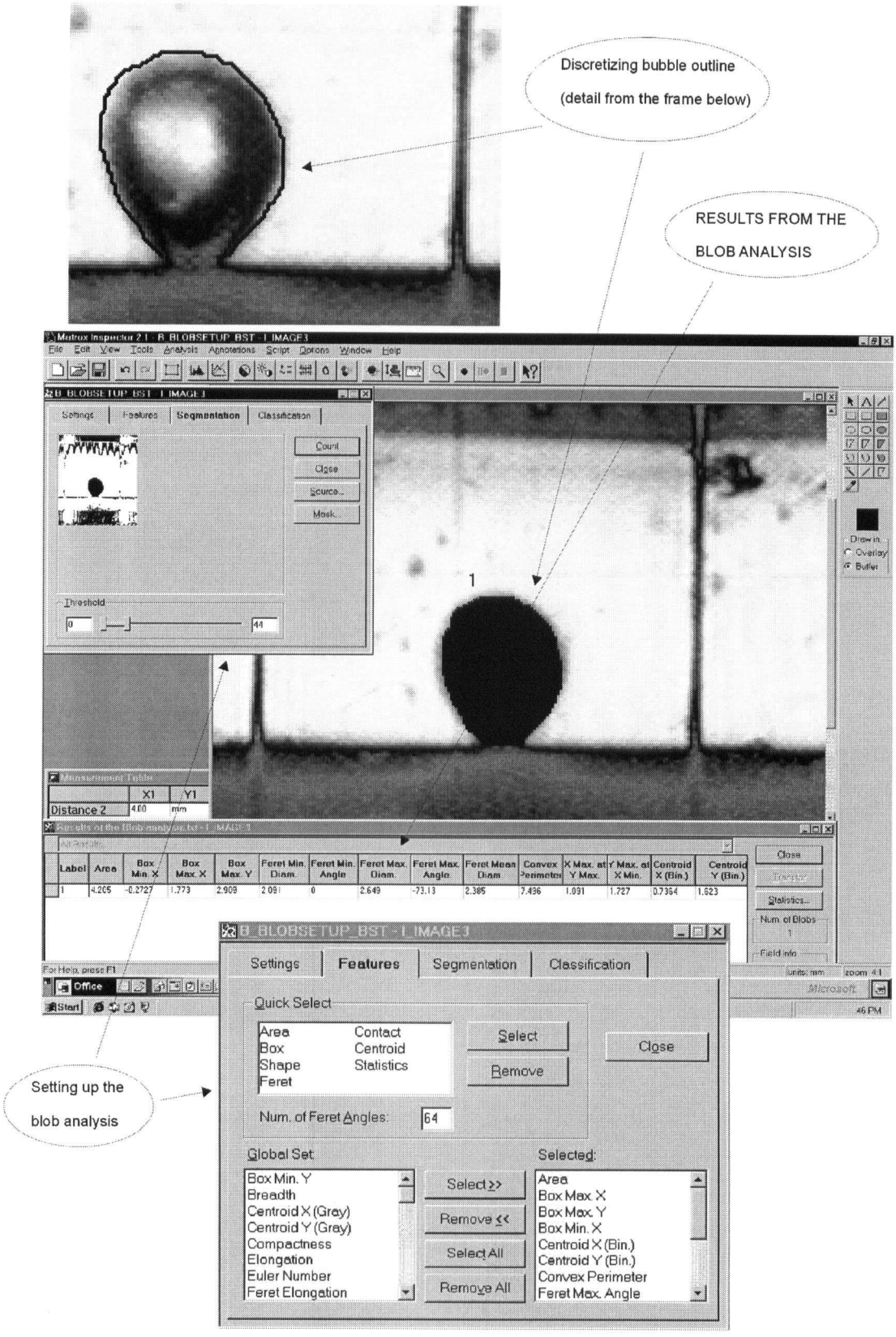

Figure 2.14 The blob analysis setup and results from the blob analysis

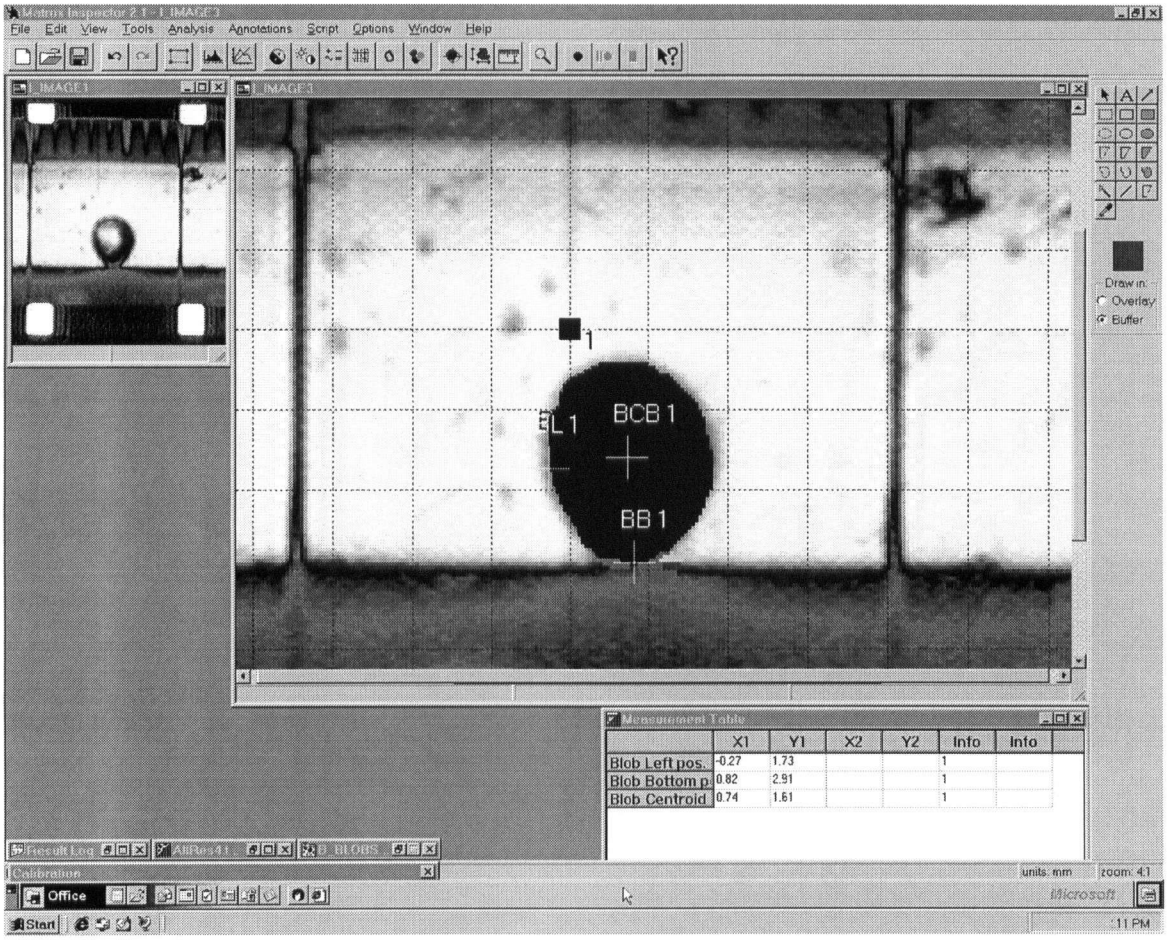

Figure 2.15 Location of the origin and bubble centroid coordinates

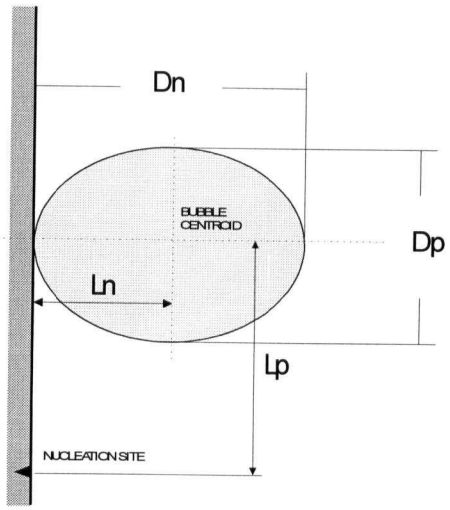

Figure 2.16 Bubble geometrical parameters

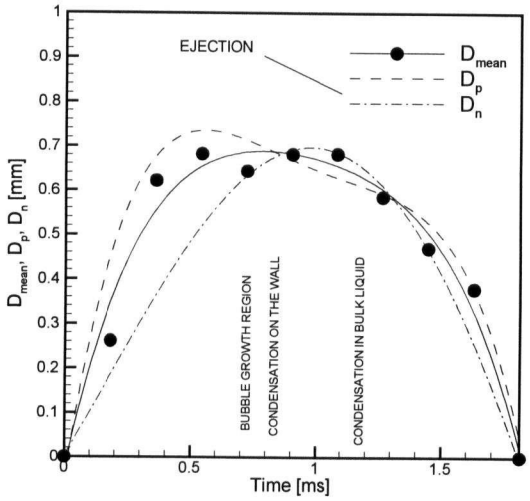

Figure 2.17 Maximum, minimum and mean diameter of a typical bubble from experiment P2-22

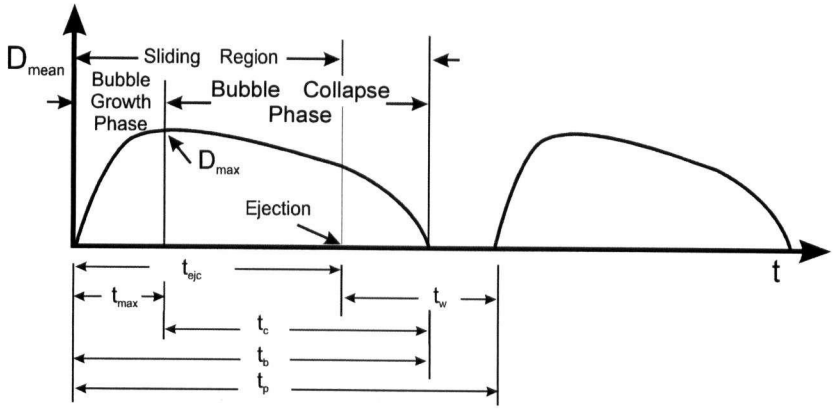

Figure 2.18 Typical bubble growth and collapse curves

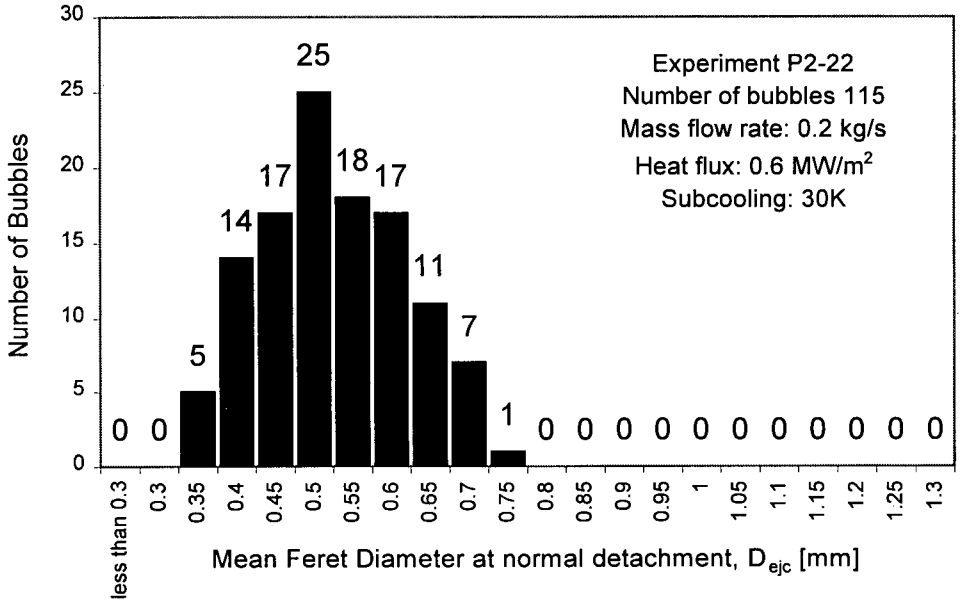

Figure 2.19 Statistical distribution of detachment diameters from experiment P2-22

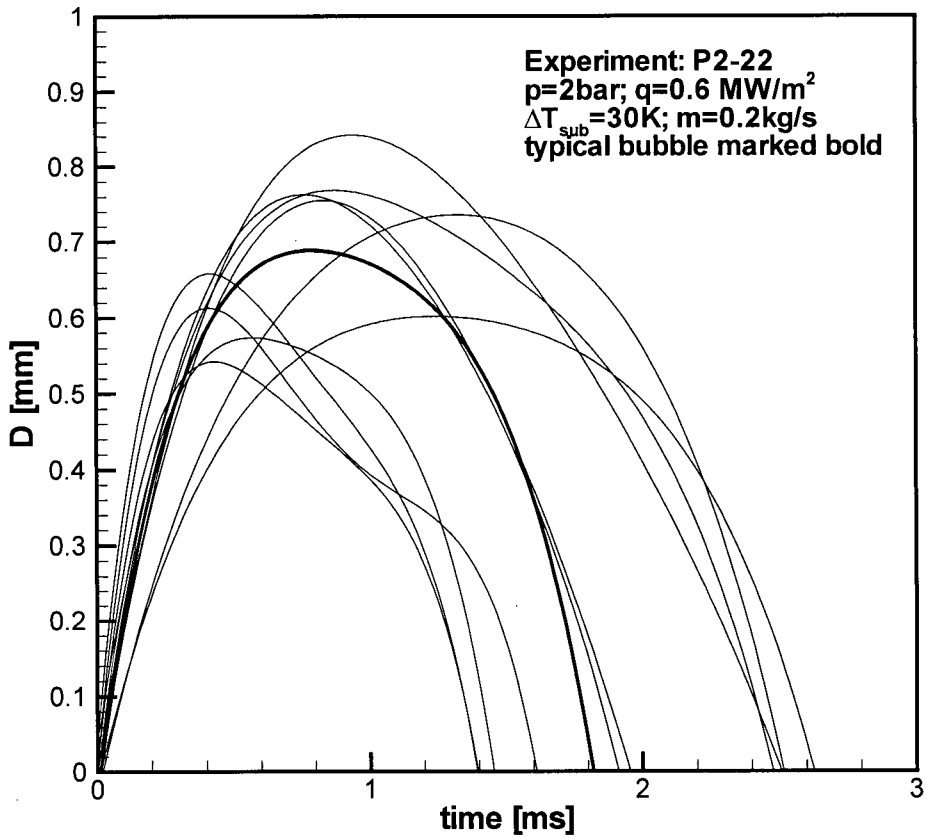

Figure 2.20 Bubbles from inception to collapse from experiment P2-22

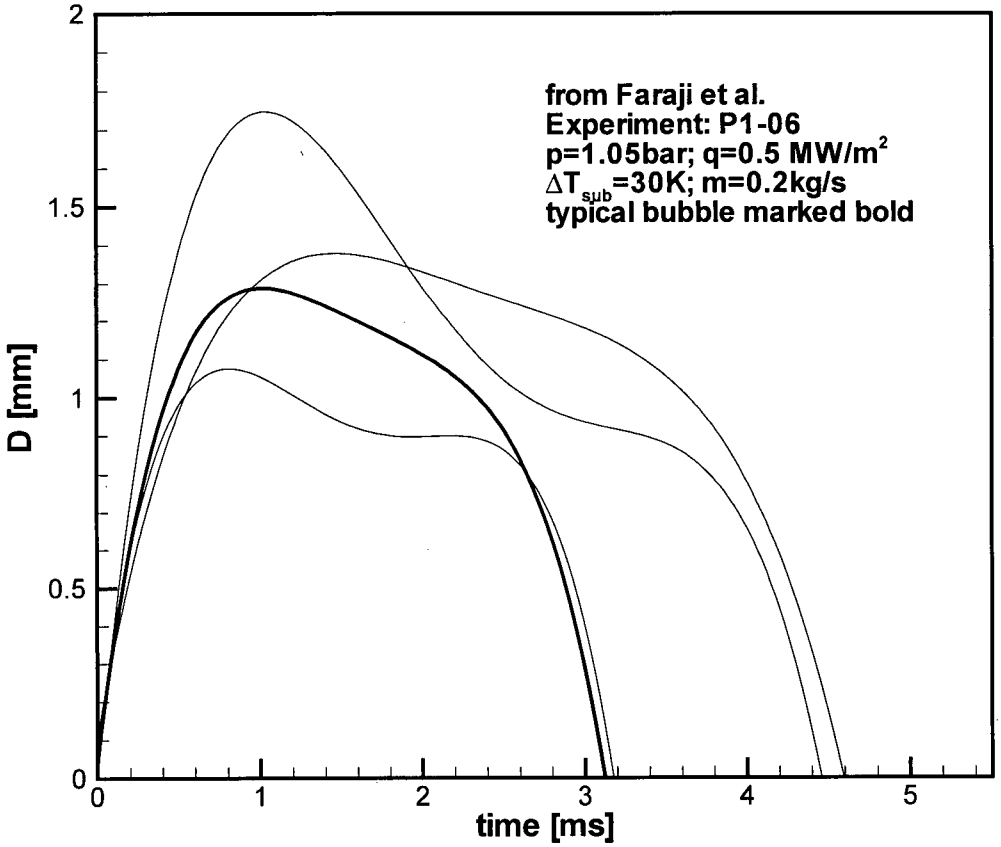

Figure 2.21 Bubbles from inception to collapse from experiment P1-06

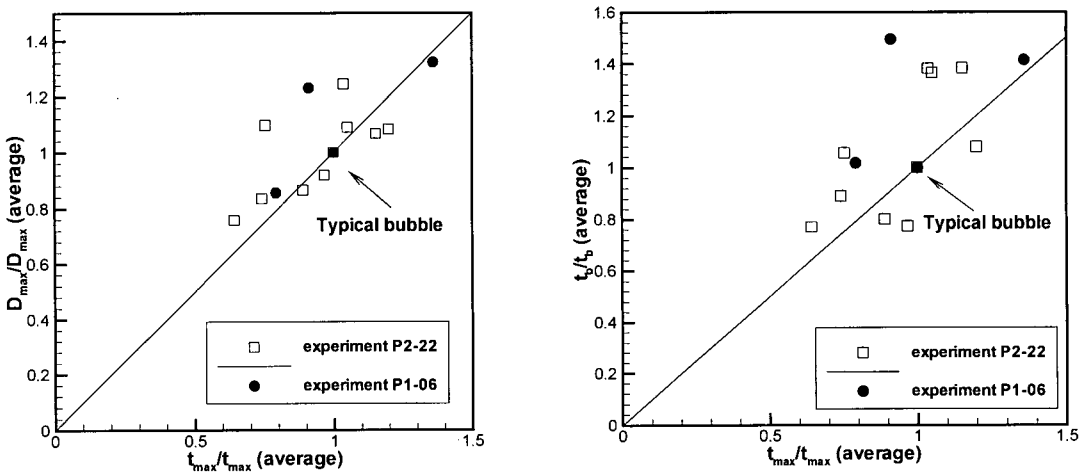

Figure 2.22 Experiments P1-06 and P2-22: comparative analysis of normalized bubble lifetimes and maximum diameters.
Parameters are scaled with average values for given experiments

Chapter 3

BUBBLE BEHAVIOUR IN SUBCOOLED FLOW BOILING

3.1 Background Information and Literature Review

The first photographic study of Gunther [57] revealed the influence of liquid subcooling, heat flux and liquid velocity on bubble size, life span and bubble population. Data were obtained for subcooled nucleate boiling of water on a vertical, electrically heated metal strip near burnout heat flux conditions. Bubbles were described as small hemispheres, growing and collapsing while sliding along the wall. Bubble size and lifetime decreased with increasing liquid velocity, subcooling and heat flux. Conversely, bubble population increased rapidly with increasing heat flux as burnout was approached. At higher subcooling bubbles did not detach from the surface of the heater, rather, they collapsed while attached to the wall.

Several researchers have focused on performing boiling experiments with water on a vertical annular test section: Frost and Kippenhan [77] investigated bubble growth and bubble size during flow boiling of water that contained surfactants. Abdelmessih et al. [78] used high-speed photography to observe the effect of liquid velocity on bubble growth and collapse from an artificial nucleation site. They concluded that the increase in liquid velocity resulted in decreased bubble size and lifetimes, whereas an increase in heat flux had an opposite effect. The latter was in contradiction with the results of Gunther [57]. Akiyama and Tachibana [79] obtained bubble growth and collapse curves from experiments with water flowing upward through a vertical annulus with an inner heater operating at atmospheric pressure. They presented data on the liquid temperature distribution normal to the heater surface. Del Valle and Kenning [80] investigated the bubble size, life span and frequency as well as the interaction of nucleation sites at high heat fluxes. Their test section was an electrically heated stainless steel plate mounted on the side of a vertical, rectangular channel. In opposition to Gunther's experiments, they found that bubbles collapsed on their nucleation sites without sliding along the wall. They also commented on an inactivation of nucleation sites with increasing heat flux.

More recently Bibeau and Salcudean [39] reported on the discrepancy between experimental investigations of bubble behaviour and void growth with theoretical predictions at low pressures and liquid velocities. They conducted a bubble visualization study during subcooled boiling of water on a vertical, electrically heated annulus. Low flow velocities at atmospheric pressure were investigated. Their experiments revealed two types of bubble detachment:

- parallel detachment, or detachment from the nucleation site that occurred almost immediately after inception and,
- normal detachment, where bubbles detached perpendicular to the heater surface and subsequently collapsed in the cooler bulk fluid.

They observed bubbles sliding and leaving the wall prior to collapse in all their experiments, including those close to ONB. Important observations were made on the shape of detaching bubbles and on the fact that detachment diameters were typically less than maximum diameters, showing that condensation started while bubbles were still attached to the wall. Similar observations were also reported by Zeitoun and Shoukri [40] in a photographic study carried out with a similar experimental setup.

Similar observations on the two types of bubble detachment were presented by Klausner et al. [81] who investigated vapor bubble departure of refrigerant R113 in saturated forced convection boiling from a horizontal, heated surface. Using the same experimental results, Zeng et al. [82] further developed a model for prediction of both departure (parallel detachment) and lift-off (normal detachment) diameters.

Recently, Thorncroft et al. [83] investigated bubble growth and detachment during vertical upflow and downflow boiling of a slightly subcooled refrigerant FC-87. They reported that bubbles were typically sliding along the surface, but remained attached to the wall in an upflow, in contrast to downflow boiling where lift-off was regularly occurring.

Tolubinsky and Kostanchuk [84] investigated the flow boiling of water on a horizontal stainless steel plate with varying pressure. It was found that there was a strong dependence on bubble size with pressure, particularly for pressures between 1 and 5 bar.

Other photographic studies of flow boiling on a horizontal surface include Koumoutsos et al. [85] and, more recently Kandlikar and Stumm [86], among others.

The present study systematically investigates the effects of liquid velocity, heat flux, subcooling and pressures on bubble dynamics. Pressure ranged from 1 to 3 bars and hence, represented the range where the most dramatic changes in bubble size occur (Tolubinsky and Kostanchuk [84]).

3.2 Experimental Observations

3.2.1 Variations of Bubble Behaviour with Heat Flux

The experiments have shown that bubble behaviour within the given range of flow rates and heat fluxes cannot be represented by a single model. This is despite the fact that most of the bubbles within the region bounded by the ONB and OSV behaved in a similar manner, as described below. Immediately after inception, typical bubbles detached from their nucleation site and started sliding. This is referred to as parallel detachment (Bibeau) or bubble departure (Klausner). The explosive bubble growth rate during the early stages was reduced in time. Bubbles, after reaching their maximum diameters, generally began shrinking while still attached to the surface of the heater. After sliding a certain distance bubbles typically detached from the surface and were propelled into the fluid core, where they collapsed. This point is known as normal detachment (Bibeau) or bubble lift-off (Klausner).

For the present study normal detachment was not observed at low heat fluxes, close to ONB. Although bubbles were occasionally seen to detach from the heater, one cannot adopt this as typical bubble behaviour. Also, at high heat fluxes, close to OSV, the significant interaction between bubbles has led to the conclusion that the bubble detachment mechanism differed from those seen at lower heat fluxes. Typical images are shown in Figures 3.1, 3.2 and 3.3. From these observations, one can divide the boiling process between ONB and OSV into three regions as follows.

The low heat flux region

Bubble behaviour in the low heat flux region is illustrated in Figure 3.4. The observed bubble population in this region was relatively low (about 3 to 8 bubbles per cm of length of the heater). Bubbles were roughly spherical and did not change significantly in size and shape. They were all observed to slide along the heater. Detachments were rarely observed and were usually preceded by some disturbance, like merging or touching between two bubbles. It can be concluded that detachments were caused by sudden changes in size and/or shape of bubbles. Also, turbulent fluctuations are believed to cause bubble detachments, although such analysis is beyond the scope of the current study.

Also typical for this region was that most detached bubbles remained close to the wall, eventually reattaching a few frames later. Very few actually collapsed in the bulk fluid. An example of reattachment is shown in Figure 3.5. Bubble reattachment in the low heat flux region was not previously reported in the open literature except in the flow boiling review by Butterworth and Shock [14]. According to this review, Mori has performed experiments on bubble growth on a vertical wall in saturated boiling at zero gravity, and noticed that, at low superheat, bubbles would detach and reattach. No detailed discussion of this phenomenon was found. Although probably insignificant relative to the overall heat transfer, a closer look at the reattachment could possibly help to understand the origin of bubble detachment. During these experiments bubble reattachment was seen regularly and can be adopted as typical low heat flux bubble behaviour.

Bubble behaviour close to ONB was previously discussed (e.g. Bibeau and Salcudean [39]) . Their first conclusion was that bubbles did not detach. This was later corrected upon closer examination of a larger area of the heater. No comments on the nature and mechanism of these detachments were offered.

The isolated bubble region

This term was "borrowed" from pool boiling terminology. It accurately describes observations at moderate heat fluxes and denotes the region in which bubbles are growing, detaching and collapsing without significant influence from neighboring bubbles. An illustration is given in Figure 3.6. Bubbles slid about a couple diameters or

less before being propelled into the fluid core. The sliding of bubbles was likely attributable to both drag and buoyancy. The experiments showed that large bubbles growing under low liquid velocity and low heat flux conditions, slid at speeds higher than the bulk liquid velocity (i.e. slip ratio >1.0). This is likely due to buoyancy effects. As the size of bubbles decreased, the sliding velocity dropped below the bulk liquid velocity, with a slip ratio of about 0.8 for high heat flux, high subcooling experiments.

Bubbles were seen to extend significantly into the bulk fluid where they collapsed rapidly. The speed at which bubbles were propelled into the bulk liquid varied with heat flux and local subcooling. Higher heat fluxes and subcooling (which produced higher temperature gradients) affected bubble motion in the direction normal to the wall by increasing their speed. Also, bubbles exposed to higher temperature gradients were seen to collapse closer to the wall. However, the location of bubble collapse measured from the wall and "normalized" with respect to the maximum diameter did not show a significant variation with heat flux. Instead, it remained relatively constant throughout the experiments.

Overall, bubbles in this region were not spherical. Upon inception, bubbles were generally flattened, likely due to strong inertial forces. As they grew while sliding on the surface, they became more rounded, having a spherical shape near the maximum diameter. After reaching their maximum size, they typically continued to slide while shrinking and becoming more elongated. The observed ratio D_p/D_n, representing the elongation of bubbles at normal detachment was between 0.8 and 0.85. These values are in agreement with previous qualitative observations of the shape of bubbles (Akiyama and Tachibana [79], Bibeau and Salcudean [39], Faraji et al. [76]). They reported that this ratio was typically around 0.8 for experiments taken at 1.05 bar.

Significant bubble coalescence region

As the heat flux was raised, approaching OSV, the bubble population increased significantly. Many merged before detachment, thus creating larger bubbles. Smaller, isolated bubbles still exhibited the behaviour described above. They were significant in number, usually growing in the wake of the larger bubbles. It was observed that various factors triggered bubble detachment. Aside from a typical normal detachment, many

bubbles detached after merging or interacting with neighboring bubbles. Detachments also occurred when a new bubble, growing underneath a passing bubble, apparently pushed the one on top away. Due to large bubble populations, significant coalescence was observed after detachment thus forming larger bubbles. These large bubbles kept sliding or travelling close to the surface of the heater and further coalesced. This is also shown in Figure 3.7.

It should be emphasized that the above three boiling regions were observed for all fixed subcoolings and flow rates. Thus, they depend on the heat flux. However, the last region (significant bubble coalescence) was not observed at p = 1.05 bar (Bibeau and Salcudean [39]) and only partially at p = 2 bar. It becomes obvious for the p = 3 bar experiments due to increasing number of active nucleation sites with increasing pressure.

Observations of different bubble behaviour lead to the conclusion that the heat transfer mechanisms in the two regions are different. In the low heat flux region the latent heat transport through sliding bubbles can be considered the main heat transfer mode, while in the isolated bubble region, bubble agitation may be dominant. With the increase in bubble population, the overall heat transfer would increase due to at least two coupled effects: increased bubble agitation and increased latent heat transport. Also, the increase of void fraction past OSV would affect the convective heat transfer (macroconvection) by accelerating the liquid phase. The link between the heat transfer modes and bubble behaviour is discussed in more detail in Chapter 4.

3.2.2 Bubble Size, Shape and Lifetime – Qualitative Observations

This study confirms that the overall bubble behaviour at pressures of p = 2 bar and p = 3 bar does not differ significantly from the bubble behaviour observed earlier by Bibeau and Salcudean [39] and several other researchers. The major observed points are:

- All bubbles are seen to slide along the surface of the heater (i.e. parallel detachment was observed for all experiments), which can be observed in Figures 3.4 and 3.6
- Bubbles detach in the direction normal to the surface of the heater and enter the fluid core where they collapse. This is true for most experiments except

those close to ONB, which characterize the low heat flux behaviour, and those close to OSV at higher pressures where significant coalescence is present.

- Bubble detachments (normal detachment, ejection) occur long before OSV. This is in agreement with recent experimental observations and contradicts the notion that the detachment of the first bubble is associated with the OSV point, as assumed by certain void growth models.
- Detachment diameters are generally smaller than maximum diameters. This suggests that the condensation rate prevails over the evaporation rate for most bubbles while they are still in contact with the heated solid surface.
- Bubble shapes deviate significantly from the spherical shape. Soon after inception they are flattened. They undergo a transition to an elongated shape, having a maximum elongation at normal detachment. This is also evident in Figure 3.6. The near spherical shape during transition coincides with the maximum bubble diameter, although this cannot be confirmed as a rule from the available experimental data.
- Normal detachments are obviously due to the strong force acting in the direction normal to the surface of the heater. Bubbles are propelled vigorously into the fluid where they collapse surrounded by a colder liquid.

3.2.3 Parallel and Normal Displacement

Typical parallel and normal displacements of the bubble subject to a high velocity of the surrounding liquid (high flow rate) are shown in Figure 3.8. Parallel and normal displacements at low flow rate are presented in Figure 3.9. The graphs show the distance between the bubble centroid and the nucleation site during bubble lifetime (as explained in Chapter 2) versus the normalized time (t/t_{ejc}). The normalized time equal to one on the horizontal axis represents the normal detachment time.

It can be observed that, at high flow rates, the bubble sliding velocity (parallel displacement) remains constant during the bubble lifetime. This can be observed in all experiments. The constancy of the bubble velocity before and after detachment indicates minor influence of the bubble base and forces associated with it on bubble dynamics.

At low flow rates, bubble sliding is not so well defined, although it has been observed in all experiments. Parallel displacements are much more affected by random factors such as turbulent fluctuations or influence of neighboring bubbles. Hence, the more chaotic pattern in Figure 3.9.

The observed normal displacements are similar in both high and low flow rate experiments. The initial fast bubble growth, determined by fast displacement of the bubble centroid in the direction normal to the heater, is being replaced by a period of stagnation or slow growth. At normal detachment, the bubble accelerates again, as it is propelled into the liquid core. The acceleration after detachment suggests the existence of a strong force in the normal direction that is responsible for bubble detachment.

3.3 Bubble Size and Lifetime – Parametric Trends

Bubble sizes and lifetimes are predominantly affected by heat flux, subcooling, bulk liquid velocity and pressure. An attempt was made in the present study to isolate and observe the effect of each of these parameters. The following is a qualitative discussion of the observed trends. The experimental results are shown in Tables 3.1 and 3.2, and also in Figures 3.10 (diameters) and 3.11 (lifetimes and ejection times). The results of Bibeau and Salcudean [39] are given in Figure 3.12 for comparison.

3.3.1 Effect of Subcooling

Bubble size decreases with increased subcooling at fixed flow rates and heat fluxes. Lower temperature gradients in the liquid surrounding a bubble reduce the condensation rates, thus allowing larger diameters. This is in agreement with most of the previous experimental studies (e.g. Gunther [57], Zeitoun and Shoukri [40], Tolubinsky and Kostanchuk [84], Faraji et al. [76], Roy et al. [87], Kandlikar et al. [88]). Bubble lifetimes and ejection times also tend to decrease with increased subcooling.

3.3.2 Effect of Heat Flux

Various opinions can be found in the literature on the effect of heat flux on maximum bubble diameters. Gunther [57] concluded that bubble size decreases with increasing heat flux, Tolubinsky and Kostanchuk [84] reported no effect of heat flux on

bubble dimensions while Abdelmessih et al. [78] observed larger bubbles and longer lifetimes with an increase in heat flux.

From the present study it can be concluded that, generally, bubble maximum diameters drop with increasing heat flux with constant flow rates and subcooling. This is particularly evident at lower heat fluxes. At higher heat fluxes, bubble diameters remained roughly constant. These findings are in agreement with the previous investigation of Bibeau and Salcudean [39]).

Bubble lifetimes and ejection times also depend on the heat flux. They show a similar behaviour as bubble maximum diameters, with the reduction of bubble life span being more evident with increasing heat flux closer to ONB. These trends have been observed within the whole pressure range.

3.3.3 Effect of Liquid Velocity

The effect of the liquid velocity on bubble sizes and lifetimes was, again, more pronounced at lower heat fluxes. Bubble diameters and lifetimes decreased with increasing flow rates. This became less pronounced as the OSV was approached.

3.3.4 Effect of Pressure

Bubble diameters appear to be strongly dependent on pressure. Experimental results from this study agree with the observations of Tolubinsky and Kostanchuk [84] (i.e., maximum diameters decrease with increasing pressure). However, from the present study, one cannot confirm their findings that increasing pressure results in an increase of the contact time between the bubble and the surface (i.e. longer ejection time). To the contrary, both bubble lifetimes and ejection times, as well as their ratio, t_{ejc}/t_b, tend to decrease with increasing pressure, as shown in Figure 3.13. Figures 3.14, 3.15 and 3.16 represent illustrations of the change in bubble size and lifetimes with pressure as well as with heat flux. All bubbles in these figures originate from the experiments with the same mass flow rate (m = 0.1 kg/s and m = 0.2 kg/s) and subcooling (ΔT_{sub} = 30 K).

3.3.5 Bubble Shapes and Active Nucleation Sites

As mentioned above, during growth, bubbles transform from a flattened to an elongated shape. This behaviour was observed at all pressures, subcoolings and flow rates, in agreement with previous observations (Bibeau and Salcudean [39], Zeitoun and Shoukri [40]). Bubble detachment diameters are smaller than maximum diameters indicating that condensation rates overcome evaporation rates while bubbles are still attached to the surface of the heater. The maximum elongation of bubbles is reached immediately before detachment.

Bubble population increases with decreasing flow rate. This is particularly evident at lower heat fluxes where single-phase forced convection still plays an important role. At lower flow rates one expects lower convection heat flux coefficients causing higher local surface temperatures and increasing the number of active nucleation sites.

Bubble population also increases with increasing heat flux. At high heat fluxes, close to OSV, large bubbles, formed as a result of significant coalescence, affect the overall bubble behaviour.

3.4 Correlations

3.4.1 Correlations for Bubble Growth and Condensation Rates

A comparison of experimental data with prediction from Zuber's [63] model revealed similar trends of bubble growth and condensation rates. However, this model generally over-predicted condensation rates, as shown in Figure 3.17. To correlate bubble growth and condensation rates in terms of maximum bubble diameter and bubble lifetime, the equation for normalized bubble diameters in the form suggested by Akiyama and Tachibana [79] was adopted. The correlation has the following form:

$$\frac{D}{D_{max}} = 1 - 2^K \left| \frac{1}{2} - \left(\frac{t}{t_b} \right)^N \right|^K \qquad (3.1)$$

where N and K are empirical constants. The values of N and K, obtained by fitting the experimental bubble size data, are compared with the parameters determined by other

investigators in Table 3.3. Predictions obtained with equation (3.1) and the current data are shown in Figure 3.18.

3.4.2 Correlations for Maximum and Detachment Diameters, Bubble Growth, Detachment and Condensation Time

Despite its importance in determining the interfacial area concentration and modeling void growth, a substantial deficit of bubble detachment diameter correlations exists in the open literature for the flow boiling conditions as compared to pool boiling. Also, many researchers equate the maximum and detachment diameters, thus not taking into account that bubbles in subcooled flow boiling start condensing while still attached to the wall.

Zuber [63] developed a model based on the assumption that the heat transfer through the vapour-liquid interface controls bubble growth. The model is based on the Bosnjakovic equation, originally developed for bubble growth in a stagnant, superheated liquid with uniform temperature. Zuber's modification accounted for the existence of a non-uniform temperature field. Another model that falls into the same category regarding the dominant heat transfer mode is that of Mikic et al. [62]. These models were presented in Chapter 1.

Unal [74] has used the microlayer evaporation concept to develop a model for maximum bubble diameters and bubble growth times. The heat is supplied to the bubble through a thin liquid microlayer separating the bubble from the solid surface. This model does not take into account the condensation effects.

Serizawa and Kenning [24] introduced the concept of a bubble boundary layer. According to this approach, bubbles detach from their nucleation sites but stay close to the surface thus creating a bubble layer adjacent to the surface. He suggested an empirical model for predicting bubble detachment diameters.

Faraji et al. [76] presented correlations for maximum bubble diameter, bubble lifetime and condensation time in terms of the Jakob number and dimensionless subcooling. They did not explicitly include pressure variations in their model. Their correlations are limited to $p = 1$ bar.

Zeitoun and Shoukri [40] presented a correlation for the Sauter diameter using a relatively complex function of Re, Ja, Bo and density ratio ρ_l/ρ_v.

A comparison of current data with these correlations is shown in Figures 3.19, 3.20 and 3.21. It can be observed that the correlations of Zuber [63] and Mikic et al. [62] significantly over-predict the maximum diameters. The concept of evaporation at the vapour-liquid interface does not seem to be appropriate for the experiments presented in this study. In fact, the microlayer concept (Unal [74]) leads to acceptable predictions for maximum bubble diameters over the whole range of pressures. The model of Zeitoun and Shoukri [40] slightly under-predicts the detachment diameters at p = 1 bar but over-predicts experimental data at higher pressures. Serizawa's [24] correlation consistently under-predicts the experimental data.

Following the suggestion by Cooper et al. [89] for the non-dimensional maximum bubble radius and applying similar procedures for the non-dimensional bubble lifetime as in Faraji et al. [76], several correlations, covering pressures up to 3 bars, were developed. The non-dimensional maximum and detachment diameters D_{max}^+, D_{ejc}^+, bubble growth time, t_m^+, bubble ejection time, t_{ejc}^+, and bubble condensation time t_c^+, are given by equations (3.2) and (3.3).

$$D_{max}^{+} = \frac{D_{max}\sigma}{\rho_l \alpha_l^{2}} \; ; \; D_{ejc}^{+} = \frac{D_{ejc}\sigma}{\rho_l \alpha_l^{2}} \tag{3.2}$$

$$t_m^{+} = \frac{t_m \alpha_l}{\left(\frac{\rho_l \alpha_l^{2}}{\sigma}\right)^{2}}; \; t_{ejc}^{+} = \frac{t_{ejc} \alpha_l}{\left(\frac{\rho_l \alpha_l^{2}}{\sigma}\right)^{2}}; \; t_c^{+} = \frac{t_c \alpha_l}{\left(\frac{\rho_l \alpha_l^{2}}{\sigma}\right)^{2}} \tag{3.3}$$

The experimental data were correlated with four parameters: the Jakob number, Ja, the non-dimensional subcooling, θ, the Boiling number, Bo, and the density ratio, ρ_l/ρ_g, These dimensionless parameters account for all relevant variables affecting bubble diameters and lifetimes. The definitions of Ja, θ, and Bo are given respectively by:

$$Ja = \frac{\rho_l c p_l (T_w - T_{sat})}{\rho_v i_{fg}} \tag{3.4}$$

$$\theta = \frac{T_w - T_b}{T_w - T_{sat}} \tag{3.5}$$

$$Bo = \frac{q}{Gi_{fg}} \tag{3.6}$$

The ratio ρ_l/ρ_v was found to represent well the influence of the pressure on bubble behaviour.

The correlation in the form shown in equation (3.7) was proven to give satisfactory results for all five dimensionless variables.

$$D_{max}^{+}, D_{ejc}^{+}, t_m^{+}, t_{ejc}^{+}, t_c^{+} = AJa^b \theta^c \left(\frac{\rho_l}{\rho_v}\right)^d Bo^e \tag{3.7}$$

The empirical parameters A,b,c,d,e are given in Table 3.4.

The negative signs for coefficients b, c and positive for d, e are in accordance with the observed trends for bubble sizes and lifetimes with changes in heat flux (Ja), subcooling, flow rates (Bo) and pressure.

The accuracy of presented correlations is satisfactory, with coefficients of correlation between 0.86 and 0.92 and coefficients of determination of about 0.75 to 0.8. The correlation for the maximum bubble diameters and normal detachment diameters are shown in Figures 3.22 and 3.23, respectively. Correlations for the bubble growth times, ejection times and condensation times are shown in Figure 3.24. The few points on these figures that are not well represented by the correlations correspond to the low heat flux region. Experimental data from the isolated bubble region are generally very well represented by given correlations. The variation of the proposed correlation for the maximum bubble diameters with pressure is shown in Figures 3.25 and 3.26. Figure 3.25 shows satisfactory agreement between the experimental data and the correlation up to the pressure of 10 bar. The results between 4 and 10 bar are more in accordance with experiments than the predictions of Unal's model.

3.5 Concluding Remarks

The experiments were carried out at pressures of 2 and 3 bar, in addition to already existing experiments at 1.05 bar, in order to cover systematically the boiling region from ONB to OSV.

Three different bubble behaviours have been distinguished as follows:

1.*Low Heat Flux Region;* Characterized by low bubble population. Nearly spherical bubbles slide long distances without changing significantly in size and shape, occasionally detaching from the surface and typically reattaching soon after.

2.Isolated Bubble Region; Covering the major part between ONB and OSV. Bubbles are flattened after inception, becoming more elongated as they grow. The transition from flat to elongated shape occurs near the maximum diameter. Bubbles typically slide a distance of a couple of diameters, detach from the surface and travel in the direction normal to the heater into the liquid core, where they collapse rapidly. The ejection diameters are smaller than maximum diameters, indicating significant condensation rates while bubbles are still attached to the wall. At ejection, bubbles are typically elongated in the direction normal to the surface of the heater.

3.Region of Significant Bubble Coalescence; Characterized by large bubbles with varying sizes and shapes. These bubbles are typically products of bubble coalescence and have different dynamics than bubbles in the isolated region. They were observed before the OSV, and were more pronounced at higher pressures particularly at low flow rates.

The transition between the low heat flux region and the isolated bubble region seems to happen abruptly leading to a change in the heat transfer mode. It is possible that this transition coincides with the transition from partial to fully developed boiling although this cannot be confirmed at this point.

The transition between the isolated bubble region and the region of significant bubble coalescence is smooth and related to increasing nucleation sites with increasing heat flux.

Bubble size and lifetime generally decrease with increasing heat flux and bulk liquid velocity. The effect of the heat flux and flow rate on bubble diameters and life span is greater at lower heat transfer rates. At higher heat fluxes the change of the bubble size becomes less obvious.

The effect of moderate (10 to 30 K) subcooling and pressure (in the low pressure range: 1 to 3 bar) on bubble size and lifetime was also investigated. Bubble size and life span decrease with increasing subcooling or pressure. The results are in accordance with most of the previous experimental studies.

New correlations for the maximum diameter, detachment diameter, bubble growth and condensation times, and bubble lifetime have been proposed

Experimental data from this study were used to develop semi-empirical correlations for determining the variation of bubble size and lifetime with the above mentioned variables. Dimensionless numbers, such as the Boiling number, Jakob number and dimensionless subcooling were used to correlate the data. The pressure dependence has been accounted for by the liquid/vapour density ratio. The coefficients of correlation between 0.86 and 0.92 indicate satisfactory agreement between experimental data and proposed correlations for the given range of experimental conditions.

The bubble growth rates were successfully correlated using the model of Akiyama and Tachibana (1974) with slightly modified constants.

Observed and measured normal detachment diameters have been compared with several models, including those of Zuber (1951), Mikic et al. (1970), Zeitoun and Shoukri (1996), Serizawa (1979) and Unal (1976). Good agreement with Unal's model has been obtained, indicating the importance of microlayer evaporation during bubble growth.

Table 3.1. Typical Bubbles p=2bar

Label	U_{bulk} [m/s]	q [MW/m^2]	ΔT_{sub} [K]	D_{max} [mm]	D_{ejc} [mm]	t_b [ms]	t_{ejc} [ms]	Lp_{ejc} [mm]
P2-02	0.41	0.4	20	0.5645	0.5361	1.728	0.96	0.2258
P2-03	0.41	1	30	0.8429	0.6769	1.827	1.218	0.320302
P2-04	0.41	0.8	30	0.8565	0.6741	2.064	1.204	0.32547
P2-05	0.41	0.6	30	0.7498	0.7193	2.502	1.39	0.269928
P2-06	0.41	0.4	30	0.9891	0.9234	3.19	1.595	0.405531
P2-10	0.08	0.4	20	0.8274	0.7569	3	1.5	0.099288
P2-20	0.82	0.4	20	0.7139	0.6517	2.592	1.44	0.656788
P2-08	0.41	0.6	20	0.7848	0.7121	2.38	1.19	0.298224
P2-09	0.82	0.6	20	0.7122	0.6306	1.862	0.931	0.334734
P2-11	0.41	0.32	10	0.7343	0.7343	3.145	1.11	0.044058
P2-18	0.82	0.36	10	0.7921	0.7791	3.64	1.43	0.570312
P2-22	0.82	0.6	30	0.6822	0.6821	1.81	1.086	0.586692
P2-23	0.82	0.8	30	0.5968	0.5784	1.379	0.788	0.364048
P2-15	0.08	0.2	30	0.7907	0.7907	2.214	0.984	0.102791

Table 3.2. Typical Bubbles p=3bar

Label	U_{bulk} [m/s]	q [MW/m^{2}s]	ΔT_{sub} [K]	D_{max} [mm]	D_{ejc} [mm]	t_b [ms]	t_{ejc} [ms]	Lp_{ejc} [mm]
P3-41	0.82	0.6	29.9	0.4708	0.4315	2.379	1.281	0.724999
P3-42	0.82	0.8	29.6	0.4231	0.4033	1.65	1.05	0.315
P3-43	0.82	1	29.5	0.4693	0.4512	1.665	0.925	0.706
P3-47	0.41	0.6	29.4	0.486	0.47	1.538	0.577	0.0980019
P3-48	0.41	0.8	30.4	0.3722	0.3662	0.828	0.414	0.1680111
P3-49	0.41	1	31.7	0.3779	0.3077	0.815	0.489	0.1519914
P3-27	0.08	0.2	28.7	0.528	0.528	2.104	1.052	0.2139614
P3-52	0.08	0.3	31	0.6043	0.6043	4	1	0.0030215
P3-37	0.82	0.6	20.2	0.516	0.4109	2.352	1.617	1.0204055
P3-39	0.82	0.8	19.1	0.5119	0.5119	3.178	1.135	0.6963017
P3-29	0.41	0.4	18.9	0.439	0.439	2.208	0.92	-0.070064
P3-24	0.41	0.6	22.5	0.388	0.363	1.27	0.762	0.0529581
P3-26	0.08	0.2	19.8	0.579	0.55	4.284	1.53	0.2521719
P3-51	0.08	0.3	20.8	0.5508	0.5064	4.446	0.936	0.2095243
P3-45	0.41	0.3	13.5	0.533	0.533	2.387	1.023	0.4106019

Table 3.3 Bubble growth and condensation correlations

Experiment	N	K
Akiyama and Tachibana	$0.25< t_m/t_b <0.5$ calculated for given range using: $D/D_m=1$ when $t/t_m=1$	3
Bankoff (Gunther's data)	$0.32< t_m/t_b <0.57$ calculated for given range using: $D/D_m=1$ when $t/t_m=1$	2
Faraji et al.	$t_m/t_b =0.33$; N=0.67	2.2
Present Study	$t_m/t_b=0.37$; N=0.7	2.5

Table 3.4 Coefficients in equation (3.7)

Variable	A	b	C	d	e
D_m^+	236.749	-0.581	-0.8843	1.772	0.138
D_{ejc}^+	440.98	-0.708	-1.112	1.747	0.124
t_m^+	9.625e8	-1.362	-1.977	2.102	0.142
t_{ejc}^+	1.522e9	-1.681	-2.182	2.459	0.262
t_c^+	1.138e8	-1.197	-1.686	2.389	0.169

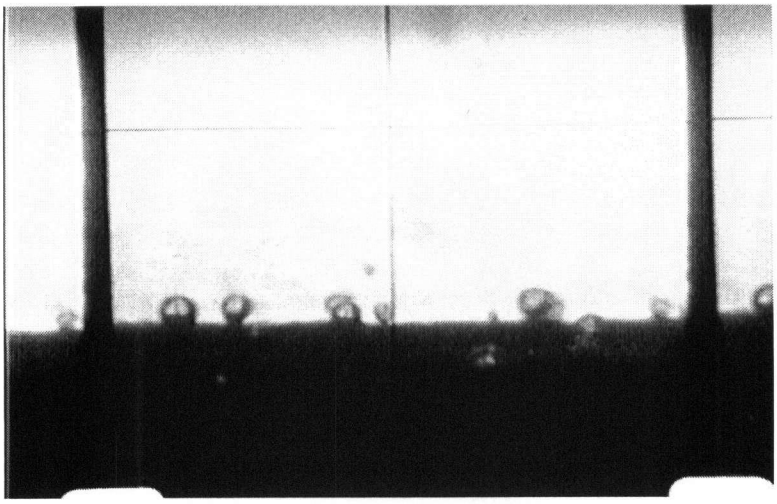

Figure 3.1 Photograph of the low heat flux region

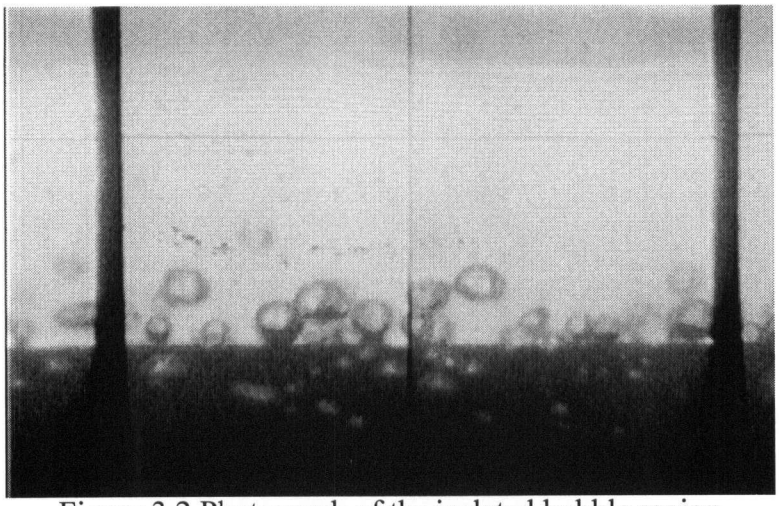

Figure 3.2 Photograph of the isolated bubble region

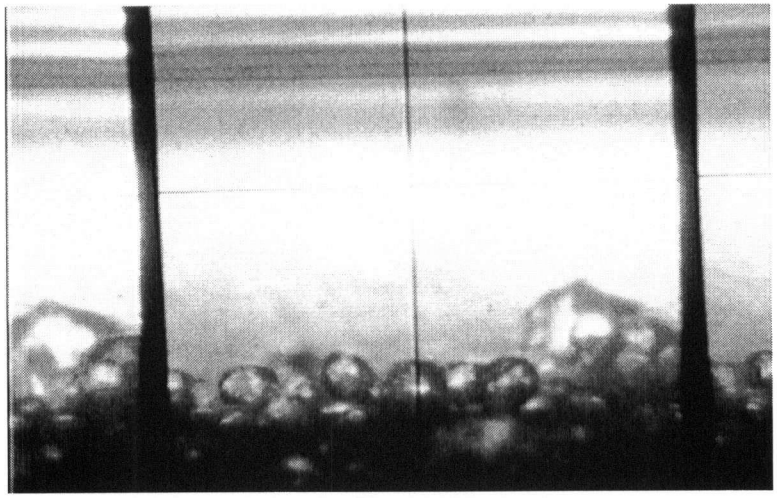

Figure 3.3 Photograph of the significant coalescence region

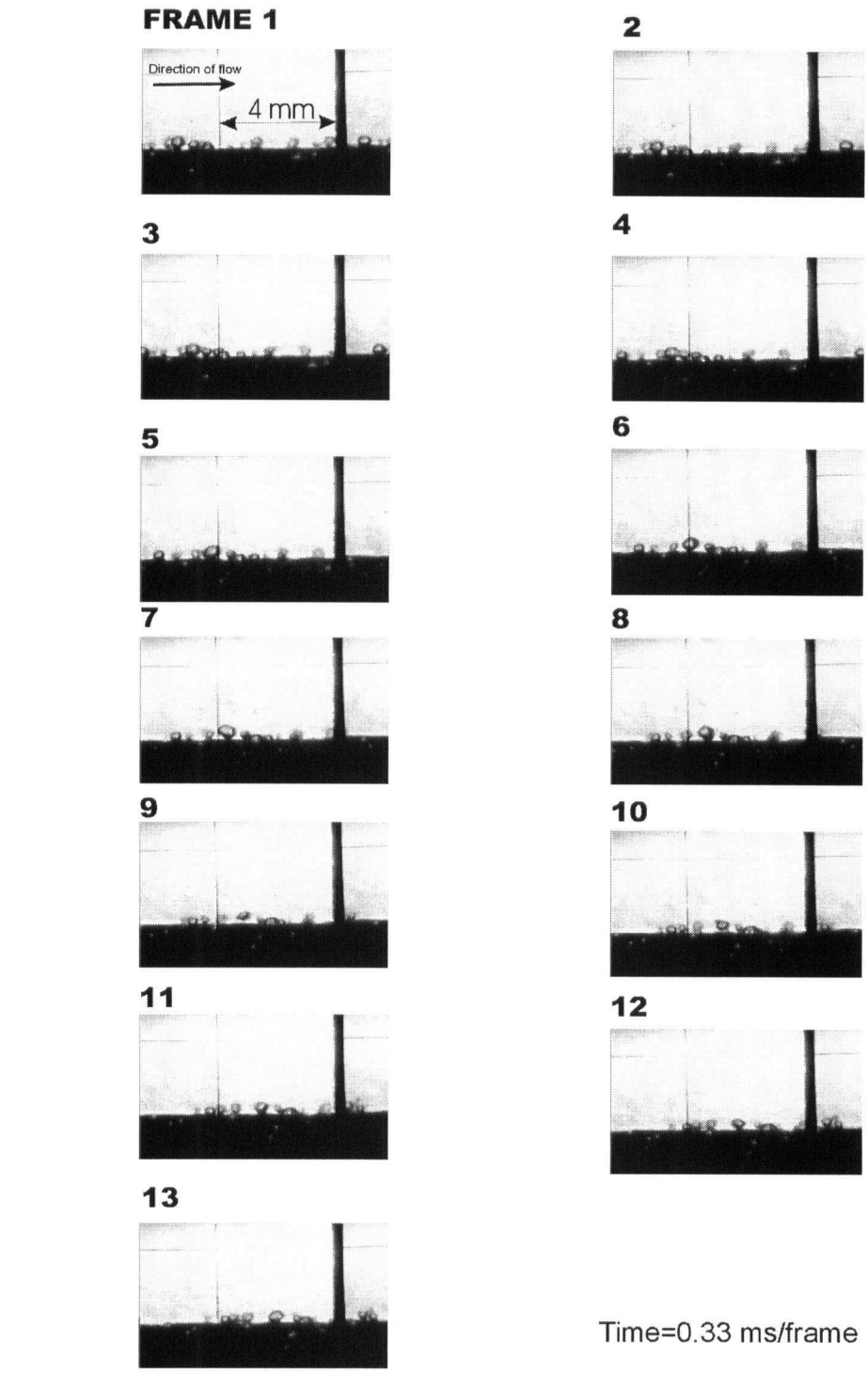

Figure 3.4 Bubble behaviour in the low heat flux region

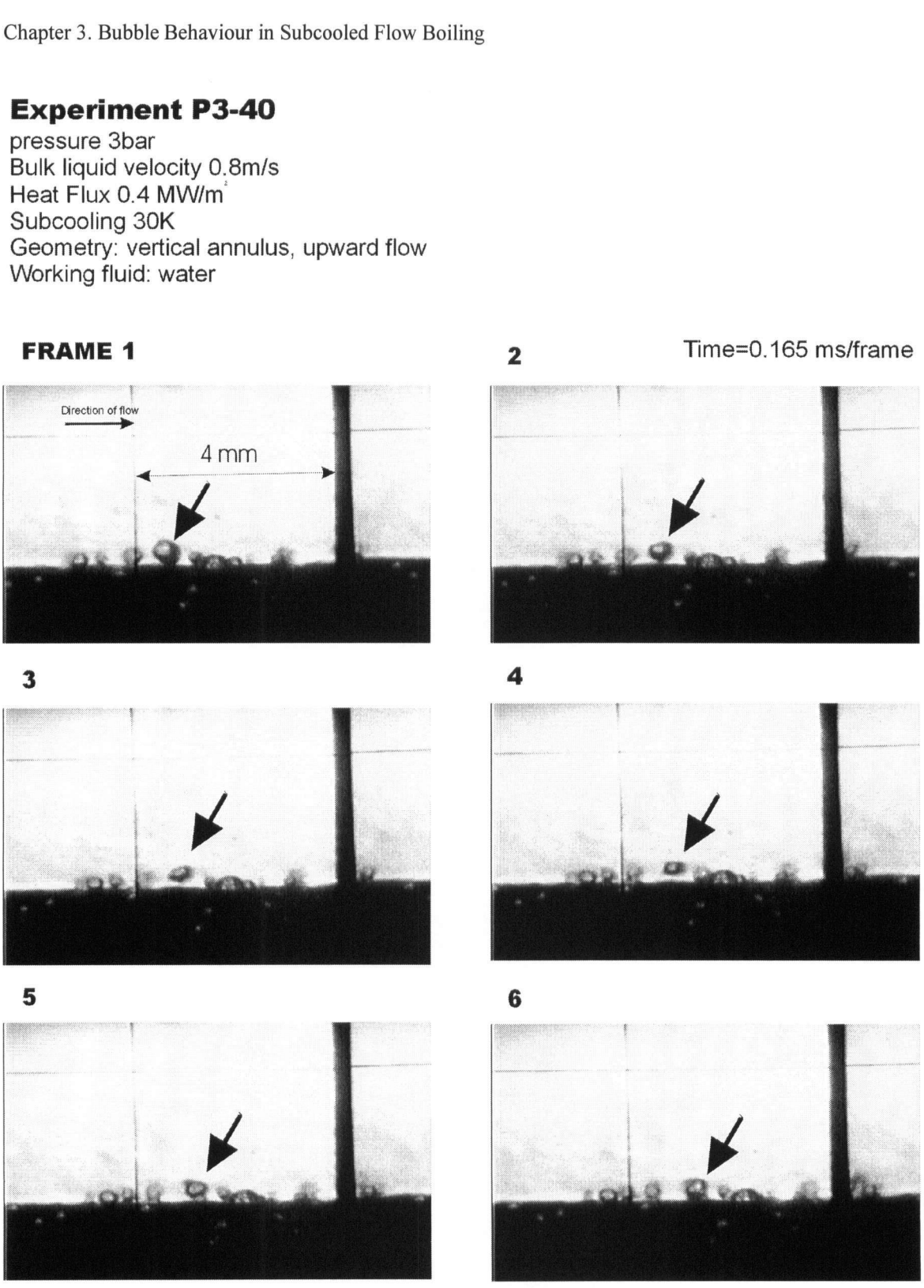

Figure 3.5 Photographs of bubble reattachment

Experiment P3-52

pressure 3bar
Bulk liquid velocity 0.08m/s
Heat Flux 0.3 MW/m^2
Subcooling 31K
Geometry: vertical annulus, upward flow
Working fluid: water

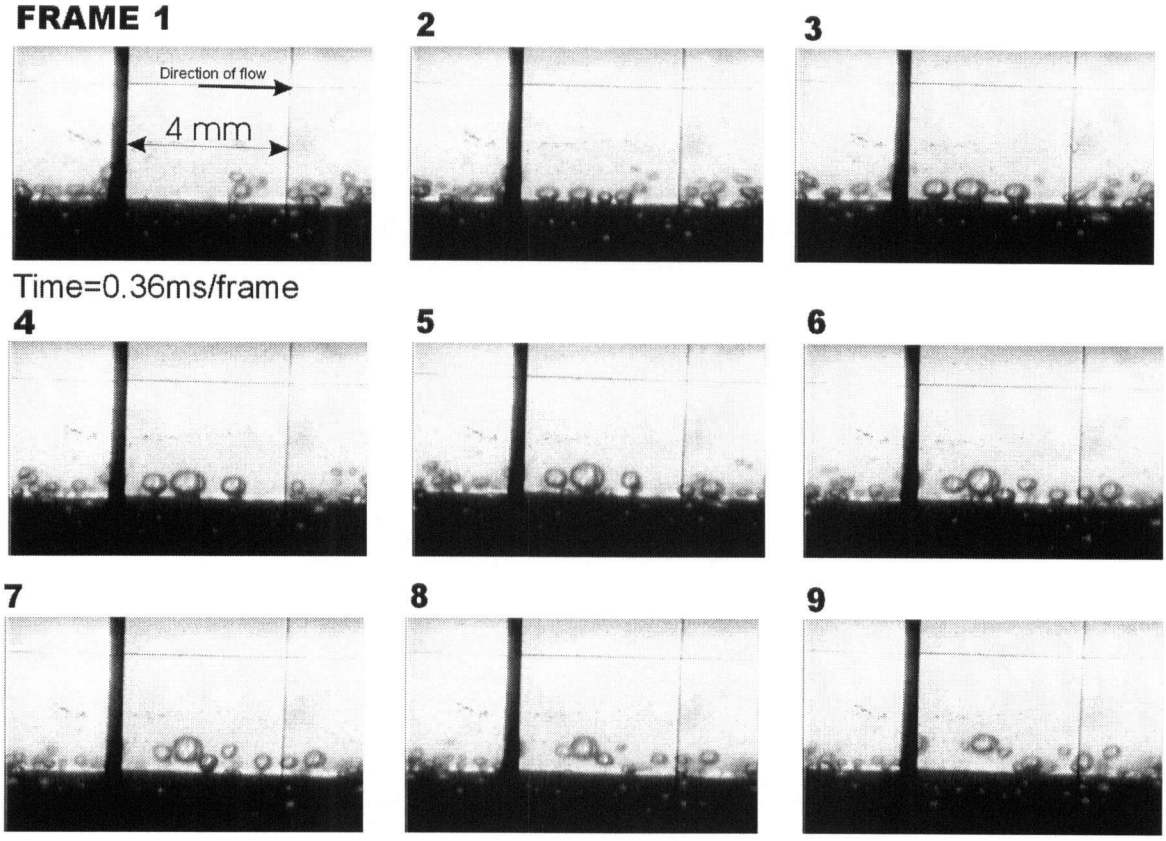

Figure 3.6 Bubble behaviour in the isolated bubble region

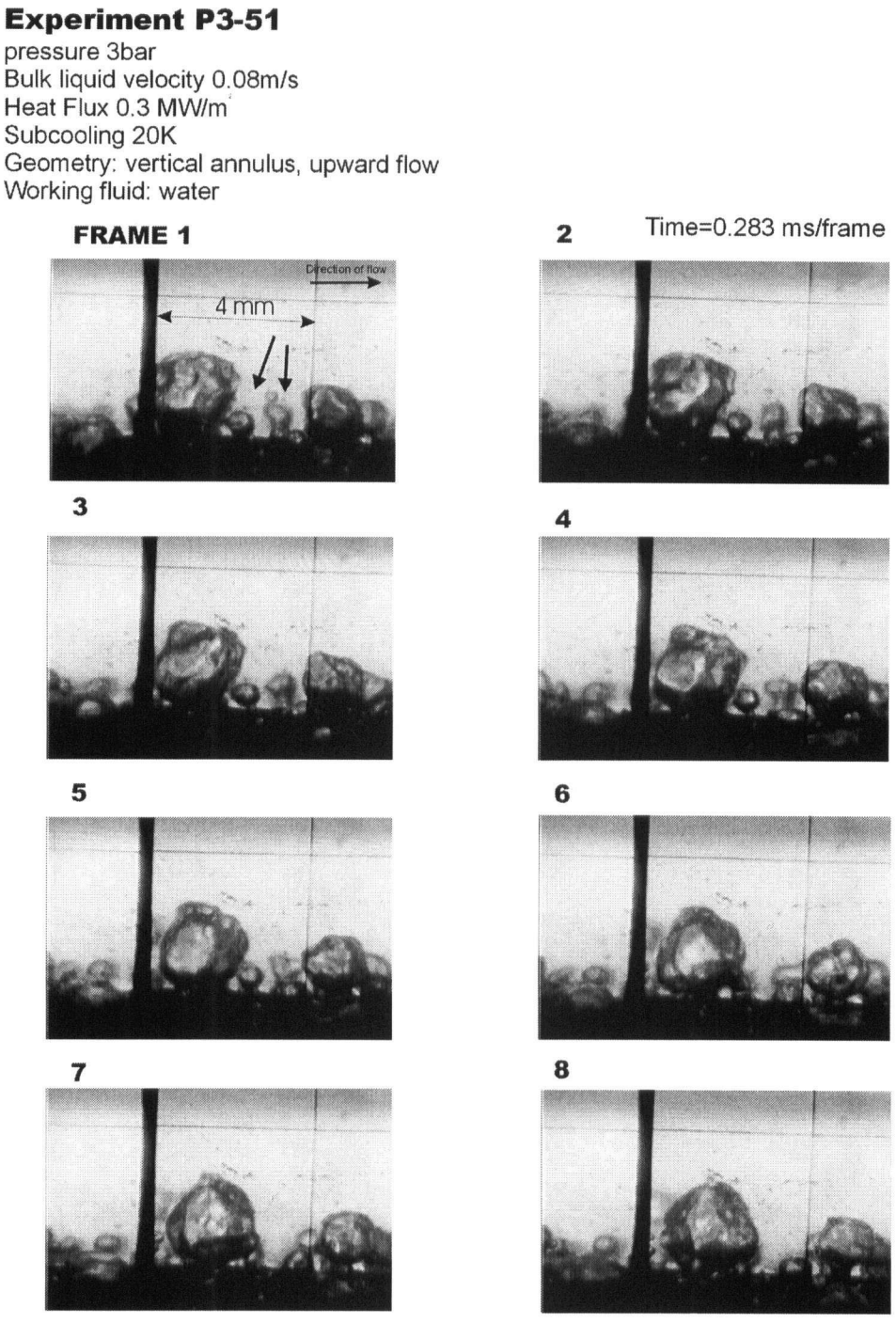

Figure 3.7 Bubble growth interrupted by coalescence with large bubble

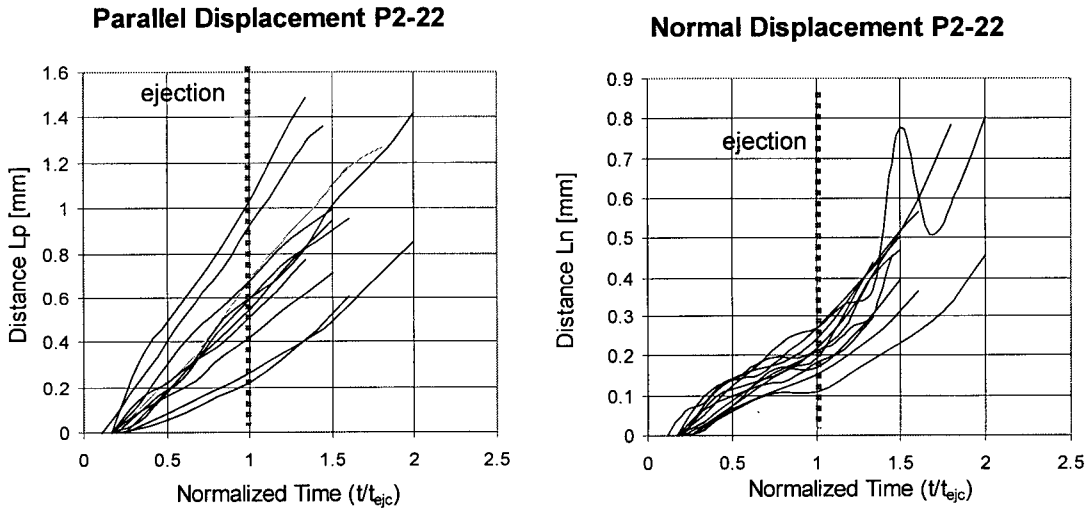

Figure 3.8 Bubble displacement at high bulk liquid velocity

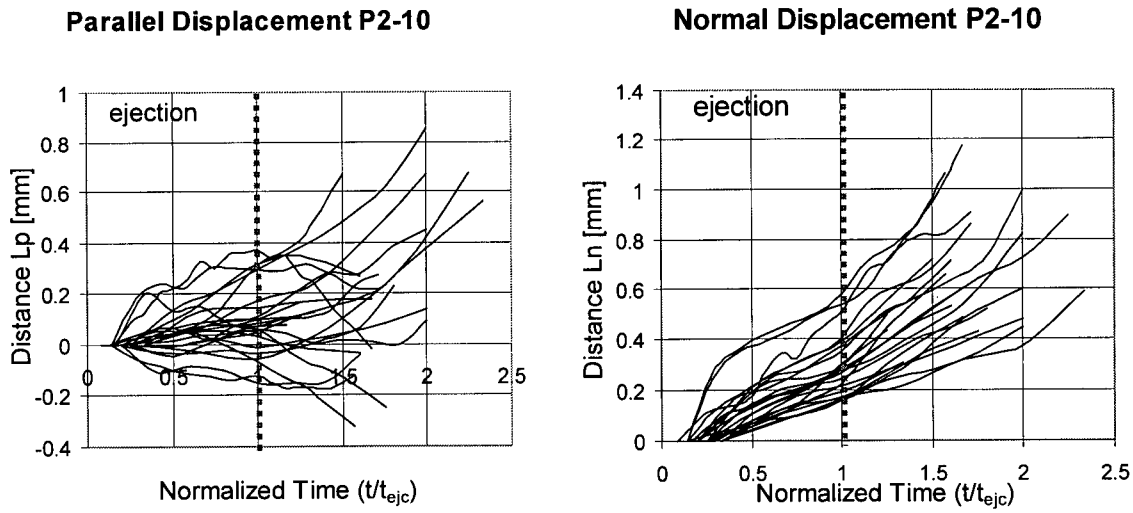

Figure 3.9 Bubble displacement at low bulk liquid velocity

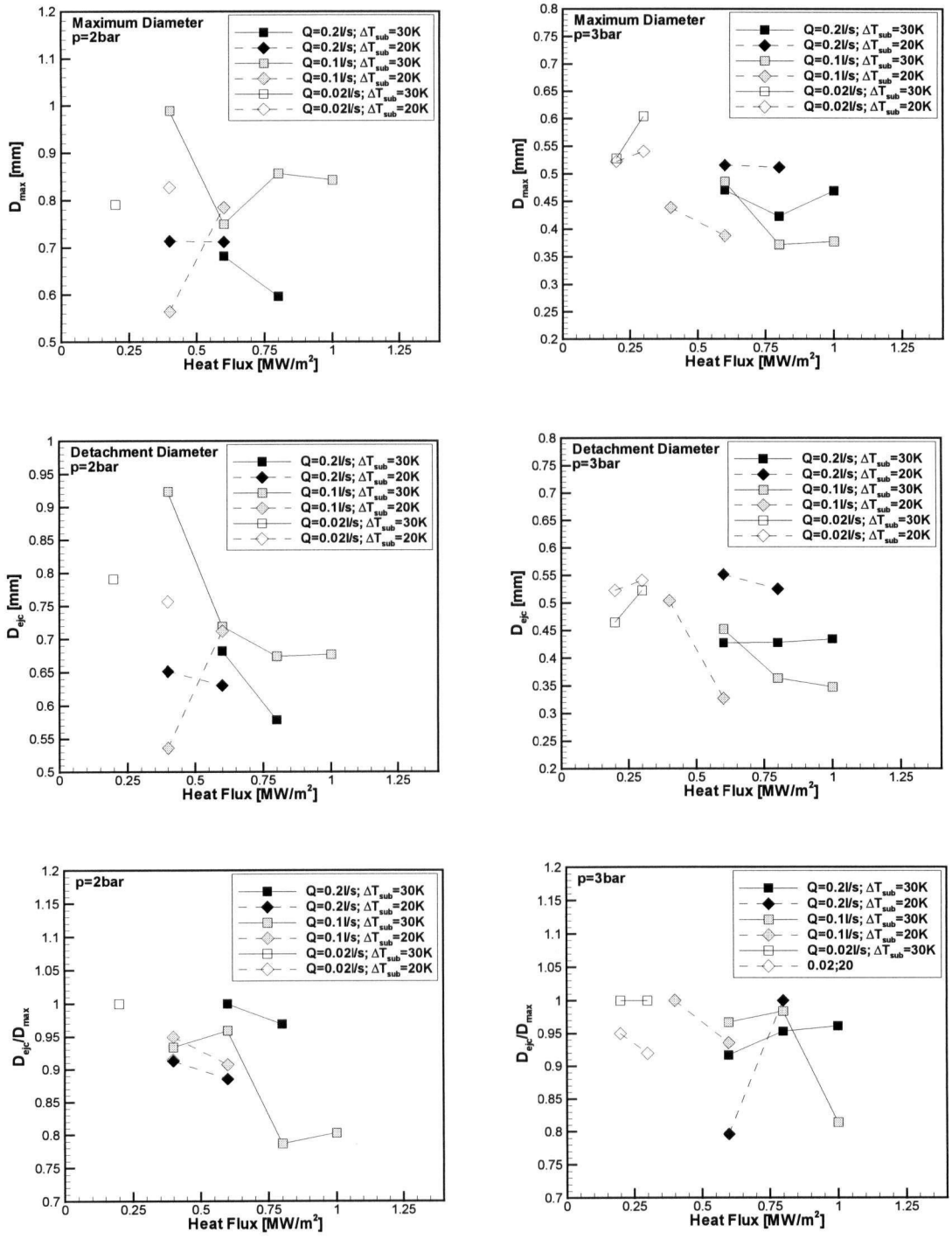

Figure 3.10 Maximum and detachment diameters – experimental data at 2 and 3 bar

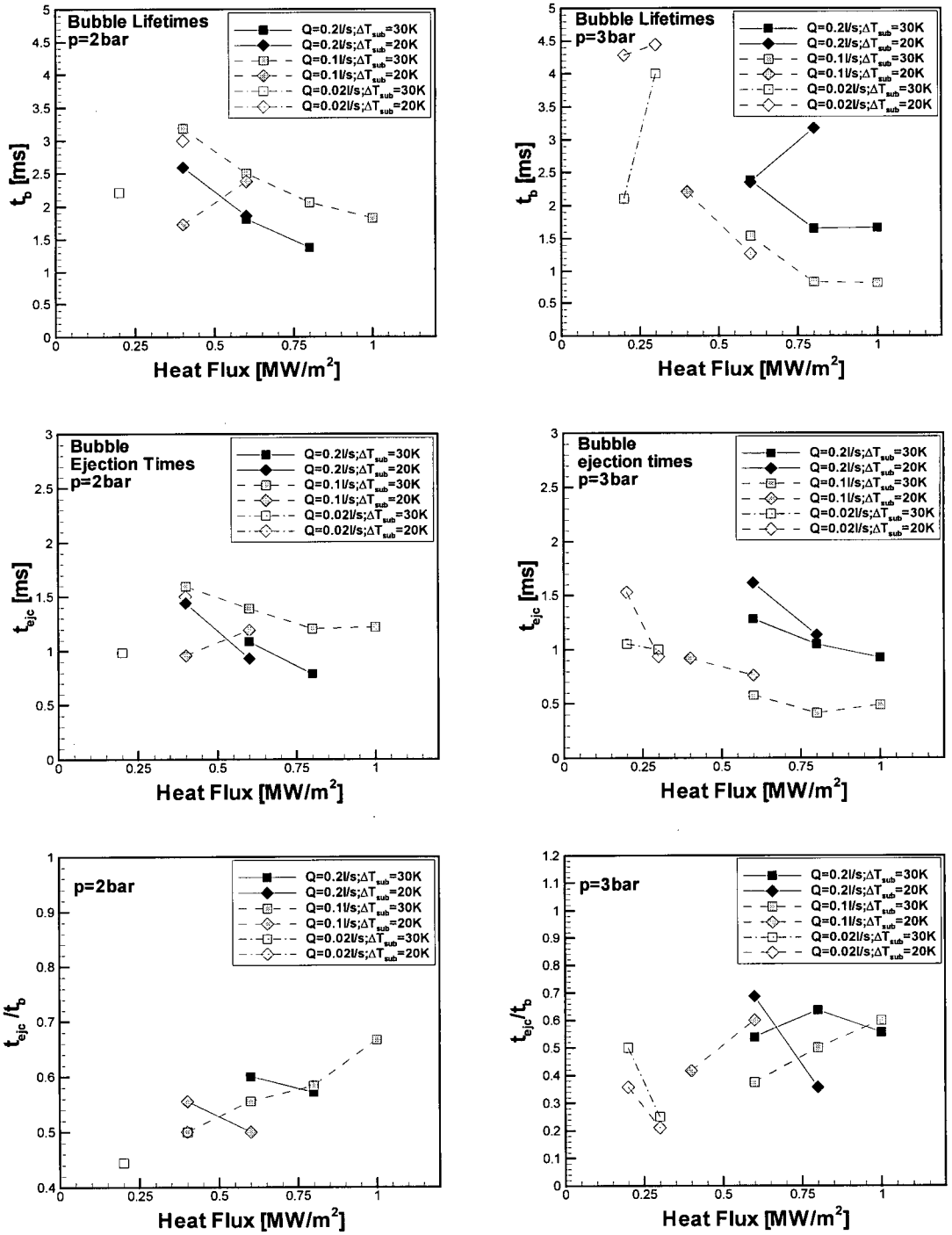

Figure 3.11 Lifetimes and ejection times – experimental data at 2 and 3 bar

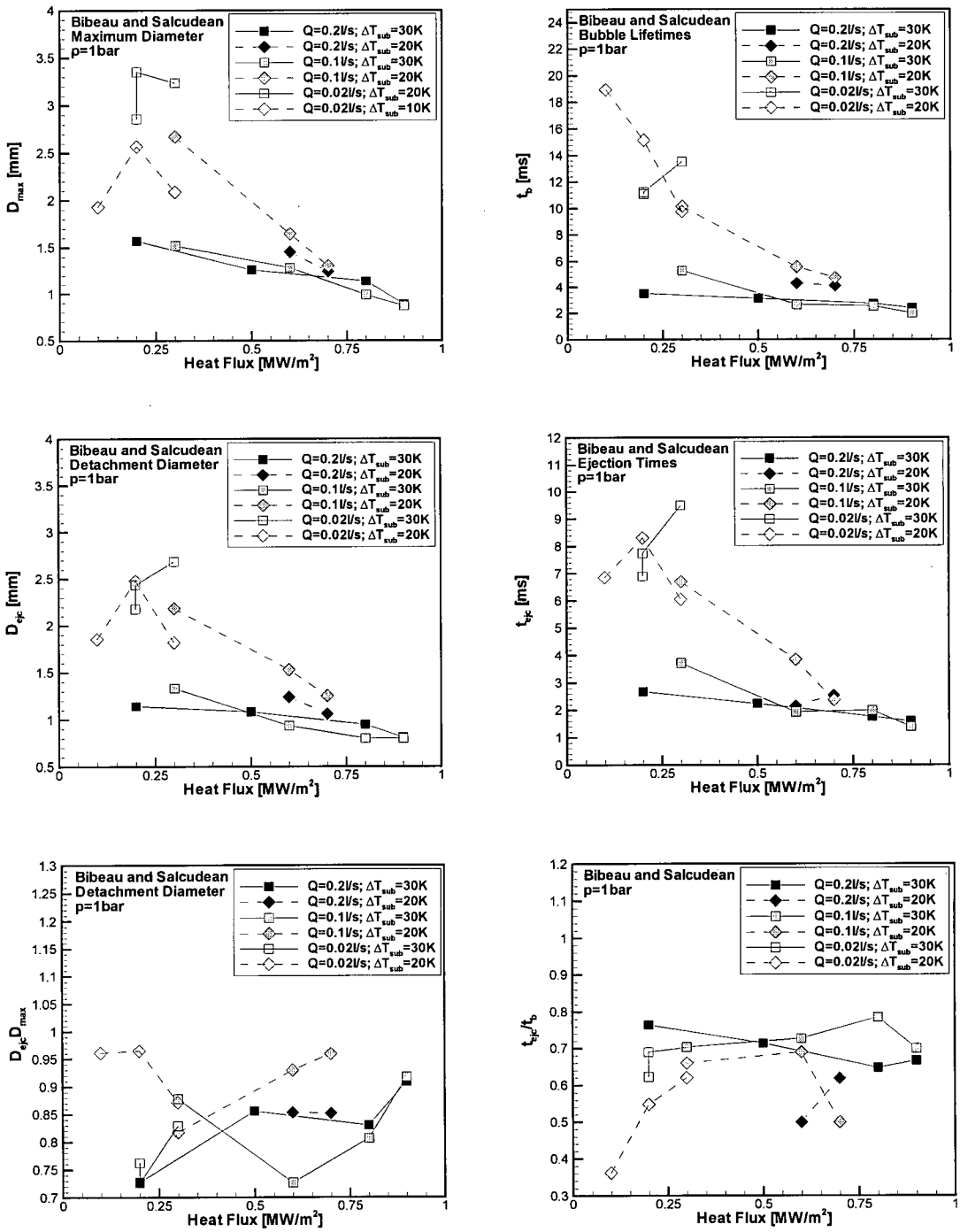

Figure 3.12 Diameters and lifetimes – from Bibeau and Salcudean, p=1bar

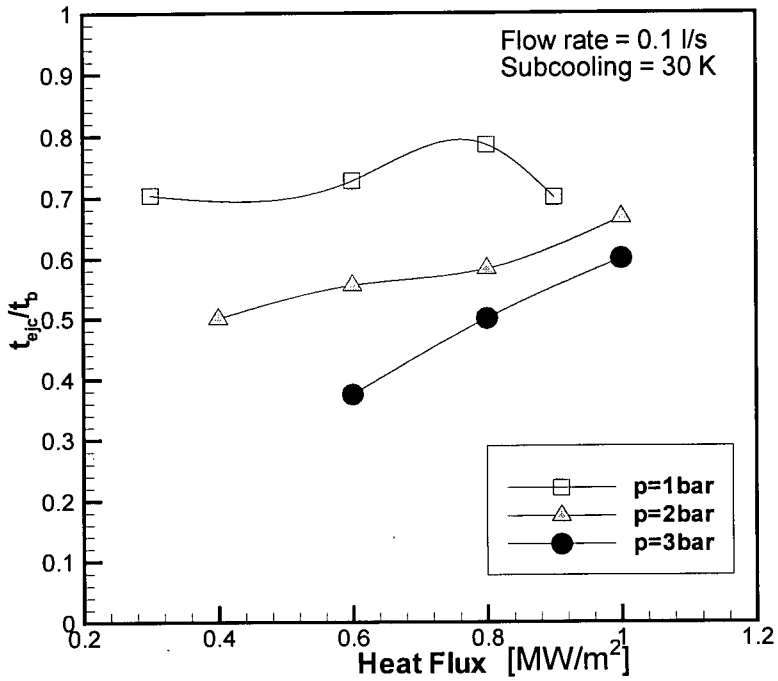

Figure 3.13 Variation of the contact time with heat flux and pressure

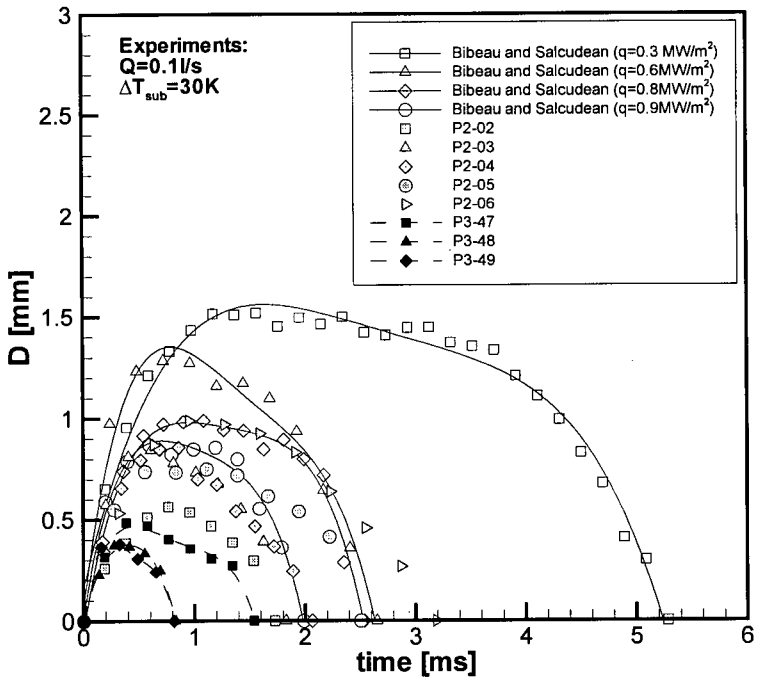

Figure 3.14 Variation of bubble diameters and lifetimes with heat flux and pressure

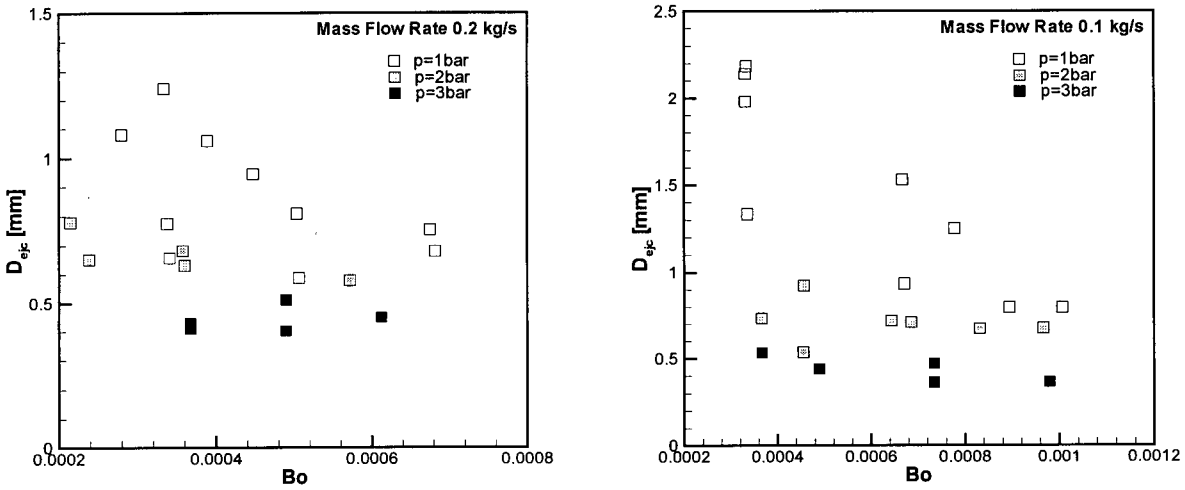

Figure 3.15 Variation of detachment diameters with Bo

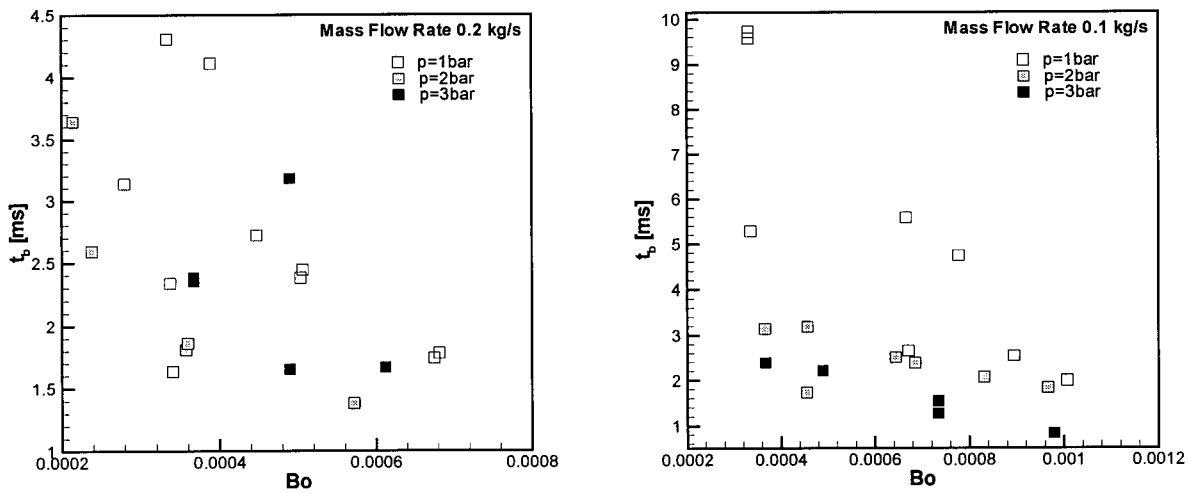

Figure 3.16 Variation of bubble lifetimes with Bo

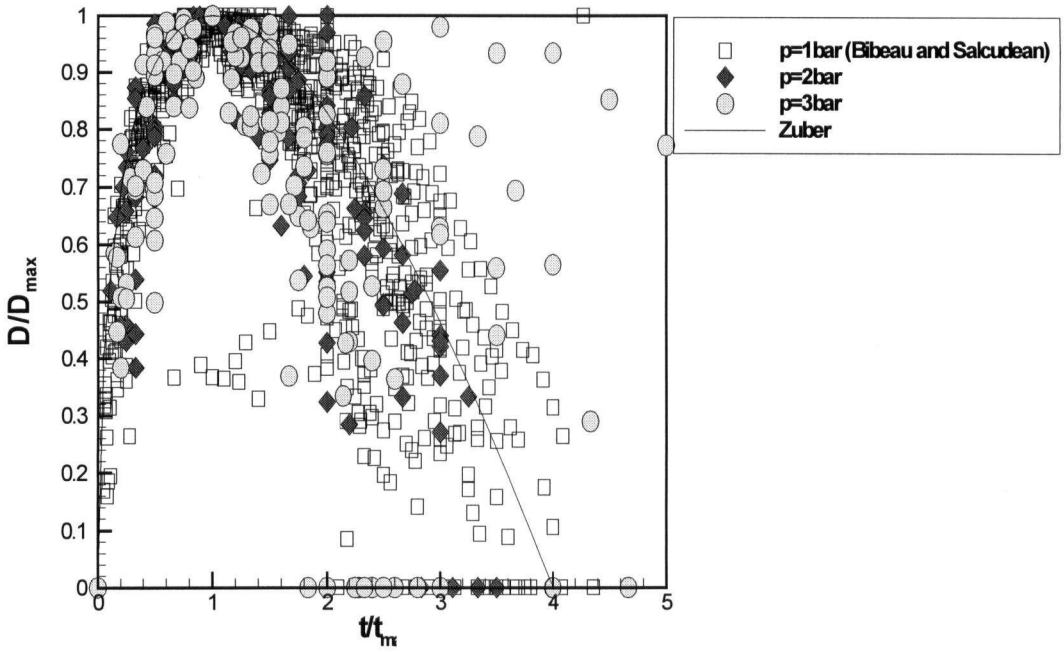

Figure 3.17 Bubble growth and condensation
Comparison with the model of Zuber

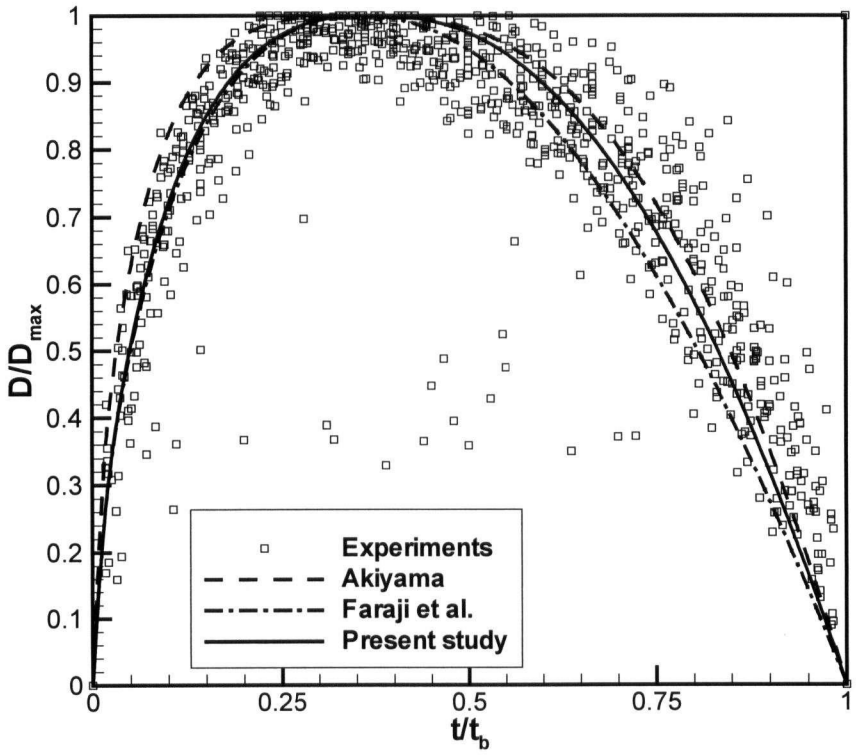

Figure 3.18 Correlations for bubble growth and condensation rates

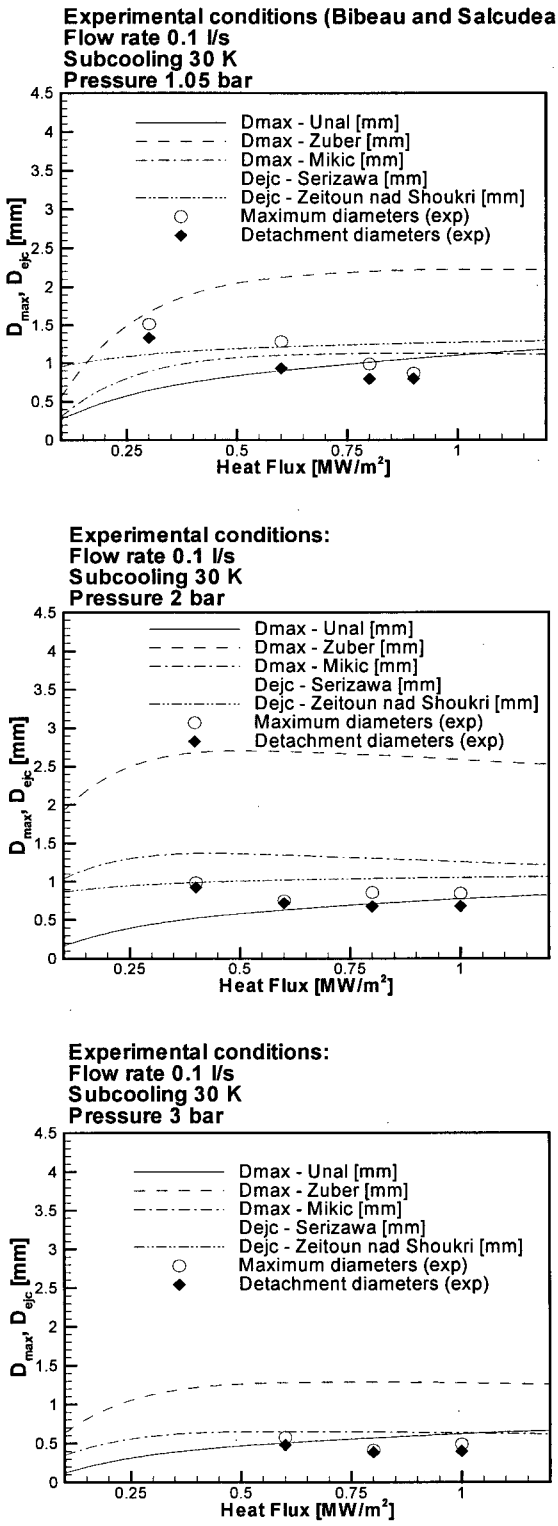

Figure 3.19 Comparison of experimental data with models for predicting maximum and detachment diameters in subcooled flow boiling

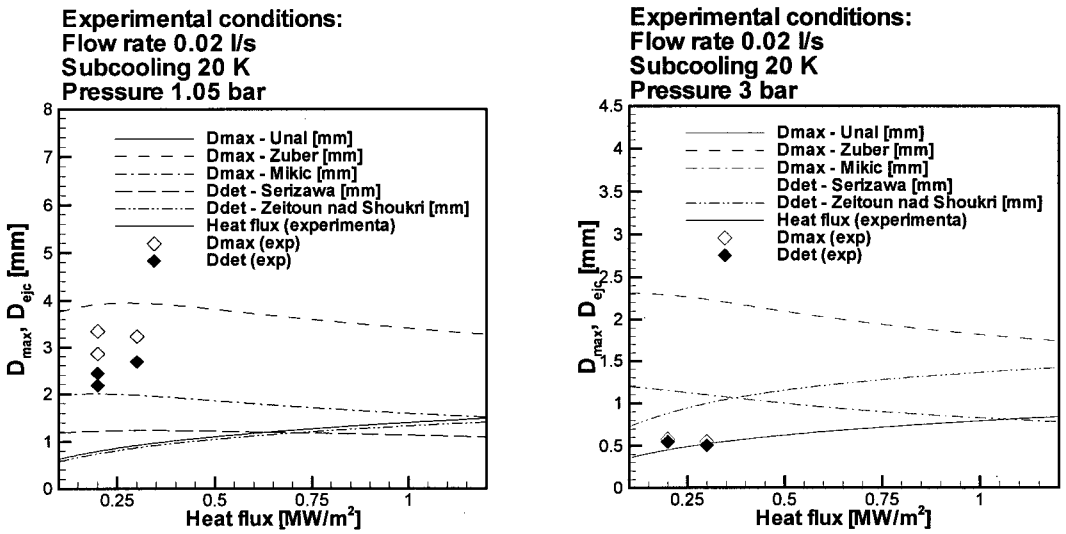

Figure 3.20 Comparison of experimental data with models for predicting maximum and detachment diameters in subcooled flow boiling – low flow rates

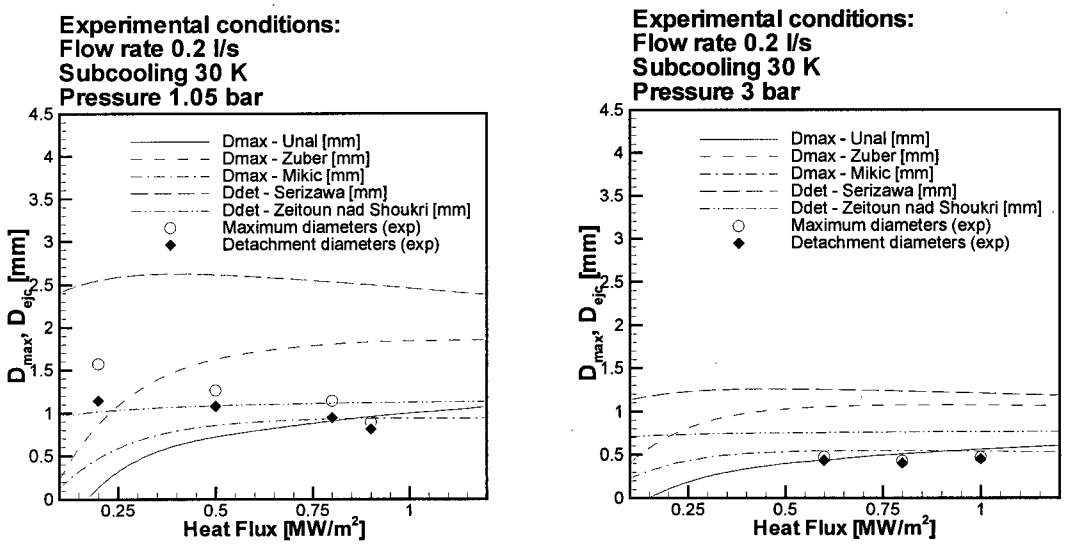

Figure 3.21 Comparison of experimental data with models for predicting maximum and detachment diameters in subcooled flow boiling – high flow rates

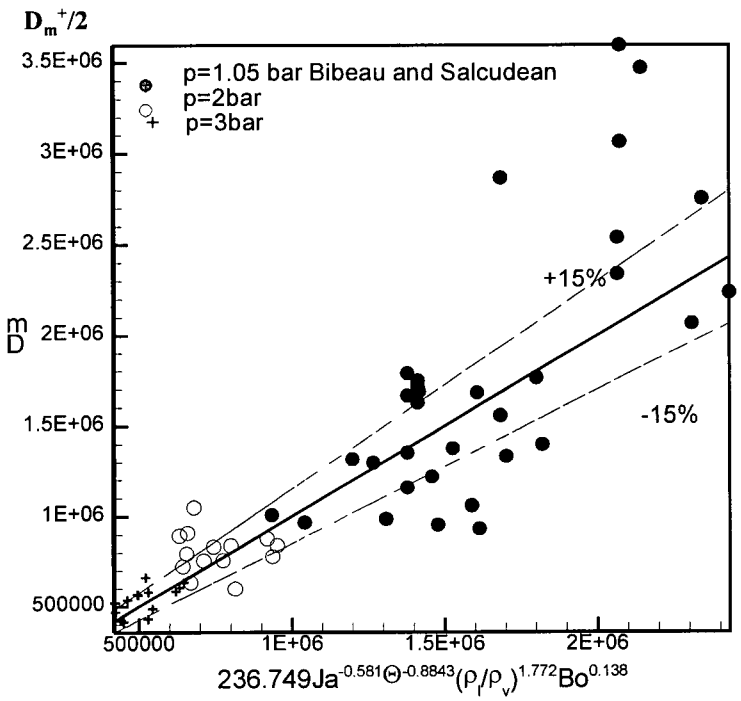

Figure 3.22 Correlation for the normalized maximum bubble diameter

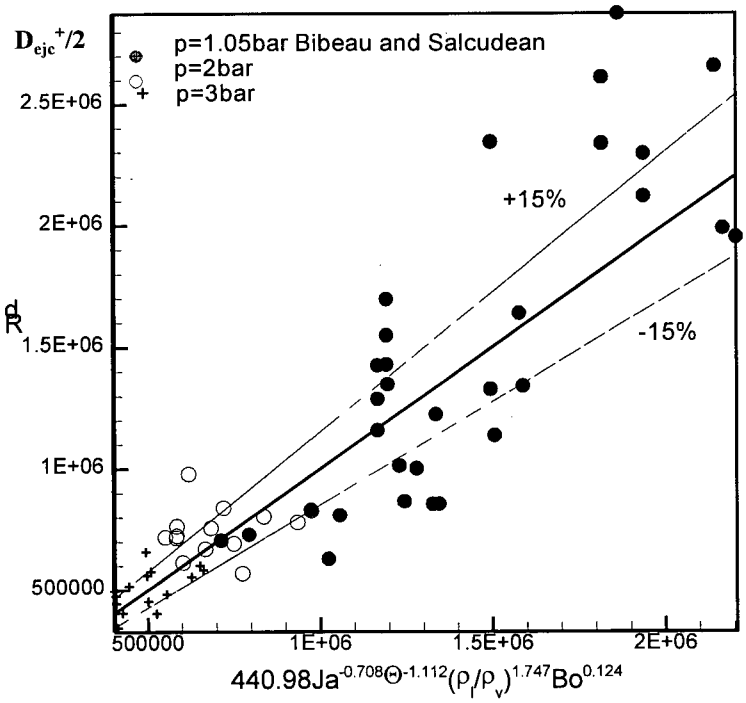

Figure 3.23 Correlation for the normalized bubble detachment diameter

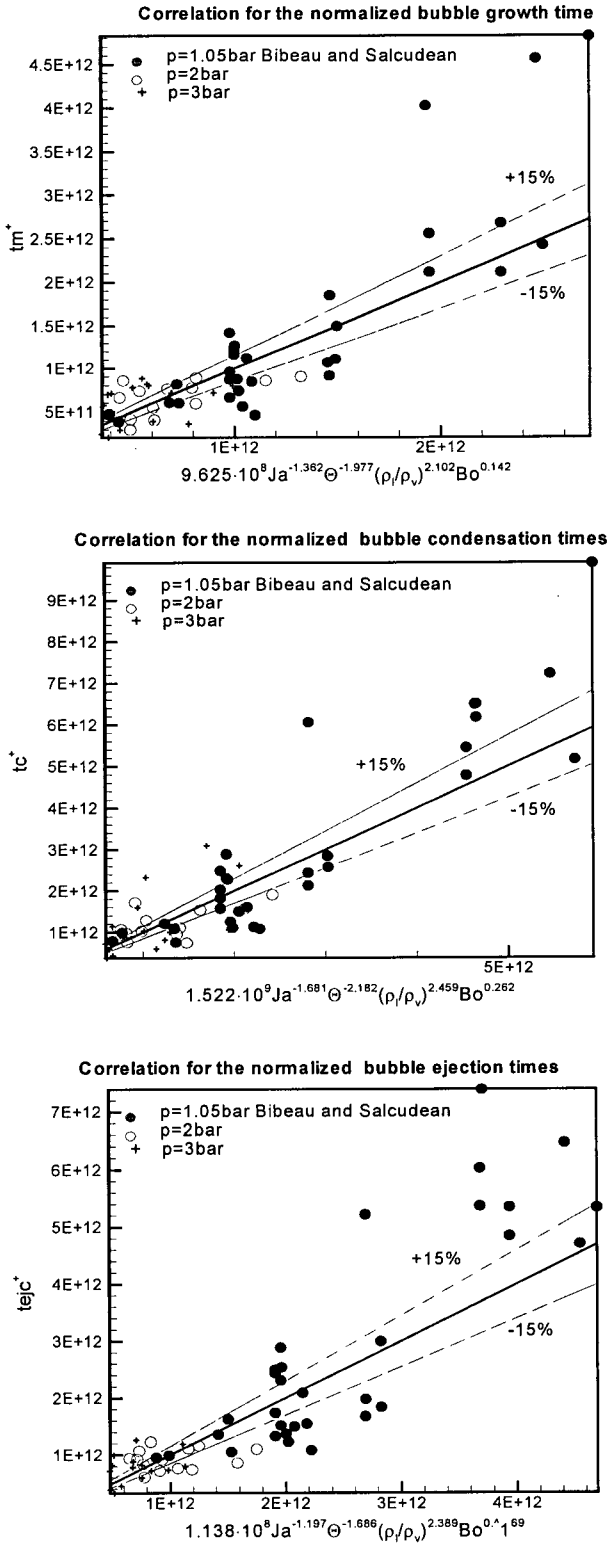

Figure 3.24 Correlation for the normalized bubble growth time, bubble condensation time and bubble ejection time

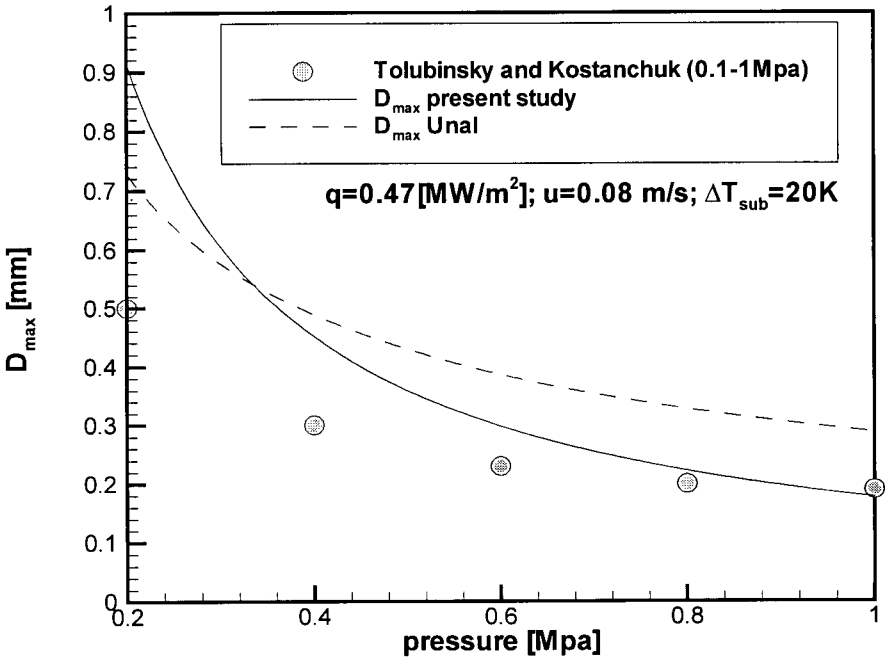

Figure 3.25 Comparison of the proposed correlation with the model of Unal

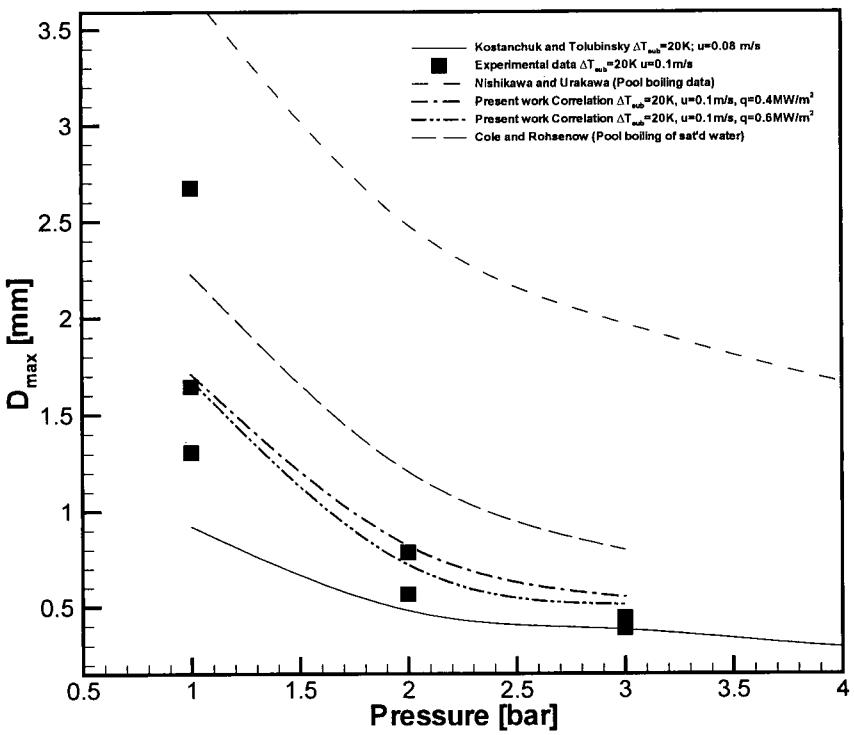

Figure 3.26 Variation of bubble diameters with pressure

Chapter 4

HEAT TRANSFER IN SUBCOOLED FLOW BOILING

4.1 Background Information and Literature Review

Forced convection is the main heat transfer mode in case of a liquid flowing over a heated solid surface. It is known that the rate of heat transfer is highly affected by the velocity of the liquid, making turbulent flow a desirable type of liquid motion in such applications. The significant amount of experimental and theoretical studies in this subject have resulted in numerous correlations for calculating heat transfer coefficients. For example, the one that is probably the most often used for circular and annular geometries is the Dittus-Boelter equation:

$$h_{FC} = 0.023 \frac{k_l}{D} Re^{0.8} Pr^{0.4} \tag{4.1}$$

Once the heat transfer coefficient is known, the rate of heat transferred per unit area between the solid wall and a liquid can then be calculated as:

$$q = h_{FC}(T_w - T_b) \tag{4.2}$$

The Dittus-Boelter equation, as well as other single-phase forced convection correlations, fail to predict the heat transfer rate in cases where a vapour phase exists in the fluid, for example, when boiling is initiated on a solid surface. At the inception of boiling, the heat fluxes become much higher due the heat removed from the surface by both forced convection and evaporation.

Shown in Figure 4.1 is the variation of the heat flux with wall temperature (boiling curve). The boiling curve upstream of point B denotes single-phase forced convection boiling. A change in the slope of the boiling curve at B indicates initiation of the boiling process. Downstream of ONB, the boiling curve deviates from the straight single-phase forced convection line due to additional heat removed through evaporation. The dual effect of convection and evaporation is notable until, at a certain location B', the evaporation effect becomes dominant. This is evident from the merger of boiling curves,

calculated from experimental data for various flow rates (shown as dotted lines) at B'. The first boiling region is called the partially developed boiling region or the highly subcooled region, while the second is known as fully developed boiling or the low subcooled region. The fully developed boiling region extends beyond OSV. Continuing on, the change of the two-phase flow pattern induces another change in the heat transfer mode. This is due to a large increase in voidage which accelerates the liquid phase, making the convective term significant again. The last region corresponds to the *Significant Void Flow* region. The flow regime here can be bubbly, slug, or annular depending on the phase structure within the flow [51].

4.1.1 Fully Developed Boiling

The heat transfer equations for the nucleate boiling region should account for the convective heat transfer contribution as well as for the heat removed by evaporation. Both of these were taken into account by the Chen [90] correlation, which has the following form:

$$h_{tp} = h_{FC} \cdot F + h_{pool} \cdot S \tag{4.3}$$

The first term on the right hand side is the convective term, the "all liquid" heat transfer coefficient, h_{FC}, which can be calculated from equation (4.1), multiplied by the enhancement factor F. The parameter F is always greater that unity and takes into account the enhancement of the convective heat transfer due to the increasing vapour quality. The second term is the evaporative term and can be obtained by using the Forster and Zuber [59] correlation for the pool boiling heat transfer coefficient, h_{pool}, multiplied by the suppression factor S. The parameter S is less that unity and accounts for the reduction of the thermal boundary layer with increasing flow. It is a function of the two-phase Reynolds number.

Chen's correlation was proposed for saturated flow boiling conditions and is widely used for low-pressure heat transfer calculations in boiling water. A question arises as to whether a correlation of this form can be used for the case of subcooled boiling. The obvious difference in the two boiling processes is the fact that bubbles condense in the presence of the cooler liquid and/or even collapse on the surface of the heater or in the

bulk fluid in subcooled boiling, thus diminishing the effect of the vapour phase on the convective term. Also, the subcooled fluid creates larger thermal gradients in the direction normal to the wall affecting the role of the suppression factor S.

As pointed out by Spindler [15], a certain amount of disagreement between researchers exists about the use of Chen's correlation in subcooled boiling. Gungor and Winterton [91] modified Chen's correlation by redefining the enhancement parameter. They made it not only a function of the Martinelli parameter as in Chen's correlation but of the Boiling number, Bo, as well. They also suggested using Cooper's [93] correlation for the pool boiling heat transfer coefficient. For the case of subcooled boiling, they recommended that the enhancement factor has to be set to unity while retaining the suppression factor.

The obvious problem in using Chen's correlation or any of its modifications is the calculation of the Martinelli parameter, X_{tt}. The parameter is used in the equations for determining F and S. One of the variables in the equation is the thermodynamic quality X_{eq}, which is negative in the case of subcooled boiling. In order to calculate the Martinelli parameter, the thermodynamic quality has to be replaced with the true mass quality X_a. According to Kandlikar [11], the Saha and Zuber [34] method is the most widely accepted method for calculating the true mass quality for the case of subcooled flow boiling. Another method that can be used is that of Ahmad [33]. The latter method is based on the prediction of the slip ratio. Both methods are shown in Appendix C. The main concern is the validity of the void fraction models for the case of low pressure and low flow rate subcooled boiling. The discrepancy between available models and the experimental data, as pointed out by Salcudean and Bibeau [109], could initiate an error in the predictions of the true mass quality.

Few models based on Kutateladze's power-type addition model, which accounts for further suppression of boiling, tend to agree better with experimental data for the case of subcooled boiling. The power-type addition model given by equation (4.4) was used by Liu and Winterton [94] for testing subcooled flow experimental data. They used the Dittus-Boelter correlation, equation (4.1), for h_{FC} and Cooper's pool boiling correlation for h_{pool} as well as equations (4.5) and (4.6) for the enhancement (E) and supression (S)

factors, respectively. Their correlation gave the best fit to subcooled boiling experimental data compared to the Chen [90] and Gungor and Winterton [91] correlations.

$$h_{tp} = \sqrt{(h_{FC} \cdot E)^2 + (h_{pool} \cdot S)^2} \tag{4.4}$$

$$E = \left[1 + X_a \, Pr_l \left(\frac{\rho_l}{\rho_v} - 1\right)\right]^{0.35} \tag{4.5}$$

$$S = \frac{1}{1 + 0.055E^{0.1} \, Re^{0.16}} \tag{4.6}$$

Other correlations of this type include those of Bjorge (1982) for saturated flow boiling in tubes at X_a>0.05, and Kandlikar [95] for saturated boiling in horizontal and vertical tubes. Good reviews on this subject can be found in Spindler [15], Darabi et al. [96] and Kandlikar [11].

Other, strictly empirical, curve fit type of correlations, give an explicit relation between the heat flux and the temperature difference (usually the wall superheat), in the form of q=f (ΔT). Recent comprehensive reviews of these correlations are given in Kandlikar [11] and Guglielmini et al. [97]. A brief summary follows here.

One of the first models was that of McAdams et al. [98] who proposed a single curve that relates the heat flux and "surface boiling potential" – wall superheat through an exponent of 3.86. They suggested that the heat transfer in the fully developed boiling region was independent of water velocity, pressure and degreee of subcooling. Several studies conducted later introduced a modification of the exponent lowering it to 2.0, as in the correlations of Shah [99] or 3.3 in Kandlikar [11]. Some of the correlations include correction factors for different pressures. These are shown in Table 4.1. Note that they were all originally proposed for heat transfer in boiling water in circular or annular geometries.

Heat transfer correlations can also be found through dimensional analysis. As shown in the following equation, the heat transfer coefficient, contained in the Nusselt number, Nu, can be expressed as a function of the Boiling number, Bo, Jacob number, Ja, Prandtl number, Pr, and density ratio, ρ_l/ρ_v.

$$Nu = f(Bo, Ja, Pr, \frac{\rho_l}{\rho_v}) \tag{4.7}$$

The boiling number takes into account the effect of heat flux and liquid velocity. The modified Jacob number (with the wall superheat replaced by the liquid subcooling) describes the ratio of sensible to latent heat. The pressure effect is accounted for by the density ratio. Shown in Table 4.2 are correlations of this type that were chosen to be tested in the current study. These correlations have been reviewed in detail by Spindler [15].

4.1.2 Partially Developed Boiling

Correlations for partial nucleate boiling are usually equations that span the single-phase forced convection curve and the fully developed boiling curve. A few authors have attempted to discuss the nature and reasons for the occurrence of partial boiling. Some correlations listed in Table 4.3 include those of Bergles and Rohsenov [17], Pokhvalov et al. [100], Shah [99] and Kandlikar [11]. Models for transition from partial to fully developed boiling are usually obtained by using various combinations of partial and fully developed boiling correlations. Little information can be found in the open literature about the nature and causes of this transition. Some models are listed in Table 4.4.

4.1.3 Transition from Partially to Fully Developed Boiling

A method of locating the transition point was first proposed by McAdams et al. [98]. They defined it as the intersection of the forced convection and fully developed boiling curves.

After compiling data from various sources, Shah [99] found that plotting $\Delta T_{sub}/\Delta T_{sat}$ versus Bo showed two distinct boiling regimes. One was dependent on subcooling and flow rate, while the other was independent of these. Transition occured at $\Delta T_{sub}/\Delta T_{sat} = 2$ and this ratio was used to indicate the change from partial to fully developed boiling.

Kandlikar [11] used the same procedure as McAdams et al., locating the intersection of the extension of the single-phase curve and fully developed curve. They

suggest the beginning of fully developed boiling can be obtained by multiplying the heat flux at that particular point by 1.4, as suggested earlier by Bowring [32].

4.2 Analysis of the Applicability of Heat Transfer Models

Two sets of experimental data have been used to test the models. Both sets involve boiling water (pressure range from 1 to 3 bar and liquid velocities from 0.08 to 0.8 m/s, Reynolds numbers ranging from 3000 to 30000) in the experimental apparatus with a vertical annular test section described in Chapter 2. The first set consists of about 1500 heat flux and surface temperatures measurements, from low temperature single-phase forced convection heat transfer to heat transfer beyond OSV. These data were taken by Bibeau and Salcudean [46] in their investigation of void growth. The second set is from the experiments described in detail in Chapter 3. The high-speed photography data (total of 61 points in the fully developed boiling region), taken along with the heat flux and surface temperature measurements, included bubble behaviour data (size and sliding distances of typical bubbles). The first set of data was used to construct boiling curves and compare them to existing heat transfer correlations. The second set provided data for modelling the transition point from partial to fully developed boiling.

Chen-type correlations typically over-predicted the heat transfer rates. Four different methods (Chen, Gungor and Winterton, Liu and Winterton, and modified Gungor and Winterton) were used with three different models for calculating the true mass fraction (Saha and Zuber, Ahmad, and Kroeger and Zuber [101]). The best results were obtained by using the correlation of Liu and Winterton and the modified Gungor and Winterton correlation. A comparison of these correlations with the experimental data of Bibeau and Salcudean is shown in Figure 4.2. for high flow rate and high subcooling and in Figure 4.3 for low flow rate and low subcooling experiments. The conclusion of poor applicability of the Chen type correlations for subcooled nucleate flow boiling is in agreement with the findings of Hasan et al. [102] who conducted experiments using R-113.

Kandlikar [11] showed good agreement between his correlation for the fully developed region and the experimental data of Bergles and Rohsenow [17]. He also

found that the correlation of Shah [99] under-predicted the heat transfer rate. Our analysis shows, however, that most models of this type, with the exception of that of Shah [99], over-predict the heat transfer coefficient for a given wall superheat. This is illustrated in Figure 4.4.

Shah's model was the only one that shows excellent agreement with our data, but only at low flow rates. Shown in Figure 4.5 is the result of applying Shah's and Kandlikar's model for both partial and fully developed boiling, to the experiments of Bibeau and Salcudean. Good agreement with the model of Shah can be noticed in the fully developed boiling (FDB) zone as well as good agreement with the model of Kandlikar in the partial boiling region (PDB). As pointed out by Shah, poor results of his correlation in the PDB zone were related to ΔT_{sat} being a strong function of h_{FC} and hence subject to accurate prediction of the convective heat transfer coefficient.

Correlations presented in Table 4.2 generally also over-predicted experimental heat transfer data of Bibeau and Salcudean. This is shown in Figure 4.6. The best results over the whole range of experiments were obtained with the correlation of Moles and Shawn [103]. However, the coefficients in the correlation were subject to modification. The modification of this correlation is discussed below.

4.3 Proposed Heat Transfer Correlation

A modification of the Moles and Shawn correlation is proposed in this study and is given by:

$$\frac{h_{tp}}{h_{FC}} = \exp(14.542)\mathrm{Bo}^{0.729}\mathrm{Ja}^{*-0.354}\left(\frac{\rho_v}{\rho_l}\right)^{1.811}\mathrm{Pr}^{7.032} \tag{4.8}$$

where Ja^* is the modified Jakob number:

$$\mathrm{Ja}^* = \frac{cp_l \Delta T_{sub}}{i_{fg}} \tag{4.9}$$

The larger exponent for the density ratio than appeared the original correlation suggests a stronger influence of pressure on the overall heat transfer rate. However, perhaps this can be expected since the bubble sizes over our pressure range (1-3 bar)

changed significantly. At higher pressures, such large variations do not occur. The single-phase heat transfer coefficient, h_{FC}, is calculated by the Dittus-Boelter correlation (4.1). As shown in Figure 4.7, the new correlation agrees very well with the experimental data. It can be shown that similar accuracy (within 20% error) can be obtained by comparing the heat transfer predictions from equation (4.8) with the experimental data of Bibeau and Salcudean [46].

4.4 Bubble Behaviour and Heat Transfer Modes

Most authors agree that, in addition to liquid single phase forced convection, there are two other main mechanisms governing heat transfer during boiling. The first mechanism has been suggested by Gunther and Kreith [104]. It is based on additional turbulent mixing (microconvection) due to the presence of the vapour phase. The second mechanism was discussed Bankoff [105] and stresses the importance of the latent heat transport to the bubble. This concept involves heat transferred to the bubble through microlayer evaporation, while heat is simultaneously transferred heat to the cooler fluid via condensation along the top of the bubble. The latent heat transport mechanism has been analyzed in detail by Bankoff and Mikesell [56] and Snyder and Robin [66], among others.

Upon analyzing the importance of microlayer evaporation in Gunther's high heat flux experimental data, Plesset and Prosperetti [106] concluded that latent heat transport represents only a small fraction of the total heat transfer. They suggested that latent heat transport may be significant in saturated and slightly subcooled boiling but becomes less important at higher subcooling, presumably due to shorter exposure time. They did not consider the sliding effect. On the other hand, Bankoff and Mikesell [56] have demonstrated that uncertain predictions of bubble internal pressure, through a kinetic theory approach, can cause large errors in the calculated amount of latent heat transport. Such heat transport was assumed to account for as much as 40% of the total heat, thus bringing to question the relative importance of these two major heat transfer mechanisms. The latent heat contribution may even prevail in the case of sliding bubbles due to significant augmentation of microlayer evaporation, as pointed out by Tsung-Chang and Bankoff [107].

There are clearly two different heat transfer modes associated with the two types of bubble behaviour described in Chapter 3. The first type, which starts right after the ONB, concerns bubbles that slide long distances on the heater before eventually being ejected into the liquid. The amount of void at the early stages of the boiling process is insignificant. The explosive bubble growth soon after nucleation is later replaced by balanced evaporation and condensation rates leaving bubbles with fairly constant size and shape for a significant amount of time. The changes in size and occasional detachments occur mainly due to local instabilities, turbulent fluctuations or bubble coalescence. It was shown earlier that bubble sliding velocities do not differ significantly from that of the bulk liquid. Hence, it can be concluded that the heat transfer in the low heat flux region is mainly associated with forced convection in the bulk liquid (macroconvection) and evaporation (latent heat). Within this region, the overall heat transfer coefficient depends on the mass flow rate. This corresponds to partial nucleate boiling. It is important to note that occasional detachments and reattachments do not significantly affect the overall heat transfer rate in this region.

With increasing heat flux at a fixed flow rate, the amount of bubbles (number of active nucleation sites) rises, thus increasing the influence of the evaporative component in the overall heat transfer. The sliding distances become much shorter. Typical bubbles slide for a maximum of a couple of diameters before being ejected into the liquid core. The bubble lifetimes are much shorter (in the order of a couple of milliseconds). The initially fast bubble growth is reduced due to increasing condensation rates at the top of the bubble and balances off at the moment the bubble reaches its maximum diameter. The condensation rate becomes larger than the growth rate while the bubble is still attached to the wall. Hence, departing bubbles are typically smaller than their maximum size. They are also elongated in the direction normal to the wall. Detachments are regular and significantly affect the overall heat transfer.

Three main effects on the overall heat transfer can be distinguished. The first two are common for both the partial nucleate boiling region and the fully developed boiling region.

Forced convection in the bulk liquid – "macroconvection": The bulk liquid is flowing mainly undisturbed by the bubbles (low void). Local disturbances certainly cause additional turbulence and microconvection although that does not seem to be affecting the heat transfer significantly. This is evident from the fact that for the low heat flux region, the heat transfer coefficients agree relatively well with those predicted from single phase forced convection correlations.

Evaporation: Most of the evaporation in the case of subcooled boiling occurs in the thin liquid layer underneath the bubble, called the microlayer. In the partial nucleate boiling region, most of the heat "consumed" by the bubble is being released at the top in form of latent heat due to condensation. If the evaporation rate is balanced by the condensation rate, as in partial boiling, the heat flux removed by evaporation remains fairly constant. As a result the q vs ΔTsat curve remains flat. A small increase in the heat transfer rate with increasing wall temperature is due to the activation of new nucleation sites.

"Microconvection" would be a characteristic of fully developed boiling. It is associated with fast bubble growth. Some hot liquid surrounding the cavity at the initial stage is pushed away from the wall by the growing bubble. Also, the bubble that detaches from the wall travels quickly into the fluid core leaving space for cooler liquid to rush in and localy cool down the surface. The experimental evidence for this type of behaviour exists and is characterized by a waiting time, i.e., the time that is needed for the surface temperature to again reach the bubble initiation level. More active nucleation sites and lower bubble lifetimes as the wall temperature rises lead to more significant "bubble agitation" and result in the dramatic increase of heat transfer rates and the slope of the q vs Tsat curve.

4.5 Model for the Transition from Partial to Fully Developed Boiling

4.5.1 Formulation of the Model

It has been experimentally observed that, as one departs from the "low heat flux region" characterized by small amount of bubbles sliding over significant lengths on the heater and rare detachments, the increase in the heat flux for a constant flow rate leads to

a dramatic drop in sliding distances. As one enters the "isolated bubble region", the heat transfer mode changes accordingly. One can suggest that this transition corresponds to the transition from partial to fully developed boiling. The change of typical sliding distances scaled with the maximum diameters vs Bo, from experimental data at p = 2 bar and p = 3 bar, is shown in Figure 4.8.

Further analysis requires the introduction of certain simplifications:

- It can be shown that the subcooling (within the experimental range 10-30K) has a relatively small influence on the overall bubble behaviour as compared to the effect of the heat flux and flow rate. A transition from the "low heat flux region" to the "isolated bubble region" was noticed at all subcoolings.
- The effect of the pressure appears to be minor in this case and it is excluded from the analysis.
- Local disturbances of the velocity field and thermal boundary layer due to turbulence or to the presence of the growing bubble as well as the roughness of the surface are not taken into account

Having adopted these simplifications, one is left with the concept that the thickness of the thermal boundary layer relative to the size of the bubble (i.e. evaporation over condensation rate) regulates the overall bubble behaviour and hence the heat transfer. In other words, there is a high heat flux and high flow rate situation which renders the same behaviour of the bubble (smaller bubble, thin thermal layer) as a corresponding low heat flux and low flow rate experiment (larger bubble, thicker thermal layer). In this simplified model it is assumed that all experimental data can be represented by a single curve, as shown in Figure 4.9. The slope of the curve shows that the flow rates (convective boiling term) do not affect the overall heat transfer in the fully developed boiling region, which was also suggested by Shah [99] . In that case the change of Bo corresponds to the change of the heat flux.

Having examined the drop of the sliding distances, one can assume that the limit of the curve Lp_{ejc}/D_{max} vs Bo when $Lp_{ejc}/D_{max} \rightarrow \infty$ yields Bo_{TRANS}, or, in other words, the heat flux that corresponds to the transition point. Figure 4.9 shows the experimental data

correlated with equation (4.10). From the limit of the equation (4.10) the transition boiling number equals $Bo_{TRANS} = 2.557*10^{-4}$.

$$\frac{Lp_{ejc}}{D_{max}} = 0.202 + \frac{1.359 \cdot 10^{-4}}{Bo - 2.557 \cdot 10^{-4}} \tag{4.10}$$

The Shah correlation can be used for comparison. Shown in Figure 4.10 is the application of Shah correlation to the experimental data of Bibeau and Salcudean at p = 2 bar. Similar graphs can be obtained for all pressures within the experimental range.

It is evident that the transition from partial to fully developed boiling occurs at $\Delta T_{sub}/\Delta T_{sat} = 2$, which is in excellent agreement with Shah's observations. In addition to this, if one calculates the Boiling number, Bo, which corresponds to the transition point, from the transition curve equation (4.11) as suggested by Shah, one will obtain the value of $Bo_{TRANS}=2.52*10^{-4}$ which corresponds to the limit of the curve Lp_{ejc}/ D_{max} vs Bo in Figure 4.9. The transition curve, as suggested by Shah [99], is given by:

$$\frac{\Delta T_{sub}}{\Delta T_{sat}} = 6.3 \cdot 10^{-4} Bo^{1.25} \tag{4.11}$$

Equation (4.11) is valid for $\Delta T_{sub}/\Delta T_{sat} \leq 2$, which corresponds to lower Bo values. For higher Bo numbers the value $\Delta T_{sub}/\Delta T_{sat}$ remains constant and equals to 2. By introducing $Bo_{TRANS} = 2.557*10^{-4}$ and $\Delta T_{sub}/\Delta T_{sat} =2$ into equation (4.8) one can obtain the heat flux corresponding to the transition from partial to fully developed boiling for the given range of pressures, subcoolings and flow rates. The proposed model for the transition point from partial to fully developed boiling is:

$$q_{TRANS} = A \cdot \Delta T_{sub}^{\ 0.646} \tag{4.12}$$

where:

$$A = \frac{3}{2} h_{FC} \exp(14.542)\left(2.557 \cdot 10^{-4}\right)^{0.729}\left(\frac{c_p}{i_{fg}}\right)^{-0.354}\left(\frac{\rho_v}{\rho_l}\right)^{1.811} Pr^{7.032} \tag{4.13}$$

The heat transfer coefficient h_{FC} can be obtained from the Dittus-Boelter equation.

4.5.2 Comparison of the Proposed Model with Previous Models

The comparison of the present model with the models of Shah and Kandlikar for the transition point is shown in Figures 4.11 and 4.12. The graphs show the transition point at various flow rates and subcoolings of 10, 20 and 30K, at pressures of p=1bar and p=3 bar. The parameter on the horizontal axis represents the normalized transition heat flux. It corresponds to the location of the transition point relative to ONB and OSV. The model used for the prediction of ONB is that of Hahne et al. [21]. The location of the OSV has been calculated using the Bibeau and Salcudean's modification of the model of Saha and Zuber, as explained in detail earlier in the text.

Excellent agreement with the model of Kandlikar has been obtained for all pressures and subcoolings. Similar observation can be made after comparing data with the model of Shah.

4.6 Concluding Remarks

A simple model for the transition point from partial to fully developed flow boiling has been proposed. The first step in modelling included the modification of the heat transfer correlation of Moles and Shawn [103]. The new heat transfer correlation agrees well within +/-20% error with the experimental data.

The transition point model is based on the observed change of the bubble behaviour with the boiling number Bo and the sharp drop of bubble sliding distances prior to ejection. The "low heat flux region" corresponds to partial boiling and the dominant heat transfer mode is that of latent heat. The change in the bubble behaviour promotes bubble agitation and microconvection as the heat transfer mode and indicates the transition to fully developed boiling.

The simplicity of the model lays in the inclusion of the parameter Lp_{ejc}/D_{max} (normalized sliding distance of the bubble prior to ejection) which is assumed to be independent of the subcooling and pressure, and hence a function of Bo solely. The limit of this function when $Lp_{ejc}/ D_{max} \rightarrow \infty$ returns the Bo number corresponding to the transition point. The obtained transition Boiling number Bo_{TRANS} and the ratio $\Delta T_{sub}/\Delta T_{sat}$ show excellent agreement with the model of Shah. With the fixed value of the transition

Boiling number and $\Delta T_{sub}/\Delta T_{sat}$, one can obtain the location of the transition from partial to fully developed boiling from the heat transfer correlation.

There are limitations due to simplicity of the model. At this stage the model is restricted to the experimental range of subcooling (10 – 30 K) and low liquid velocities (0.08 – 0.8 m/s) corresponding to available experimental data. Although it appears to be within accepted limits of accuracy for the given range of experiments, it is generally not acceptable that the transition is limited to one particular point (i.e. $Bo_{TRANS}=2.557*10^{-4}$ and $\Delta T_{sub}/\Delta T_{sat}=2$). The transition curves in Shah's model permit more flexibility, which explains the discrepancy between the two models in Figures 4.11 and 4.12. However, the the observed link between the sliding distances (bubble behaviour) and changes in heat transfer represents a step forward toward better understanding of the transition from partial to fully developed boiling.

Table 4.1 Heat transfer correlations for fully developed subcooled flow boiling

McAdams et al. (1949)	$q = 4.77\Delta T_{sat}^{3.86}$
Jens and Lottes (1951)	$\Delta T_{sat} = 25q^{0.25} \exp(p / 62)$
Thom et al. (1965)	$\Delta T_{sat} = 22.65q^{0.5} \exp(p / 87)$
Shah (1977)	$q = h_{FC} 230Bo^{0.5} \Delta T_{sat}$ where h_{FC} from Dittus-Boelter correlation
Aladiev (1957)	$\Delta T_{sat} = \left[39.2 - 0.1\left(T_{sat} - 273.16\right)\right]q^{0.3}$
Labuntzov (1972)	$\Delta T_{sat} = \frac{1 - 0.0045p}{3.4p^{0.18}} q^{0.3}$
Kandlikar (1998)	$q = \left[1058h_{FC}\Delta T_{sat}(Gi_{fg})^{0.7}\right]^{3.33}$ where h_{FC} from Petukhov and Popov (1963) correlation

Table 4.2 Heat transfer correlations for subcooled flow boiling based on dimensional analysis

Papell (1963)	$Nu_{tp}/Nu_l = 90Bo^{0.7}Ja^{*-0.84}(\rho_v/\rho_l)^{0.056}$
Badiuzzaman (1967)	$Nu_{tp}/Nu_l = 178Bo^{0.75}Ja^{*-0.9}(\rho_v/\rho_l)^{-0.06}(\Delta T_{sub}/T_{sat})^{0.45}$
Moles and Shaw (1972)	$Nu_{tp}/Nu_l = 78.5Bo^{0.67}Ja^{*-0.5}(\rho_v/\rho_l)^{-0.03}Pr^{0.45}$

Table 4.3 Heat transfer correlations for partially developed subcooled flow boiling

Bergles and Rohsenow (1964)	$\frac{q}{q_{FC}} = \left[1+\left[\frac{q_{FDB}}{q_{FC}}\left(1-\frac{q_{FDBi}}{q_{FDB}}\right)\right]^2\right]^{0.5}$ q_{FDB} – not specified; correlation suitable for particular boiling conditions q_{FDBi} – represents q_{FDB} at ONB
Pokhvalov et al. (1966)	$\Delta T_{sat} = \Delta To\left[1+\left(\frac{\Delta To}{\Delta q}h_{FC}\right)^{1.5}\right]^{-\frac{2}{3}}$ $\Delta To = 0.11\frac{T_{cr}^{0.82}M^{0.18}}{p^{0.36}}\Delta q^{0.36}e^{-5.6\frac{T_{sat}}{T_{cr}}}$ $\Delta q = q - h_{FC}\Delta T_{sub}$
Shah (1977)	$\Delta T_{sat} = \left(\frac{q}{0.54\Psi_0 h_{FC}}\right)^{8.33}\Delta T_{sub}^{-7.83}$ $\Psi_0 = \begin{cases} Bo > 0.3\cdot10^{-4} \Rightarrow 230Bo^{0.5} \\ Bo < 0.3\cdot10^{-4} \Rightarrow 1+46Bo^{0.5} \end{cases}$ where h_{FC} from Dittus-Boelter correlation
Kandlikar (1998)	$q = a + b\Delta T_{sat}^{\ m}$ $a = q_{ONB} - b(\Delta T_{sat,ONB})^m$ $b = \frac{\left[1058h_{FC}\Delta T_{sat,TRANS}(Gi_{fg})^{-0.7}\right]^{3.33} - q_{ONB}}{\Delta T_{sat,TRANS}^{\ m} - \Delta T_{sat,ONB}^{\ m}}$ $m = n + cq$ $c = \frac{2.33}{\left[1058h_{FC}\Delta T_{sat,TRANS}(Gi_{fg})^{-0.7}\right]^{3.33} - q_{ONB}}$ $n = 1 - cq_{ONB}$ where the $DT_{sat,ONB}$ and q_{ONB} are from Hsu (1962), and Sato and Matsumura (1964) h_{FC} from Petukhov and Popov (1963) correlation

Table 4.4 Transition from partially to fully developed subcooled flow boiling

Bowring (1962)	$q_{TRANS} = 1.4q_{INTERSECT}$ where $q_{INTERSECT}$ is the intersection between the single-phase forced convection curve and the fully developed boiling curve
Shah (1977)	$\frac{\Delta T_{sub}}{\Delta T_{sat}} = 2\ ;\ q_{TRANS} = h_{FC}230\left(\frac{q_{TRANS}}{Gi_{fg}}\right)^{0.5}\frac{\Delta T_{sub}}{2}$
Kandlikar (1998)	$q_{TRANS} = \frac{1.4\left[\left(\frac{q_{TRANS}}{1.4}\right)^{0.3} + 1058h_{FC}(Gi_{fg})^{-0.7}\Delta T_{sub}\right]}{1058(Gi_{fg})^{-0.7}}$ iterative procedure needed; ΔT_{sub} calculated for $q=q_{TRANS}/1.4$

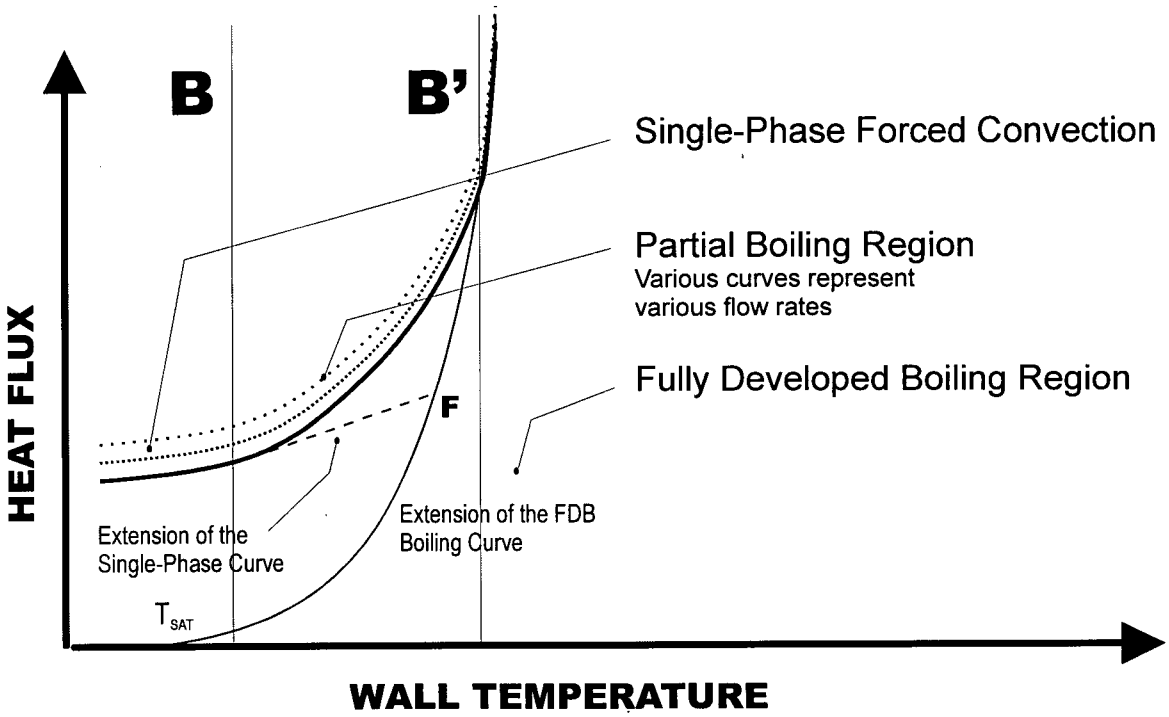

Figure 4.1 The flow boiling curve

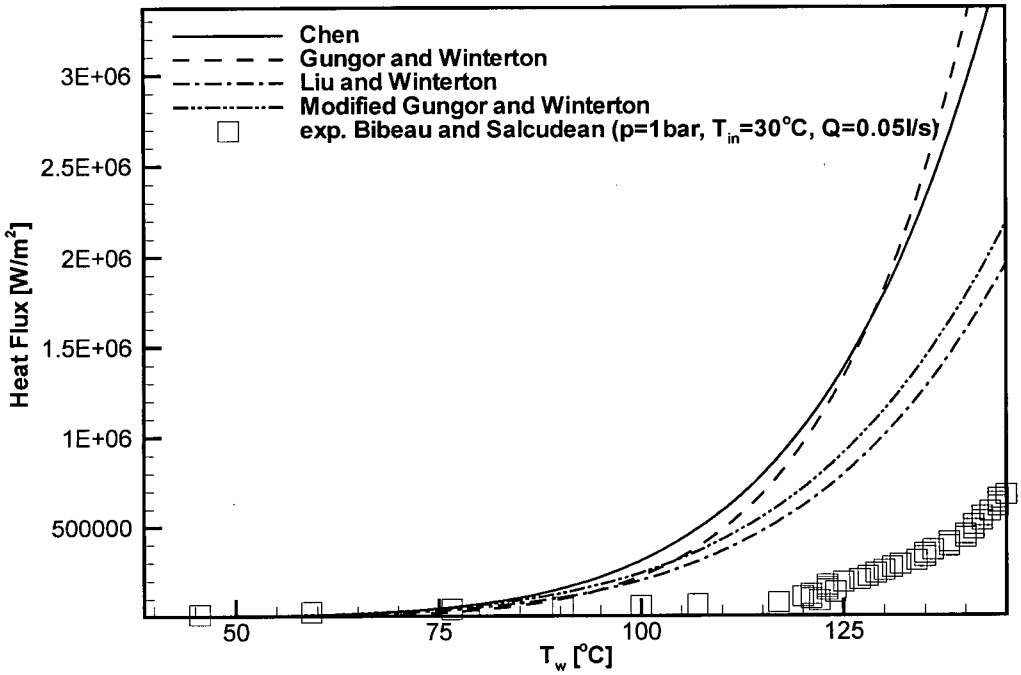

Figure 4.2 Chen-type correlations compared with experiments at p=1bar

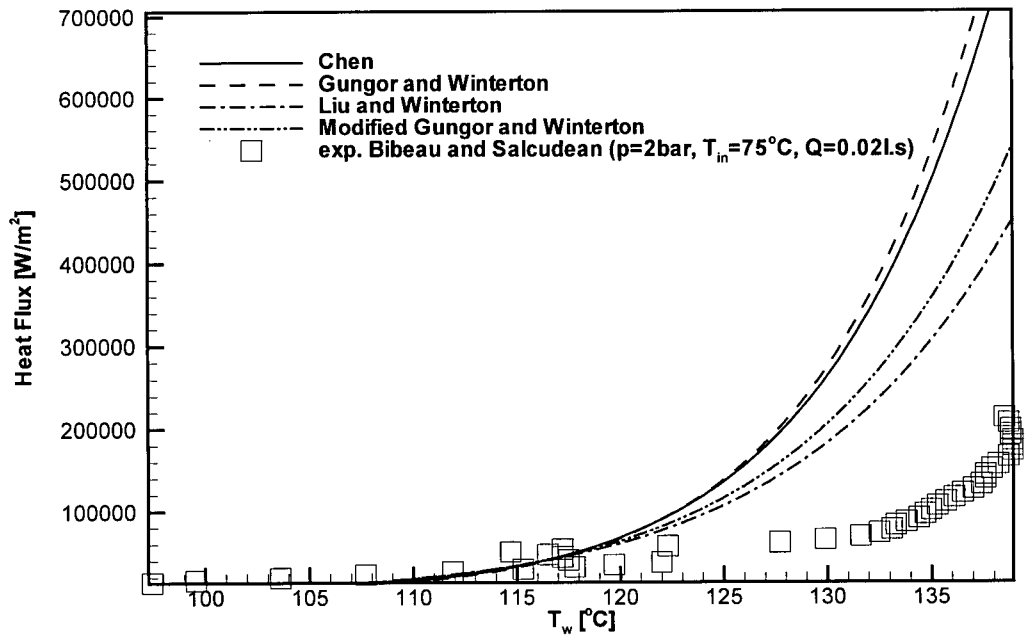

Figure 4.3 Chen-type correlations compared with experiments at p=2bar

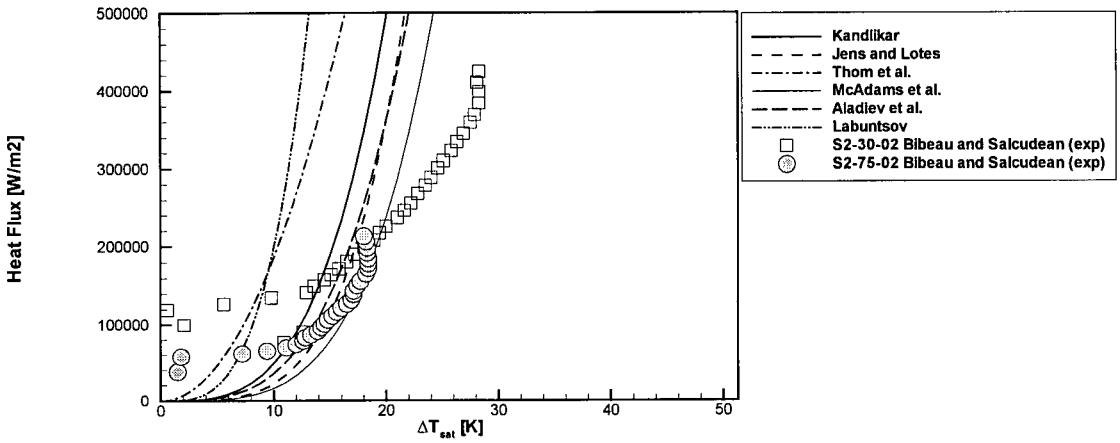

Figure 4.4 Fully developed boiling (FDB) correlations
Experiment S2-30-02 (p=2bar, T_{in}=30°C, Q=0.02l/s) – high subcooling
Experiment S2-75-02 (p=2bar, T_{in}=75°C, Q=0.02l/s) – low subcooling

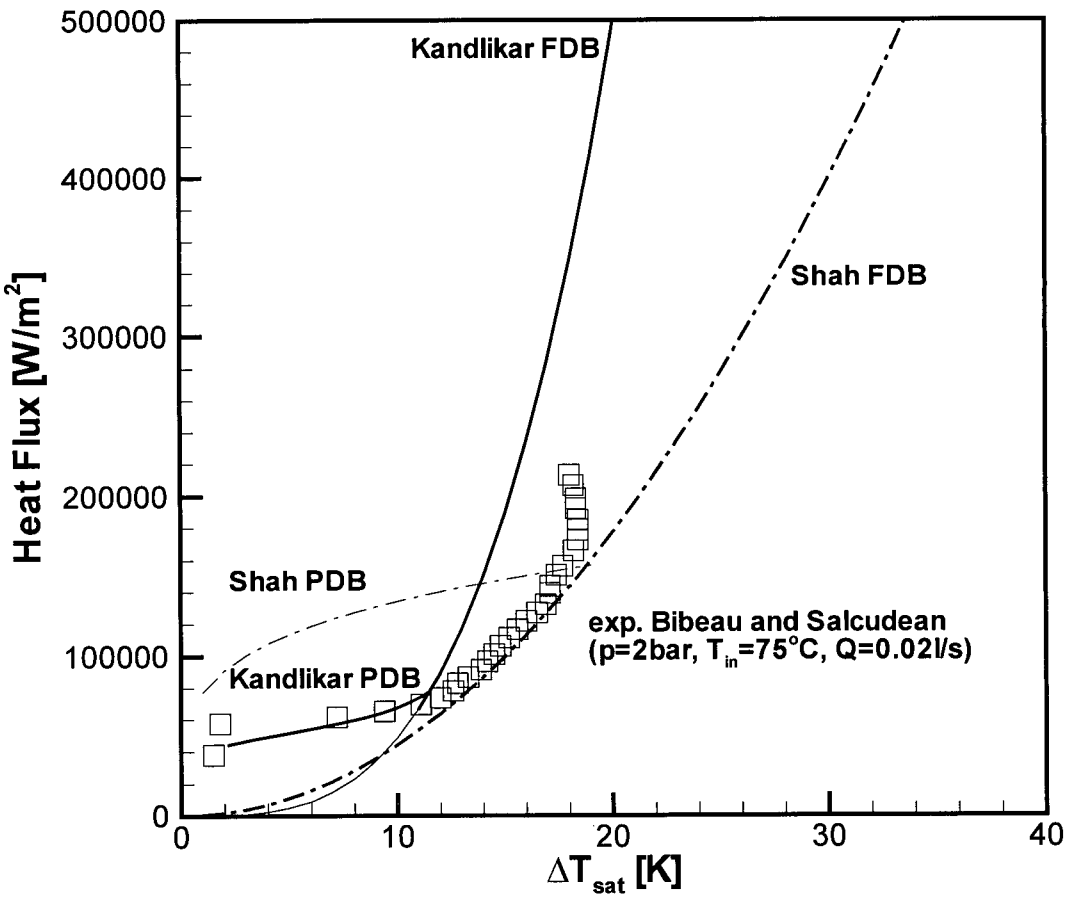

Figure 4.5. Correlations of Shah and Kandlikar in partial and fully developed boiling

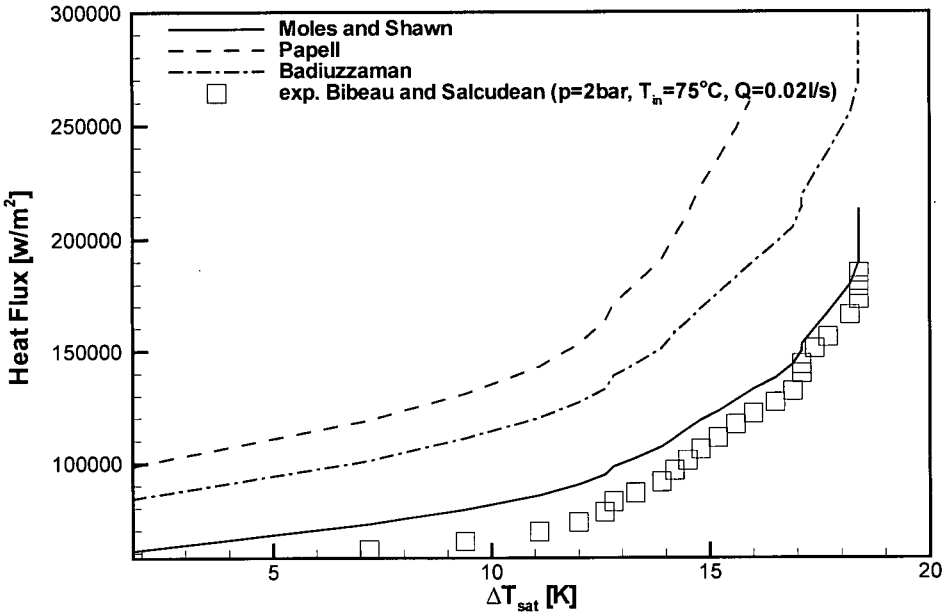

Figure 4.6 Correlations based on dimensional analysis

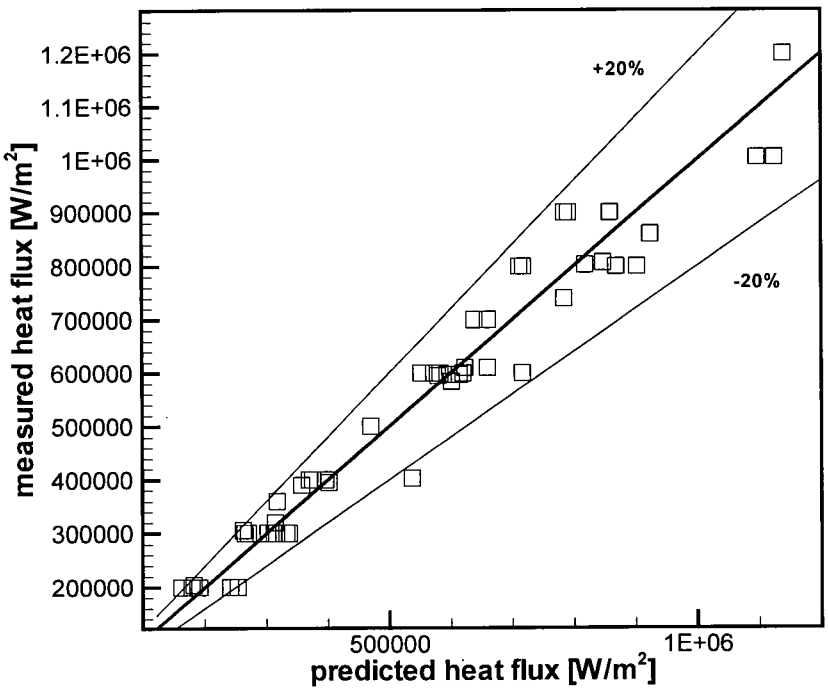

Figure 4.7 Proposed heat transfer correlation compared with combined experimental data of Faraji et al. (1994) at p=1bar and from the present study at p=2bar and p=3bar

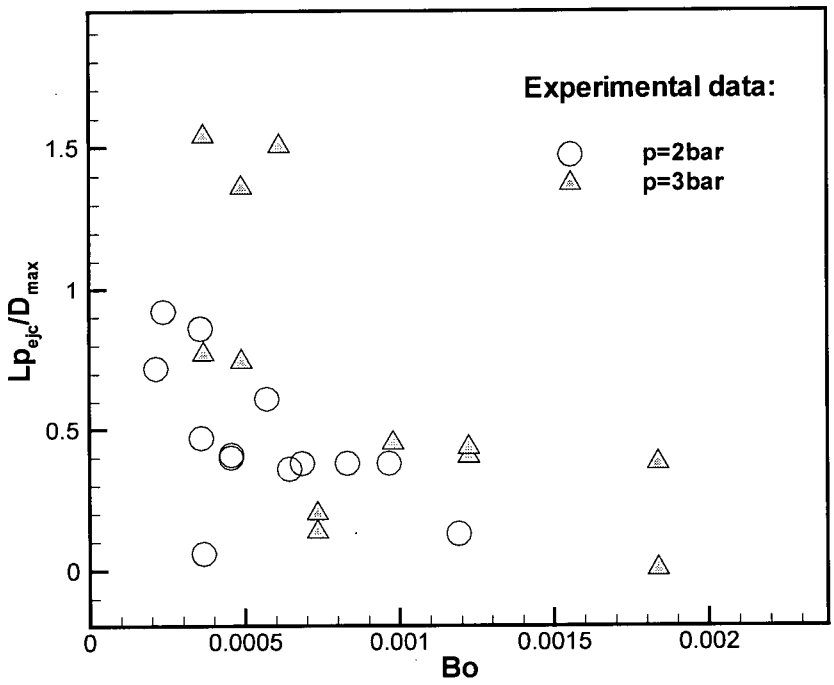

Figure 4.8 Normalized parallel displacement – experimental data

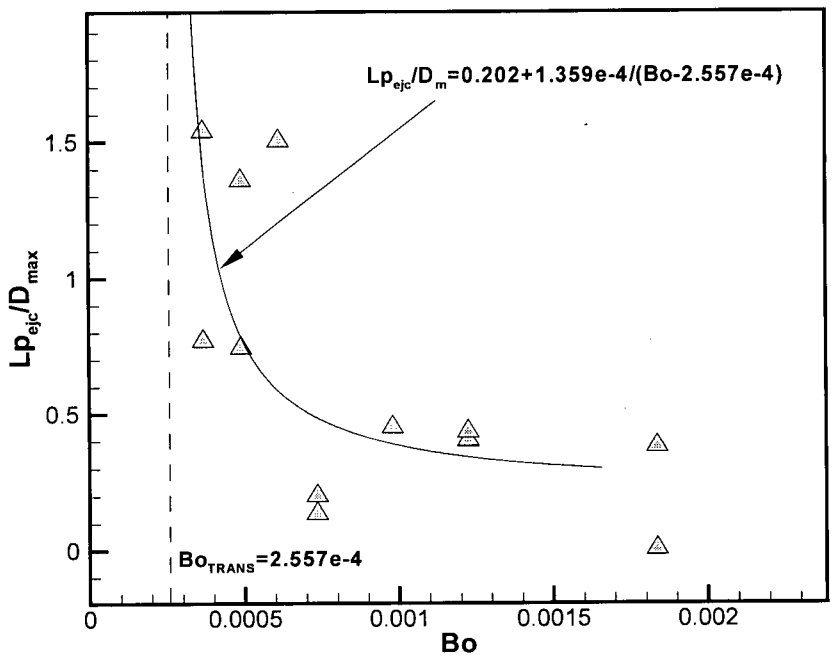

Figure 4.9 Normalized parallel displacement correlation shown with experimental data at p=3bar

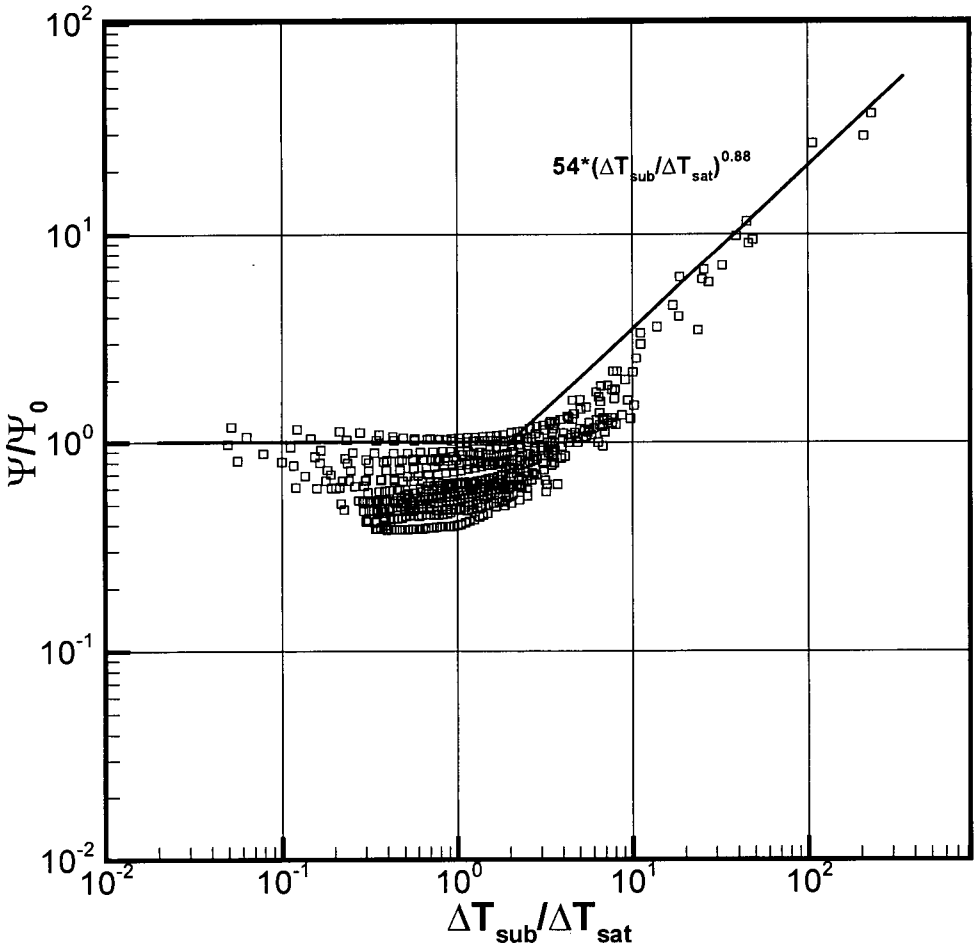

Figure 4.10 Transition point prediction from Shah model
Compared with experimental data of Bibeau and Salcudean

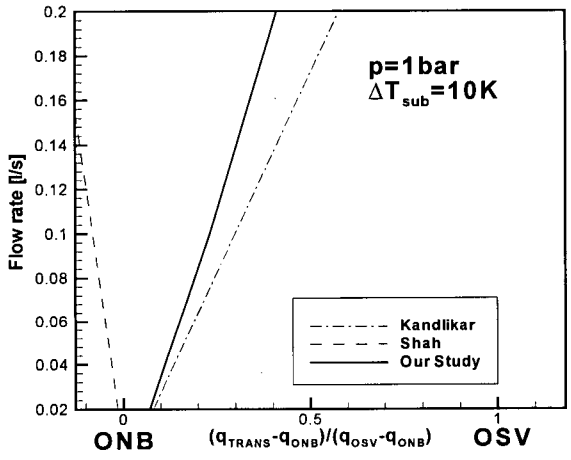

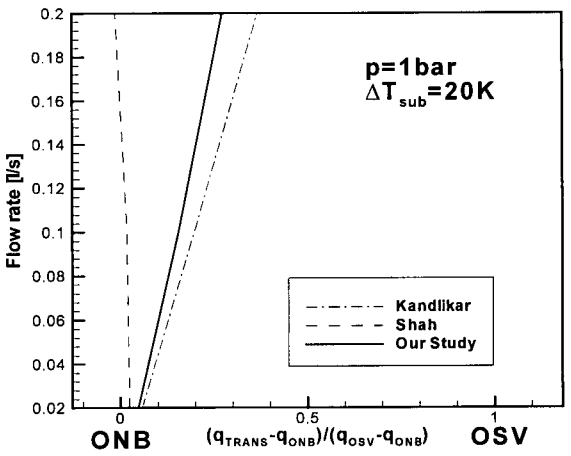

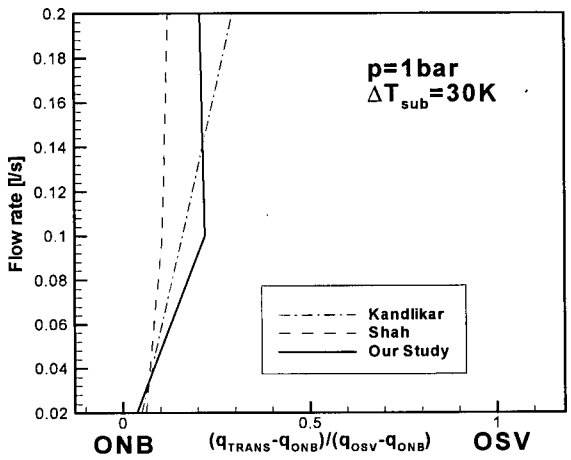

Figure 4.11 Prediction of the transition point

Comparison of the proposed model
with models of Shah and Kandlikar for p=1bar

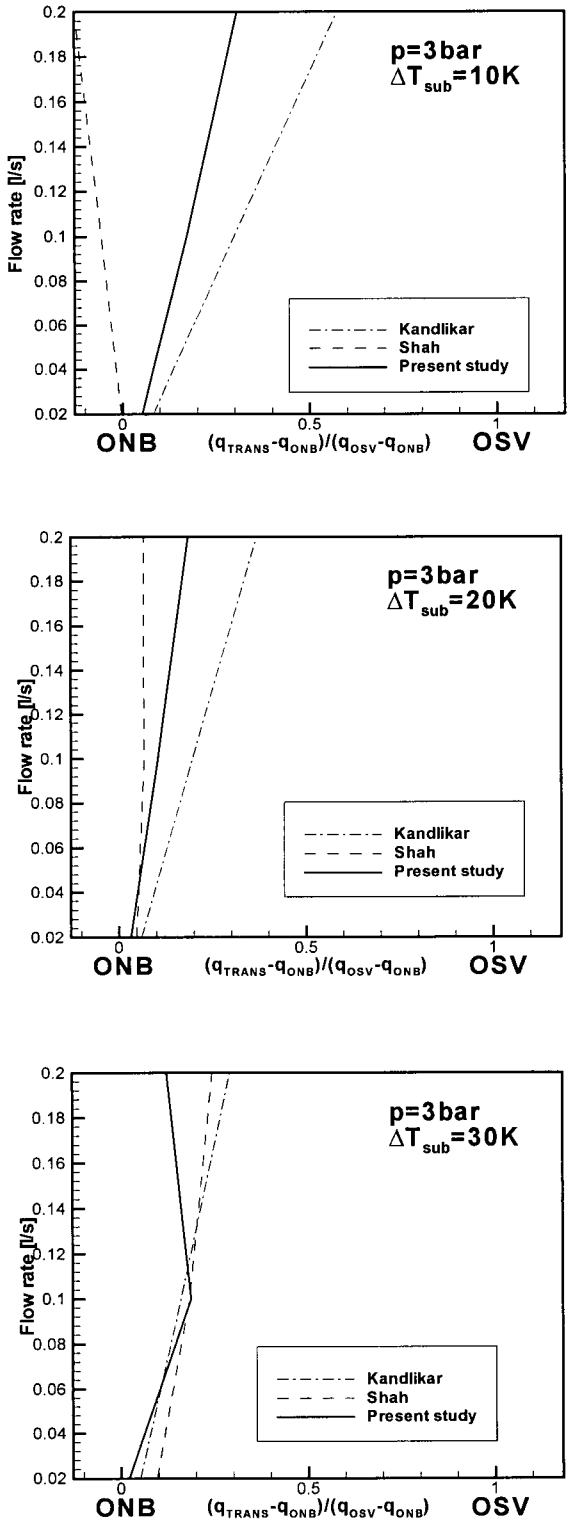

Figure 4.12 Prediction of the transition point

Comparison of the proposed model
with models of Shah and Kandlikar for p=3bar

Chapter 5

FORCES ACTING ON A SINGLE BUBBLE IN SUBCOOLED FLOW BOILING

In this section, the major forces exerted upon bubbles are discussed and the most important force balance models in subcooled flow boiling are critically reviewed. A new force balance model is suggested. Also, an attempt is made to establish a new criterion for normal bubble detachment, based on experimental observations and the proposed force balance.

5.1 Background Information and Literature Review

Models for prediction of the bubble detachment diameter are typically based on force balances. Therefore, the investigation of forces acting on individual bubbles during their growth on the heated surface is an important part of void growth modelling. It is also crucial in investigating the microconvective component of the heat transfer.

Fritz (1935) derived a criterion for bubble departure by considering a balance of the buoyancy and the surface tension forces in a superheated liquid. This is the earliest known relation for the departure radius based on a force balance. Following these early studies, the process of bubble inception, growth and detachment in the pool boiling domain has been described by many other authors. Fewer studies appear in the open literature for the case of flow boiling.

Chang [27] categorized the forces exerted on a growing bubble in a flowing liquid as follows:

- Gravitational forces
- Surface tension
- Pressure gradient forces
- Inertia forces of the vapor and liquid

- Resistance due to molecular and eddy viscosities
- Forces due to circulation inside the bubble
- Virtual mass and "Basset" force

He also suggested a set of initial assumptions which would simplify attempts to quantitatively predict these forces:

- Parameters such as bubble size or bubble frequency can be approximated by statistically mean values
- Bubbles are considered as spheres or as equivalent spheres
- Bubbles detach or are about to detach at their maximum size (hydrodynamic and thermodynamic equilibrium)

However, one can conclude from recent experimental data that, in the case of subcooled flow boiling, the latter two assumptions are generally not valid.

Most earlier models take into account only static forces (buoyancy, flow drag and surface tension) neglecting the dynamics of the bubble growth. Levy [35] obtained a vapour bubble detachment diameter for upflow subcooled boiling of water by considering a balance of buoyancy, shear and surface tension forces. Koumoutsos et al. [85] considered the case of horizontal forced convection saturated boiling of water from an artificial nucleation site. They arrived at a bubble departure criterion by balancing the drag, surface tension and gravitational forces.

In a detailed analysis of the forces acting on the bubble in pool boiling, Beer et al. [108] suggested that dynamic forces such as inertia, dynamic drag and pressure must be included in addition to static forces. The order of magnitude of dynamic forces depends on bubble growth rate or acceleration of the bubble. Beer's analysis included the buoyancy force, the pressure force (consisting of the dynamic excess vapor pressure and the capillary pressure both of which contribute to bubble detachment), inertia forces (which may support or oppose bubble detachment, depending on whether the bubble is decaying or growing), the surface tension force and drag forces (both of which oppose bubble detachment).

Very few similar studies have been carried out for flow boiling. Due to the forced convection effects and disturbances in the flow field caused by the growth of the bubble in the flowing liquid, models developed in the pool boiling domain are usually not applicable to flow boiling. In general, simple force balances which take into account only static forces (Levy, Koumoutsos et al.) were insufficient for modeling vapor bubble departure data in forced convection boiling, as concluded by Cooper et al. [89].

It is well accepted that, during flow boiling, bubbles are typically inclined in the direction of flow. Models for flow boiling should take into consideration the difference between the receding and advancing contact angles of the attached bubble, as well as the importance of the inclination angle of the bubble. The asymmetrical growth of a bubble produces parallel components of forces which, in pool boiling, are assumed to act only in the normal direction.

Al-Hayes and Winterton [109] developed a force model by assuming that the bubble has the form of a truncated sphere. A major improvement of the Al-Hayes and Winterton model is the consideration of the effect of different upstream and downstream contact angles. When this difference is taken into account, a parallel component of the surface tension force results. This force is opposed by the buoyancy and flow drag force for vertical upward flow. Rogers et al. [37] used this model for predicting bubble detachment in vertical flow boiling at low pressures. The three forces are:

The buoyancy force:

$$F_b = \rho_l g \frac{\pi R^3}{3}\left(2 + 3\cos\theta - \cos^3\theta\right) \tag{5.1}$$

The drag force:

$$F_d = C_d R^2 \frac{\rho_l U^2}{2}\left(\pi - \theta + \cos\theta\sin\theta\right) \tag{5.2}$$

The surface tension force:

$$F_\sigma = C_s \frac{\pi R}{2}\sigma \sin\theta\left(\cos\beta - \cos\alpha\right) \tag{5.3}$$

where U is the velocity of the fluid at the position of the center of mass of the bubble, C_d is the drag coefficient (1.22 for $20<Re_B<400$), and θ is the equilibrium contact angle (assumed to have values between the receding, β, and advancing contact angle, α). The surface tension coefficient has the following form:

$$C_s = \frac{58}{\theta + 5} + 0.14 \tag{5.4}$$

where θ is in degrees.

Bibeau [6] concluded that a static force model was sufficient to predict the diameter for parallel detachment (the beginning of the sliding phase). He found that the model of Al-Hayes and Winterton [109] approximated the radius of the bubble at parallel detachment for given experimental conditions. At low liquid velocities the model over-predicted the experimental data. Bibeau also showed that the pool boiling model of Beer et al. [108] was not sufficient to predict the point of normal detachment for vertical upward flow boiling at atmospheric pressure for low liquid velocities.

Klausner et al. [81] investigated bubble departure (parallel detachment) and lift-off (normal detachment) during horizontal, saturated flow boiling of R113. Their experimental observations of bubble behaviour agree with the results of Bibeau and Salcudean [39] and those from the present study. Bubbles were seen to slide after nucleation and prior to lift-off. Bubbles were also seen to be inclined in the direction of flow due to the hydrodynamic drag force. Asymmetric bubble growth creates an additional force due to the resistance of the liquid, which opposes the flow and prevents the bubble from departing from the nucleation site. They concluded that two major parameters influencing departure diameters are the liquid velocity and wall superheat.

Zeng et al. [110], [82] used the same force balance to create a unified model for both pool boiling and flow boiling of saturated liquids. The apparent difficulties in defining the inclination angle and the bubble base in the model of Klausner et al. [81] were overcome by assuming that the contact area of the bubble at points of departure and lift-off is small. This leads to a negligible surface tension force. The model allows for simultaneous solution of bubble diameters and inclination angles.

Van Helden et al. [111] examined the relative importance of various forces on bubbles growing from an artificial cavity in a vertical upward flow. Two types of experiments were reported. In the first experiment, vapour bubbles were generated by local heating of the cavity. In the second experiment, nitrogen bubbles of about the same size were injected isothermally. Differences were noticed in bubble trajectories. Steam bubbles were seen to take off into the liquid while nitrogen bubbles were typically sliding parallel to the wall. Major contributions accounted for in the force balance were buoyancy, lift, drag and surface tension. Van Helden et al. [111] explained the differences in observed bubble behaviour of steam and nitrogen bubbles due to the action of the temperature drop force. The temperature drop force represents an additional force due to the gradient of surface tension in a non-uniform temperature field. The temperature gradient was present in the experiment with vapour bubbles and absent in the second experiment. The variation of surface tension induces flow in the fluid along the bubble, called Marangoni flow. The effect of Marangoni convection on the growth of bubbles has been investigated elsewhere (Gaddis [112], Kao and Kenning [113]).

Kandlikar and Stumm [86] used a control-volume approach in order to investigate separately the forces on the upstream and downstream facing portions of the bubble. The forces due to surface tension, drag, buoyancy, pressure difference and momentum changes were considered. They concluded that, for small bubbles (less than 0.5mm in diameter), bubble detachment was initiated at the front edge through a sweep-removal mechanism.

One model gaining significant interest and divided opinions amongst researchers is that of Buyevich and Webbon [73]. They presented a force model that applies to nucleate pool boiling conditions. Their model is based on the conservation of mechanical energy for a truncated sphere with a clear distinction between two independent dynamic equations that describe bubble expansion and translational motion. This approach allows for estimating the portion of any accounted force that affects either bubble expansion or translational motion.

Buyevich and Webbon concluded that surface tension produces an effective force that facilitates bubble detachment. This statement is in contradiction with all preceding

theoretical papers on the subject. However, it gives a reasonable explanation for a number of visual observation during bubble ejection, when bubbles are propeled into the liquid core in the direction normal to the heater surface. This statement is in accordance with an explanation of the bubble ejection process given earlier by Bibeau [6]. Bibeau also concluded that the surface tension gradient actually produces a force which facilitates detachment.

The present analysis is driven by the fact that most bubble detachment models are based on force balances that disagree with experimental evidence at low pressure and low flow rate subcooled boiling. Significant variations of bubble shapes and deviations from spherical, as well as sliding and partial condensation on the wall, have to be included in the force model. Experimental evidence on bubble behaviour decribed in Chapter 3 as well as experimental results of Bibeau and Salcudean [39] with the same experimental apparatus were used in the analysis.

5.2 Identification of Forces

The most recent and probably one of the most complete reviews on bubble forces and detachment models is presented by Klausner [114]. The following text is based on this review and includes a quantification of these forces based on the experimental data of the current study.

The analysis is restricted to isolated bubbles and, hence, excludes thermal or fluid-dynamic influences from neighbouring bubbles. Shown in Figure 5.1a is a bubble modelled as spherical segment on the vertical wall. Major forces acting on such bubble are shown in Figure 5.1b. According to Newton's second law, the sum of forces acting on an isolated bubble has to be equal to the rate of change of the momentum:

$$\vec{F}_g + \vec{F}_\sigma + \underset{S1}{\iint} \sigma \vec{n} dS + \underset{S2}{\iint} p_v(-\vec{n})dS + \vec{R} = m\frac{d\vec{V}}{dt} \qquad (5.5)$$

In equation (5.5) $\vec{F}_g$ is the *body* or *gravitational force*. It represents the effect of the mass of vapour. It is given as:

$$\vec{F}_g = \rho_v \vec{g} V_B \qquad (5.6)$$

The body force acts at the center of gravity. For the case of upward vertical flow this force prevents bubbles from sliding. It is generally very small compared to other forces. The estimated order of magnitude for the present experiments is 10^{-9} N.

$\vec{F}_\sigma$ is the *surface tension force*. It acts on the edge of the circular bubble base, S2. It is defined by equations (5.3) and (5.4). It is obvious that bubbles growing symmetrically with respect to the normal of the heater surface will have only a normal component of the surface tension force. Inclined bubbles will create a component parallel to the surface of the heater. For bubbles inclined in the direction of flow, the parallel component will oppose bubble sliding motion. The surface tension force is important for the type of boiling found in present experiments. However, the action of this force is subject to discussion. Particular attention to defining this force will be given in subsequent sections.

The third term in equation (5.5) represents the liquid stress at the liquid –vapour interface, S1. It includes both, normal and tangential components of the stress tensor. The fourth term is the normal stress due to vapour pressure at the vapour-solid interface, S2. It creates a net pressure force which acts to remove the bubble from the surface. The variable $\vec{n}$ represents an outward pointing vector in the direction normal to the bubble surface.

$\vec{R}$ is the reaction force introduced by Klausner [114]. It results from the London-van der Waals force acting through a thin liquid film close to the three-phase line (TPL) in the microlayer, which resides underneath the bubble. The size of this thin film is of molecular scale. The widely accepted normal detachment criterion is that the sum of forces in the direction normal to the heater becomes zero, hence, according to Klausner $R_y = 0$. This reaction force will not be analyzed in the present study.

After a redistribution of parameters in the two surface integrals in equation (5.5) a relatively simple mathematical procedure [114] returns three important forces: buoyancy, contact pressure and the hydrodynamic force. Only final equations will be given.

The *buoyancy force* is given by:

$$\vec{F}_b = -\rho_l \vec{g} V_B \tag{5.7}$$

For the case of vertical upward flow, the buoyancy force aids sliding. The order of magnitude of this force for typical vapour bubbles under present experimental conditions is about 10^{-5} N.

The *contact pressure force* acts upon the vapour-solid contact area in a direction normal to the surface, thus facilitating bubble detachment. It can be expressed as:

$$\vec{F}_{cp} = \frac{d_{base}{}^2\pi}{4}\left(\frac{2\sigma}{r_c}\right)\vec{e}_y \tag{5.8}$$

where r_c is the radius of curvature on the top of the bubble and $\vec{e}_y$ is the unit vector in the y-direction. The contact pressure force has to be taken into account as long as a stable vapour-solid interface at the bubble base exists. Close to the normal detachment, the surface of the bubble base diminishes, thus making the contact pressure force insignificant.

The *hydrodynamic force* is a complex parameter. It accounts for effects due to the motion of the liquid and vapour phase. According to Mei and Klausner [115], for a bubble translating at a velocity $U_B(t)$ and growing in an unbounded, unsteady uniform flow field of velocity U(t), it consists of the history force, quasi-steady drag force, added-mass force, and the free stream acceleration. These are each addressed below.

The *history (or Basset) force* is due to the acceleration of a bubble in an unsteady flow field. A rather complicated mathematical formulation for defining this force is excluded from this analysis. The reason is that from present experiments, a stationary flow with small variations of liquid and vapour velocities leads to very small values of the history force, which can therefore be neglected.

The *drag force* results from the viscous action of liquid motion on the vapour-liquid interface. The limiting case of very slow motion (creeping flow) allows for neglecting the inertial terms in the Navier-Stokes equations [116], returning the force that acts on the spherical particle, in the form known as the classical Stokes solution:

$$\vec{F}_D = -6\pi\rho_l\nu_l\left(\vec{U} - \vec{U}_B\right)R \tag{5.9}$$

Mei and Klausner carried out a numerical analysis on a spherical bubble at higher Reynolds numbers. This led to a novel equation for the quasi-steady drag given below in a modified form [115]:

$$\vec{F}_D = -6\pi\rho_l\nu_l\left(\vec{U}-\vec{U}_B\right)R\left\{\frac{2}{3}+\left[\frac{12}{Re_B}+0.75\left(1+\frac{3.315}{Re_B^{0.5}}\right)\right]^{-1}\right\} \tag{5.10}$$

It can be seen that for the limiting case of $Re_B \to 0$ equation (5.10) becomes equal to the Hadamard- Rybczynski solution for creeping flows.

In order to simplify the calculation procedure, if the flow is steady and the bubble sliding velocity is without large fluctuations, the drag force can be obtained using:

$$\vec{F}_D = C_D S_{proj}\frac{1}{2}\rho_l\left(\vec{U}-\vec{U}_B\right)\left|\vec{U}-\vec{U}_B\right| \tag{5.11}$$

An empirical correlation for the drag coefficient C_D, from Schiller and Nauman (in [116]), was used in this study. The drag coefficient is given as a function of the bubble Reynolds number, Re_B:

$$C_D = \frac{24}{Re_B}\left(1+0.15\,Re_B^{0.687}\right) \tag{5.12}$$

The effect of *freestream acceleration* on a spherical bubble can be determined from the following equation:

$$\vec{F}_{FS} = \frac{4}{3}\pi\rho_l R^3\frac{d\vec{U}}{dt} \tag{5.13}$$

The conventional way of calculating the *added-mass force* is to use:

$$\vec{F}_{AM} = C_A\frac{4}{3}\pi\rho_l R^3\frac{d\left(\vec{U}-\vec{U}_B\right)}{dt} \tag{5.14}$$

The virtual mass coefficient can be estimated from an equation given by Odar and Hamilton [117] as:

$$C_A = 1.05 - \frac{0.066}{\left(\frac{\left|\vec{U} - \vec{U}_B\right|^2}{D_{eq}\left|\frac{d\left|\vec{U} - \vec{U}_B\right|}{dt}\right|} + 0.12 \right)^2} \tag{5.15}$$

Klausner [114] obtained the hydrodynamic force by assuming a spherical bubble growing in an inviscid, uniform, unsteady flow field. The result is given as:

$$\vec{F}_{H(partial)} = \frac{4}{3}\pi\rho_l R^3 \frac{d\vec{U}}{dt} + \frac{1}{2}\frac{4}{3}\pi\rho_l R^3 \frac{d\left(\vec{U} - \vec{U}_B\right)}{dt} + 2\pi\rho_l R^2\left(\vec{U} - \vec{U}_B\right)\frac{dR}{dt} \tag{5.16}$$

The first term is the freestream acceleration, the second represents the conventional added-mass and the third term is the added-mass force due to bubble expansion.

The equations for the hydrodynamic force were mainly developed for the case of a bubble growing in an unbounded liquid. In the presence of a wall, the corresponding forces differ. Klausner [114] reported that the quasi-steady drag on a bubble adjacent to a wall will increase approximately 10-25%. However, the most important effect of shear velocity distribution is the generation of a lift force, which acts in a direction normal to the heater surface.

The *shear lift force* has been often estimated by using models which consider solid particles in unbounded or bounded shear flows. Among these models, one should mention the well-known paper of Saffman [118]. Here, the expression for the lift force on a solid spherical particle in a low Reynolds number shear flows was presented. Recently, attempts have been made to define the lift force on a spherical bubble (Mei and Klausner [119], Legendre and Magnaudet [120]). In this study, the following expression developed by Thorncroft (1997) will be used, as given by Klausner [114]:

$$\vec{F}_L = \frac{\rho_l \pi R^2}{2}\left(\vec{U} - \vec{U}_B\right)\left|\vec{U} - \vec{U}_B\right| Sr^{0.5}\left\{\left[\frac{1.146J(\varepsilon)}{Re_B^{0.5}}\right]^2 + \left(\frac{3}{4}Sr^{0.5}\right)^2\right\}^{0.5} \tag{5.17}$$

where the non-dimensional shear rate, Sr, and the scalar function, J(ε), are expressed by:

$$Sr = \frac{\partial U}{\partial y}\frac{R}{|U - U_B|} \tag{5.18}$$

$$\varepsilon = \sqrt{\frac{2Sr}{Re_B}} \tag{5.19}$$

$$J(\varepsilon) \approx \begin{cases} 0.6765\{1 + \tanh[2.5\log_{10}\varepsilon + 0.191]\}\{0.667 + \tanh[6(\varepsilon - 0.32)]\}, \varepsilon \le 1000 \\ 2.255, \varepsilon > 1000 \end{cases} \tag{5.20}$$

After reviewing important forces, one can rewrite the conservation of momentum (5.5) as given by Klausner as:

$$\vec{F}_g + \vec{F}_\sigma + \vec{F}_b + \vec{F}_{cp} + \vec{F}_D + \vec{F}_L + \vec{F}_{FS} + \vec{F}_{AM} + \vec{R} = m\frac{d\vec{V}}{dt} \tag{5.21}$$

5.3 Bubble Detachment Model (Normal Detachment)

5.3.1 Formulation of the Model

The experimentally observed bubble behaviour was described in detail in Chapter 3. Several points, such as the fact that bubbles start shrinking while still attached to the wall and their shape deviates largely from that of a sphere, indicate that bubble detachment models based on spherical bubbles are not applicable to subcooled flow boiling at low pressures. In this model, it is assumed that bubbles have ellipsoidal shapes. The physical model, described in section 5.3.2, is used to determine geometrical bubble parameters. Once the geometry of the bubbles is known, one can proceed to obtain a force balance as follows:

- Only forces acting in a direction normal to the surface of the heater are considered. The gravitational force, buoyancy force and drag force do not affect normal detachment of the bubble (lift-off) in vertical flow boiling. Also, given that the flow is one-dimensional and steady, the freestream acceleration can be neglected;

- Qualitative observations of bubble behaviour indicate that the vapour-solid interface on the bubble base, if it exists, has a minor influence on normal detachment. The model, therefore, excludes the existence of such a contact area. It is assumed that the liquid microlayer (of negligible thickness) covers completely the bubble base, which is assumed to be flat. Exclusion of the vapour-solid interface sets the contact pressure force and reaction force to zero. This gives a new meaning for the surface tension force (as explained in the following section).
- The Marangoni effect was not considered in the analysis;
- The thermo-physical properties of the vapour and liquid were taken at saturation. Variation with temperature was omitted;
- The inclination angle of the bubble was neglected. Although it appears to have a significant role in experiments performed at p=1bar, it is not so evident at elevated pressures. Also, it is believed, that inclusion of the inclination angle will not invalidate the concept of the model;
- The mass of the bubble is small. Calculations show that the change of momentum on the right hand side of equation (5.21) can therefore be omitted;

Having adopted these constraints, the simplified force balance at normal detachment is given by:

$$\vec{F}_\sigma + \vec{F}_L + \vec{F}_I \approx 0 \qquad (5.22)$$

The *inertial force*, the third term in the equation (5.22), represents the integral form of the equation (5.16). It represents the remaining part of the hydrodynamic force.

5.3.2 Physical Modelling – Ellipsoidal Bubble

In the past, bubbles were modelled as truncated spheres. It has been experimentally observed, however, that during subcooled nucleate boiling bubble shapes deviate significantly from that of a sphere. Bubbles, initially flattened after inception, tend to elongate in a direction normal to the heater surface as they grow. Hence, the spherical shape is only reached during the transition from a flattened to an elongated

shape. This occurs near the position of a maximum bubble radius, well before normal detachment.

During subcooled flow boiling it is more appropriate to consider a bubble as a truncated ellipsoid with the base parallel to the wall, as shown in Figure 5.1c. Three parameters are needed to determine the volume, V_B, total surface area, S, and the distance from the center of mass to the wall, z:

$$V_B = a^2\pi\left(b + s - \frac{b^3 + s^3}{3b^2}\right) \tag{5.23}$$

$$S_{a>b} = \frac{a\pi}{b^2}\left[ab^2 + s\sqrt{s^2a^2 + b^2\left(b^2 - s^2\right)}\right.$$
$$\left. + \frac{b^4}{\sqrt{a^2 - b^2}} \ln \frac{b\left(1 + \frac{a}{\sqrt{a^2 - b^2}}\right)}{\frac{\sqrt{s^2a^2 + b^2\left(b^2 - s^2\right)}}{\sqrt{a^2 - b^2}} - s} + a\left(b^2 - s^2\right)\right] \tag{5.24a}$$

$$S_{a<b} = \frac{a\pi}{b^2}\left[ab^2 + s\sqrt{s^2a^2 + b^2\left(b^2 - s^2\right)}\right.$$
$$\left. + \frac{b^4}{\sqrt{b^2 - a^2}}\left(a\sin\frac{\sqrt{b^2 - a^2}}{b} + a\sin\frac{s\sqrt{b^2 - a^2}}{b^2}\right) + a\left(b^2 - s^2\right)\right] \tag{5.24b}$$

$$z = \frac{a^2\pi\left[\frac{b^2}{2} - s\left(1 - \frac{s^2}{2b^2}\right)\right]}{2V} + s \tag{5.25}$$

where:

$$s = \sqrt{\frac{b^2}{\frac{a^2}{b^2}\tan^2\beta + 1}} \tag{5.26}$$

The parameters a and b represent half-diameters along the two principal axes of the ellipsoidal bubble. The parameter, s, is the distance to the ellipse center from the wall. It should be emphasized that the total surface area, S, includes the contact area between

the bubble base and the solid surface, S2. The thickness of the liquid microlayer (separating the bubble from the wall) is considered small compared with the bubble diameter. Hence, the surface of the bubble base is taken as flat.

The angle β represents the angle between the tangent to the bubble interface adjacent to the wall and the wall itself. Significant difficulties associated with experimental evaluation of these angles have led to an approximate evaluation of the third parameter needed to determine the bubble geometry. The projected area (proportional to bubble volume if it is axisymmetric) is compared with the projected area of an ellipsoid having the same maximum and minimum diameters. The difference accounts for the missing segment, which leads to the evaluation of the parameter s.

5.3.3 Modelling of Forces

Only inertia, surface tension and lift forces were considered as discussed in the following.

5.3.3.1 Inertial Force

The typical assumption of a spherical bubble growing in an unbound liquid is not valid in subcooled flow boiling. The bubble deviates from a spherical shape creating a velocity field that differs from that calculated assuming a spherical shape. Therefore, it was necessary to calculate the velocity distribution over an ellipsoidal bubble.

The details for determining a velocity field produced by an expanding ellipsoidal bubble are given in Appendix E. The velocity in equation (E.27) can be averaged over the range of ξ from 0 to 90° at η = const. Since it was assumed that velocity does not depend on ϕ, this led to a reduction in the number of independent variables to one ($\bar{u} = f(\eta)$). Furthermore, curve fitting has shown that the average velocity $\bar{u} = f(\eta)$ can be approximated from the following equation:

$$\bar{u} = \left(\frac{b_0}{\eta}\right)^{\frac{2}{\varepsilon}} \frac{db_0}{dt} \tag{5.27}$$

where $\varepsilon = a/b$ represents the non-sphericity of the ellipsoidal bubble. The parameter a is the maximum half-diameter and b the minimum half-diameter along the principal axes of the ellipsoid. Equation (5.27) is transformed into equation (1.4) for the limiting case of $\varepsilon = 1$ (spherical bubble), when b_0 becomes R and, hence, the coordinate η equals r.

Following the standard procedure for defining the kinetic energy associated with bubble expansion (i.e., Mikic et al. [62]), the case of an ellipsoidal bubble yields:

$$E_{ke} = \frac{\rho_l}{2} \int_{\eta=b_0}^{\infty} [\bar{u}(\eta)]^2 dV_{BUBBLE} = \frac{\rho_l}{2} \int_{\eta=b_0}^{\infty} [\bar{u}(\eta)]^2 S(\eta) d\eta \tag{5.28}$$

where the surface area of the expanding bubble is obtained from equation (5.24a):

$$S(\eta) = \varepsilon\pi \left\{ 2\varepsilon + \frac{1}{\sqrt{\varepsilon^2 - 1}} \ln\left[\frac{\varepsilon + \sqrt{\varepsilon^2 - 1}}{\varepsilon - \sqrt{\varepsilon^2 - 1}} \right] \right\} \eta^2 \tag{5.29}$$

After integrating (5.28) one can obtain:

$$E_{ke} = \varepsilon\pi \left\{ 2\varepsilon + \frac{1}{\sqrt{\varepsilon^2 - 1}} \ln\left[\frac{\varepsilon + \sqrt{\varepsilon^2 - 1}}{\varepsilon - \sqrt{\varepsilon^2 - 1}} \right] \right\} \frac{\varepsilon}{4 - 3\varepsilon} \frac{\rho_l}{2} b_0^3 \left(\frac{db_0}{dt} \right)^2 \tag{5.30}$$

By differentiating equation (5.30) with respect to b_0, one can determine the following expression for the inertial force associated with bubble expansion:

$$F_I = \frac{\partial E_{ke}}{\partial b_0} = \varepsilon\pi \left\{ 2\varepsilon + \frac{1}{\sqrt{\varepsilon^2 - 1}} \ln\left[\frac{\varepsilon + \sqrt{\varepsilon^2 - 1}}{\varepsilon - \sqrt{\varepsilon^2 - 1}} \right] \right\} \frac{\varepsilon}{4 - 3\varepsilon} \frac{\rho_l}{2} \left[3b_0^2 \left(\frac{db_0}{dt} \right)^2 + 2b_0^3 \frac{d^2 b_0}{dt^2} \right] \tag{5.31}$$

It can be shown that, again, for the limiting case of $\varepsilon = 1$ (spherical bubble), equation (5.31) becomes the well known Rayleigh equation for inertial force on a sphere growing in the unbounded liquid.

5.3.3.2 The Surface Tension Force

The present definition of surface tension force is based on the model introduced by Buyevich and Webbon [73]. It relies on the assumption that bubbles are closed

structures surrounded only by liquid. The bubble base is completely separated from the surface of the heater by a liquid microlayer. If such an assumption is adopted, a net surface tension force different from zero will be created on the surface of the bubble due to asymmetrical bubble shape (truncated ellipsoid). Furthermore, if one assumes that bubbles are not inclined in the flow direction and are symmetrical about the y-axes, the resulting surface tension force will act normal to the heater (y-direction) opposing or facilitating bubble detachment. The direction and size of this force will depend on the changes in bubble shape.

The effect of surface tension on a deformed object can be regarded as a potential energy stored on the surface of that object. According to Buyevich and Webbon the change of the surface tension potential energy is equal to:

$$\delta E_\sigma = \sigma \delta S \tag{5.32}$$

The change of the surface tension potential energy affects the translational motion of the bubble. The corresponding net surface tension force, which affects the translational motion of the bubble, (i.e. the change of location of the bubble center of mass, δz) can be defined as:

$$F_\sigma = \frac{\partial E_\sigma}{\partial z} = \sigma\left(\frac{\partial S}{\partial a}\frac{\partial a}{\partial z} + \frac{\partial S}{\partial b}\frac{\partial b}{\partial z} + \frac{\partial S}{\partial s}\frac{\partial s}{\partial z}\right) \tag{5.33}$$

5.3.3.3 The Lift Force

The lift was calculated using equation (5.17). In order to determine the non-dimensional shear rate (equation (5.18)), an estimate of the velocity profile has to be made. A review of several models for velocity and temperature profiles is given in Appendix D. In this case, the model of Knudsen and Katz, given by equation (D.8) was adopted.

5.4 Comparison of the Model with Experimental Data

The model was tested with the experimental data (typical bubbles – as explained in Chapters 2 and 3) at pressures p = 2 bar and p = 3 bar, as well as with the experimental data of Faraji et al. [76] at p = 1.05 bar. Typical results (experiments at 2 and 3 bar) are

shown in Figures 5.2, 5.3, 5.4 and 5.5. Graphs at the top of each page show the two half-diameters fitted by fourth-order polynomials, that were used for evaluating forces. The parameter, a, represents the half-diameter parallel to the surface while the parameter, b, denotes the half-diameter normal to the heater surface. The graphs at the bottom of each page represent the calculated forces as well as summation of lift, inertial, and surface tension forces.

The lift force is small. A typical value for lift in the range of our experimental conditions is about 10^{-7} N. This is expected because of the small difference between bubble sliding velocity and the bulk liquid velocity (typically about 10% of the bulk velocity). The effect of the lift force on bubble detachment is, hence, minor.

The trend of the inertial force is expected, although quantitatively it is surprisingly large. A large negative inertial force is expected in the early stage of bubble growth due to its significant growth rate. However, one can estimate substantially lower values as the bubble approaches its maximum diameter. Further testing indicates that the calculation is extremely sensitive to the last two terms in equation (5.31). This also explains the small initial positive value of the inertial force.

The uncertainty of applying equation (5.31) to determine the inertial force is increased by the fact that the model was developed for an ellipsoid growing in the unbounded stagnant liquid. However, one has to account for the presence of the wall and flow of liquid, as well. Finally, experimental evidence is that bubbles, after reaching their maximum diameters, start shrinking while still attached to the wall. It is not clear what the effect of the inertia of the liquid is on a shrinking bubble.

The surface tension force, as formulated in the previous section, is a consequence of the change of shape of the bubble. It represents a net force due to the asymmetry (truncated ellipsoid) of the bubble shape. Its size and direction depend on the rate of change of the parameters defining the bubble geometry. It has been assumed that the bubble can be described by three parameters (two half-diameters along principal axes and the distance of the bubble center of mass from the surface) and, hence, the surface tension force is defined by equation (5.33).

Comparisons with experimental data show that the typical surface tension force has a negative value during most of the bubble growth stage, thus preventing the bubble from detaching. As the bubble becomes more elongated, this force becomes positive. A strong, positive surface tension force at the location of normal detachment suggests that this force is responsible for ejection. The transition point of the surface tension force shows excellent agreement with experimentally observed points of normal detachment. These results are consistent with all experimental data used for testing. The validity of the model is shown in Figures 5.6 and 5.7. The same results were obtained with the p = 3 bar experiments. The accuracy in predicting experimental data is well within +/-10%.

5.5 Concluding Remarks

After identifying and quantifying forces that act on a single, isolated bubble in subcooled flow boiling, it has been concluded that three forces affect the normal detachment of bubbles in vertical upward flow. They are: lift, inertia and surface tension forces. These three forces were calculated using experimental bubble growth data and the assumption of an ellipsoidal bubble shape. The results indicate that the effect of a lift force on bubble dynamics is minor. The model cannot correctly predict the inertial force, which is expected to be negligible (slow bubble growth or stagnation). It is, therefore, assumed that the primary force leading to normal bubble detachment is the surface tension force.

The transition of the surface tension force from negative (opposing detachment) to positive (facilitating detachment) shows good agreement with experimentally observed ejection points over the whole range of experimental data. Hence, it appears that a bubble detachment criterion can be based solely on the behaviour of the surface tension force during bubble growth.

Unfortunately, the nature of bubble ejection is not well understood. One has to note that the surface tension force described in this model represents, in fact, a reaction force. It is a consequence of bubble stretching and elongation. It does not explain the cause for detachment but rather the events on the vapour-liquid interface that lead to detachment. What is still unknown is the force which elongates the bubble. One can

speculate that this unknown force depends on the thermal gradient and is related to bubble shape and shrinkage. A step forward in defining this force would be to understand the relation between the bubble elongation and boiling parameters such as heat flux, subcooling and liquid velocity.

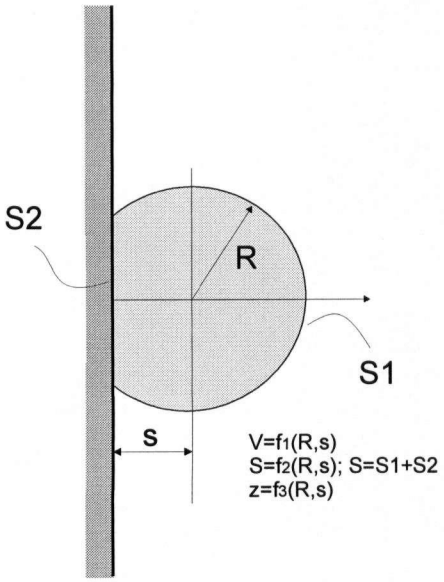

Figure 5.1a Bubble modelled as spherical segment

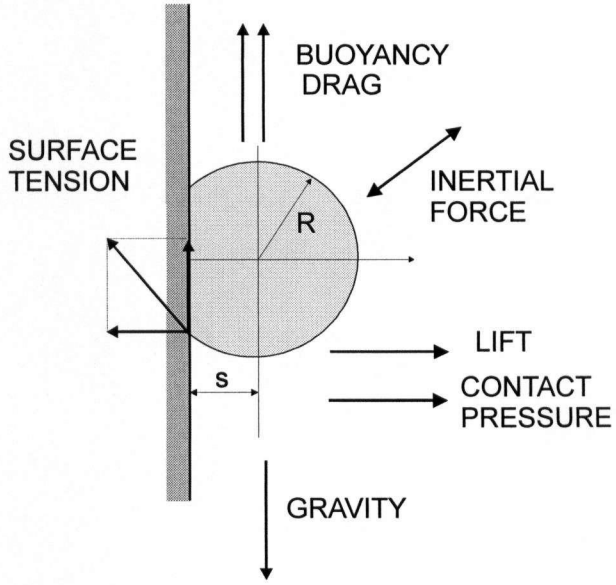

Figure 5.1b Forces acting on a bubble

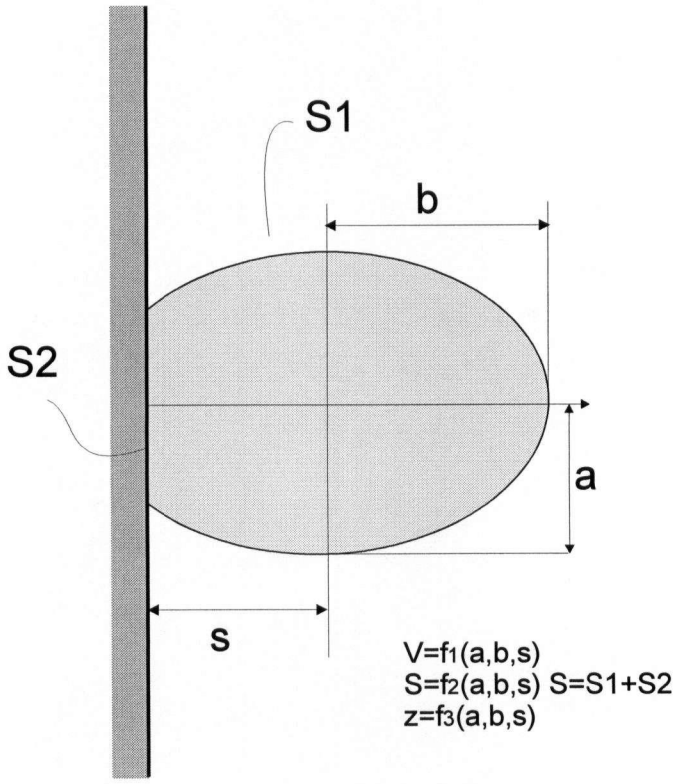

Figure 5.1c Bubble modelled as ellipsoidal segment

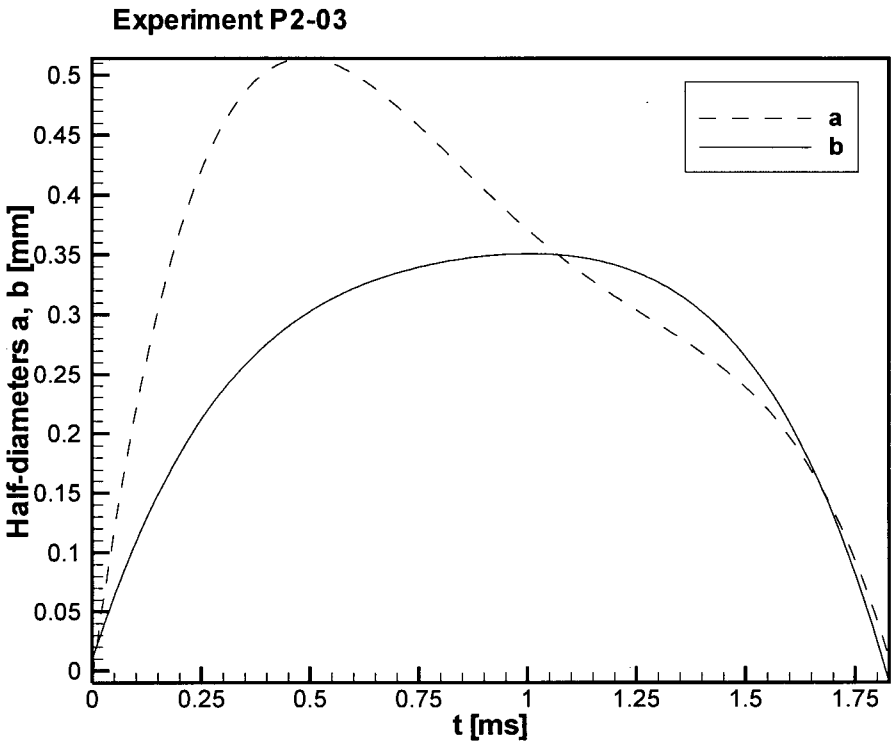

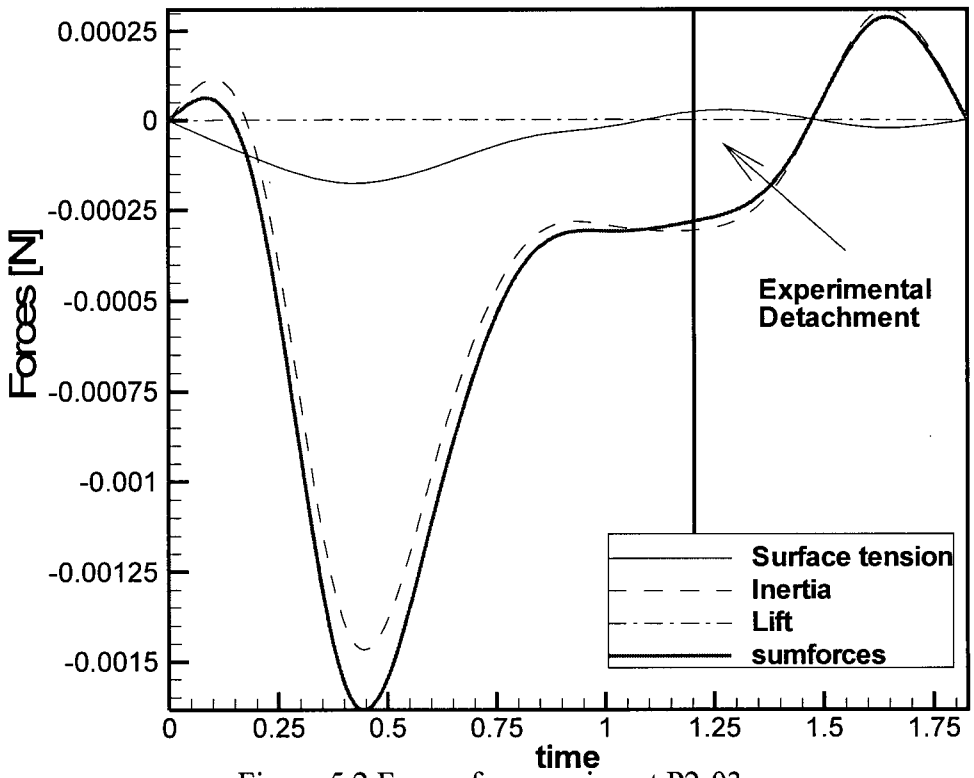

Figure 5.2 Forces for experiment P2-03

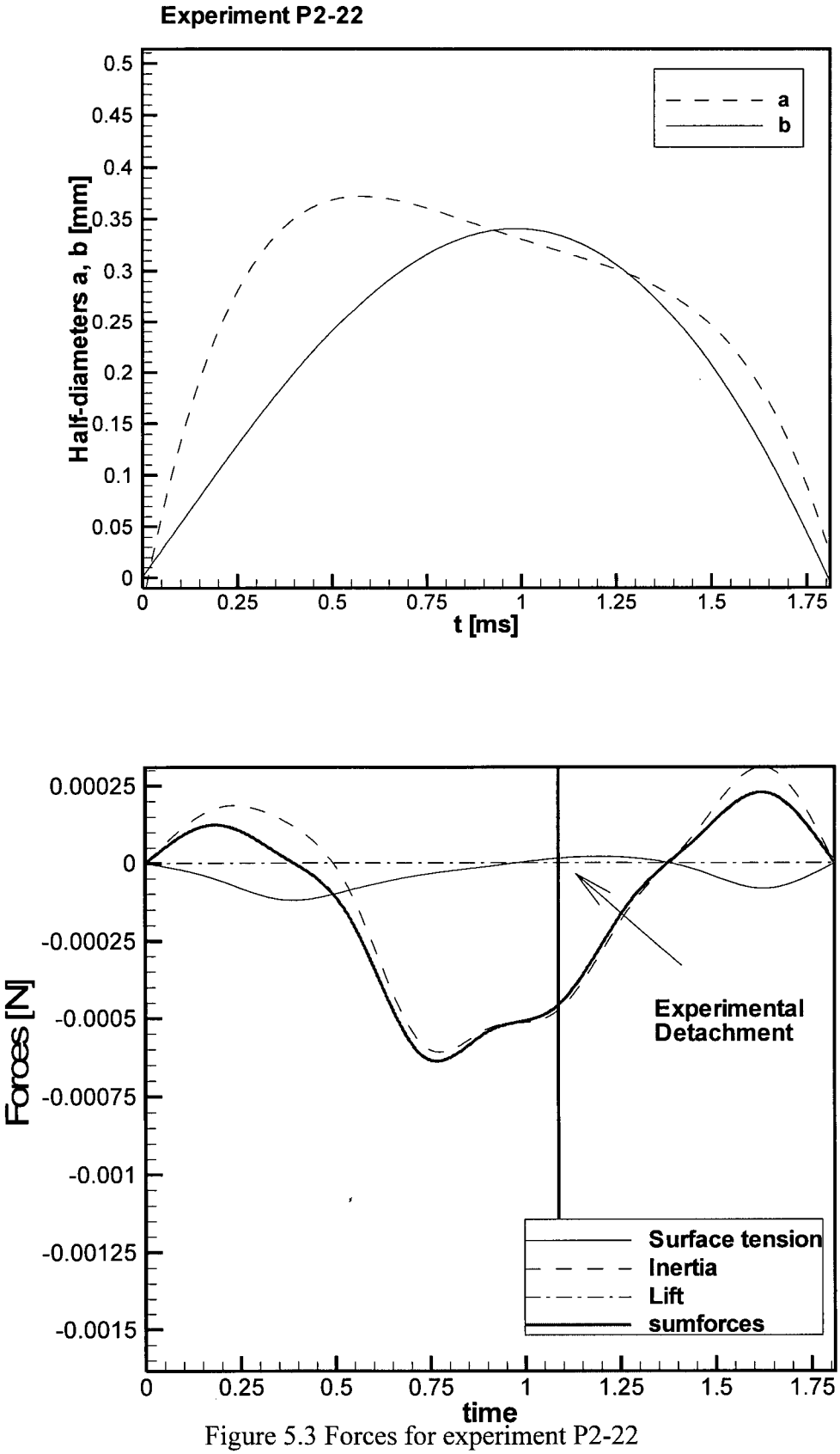

Figure 5.3 Forces for experiment P2-22

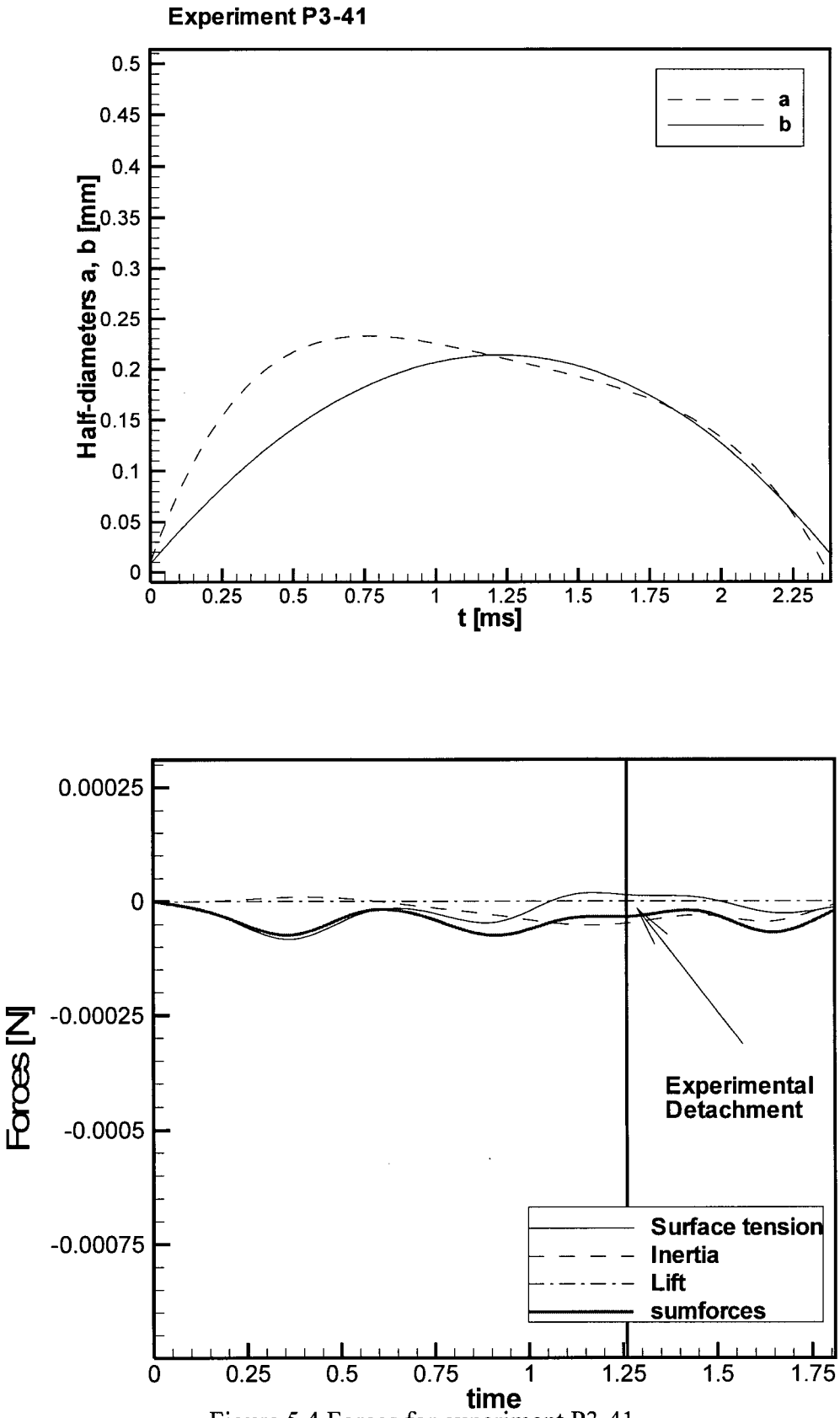

Figure 5.4 Forces for experiment P3-41

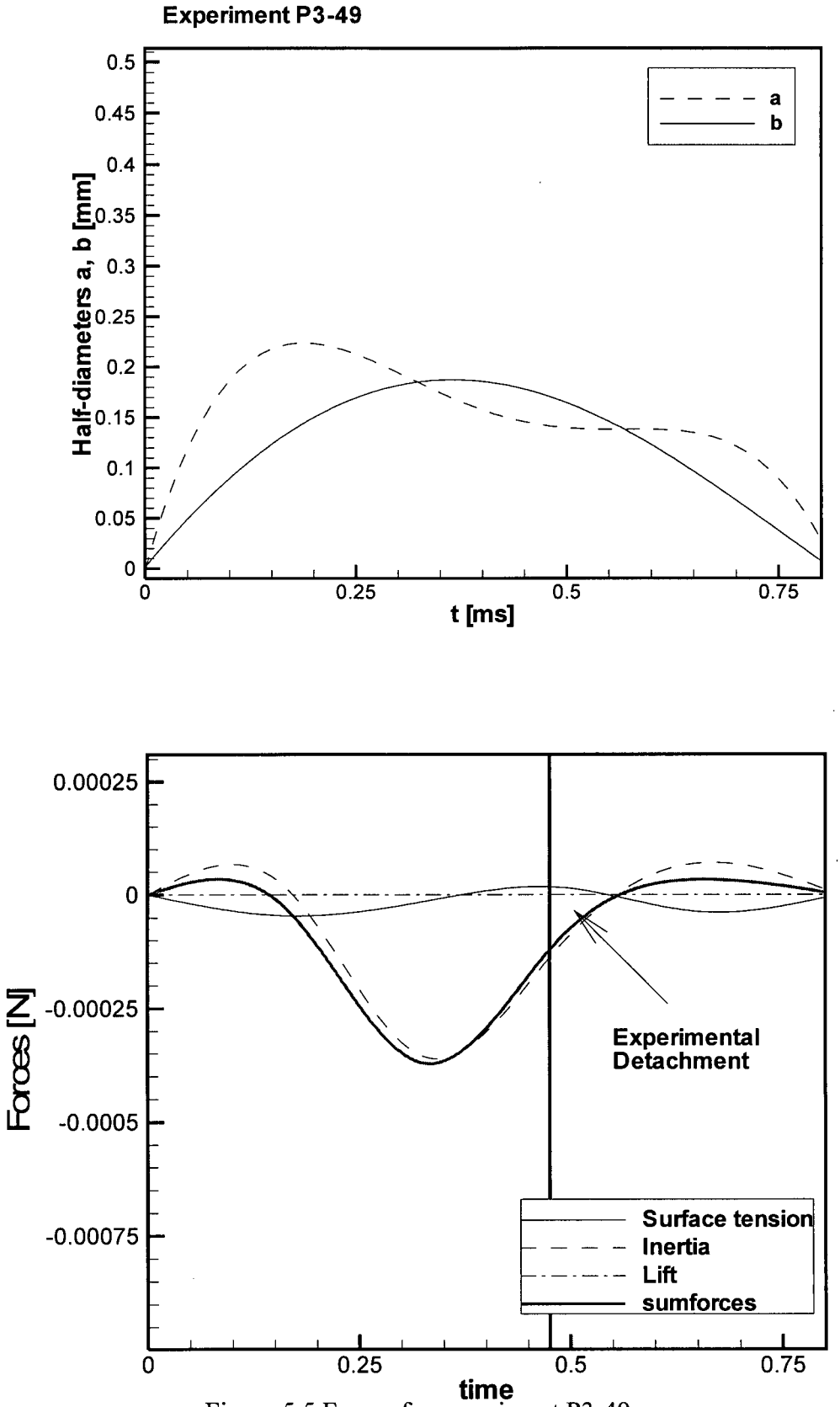

Figure 5.5 Forces for experiment P3-49

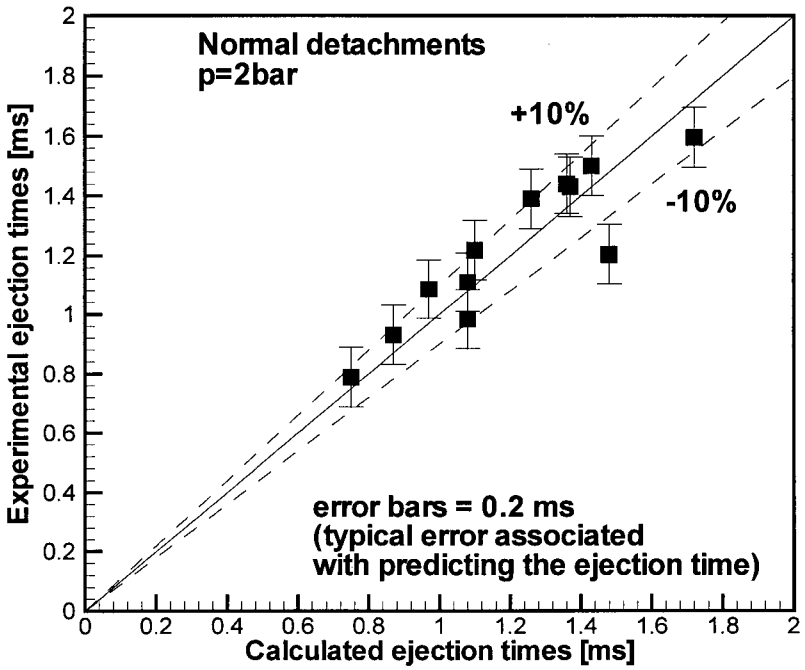

Figure 5.6 Comparison of the detachment criterion (transition of the surface tension force) with experiments p=2bar

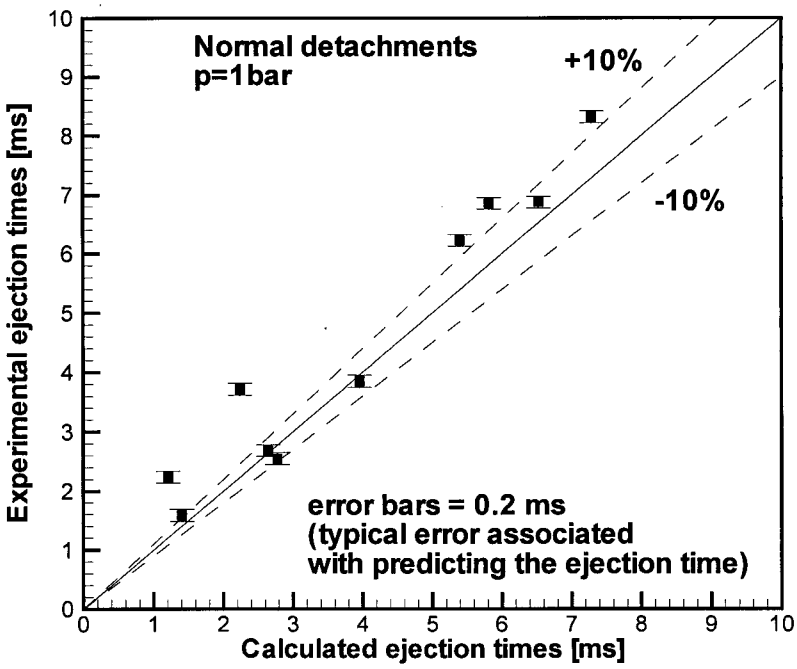

Figure 5.7 Comparison of the detachment criterion (transition of the surface tension force) with experiments p=1bar

Chapter 6

CONCLUSIONS AND RECOMMENDATIONS

6.1 Conclusions

Subcooled flow boiling experiments were performed on an apparatus with a vertical annular test section (inner heated surface), with an upward flow of water. Data were obtained using high-speed photographic techniques. Experimental results consisted of 61 films taken at pressures of 2 and 3 bar. The range of experimental conditions included: mass flow rates from 0.02 to 0.2 kg/s, subcoolings of 10, 20 and 30 K at the filming location, and heat fluxes from 0.2 to 1 MW/m^2. Bubble behaviour was analyzed qualitatively and quantitatively. Based on observed bubble behaviour, new models for heat transfer (transition from partially to fully developed boiling) and bubble detachment were developed.

Since the thesis can be thought of as addressing three very important areas (given by Chapters 3, 4 and 5), the main conclusions for these areas are outlined below.

6.1.1 Bubble behaviour

1. Bubble behaviour was systematically analyzed for the region between ONB and OSV. Past researchers have not addressed any distinct regions occurring between ONB and OSV. However, for this study there has been a distinction made between three separate regions with respect to heat flux. :

   - *Low heat flux region*: small bubble populations slide long distances without changing significantly in size and shape. Rare detachments are often followed by reattachments;

   - *Isolated bubble region*: moderate bubble populations grow, slide, detach from the surface and collapse in the bulk liquid without significant interference with neighboring bubbles. Bubbles detach from the surface after sliding for a distance of around 1-2 diameters along the heater;

- *Region of significant coalescence*: occurs before OSV is reached. Large bubble populations affect overall bubble behaviour. Significant interference between neighboring bubbles is noticed as well as formation of large bubbles due to coalescence. These bubbles travel with the flow attached or close to the heater surface without collapsing;

2. Observations of bubble shapes are in accordance with previous experimental work. Bubbles are flat after inception and become more spherical as they grow. The initial high growth rate is followed by a stagnation period as the bubble reaches the maximum diameter approximately at the same time it reaches its spherical shape. At this point, as condensation rates prevail over the evaporation rate, the bubble, still attached to the surface, starts shrinking and becomes elongated. The detachment diameter is generally smaller than the maximum diameter. After detachment, bubbles collapse into the cooler liquid. Detachment is often followed by oscillations in size before collapse;
3. Parallel detachment occurs almost immediately after inception. All bubbles slide, approximately at the same speed as the bulk fluid (slip ratio close to unity), before normal detachment. Bubble sliding velocity is constant at moderate and high flow rates, and remains the same after detachment. Bubble sliding velocity varies at low flow rates.
4. All bubbles in the isolated bubble region depart from the surface. After detachment they are propelled into the liquid in a direction normal to the heater surface. Detachments occur long before the OSV is reached;
5. No bubble layer was observed;
6. Bubble size and lifetime generally decrease with increasing heat flux, subcooling, bulk liquid velocity and pressure. Correlations for maximum diameters, detachment diameters, bubble growth times, lifetimes and condensation times were developed.
7. Bubble growth is thermally controlled. Experimental detachment diameters agree well with estimates from the models based on the microlayer evaporation theory.

Models based on heat conduction at the liquid-vapour interface largely over-predict detachment diameters;

6.1.2 Heat transfer

An attempt was made to link the observed changes in bubble behaviour with changes in boiling heat transfer. The transition from the *low heat flux region* to an *isolated bubble region* was associated with transition from *partially developed boiling* to *fully developed boiling*. Changes in the heat transfer mode were discussed assuming that heat transfer in partially developed boiling is mainly maintained by evaporation and macroconvection, while microconvection becomes the most important contribution in the fully developed boiling region. Following the heat transfer analysis:

1. A new heat transfer correlation was proposed. The correlation is in the form of $Nu=f(Bo, Ja, Pr, \rho_l/\rho_v)$;
2. A new model for transition from partially to fully developed boiling was developed. The model represents a step forward in understanding the physical nature of the transition point. It is based on observations that a significant and abrupt drop in bubble sliding distances coincide with a change in heat transfer rate;
3. The OSV point is not associated with a transition from partial to fully developed boiling;

6.1.3 Detachment Model

Most bubble detachment models fail to explain the physics of detachment in subcooled flow boiling. Observed bubble behaviour indicates at least two reasons for this failure. One is the fact that detachment diameters are smaller than maximum diameters, suggesting an opposite trend in bubble growth (i.e. condensation and shrinking) than the trend that past detachment models assume. Another reason is the significant deviation from the typically assumed spherical shape during most of the bubble lifetime, and particularly, at normal detachment. The model described in Chapter 5, represents an attempt to account for the two above mentioned characteristics of subcooled flow boiling. In addition, vapour bubbles are assumed to be completely separated from the solid

surface giving a new role to surface tension forces. The following are the main conclusion about the modelling of bubble detachment:

1. Bubbles were regarded as truncated ellipsoids and a corresponding physical model was developed. The model has three degrees of freedom, which means that three variables are needed to determine the geometrical parameters. The three variables, two half-diameters along the principal axes and distance of the center of mass of the full ellipsoid from the wall, were obtained from the experimental data;
2. The three forces considered to have a significant impact on bubble dynamics in vertical subcooled flow boiling are: the lift force, the inertial force and the surface tension force;
3. The calculated lift force is about two orders of magnitude smaller than the other two forces during bubble lifetime. This is due mainly to the low bubble velocity (relative to bulk liquid velocity) in the range of operating conditions studied;
4. The inertial force was modelled for an ellipsoid growing in an unbounded, stagnant liquid. The calculated inertial force is larger than expected based on experimental observations. However, the sensitivity of the inertial force on the bubble growth models brings uncertainty into its role in modelling bubble detachment. Visual observations suggest that inertia at the point of normal detachment is rather small. Bubble size at detachment is reduced due to condensation although the process is relatively slow compared to the initial bubble growth. Also the effect of inertia during bubble condensation is not well understood.
5. The remaining surface tension force has a crucial effect on normal detachment. The net surface tension force is obtained from the rate of change of the surface tension potential energy with respect to the location of the center of mass (translational motion). The net surface tension force exists due to asymmetry of the truncated ellipsoid and, if the inclination of the bubble is neglected, it acts in a direction normal to the surface of the heater. It is highly affected by variations of the bubble shape. Comparisons with experiments show that, at the point of normal detachment, the surface tension force undergoes a transition from negative (opposing detachment)

to positive (facilitating detachment), thus becoming an important criterion for determining detachment;

6. It is important to stress that the detachment model is based on the assumption that bubble contact with the solid surface is unstable. The bubble base is separated from the wall by a thin microlayer through which most of the evaporation occurs. This assumption is based on experimental evidence that bubble motion is not notably affected by so-called attachment to the wall. Measurements of the parallel displacement before and after detachment showed no difference. This would not be possible if a stable bubble base existed. As an example, the three phase contact solid, liquid, vapor line would be stable for a gas bubble attached to the surface in a flow.
7. Excellent agreement between the model and experiments were obtained for all the data.

6.2 Recommendations

This study introduced several new elements for the analysis of subcooled flow boiling, which need to be further investigated. The most important are: the surface tension force whose role may be to facilitate bubble detachment, the change in bubble behaviour associated with the transition from partial to fully developed boiling, and the observed bubble reattachment in the low heat flux region. Recommendations for future work with regard to these are:

1. Photographic boiling experiments with fluids for which surface tension coefficients are substantially different than the surface tension coefficients for water (i.e. well-wetting fluids) are recommended. Fluid-to-fluid scale modelling should be used to simulate present experimental conditions and to isolate the effect of surface tension from other parameters. These results should help to better understand the role and order of magnitude of the surface tension force;
2. The surface tension force is highly dependent on the shape of the bubble. There is reason to believe that bubble non-sphericity can be related to heat flux, flow rate and subcooling. The present experiments with random bubbles did not clarify this point. Future investigation should include experiments using a predefined nucleation site

and with an improved photographic setup. The predefined or artificial nucleation site will reduce the number of stochastic parameters involved;

3. The heat transfer model should be improved by taking into account the effect of subcooling. This was neglected in the present simplified model;

4. Both the heat transfer (transition) model and bubble detachment model should be tested and validated with different fluids under different boiling conditions. Measurements of sliding distances are necessary for the heat transfer (transition) model and knowledge of bubble non-sphericity is a requirement for modelling of bubble detachment;

5. Bubble reattachment should be further investigated. Reattachments occur regularly in the low heat flux region. At present there is no force that can explain the nature of reattachment. Detachment and reattachment times as well as bubble displacements should be investigated with respect to turbulence time and length scales;

6. Bubble behaviour in real boiling systems is a stochastic process. All relevant parameters such as bubble geometry, lifetimes, ejection or eventually waiting times have to be statistically processed.

Bibliography

1. Kay R.E., Stevens-Guille P.D., Hilborn J.W., Jervis R.E.;"SLOWPOKE: A New Low-Cost Laboratory Reactor", International Journal of Applied Radiation and Isotopes, Vol 24, pp. 509-518 (1973)
2. Salcudean M., Rogers J.T., Tahir A., Abdullah Z., Graham K.,"Investigation of two-phase flow characteristics and heat transfer limitations in fuel elements for the 2 MW SLOWPOKE reactor", Report to AECL, Dept.of Mech.Eng., University of Ottawa (1984)
3. Salcudean M., Rogers J.T., Tahir A., Abdullah Z., Graham K.,"Investigation of two-phase flow characteristics and heat transfer limitations in fuel elements for the 2 MW SLOWPOKE reactor", Report to AECL, Dept.of Mech.Eng., University of Ottawa (1985)
4. McLeod R.D.,"Investigation of subcooled void fraction growth in water under low pressure and low flow rate conditions", Master Thesis, Carleton University, Ottawa (1986)
5. Bibeau E.L.,"Experimental investigation of subcooled void growth for upflow and downflow at low velocities and low pressure", Master Thesis, University of British Columbia, Vancouver, BC (1988)
6. Bibeau E.L.,"Void growth in subcooled flow boiling for circular and finned geometries for low values of pressure and velocity", PhD Thesis, University of British Columbia, Vancouver, BC (1993)
7. Farajisarir D,"Growth and collapse of vapour bubbles in convective subcooled boiling of water", Master Thesis, University of British Columbia, Vancouver, BC (1993)
8. Zeitoun O.,"Subcooled flow boiling and condensation", PhD Thesis, McMaster Unversity, Hamilton, ON (1994)
9. Kowalski J.E., Harvel G.D.,"Void fraction in a vertical finned annulus", Recent advances in Heat Transfer, pp. 256-276, Elsevier Science Publishers B.V. (1992)
10. Collier J.G.,"Convective boiling and condensation", McGraw Hill Book Co. (1972)
11. Kandlikar S.G.,"Heat transfer characteristics in partial boiling, fully developed boiling, and significant void flow regions of subcooled flow boiling",Trans ASME Journal of Heat Transfer, Vol 120, pp. 395-401 (1998)
12. Bankoff S.G.,"Entrapment of gas in the spreading of liquid over a rough surface", A.I.Ch.E. Journal, Vol 4, pp. 24-26 (1958)
13. Clark H.B., Strenge P.S., Westwater J.W.,"Active sites for nucleate boiling", Chem.Eng. Progress Symposium series, Vo. 55, No 29. pp. 103-110 (1959)
14. Butterworth D., Shock R.A.W.,"Flow boiling", Proc. 7th Int. Heat Transfer Conference, vol 1, pp. 11-30 (1982)

15. Spindler K.,"Flow boiling", 10th Int. Heat Transfer Conference, GK-12, pp. 349-368 (1994)
16. Hsu Y.Y.,"On the size range of active nucleation cavities on a heating surface", Trans ASME Journal of Heat Transfer, pp. 207-216 (1962)
17. Bergles A.E., Rohsenow W.M.,"The determination of forced convection surface boiling heat transfer", Trans ASME Journal of Heat Transfer, Vol 86, pp. 365-372 (1964)
18. Davis E.J., Anderson G.H.,"The incipience of nucleate boiling in forced convection flow", A.I.Ch.E. Journal, Vol 12, No 4. pp.774-780 (1966)
19. Sato T., Matsumura H.,"On the conditions of incipient subcooled boiling with forced convection", Bull. of JSME, Vol 7, No 26. pp. 392-398 (1964)
20. Hino R., Ueda T.,"Studies on heat transfer and flow characteristics in subcooled flow boiling - Part 1 Boiling characteristics", Int. J. Multiphase Flow, Vol 11, No 3. pp. 269-281 (1985)
21. Hahne E., Spindler K., Shen N.,"Incipience of flow boiling in subcooled well wetting fluids", 9th Int.Heat Transfer Conference, Vol 2, pp. 69-74 (1990)
22. Unal H.C.,"Void fraction and incipient point of boiling during the subcooled nucleate flow boiling of water", Int. J. Heat Mass Transfer, Vol 20, pp. 409-419 (1977)
23. Unal H.C.,"Determination of the initial point of net vapor generation in flow boiling systems", Int. J. Heat Mass Transfer, Vol 18, pp. 1095-1099 (1975)
24. Serizawa A., Kenning D.B.R.,"A study of forced convective subcooled flow boiling", Kyoto University, Tech.Rep. (1979)
25. Rouhani S.Z.,"Calculation of steam volume fraction in subcooled boiling", Trans ASME Journal of Heat Transfer, February (1968)
26. Lahey R.T. Jr.,"A mechanistic subcooled boiling model", 6th Int.Heat Transfer Conference, Toronto Canada Vol 1 (1978)
27. Chang Y.P.,"Some possible critical conditions in nucleate boiling", Trans ASME Journal of Heat Transfer, May (1963)
28. Hsu Y.Y., Graham R.W.,"An analytical and experimental study of the thermal boundary layer and ebulition cycle in nucleate boiling", Technical note D-594
29. Griffith P., Clark J.A., Rohsenow W.M.,"Void volumes in subcooled boiling systems", Trans ASME, 58-HT-19 (1958)
30. Zeitoun O., Shoukri M.,"On the net vapour generation phenomenon in low pressure and low mass flux subcooled flow boiling", Engrng. Foundation Conf. on Convective Boiling, Banff, Proc. II-3 (1995)
31. Kocamustafaogullari G., Ishii M.,"Interfacial area and nucleation site density in boiling systems", Int. J. Heat Mass Transfer, Vol 26, pp. 1377-1387 (1983)

32. Bowring R.W.,"Physical model, based on bubble detachment and calculation of steam voidage in the subcooled region of a heated channel", HPR-29, Institutt for Atomenergy, Halden, Norway (1962)

33. Ahmad S.Y.,"Axial distribution of bulk temperature and void fraction in a heated channel with inlet subcooling", Trans ASME Journal of Heat Transfer, Vol 92, pp. 595-608 (1970)

34. Saha P., Zuber N.,"Point of net vapor generation and vapor void fraction in subcooled boiling", 5th Int.Heat Transfer Conference, Vol 4, B4.7 Proc. (1974)

35. Levy S.,"Forced convection subcooled boiling - prediction of vapor volumetric fraction", Int. J. Heat Mass Transfer, Vol 10, pp. 951-964 (1967)

36. Staub F.W.,"The void fraction in subcooled boiling - Prediction of the initial point of net vapor generation", Trans ASME Journal of Heat Transfer, Vol 90, pp. 151-157 (1968)

37. Rogers J.T., Salcudean M., Abdullah Z., McLeod D., Poirier D.,"The onset of significant void in up-flow boiling of water at low pressure and velocities", Int. J. Heat Mass Transfer, Vol 30, No 11. pp. 2247-2260 (1987)

38. Dix G.E.,"Vapour void fraction for forced convection with subcooled boiling at low flow rates", General Electric Report, No NEDO-10491 (1970)

39. Bibeau E.L., Salcudean M.,"A study of bubble ebullition in forced-convective subcooled nucleate boiling at low pressure", Int. J. Heat Mass Transfer,Vol 37, No 15. pp. 2245-2259 (1994)

40. Zeitoun O., Shoukri M.,"Bubble behaviour and mean diameter in subcooled flow boiling", Trans ASME Journal of Heat Transfer, Vol 118, pp.110-116 (1996)

41. Rouhani S.Z., Axelsson E.," Calculation of void volume fraction in the subcooled and quality boiling regions", Int. J. Heat Mass Transfer, Vol 13, pp. 383-393 (1970)

42. Zuber N., Findlay J.A.,"Average volumetric concentration in two-phase flow systems", Trans ASME Journal of Heat Transfer, Vol 87, pp. 453-468 (1965)

43. Evangelisti R., Lupoli P.,"The void fraction in an annular channel at atmospheric pressure", Int. J. Heat Mass Transfer, Vol 12, pp. 699-711 (1969)

44. Edelman Z., Elias E.,"Void fraction distribution in low flow rate subcooled boiling", Nuclear Engrg.and Design, Vol 66, pp. 375-382 (1981)

45. Shoukri M., Donevski B., Judd R.L., Dimmick G.R.,"Experiments on subcooled flow boiling and condensation in vertical annular channels", Int Congress on Multiphase flow, Dubrovnik, YU May (1990)

46. Bibeau E.L., Salcudean M.,"Subcooled void growth mechanisms and prediction at low pressure and low velocity ", Int. J. Multiphase Flow, Vol 20, No 5. pp. 837-863 (1994)

47. Plesset M.S., Prosperetti A.,"Bubble dynamics and cavitation", Annu.Rev.Fluid Mech., Vol 9, pp. 145-185 (1977)

48. Feng Z.C., Leal L.G.,"Nonlinear bubble dynamics", Annu.Rev.Fluid Mech., Vol 29, pp. 201-243 (1997)

49. Tong L.S.,"Boiling heat transfer ant two-phase flow",John Wiley & Sons, Inc. (1965)

50. Brennen C.E.,"Cavitation and bubble dynamics", Oxford University Press, Inc. (1995)

51. Kandlikar S.G., Shoji M., Dhir V.K.,"Handbook of phase change: Boiling and condensation", Taylor & Francis (1999)

52. Lee R.C., Nydahl J.E.,"Numerical calculation of bubble growth in nucleate boiling from inception through departure", Trans ASME Journal of Heat Transfer, Vol 111, pp. 474-478 (1989)

53. Welch S.W.J.,"Direct simulation of vapor bubble growth", Int.J.Heat Mass Transfer, Vol 41, No 12. pp. 1655-1666 (1998)

54. Legendre D., Boree J., Magnaudet J.,"Thermal and dynamic evolution of a spherical bubble moving steadily in a superheated or subcooled liquid", Phys.Fluids, Vol 10, No 6. pp. 1256-1272 (1998)

55. Lord Rayleigh,"On the pressure developed in a liquid during the collapse of a spherical cavity", Philosophical Magazine, Vol XXXIV, pp.94-98 (1917)

56. Bankoff S.G., Mikesell R.D.,"Bubble growth rates in highly subcooled nucleate boiling", Chem.Eng. Progress Symposium Series, Vol 55, No 29. pp. 95-102 (1959)

57. Gunther F.C.,"Photographic study of surface boiling heat transfer to water with forced convection", Trans. ASME (1951)

58. van Stralen S., Cole R.,"Boiling phenomena; Physicochemical and engineering fundamentals and applications, Volume 1", McGraw Hill Book Co. (1979)

59. Forster H.K., Zuber N.,"Growth of a Vapor Bubble in a Superheated Liquid", Journal of Applied Physics, Vol 25, No 4. pp. 474-478 (1954)

60. Plesset M.S., Zwick S.A.,"The growth of vapor bubbles in superheated liquids", Journal of Applied Physics, Vol 25, No 4. pp.493-500 (1954)

61. Scriven L.E.,"On the dynamics of phase growth", Chemical Engineering Science, Vol 10, pp. 1-13 (1959)

62. Mikic B.B., Rohsenov W.M., Griffith P.,"On bubble growth rates", Int.J.Heat Mass Transfer, Vol 13, pp. 657-665 (1970)

63, Zuber N.,"The dynamics of vapor bubbles in nonuniform temperature fields"' Int.J.Heat Mass Transfer, Vol 2, pp. 83-98 (1961)

64. van Stralen S.J.D.,"The mechanism of nucleate boiling in pure liquids and in binary mixtures – III", Int.J.Heat Mass Transfer, Vol 10, pp. 1469-1484 (1967)

65. Mikic B.B., Rohsenov W.M.,"Bubble growth rates in non-uniform temperature field", Progress in Heat and Mass Transfer II, pp. 83-293 (1964)

66. Snyder N.W., Robin T.T.,"Mass-transfer model in subcooled nucleate boiling", Trans ASME Journal of Heat Transfer, Vol 91C, pp. 404-412 (1969)

67. Moore F.D., Messler R.B.,"The measurement of rapid surface temperature fluctuations during nucleate boiling of water", A.I.Ch.E. Journal, December (1961)

68. van Ouwerkerk H.J.,"The rapid growth of a vapour bubble at a liquid-solid interface", Int J. Heat Mass Transfer, Vol 14, pp. 1415-1431 (1971)

69. Cooper M.G., Lloyd A.J.P.,"The microlayer in nucleate pool boiling", Int.J.Heat Mass Transfer, Vol 12, pp. 895-913 (1969)

70. Jawurek H.H.,"Simultaneous determination of microlayer geometry and bubble growth in nucleate boiling", Int.J.Heat Mass Transfer, Vol 12, pp. 843-848 (1969)

71. Koffman L.D., Plesset M.S.,"Experimental observations of the microlayer in vapor bubble growth on a heated solid", Trans ASME Journal of Heat Transfer, Vol 105, pp.625-632 (1983)

72. Mitrovic J.,"The flow and heat transfer in the wedge-shaped liquid film formed during the growth of a vapour bubble", Int.J.Heat Mass Transfer, Vol 41, No 12. pp. 1771-1785 (1998)

73. Buyevich YU.A., Webbon B.W.,"Dynamics of vapour bubbles in nucleate boiling", Int.J.Heat Mass Transfer, Vol 39, No 12. pp. 2409-2426 (1996)

74. Unal H.C.,"Maximum bubble diameter, maximum bubble growth time and bubble growth rate during the subcooled nucleate flow boiling of water up to 17.7 MN/m2", Int.J.Heat Mass Transfer, Vol 19, pp. 643-649 (1976)

75. Bibeau E.L., Salcudean M.,"Subcooled void growth for finned and circular annular geometries at low pressures and low velocities", 3rd World Conf. on Exp.Heat Trans., F.Mech. and Thermodyn., Honolulu, Hawaii USA 10/31-11/05/93 (1993)

76. Faraji D., Barnea Y., Salcudean M.,"Visualization study of vapour bubbles in convective subcooled boiling of water at atmospheric pressure", 10th Int.Heat Transfer Conference, Proc. pp. 425-430 (1994)

77. Frost W., Kippenhan C.J.,"Bubble growth and heat transfer mechanisms in the forced convection boiling of water containing a surface active agent", Int.J.Heat Mass Transfer, Vol 10, pp. 931-949 (1967)

78. Abdelmessih A.H., Hooper F.C., Nangia S.,"Flow effects on bubble growth and collapse in surface boiling", Int.J.Heat Mass Transfer, Vol 15, pp. 115-125 (1972)

79. Akiyama M., Tachibana F.,"Motion of vapor bubbles in subcooled heated channel", Bulletin of J.S.M.E., Vol 17, No 104. pp. 241-247 (1974)

80 Del Valle V.H., Kenning D.B.R.,"Subcooled flow boiling at high heat flux", Int.J.Heat Mass Transfer, Vol 28, No 10. pp. 1907-1920 (1985)

81. Klausner J.F., Mei R., Bernhard D.M., Zeng L.Z.,"Vapor bubble departure in forced convection boiling", Int.J.Heat Mass Transfer, Vol 36, No 3. pp. 651-662 (1993)

82. Zeng L.Z., Klausner J.F., Bernhard D.M., Mei R.,"A unified model for the prediction of bubble detachment diameters in boiling systems -II. Flow boiling", Int.J.Heat Mass Transfer, Vol 36, No 9. pp. 2271-2279 (1993)

83. Thorncroft G.E., Klausner J.F., Mei R.,"An experimental investigation of bubble growth and detachment in vertical upflow and downflow boiling", Int.J.Heat Mass Transfer, Vol 41, No 23. pp. 3857-3871 (1998)

84. Tolubinsky V.I., Kostanchuk D.M.,"Vapour bubbles growth rate and heat transfer intensity at subcooled water boiling", 4th Int.Heat Transfer Conference, Vol 5. (1970)

85. Koumoutsos N., Moissis R., Spyridonos A.,"A study of bubble departure in forced convection boiling", Trans ASME Journal of Heat Transfer, Vol 90, pp.223-230 (1968)

86. Kandlikar S.G., Stumm B.J.,"A control volume approach for investigating forces on a departing bubble under subcooled flow boiling", Trans ASME Journal of Heat Transfer, Vol 117, pp. 990-997 (1995)

87. Roy R.P., Velidandla V., Kalra S.P., Peturaud P.,"Local measurements in the two-phase region of turbulent subcooled boiling flow", Trans ASME Journal of Heat Transfer, Vol 116, pp. 660-669 (1994)

88. Kandlikar S.G., Mizo V.R., Cartwright M.D.,"Investigation of bubble departure mechanism on subcooled flow boiling of water using high speed photography", Proc. Of Convective FLow Boiling, Banff AB, Canada pp 161-166 (1995)

89. Cooper M.G., Mori K., Stone C.R.,"Behaviour of vapour bubbles growing at a wall with forced flow", Int.J.Heat Mass Transfer, Vol 26, No 10. pp. 1489-1507 (1983)

90. Chen J.C.,"Correlation for boiling heat transfer to saturated fluids in convective flow", I&EC Process Design and Development, Vol 5, No 3. pp. 322-329 (1966)

91. Gungor K.E., Winterton R.H.S.,"A general correlation for flow boiling in tubes and annuli", Int.J.Heat Mass Transfer, Vol 29, No 3, pp. 351-358 (1986)

92. Salcudean M., Bibeau E.L.,"Experimental investigation of subcooled void growth for upward and downward flow at low velocities and low press.", Experimental Heat Transfer, Fluid Mech. and Thermodynamics (1991)

93. Cooper M.G.,"Saturation nucleate pool boiling: A simple correlation", Int.Chem.Eng. Symposium Series, Vol 86, pp 785-793 (1984)

94. Liu Z., Winterton R.H.S.,"A general correlation for saturated and subcooled flow boiling in tubes and annuli based on a nucleate pool boiling", Int.J.Heat Mass Transfer, Vol 34, pp 2759-2765 (1991)

95. Kandlikar S.G.,"A general correlation for saturated two-phase flow boiling heat transfer inside horizontal and vertical tubes", Trans ASME Journal of Heat Transfer, Vol 112, pp. 219-228 (1990)

96. Darabi J., Salehi M., Saeedi M.H., Ohadi M.M.,"Review of available correlations for prediction of flow boiling heat transfer in smooth and augmented tubes", ASRAE Transactions: Symposia, CH-95-12-2, pp. 965-975 (1995)

97. Guglielmini G., Nannei E., Pisoni C.,"Survey of heat transfer correlations in forced convection boiling", Warme- und Stoffubertragung, Vol 13, pp. 177-185 (1980)

98. McAdams W.H., Kennel W.E., Minden C.S., Carl R., Picornell P.M., Dew J.E.,"Heat transfer at high rates to water with surface boiling", Industrial and Engineering Chemistry, Vol 41, No 9. pp.1945-1953 (1949)

99. Shah M.,"A general correlation for heat transfer during subcooled boiling in pipes and annuli", ASHRAE Trans. Vol 83, Part 1. Pp 205-215 (1977)

100. Pokhvalov Yn.E., Kronin G.H., Kurganova I.V.,"Correlation on experimental data on heat transfer with nucleate boiling of subcooled liquid in tubes", Teploenergetika, Vol 13, pp. 63-68 (1966)

101. Kroeger P.G., Zuber N.,"An analysis of the effects of various parameters on the average void fractions in subcooled boiling", (1967)

102. Hasan A., Roy R.P., Kalra S.P.,"Experiments on subcooled flow boiling heat transfer in a vertical annular channel", Int.J.Heat Mass Transfer, Vol 33, NO 10. pp. 2285-2293 (1990)

103. Moles F.D., Shaw J.F.G.,"Boiling heat transfer to subcooling liquids under condition of forced convection", Trans.Inst.Chem.Engrs. Vol 50, pp. 76-84 (1972)

104. Gunther F.C., Kreith F.,"Photographic study of bubble formation in heat transfer to subcooled water", Jet Propulsion Lab. Pasadena CA Progress Report No 4-75 (1950)

105. Bankoff S.G.,"On the mechanism of subcooled nucleate boiling, Part I: Preliminary considerations", 4th. National Heat Transfer Conference, (1960)

106. Plesset M.S., Prosperetti A.,"The contribution of latent heat transport in subcooled nucleate boiling", Int J. Heat Mass Transfer, Vol 21, pp. 725-734 (1978)

107. Tsung-Chang G., Bankoff S.G.,"On the mechanism of forced convection subcooled nucleate boiling", Trans ASME Journal of Heat Transfer, Vol 112, pp. 213-218 (1990)

108. Beer H., Burrow P., Best R.,"Bubble Growth, Bubble Dynamics and Heat Transfer in Nucleate Boiling, Viewed with Laser Interferometer", Heat Transfer in Boiling edited by Hahne E. and Grigull U. Chapter 2 (1977)

109. Al-Hayes R.A.M., Winterton R.H.S.,"Bubble diameter on detachment in flowing liquids", Int.J.Heat Mass Transfer, Vol 24, pp. 223-229 (1981)

110. Zeng L.Z., Klausner J.F., Mei R.,"A unified model for the prediction of bubble detachment diameters in boiling systems -I. Pool boiling", Int.J.Heat Mass Transfer, Vol 36, No 9. pp. 2261-2270 (1993)

111. Van Helden W.G.J., Van Der Geld C.W.M., Boot P.G.M.,"Forces on bubbles growing and detaching in flow along a vertical wall, Int.J.Heat Mass Transfer, Vol 38, No 11. pp. 2075-2088 (1995)

112. Gaddis E.S.,"The effect of liquid motion induced by phase change and thermocapillarity on the thermal equilibrium of vapour bubbles", Int.J. Heat Mass Transfer, Vol 15, pp. 2241-2250 (1972)

113. Kao Y.S., Kenning D.B.R,"Thermocapillary flow near a hemispherical bubble", J.Fluid Mech., Vol 53, No 4. pp. 715-735 (1972)

114. Klausner J.F,"Bubble forces and detachment models", Boiling 2000: Phenomena & Emerging Applications, Keynote Lecture (2000)

115. Mei R., Klausner J.F.,"Unsteady force on a spherical bubble at finite Reynolds number with small fluctuations in the free-stream velocity", Phys.Fluids, A4, No 1., pp.63-70 (1992)

116. Clift R., Grace J.R., Weber M.E.,"Bubbles, drops and particles", Acad. Press (1978)

117. Odar F., Hamilton W.S.,"Forces on sphere accelerating in a viscous fluid", J. Fluid Mech., Vol 18, pp. 302-314 (1964)

118. Saffman P.G.,"The lift on a small sphere in a slow shear flow", J.Fluid Mech., Vol 22, part 2. pp. 385-400 (1965)

119. Mei R., Klausner J.F.,"Shear lift force on spherical bubbles", Int.J.Heat and Fluid Flow, Vol 15, No 1. pp. 62-65 (1994)

120. Legendre D., Magnaudet J.,"A note on the lift force on a spherical bubble or drop in a low-Reynolds-number shear flow", Phys.Fluids, Vol 9, No 11. pp. 3572-3574 (1997)

Appendix A

PROPAGATION OF LIGHT THROUGH THE TEST SECTION

The fact that the ray of light passing through different media changes its direction of propagation, causes an error in the analysis of photographs taken through cylindrical surfaces. The phenomenon is known as refraction of light. If indexes of refraction for particular media are known, the deviation of a ray of light from its original path can be calculated using Snell's Law, given by equation (A.1). The difference between angles of incidence and refraction are shown in Figure A.1.

$$n_1 \cdot \sin\alpha_1 = n_2 \cdot \sin\alpha_2 \qquad (A.1)$$

In the test section the light passes through water, a circular glass tube and finally through air. This deviates the image for about 37%, as shown in Figures A.2 and A.3. In order to decrease the error associated with the refraction of light, a square cross-sectional glass box was built and mounted around the circular test section.

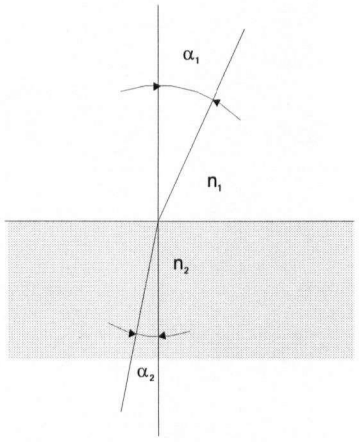

Figure A.1. Angles of incidence and refraction between two media

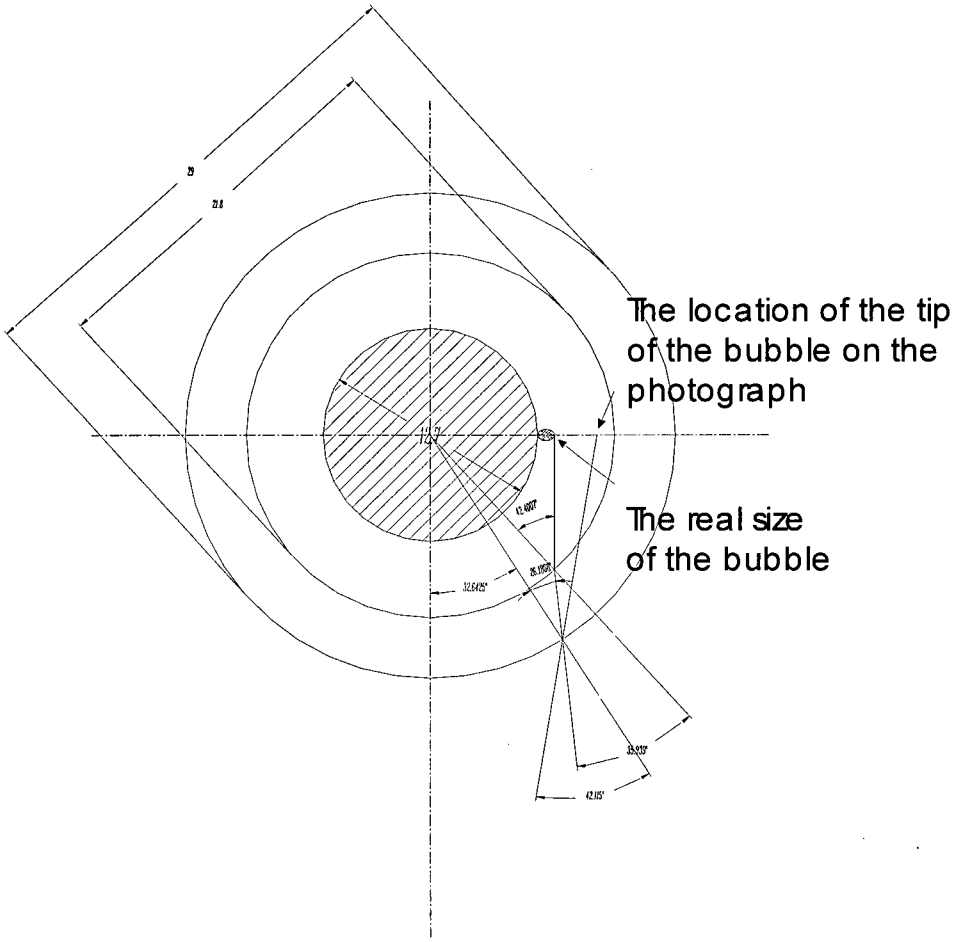

Figure A.2 Location of the tip of the bubble on the photograph and the real location

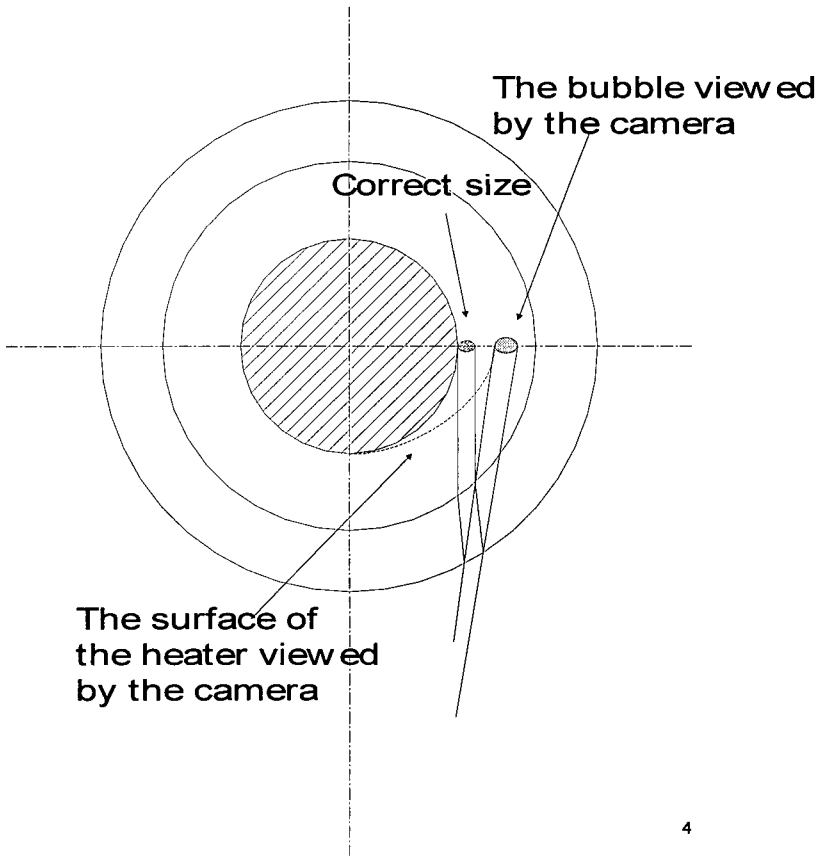

Figure A.3 The size of the bubble "seen" on the photograph and the real size

Appendix B

BUBBLE DETACHMENT MODELS

B.1 Model of Unal

Assumptions:

- Subcooled nucleate flow boiling coincides with the partial nucleate boiling region;

- Bubble parameters (diameters, bubble growth time) are stochastic in nature. Averages are used;

-Heat transfer through evaporation of a microlayer. The ratio D_{base}/D_{bubble} is assumed to be constant for a given pressure. Bubbles release heat at the upper-half surface (corresponds to the latent heat transport);

- Bubble growth is thermally controlled (slower);

- Bubble growth is isobaric with respect to the surrounding liquid;

$$D(t) = \frac{2a\alpha t^{\frac{1}{2}}(1 + 0.33bC\Phi t)}{1 + bC\Phi t} \tag{B.1}$$

$$a = \frac{(q - h\Delta T_{sub})^{\frac{1}{3}} k_l \gamma}{2C_l^{\frac{1}{3}} \rho_v \lambda (\pi \alpha_l)^{\frac{1}{2}}} \tag{B.2}$$

$$\alpha_l = \frac{k_l}{\rho_l c_{p_l}} \qquad C_l = \frac{\lambda \mu_l \left(\frac{c_{p_l}}{0.013 \lambda \, Pr_l^{1.7}} \right)^3}{\left(\frac{\sigma}{(\rho_l - \rho_v) g} \right)^{0.5}} \tag{B.3}$$

$$\gamma = \left(\frac{k_s \rho_s c_{p_s}}{k_l \rho_l c_{p_l}} \right)^{\frac{1}{2}} \text{; index s refers to heater material} \tag{B.4}$$

$$b = \frac{\Delta T_{sub}}{2\left(1-\frac{\rho_v}{\rho_l}\right)} \tag{B.5}$$

$$\Phi = \left(\frac{u}{u_0}\right)^{0.47} ; u_0 = 0.61 m/s \quad \text{for } u>0.61 m/s \tag{B.6a}$$

$$\Phi = 1 \qquad \text{for } u<0.61 m/s \tag{B.6b}$$

$$D_m = 1.21\frac{a\alpha}{(bC\Phi)^{\frac{1}{2}}} \tag{B.7}$$

$$D_m = \frac{1}{1.46bC\Phi} \tag{B.8}$$

$$\frac{\alpha}{C^{\frac{1}{2}}} = 2.10^{-5} p^{0.709} \tag{B.9}$$

$$C = 65 - 5.69\cdot 10^{-5}\left(p - 10^5\right) \quad ; \quad 0.1 \le p[MPa] \le 1 \tag{B.10}$$

B.2. Model of Zuber

$$D_m = Ja \cdot \frac{k\Delta T_w}{q} \tag{B.11}$$

B.3. Model of Mikic

$$R_m = \frac{2}{\pi}\cdot\sqrt{3}\cdot Ja\cdot\frac{k\Delta T_w}{q}\left\{1-\theta\left[\theta-\left(\sqrt{\theta^2-1}\right)\right]\right\} \tag{B.12}$$

where

$$\theta = \frac{T_w - T_b}{T_w - T_{sat}} \tag{B.13}$$

represents the degree of subcooling.

B.4 Model of Zeitoun and Shoukri

They suggested the following equation for detachment diameters. For their experiments, they used water at pressures close to atmospheric:

$$\frac{D_s}{\sqrt{\frac{\sigma}{g(\rho_l-\rho_v)}}}=\frac{0.0683\left(\frac{\rho_l}{\rho_v}\right)^{1.326}}{Re^{0.324}\left(Ja+\frac{149.2\left(\frac{\rho_l}{\rho_v}\right)^{1.326}}{Bo^{0.487}\,Re^{1.6}}\right)} \tag{B.14}$$

B.5 Model of Serizawa and Kenning

Serizawa reported that, upon analyzing experimental data from othe investigators (Gunther, Griffith, Cumo et al., Tolubinsky and Kostanchuk, Sato et al), bubble diameter decreases linearly with increasing the liquid subcooling and flow velocity. The slope changes at around 0.7 m/s. This value is close to Unal's 0.61 which he attributed to the abrupt change in condensation characteristics of vapour bubbles.

$$D_b = D_0 \Psi \exp(-K_1 \Delta T_{sub} - K_2 q) \tag{B.15}$$

where D_0 is the characteristic diameter used in the Re* along with the bubble rise velocity u*

$$Gr=\frac{\left(\frac{\sigma}{g(\rho_l-\rho_v)}\right)^{0.5}}{\frac{\rho_v {\nu_l}^2}{\sigma}};\qquad Re^*=\frac{u^* D_0}{\nu_l};\ u^*=1.18\left(\frac{\sigma g(\rho_l-\rho_v)}{{\rho_l}^2}\right)^{0.25} \tag{B.16}$$

for:

$$Gr>7x10^8 \qquad Re^* Pr^{0.5}=\frac{40}{3}\left(\frac{Gr}{10^8}\right)^{1.6} \tag{B.17a}$$

$$Gr<7x10^8 \qquad Re^* Pr^{0.5}=300 \tag{B.17b}$$

$$\frac{\frac{K_l}{k_l}}{qD_e} = 11.5 + 3\cdot 10^{-4}\left(\frac{\rho_l}{\rho_v}\right)\frac{R_H}{\eta Pr_l^{0.8}} \tag{B.18}$$

where:

$$\eta = \frac{\sigma}{\rho_v i_{fg}\left(\frac{\sigma}{g(\rho_l-\rho_v)}\right)^{0.5}}; \quad R_H = \frac{\dot{m}v_l}{\sigma} \tag{B.19}$$

$$\left[K_2\rho_l i_{fg}u^* + 0.4\frac{u}{u^*}\right]^2 = \frac{\left[40\left(\frac{Gr}{10^9}\right)^{0.07}\right]^2 + \left[14\left(\frac{Gr}{10^9}\right)^{2.2}\right]^2}{Pr^2} \tag{B.20}$$

u_0=0.7 m/s; $u^+=u/u_0$; $Qn = \frac{q}{\rho_l i_{fg} u^*}$ (B.21)

for:

$u<u_0 \quad \Psi = 1$ (B.22a)

$u>u_0 \quad \Psi = 1 - 0.75\,Pr_l^{-0.8}\,FpFqFu$ (B.22b)

where:

$$Fp = 1 - 2.5\left(\frac{\rho_l-\rho_v}{\rho_l}\right)^{-0.006\frac{\rho_l}{\rho_v}} \tag{B.23a}$$

$$Fq = \begin{cases} 1 & Qn \geq 4\cdot 10^{-4} \\ 2500Qn & Qn < 4\cdot 10^{-4} \end{cases} \tag{B.23b}$$

$$Fu = \left(1-u^+\right)^{2.1u^+} \tag{B.23c}$$

Appendix C

SAMPLE CALCULATION PROCEDURE (in MathCad) FOR PREDICTING HEAT TRANSFER COEFFICIENTS USING CHEN-TYPE HEAT TRANSFER MODELS

Comparison of heat transfer models based on the addition of convective and evaporation terms with experimental data

Thermophysical data

Data for p=1bar

$p_{crit} := 22.09 \cdot 10^{6}$ $p_{sat} := 1.05 \cdot 101325$ [Pa]

$Pr_l := 1.75$ $T_{sat} := 102.3$

$k_l := 0.683$ [W/mK] $\mu_l := 2.82 \cdot 10^{-4}$ [Pas]

$D := 9.1 \cdot 10^{-3}$ [m] $\rho_l := 956.7$

$i_{fg} := 2250 \cdot 10^{3}$ [J/kg] $\rho_v := 0.645$

$\sigma := 5.88 \cdot 10^{-2}$ $\mu_v := 12.7 \cdot 10^{-6}$ [Pas]

$cp_l := 4217$ [J/kgK] $M := 18.02$ [kg/kmol]

$m_i := Flow_i \cdot 10^{-3} \cdot \rho_l$ mass flow rate [kg/s]

$$G_i := \frac{m_i}{2.47 \cdot 10^{-4}} \qquad u_i := \frac{G_i}{\rho_l} \qquad Re_{l_i} := \rho_l u_i \frac{D}{\mu_l}$$

$\Delta T_{sat_i} := T_{surface_i} - T_{sat}$

$$Bo_i := \frac{q_i}{G_i \cdot i_{fg}} \qquad p_r := \frac{p_{sat}}{p_{crit}}$$

Input:matrix with experimental data

Input:matrix with experimental data

MATRIX =

D:\...\Void experiments p=1bar.txt

$i := 0 .. \text{rows}(MATRIX) - 1$

$Flow := MATRIX^{\langle 1 \rangle}$

$T_{surface} := MATRIX^{\langle 5 \rangle}$

$\Delta T_{sub} := MATRIX^{\langle 14 \rangle}$

$q := MATRIX^{\langle 6 \rangle}$

$x := \frac{MATRIX^{\langle 15 \rangle}}{100}$

$VOID := MATRIX^{\langle 16 \rangle}$

Calculation of the sat'd pressure corresponding to surface temperature

$A_0 := 0.104592 \cdot 10^{2}$ $\quad A_6 := 0.903668 \cdot 10^{-15}$

$A_1 := -0.404897 \cdot 10^{-2}$ $\quad A_7 := -0.19969 \cdot 10^{-17}$

$A_2 := -0.41752 \cdot 10^{-4}$ $\quad A_8 := 0.779287 \cdot 10^{-21}$

$A_3 := 0.36851 \cdot 10^{-6}$ $\quad A_9 := 0.191482 \cdot 10^{-24}$

$A_4 := -0.10152 \cdot 10^{-8}$ $\quad A_{10} := -0.396806 \cdot 10^{4}$

$A_5 := 0.86531 \cdot 10^{-12}$ $\quad A_{11} := 0.395735 \cdot 10^{2}$

From Irvine and Liley "Steam and Gas Tables with Computer Equations" 1984

$$p_{surface_i} := e^{\left[\sum_{j=0}^{9} A_j \cdot \left(T_{surface_i} + 273.16\right)^j + \frac{A_{10}}{T_{surface_i} + 273.16 - A_{11}}\right]} \cdot 10^{6}$$

Calculation of the true mass fraction

Ahmad (1970) - using the slip ratio:

$$SLIP_i := \left(\frac{\rho_l}{\rho_v}\right)^{0.205} \cdot \left(Re_{l_i}\right)^{-0.016}$$

$$x_{aAHMAD_i} := \frac{\frac{VOID_i}{100} \cdot \left(\frac{\rho_v}{\rho_l}\right) \cdot SLIP_i}{1 + \frac{VOID_i}{100} \cdot \left[\left(\frac{\rho_v}{\rho_l}\right) \cdot SLIP_i - 1\right]}$$

Saha and Zuber (1974)

$$x_{OSV_i} := -0.0022 \cdot Bo_i \cdot Re_{l_i} \cdot Pr_l \qquad \text{for Pe<70000}$$

$$x_{aSAHA_i} := \text{if}\left[VOID_i > 0, \frac{x_i - x_{OSV_i} \cdot e^{\left(\frac{x_i}{x_{OSV_i}} - 1\right)}}{1 - x_{OSV_i} \cdot e^{\left(\frac{x_i}{x_{OSV_i}} - 1\right)}}, 0\right]$$

Kroeger and Zuber (1968) using the drift flux model

$$U_{gj} := 1.41 \cdot \left[\frac{\sigma \cdot 9.81 \cdot \left(\rho_l - \rho_v\right)}{\rho_l^2}\right]^{0.25} \qquad \text{from Zuber and Findlay}$$

$$x_{aKROEGER_i} := \frac{VOID_i}{100} \cdot \frac{\left(\rho_v \cdot \frac{U_{gj}}{G_i} + 1.13 \cdot \frac{\rho_v}{\rho_l}\right)}{1 - \frac{VOID_i}{100} \cdot \frac{\left(\rho_l - \rho_v\right) \cdot 1.13}{\rho_l}}$$

Chen correlation

NOTE: in subcooled boiling the quality x has to be replaced with the trus mass fraction

Martinelli parameter

$$X_{tt_i} := \text{if}\left[VOID_i > 0, \left(\frac{1 - x_{aKROEGER_i}}{x_{aKROEGER_i}}\right)^{0.9} \cdot \left(\frac{\rho_v}{\rho_l}\right)^{0.5} \cdot \left(\frac{\mu_l}{\mu_v}\right)^{0.1}, 0\right]$$

Calculate only for the boiling region

$$F := 2.35 \cdot \left(0.213 + \frac{1}{X_{tt}}\right)^{0.736} \qquad \text{if } 1/x_{tt} > 0.1$$

$$F := 1 \qquad \text{if } 1/x_{tt} < 0.1$$

These equations were proposed by Collier (1981) to fit Chen's original curves

$$S := \frac{1}{1 + 2.56 \cdot 10^{-6} \cdot Re_{tp}^{1.17}}$$

Later modifications of the parameters as discussed by Kandlikar (2000)

$$F_i := \text{if}\left[VOID_i > 0, \left[1 + \left(X_{tt_i}\right)^{-0.5}\right]^{1.78} \cdot \left(\frac{Pr_l + 1}{2}\right)^{0.444}, 1\right]$$

$$S_i := \text{if}\left[VOID_i > 0, \left[0.9622 - \text{atan}\left[Re_{l_i} \cdot \frac{\left(F_i\right)^{1.25}}{6.18 \cdot 10^4}\right]\right], 0\right]$$

Dittus-Boelter single-phase correlation

$$h_{lDB_i} := 0.023 \cdot \left(Re_{l_i}\right)^{0.8} \cdot Pr_l^{0.4} \cdot \frac{k_l}{D}$$

Forster and Zuber pool boiling correlation

$$h_{poolFZ_i} := 0.00122 \cdot \frac{k_l^{0.79} \cdot cp_l^{0.45} \cdot \rho_l^{0.49}}{\sigma^{0.5} \cdot \mu_l^{0.29} \cdot i_{fg}^{0.24} \cdot \rho_v^{0.24}} \cdot \left(\Delta T_{sat_i}\right)^{0.24} \cdot \left(p_{surface_i} - p_{sat}\right)^{0.75}$$

$$h_{tpChen_i} := h_{lDB_i} \cdot F_i + h_{poolFZ_i} \cdot S_i$$

Gungor and Winterton correlation

$$E_i := \left[\text{if}\left(VOID_i > 0, 1 + 24000 \cdot \left(Bo_i\right)^{1.16} + 1.23 \cdot \left(\frac{1}{X_{tt_i}}\right)^{0.86}, 1\right) \right]$$

Cooper's pool boiling correlation

$$h_{poolCOOPER_i} := 55 \cdot p_r^{0.12} \cdot \left(-\log\left(p_r\right)\right)^{-0.55} \cdot M^{-0.5} \cdot \left(q_i\right)^{0.67}$$

$$h_{tpGW_i} := E_i \cdot h_{lDB_i} + S_i \cdot h_{poolCOOPER_i} \qquad h_{tpGWSUB_i} := S_i \cdot h_{poolCOOPER_i} + h_{lDB_i}$$

Liu and Winterton correlation

$$E_{LW_i} := \left[1 + x_{aKROEGER_i} \cdot Pr_l \cdot \left(\frac{\rho_l}{\rho_v} - 1\right) \right]^{0.35}$$

$$S_{LW_i} := \left[\text{if}\left(VOID_i > 0, \frac{1}{1 + 0.055 \cdot \left(E_{LW_i}\right)^{0.1} \cdot \left(Re_{l_i}\right)^{0.16}}, 0\right) \right]$$

$$h_{tpLW_i} := \sqrt{\left(E_{LW_i} \cdot h_{lDB_i}\right)^2 + \left(S_{LW_i} \cdot h_{poolCOOPER_i}\right)^2} \qquad h_{tpLWSUB_i} := \sqrt{\left(h_{lDB_i}\right)^2 + \left(S_{LW_i} \cdot h_{poolCOOPER_i}\right)^2}$$

Appendix D

RADIAL VELOCITY AND TEMPERATURE DISTRIBUTION IN A VERTICAL ANNULUS WITH AN INNER HEATER

The conservation equations for hydrodynamically fully developed turbulent flow with constant properties, axially uniform heating and insignificant axial conduction are:

Continuity:

$$\frac{1}{r}\frac{\partial}{\partial r}(r \cdot u_r) + \frac{\partial u}{\partial x} = 0 \qquad (D.1)$$

x-momentum[1]:

$$\frac{1}{\rho}\frac{dp}{dx} = \frac{1}{r}\frac{\partial}{\partial r}\left[r(\nu + \varepsilon_m)\frac{\partial u}{\partial r}\right] \qquad (D.2)$$

Energy:

$$u\frac{dT}{dx} = \frac{1}{r}\frac{\partial}{\partial r}\left[r(\alpha + \varepsilon_h)\frac{\partial T}{\partial r}\right] \qquad (D.3)$$

D.1. Velocity distribution

Given that the entrance length of an annulus is sufficiently long to allow for fully developed velocity profiles and also that the flow is (for most of the experiments) turbulent, one can assume that the flow region over the surface of the heater can be divided into three zones:

[1] ε_m is the eddy diffusivity of momentum. According to Boussinesq (1877) the relation between ε_m and the turbulent shear stress is: $\tau = (\mu + \rho\varepsilon_m)\frac{\partial u}{\partial y}$; u is the time average velocity in the axial direction and y is the distance from the wall (point of interest in this study – the inner wall of the annulus). Consequently, the eddy diffusivity of heat, ε_h, in the equation (D.3) is related to the heat flux as $q'' = -(k + \rho c_p \varepsilon_h)\frac{\partial T}{\partial y}$

The laminar sublayer: $(y^+<5)^2$ also known as the viscous layer is a thin layer adjacent to the heater surface. Flow is laminar and viscous forces are dominant. The transfer of heat is governed by molecular diffusion;

The buffer layer ($5<y^+<30$) represents the transition region between laminar sublayer and turbulent core;

The turbulent core ($y^+>30$) is the region where the eddy diffusivity of momentum and heat predominates;

The universal velocity distribution has the form as suggested by Prandtl and Taylor:

$$u^+ = A \ln y^+ + B \tag{D.4}$$

D.1.1. Von Karman (1939)

Von Karman Provided a set of equations for the three layer ensuring the smooth transition of velocity vectors between layers. The equations are as follows:

The laminar sublayer	$u^+ = y^+$
The buffer layer	$u^+ = 5 \ln y^+ - 3.05$
The turbulent core	$u^+ = 2.5 \ln y^+ + 5.5$

The use of the universal velocity distribution equations are questionable. First, the transition from laminar to turbulent motion is gradual and obviously present at all distances from the wall. In that matter, a fixed transition at $y^+=5$ seems somewhat awkward, as well as the fact that three equations are used for a single curve. Also, the boundary condition of zero velocity gradient at some point in the flow region (centerline

---

[2] y^+ is a dimensionless distance from the wall defined as $y^+ = y\frac{\sqrt{\tau_w/\rho}}{\nu}$; $\sqrt{\tau_w/\rho}$ is the so-called friction velocity. The corresponding dimensionless velocity is $u^+ = \frac{u}{\sqrt{\tau_w/\rho}}$

for tubes, point of maximum velocity for annulus) are not met when using the universal velocity profile.

D.1.2. Deissler (1955)

In an attempt to overcome the above mentioned inconsistencies, Deissler has developed a single velocity profile equation for the region $y^+<26$ based on the following assumption:

$$\varepsilon_m = n^2 u y \tag{D.5}$$

where n is a constant to be determined experimentally.Deissler's equation can be found in two forms:

$0<y^+<26$	$y^+ = \frac{1}{n}\frac{1/\sqrt{2\pi}\int_0^{nu^+} e^{-\left[(nu^+)^2/2\right]} d(nu^+)}{(1/\sqrt{2\pi})\cdot e^{-\left[(nu^+)^2/2\right]}}$; $n = 0.109$ $\frac{du^+}{dy^+} = \frac{1}{1+n^2u^+y^+\left[1-e^{-n^2u^+y^+}\right]}$; $n = 0.124$
$y^+>26$	$u^+ = 2.78 \ln y^+ + 3.8$

A significant problem in determining velocity profiles for turbulent flow in an annulus is the calculation of the location of maximum velocity. This location is at the zero shear stress point. The corresponding experimental data is scarce given that direct shear stress measurement are extremely difficult and that, due to very flat turbulent velocity profile in the vicinity of the maximum velocity, its location cannot be accurately determined.

The related problem is determination of the ratio of shear stresses on two surfaces. The shear stresses are not equal. The location of the maximum velocity is not midway between the walls. The velocity distribution is not symmetrical. The relation between the two parameters has the following form[3]:

$$\frac{\tau_{wi}}{\tau_{wo}} = \frac{r_o\left(r_{max}^2 - r_i^2\right)}{r_i\left(r_o^2 - r_{max}^2\right)} \tag{D.6}$$

Few models related to turbulent flows in annuli can be found in the literature. A good representation is given by Knudsen and Katz (1958):

For the inner tube:

$$u_i^+ = 4.4 \log y_i^+ + 6.2 \tag{D.7}$$

also based on the mean velocity, U:

$$u_i = 1.14U\left(\frac{r - r_i}{r_{max} - r_i}\right)^{0.102} \tag{D.8}$$

For the outer tube:

$$u_o^+ = 6.1 \log y_o^+ + 3.0 \tag{D.9}$$

also based on the mean velocity, U:

$$u_o = 1.14U\left(\frac{r_o - r}{r_o - r_{max}}\right)^{0.142} \tag{D.10}$$

Equations (D.8) and (D.10) have been derived taking into account that $U/u_{max}=0.876$ (+/-1.8%). The indexes i and o denotes the parameter related to the inner and outer type (i.e. $y_i^+ = y_i \frac{\sqrt{\tau_{wi}/\rho}}{\nu}$).

[3] The equation (D.6) has been originally developed for the laminar flow in a circular annulus by differentiating the velocity profile with respect to r. It can also be derived by writing a force balance for a differential length dx of the annular fluid. Even though it has been derived for laminar flow, it holds for turbulent flow in annuli as well. It was also used by Kays and Leung.

D.1.3. Kays and Leung (1963)

They used Deissler's approach in evaluating the velocity distribution for fully turbulent flow in annuli. The equation they suggested for the location of the maximum velocity was given as[4]:

$$\frac{r_{max} - r_i}{r_o - r_{max}} = \left(\frac{r_i}{r_o}\right)^{0.343} \tag{D.11}$$

They calculated the eddy diffusivity of momentum from:

$$\frac{\varepsilon_m}{\nu} = mu_i^+ \eta_i^+ \left[1 - e^{-\left(mu_i^+ \eta_i^+\right)}\right]; \qquad m = 0.0154 \tag{D.12}$$

where:

$$\eta_i^+ = 1.5y^+ \frac{1+\eta_i}{1+2\eta_i^{\,2}}; \qquad \eta_i = \frac{r_{max} - r}{r_{max} - r_i} \tag{D.13}$$

Kays and Leung divided the flow region into four zones: Two sublayers (inner and outer) and two turbulent cores joining each other at the location of maximum velocity. For the outer turbulent core the von Karman equation was used. For the inner turbulent core the coefficients A and B from (D.4) had to be calculated in order to match the outer turbulent core profile and inner sublayer, which ended at $\eta_i^+ = 42$.

D.2. Temperature distribution

The main tool to determine the temperature profiles in forced convection flows is the assumption that heat and momentum propagate through the fluid equally. Several analogies have been proposed stemming from the remarkable work of Reynolds (1874) and Prandtl (1910). It was pointed out by Kays and Leung that: "the essence of the heat and momentum analogy lies in the assumption of a definite relationship between the

---

[4] Same equation can be found modified latter as: $\frac{r_{max}}{r_o} = \left(\frac{r_i}{r_o}\right)^{0.343}\left[1 + \left(\frac{r_i}{r_o}\right)^{0.657} - \left(\frac{r_i}{r_o}\right)\right]$; in W.M.Kays and M.E.Crawford;"Convective Heat and Mass Transfer" Third Edition – Mcgraw-Hill,Inc.

thermal and momentum eddy diffusivities." Most analogies recognize the proportionality between ε_m and ε_h, their ratio being known as the turbulent Prandtl number:

$$Pr_t = \frac{\varepsilon_m}{\varepsilon_h} \tag{D.14}$$

D.2.1 The Martinelli Analogy (1947)

Only the essence will be given here:

Initial conditions:

Velocity and temperature profiles are fully developed (i.e. dT/dx=0);

Fluid properties are independent of temperature;

Uniform heat flux along the tube;

Linear variation of the shear stress and heat flux in the radial direction:

$$\frac{\tau_w}{\rho}\left(1-\frac{y}{r_w}\right)=(\nu+\varepsilon_m)\frac{du}{dy}; \qquad \frac{q''_w}{\rho c_p A_w}\left(1-\frac{y}{r_w}\right)=(\nu+\varepsilon_h)\frac{dT}{dy}; \qquad r=r_w-y \tag{D.15}$$

The equations (D.15) are derived for circular tubes. If the analogy is used for flows in annuli, modifications have to be made to recognize the direction of y and the location of the centerline relative to the walls. Also, different wall shear stresses on the two walls have to be taken into account.

The temperature distributions derived by Martinelli are as follows:

- Laminar sublayer ($0<y^+<5$)

$$\frac{T_w-T}{T_w-T_c}=\frac{\dfrac{Pr}{Pr_t}\dfrac{y}{y_1}}{\dfrac{Pr}{Pr_t}+\ln\left(1+5\dfrac{Pr}{Pr_t}\right)+0.5F_1\ln\dfrac{Re}{60}\sqrt{\dfrac{f}{2}}} \tag{D.16}$$

where y_1 is the value of y at $y^+=5$

- Buffer layer ($5<y^+<30$)

$$\frac{T_w - T}{T_w - T_c} = \frac{\frac{Pr}{Pr_t} + \ln\left[1 + \frac{Pr}{Pr_t}\left(\frac{y}{y_1} - 1\right)\right]}{\frac{Pr}{Pr_t} + \ln\left(1 + 5\frac{Pr}{Pr_t}\right) + 0.5F_1 \ln\frac{Re}{60}\sqrt{\frac{f}{2}}} \qquad (D.17)$$

- Turbulent core ($y^+>30$)

$$\frac{T_w - T}{T_w - T_c} = \frac{\frac{Pr}{Pr_t} + \ln\left(1 + 5\frac{Pr}{Pr_t}\right) + 0.5F_1 \ln\frac{Re}{60}\sqrt{\frac{f}{2}}\frac{y}{r_w}}{\frac{Pr}{Pr_t} + \ln\left(1 + 5\frac{Pr}{Pr_t}\right) + 0.5F_1 \ln\frac{Re}{60}\sqrt{\frac{f}{2}}} \qquad (D.18)$$

The value of the function F_1 depends of the Reynolds and Prandtl number. It can be obtained from the following table:

Re / Pe	10^4	10^5	10^6
10^2	0.18	0.098	0.052
10^3	0.65	0.45	0.29
10^4	0.92	0.83	0.65
10^5	0.99	0.985	0.98
10^6	1.00	1.0	1.00

D.2.2 Deissler (1954)

Initial conditions:

Velocity and temperature profiles are fully developed; no entrance effects;

$Pr_t=1$;

Prandtl number and heat capacity are constant;

The temperature distribution for liquids has the following form:

$$T^+ = \int_0^{y^+} \frac{dy^+}{\frac{1}{Pr} + n^2 u^+ y^+ \left(1 - e^{-n^2 u^+ y^+}\right)}; \qquad y^+ < 26 \tag{D.19}$$

$$T^+ = C + \frac{1}{\kappa} \ln y^+; \qquad y^+ > 26 \tag{D.20}$$

where:

$$T^+ = \frac{1}{\omega}\left(1 - \frac{T}{T_w}\right); \qquad \omega = \frac{q''_w \sqrt{\tau_w / \rho}}{c_p T_w \tau_w} \tag{D.21}$$

and n=0.109 (Knudsen and Katz), C is a constant evaluated at $y^+=26$ and $\kappa=0.36$.

A relatively simple expression for the friction factor in plain annuli is that of Davis (1943):

$$f = \frac{0.055 \cdot Re^{-0.2}}{\left(\frac{r_o / r_i - 1}{r_o / r_i}\right)^{-0.1}} \tag{D.22}$$

The notable study of Kays and Leung (1963) to calculate the temperature profiles with arbitrary prescribed heat flux was based on an application of Deissler's analysis for the velocity profiles in the sublayers and von Karman analysis for the turbulent core. The eddy diffusivity of heat was assumed to be equal to the eddy diffusivity of momentum (i.e. $Pr_t=1$). Once these parameters were obtained, the energy equation (D.3) was solved numerically.

Appendix E

THE INERTIAL FORCE DURING GROWTH OF AN ELLIPSOIDAL BUBBLE

Following the procedure described by Lord Rayleigh, the velocity distribution comes from the steady-state equation of continuity which has the general form:

$$\frac{\partial u}{\partial x}+\frac{\partial v}{\partial y}+\frac{\partial w}{\partial z}=0 \tag{E.1}$$

Transformation of coordinates is needed. It is convenient to use the transform coordinates η (the half diameter of concentric ellipsoids measured along the y-axes), ξ (represents lines that are perpendicular to the ellipsoidal surface of the bubble – conii in 3D) and ϕ (whis is the angle the the projection of the velocity vector on the x-z plane forms with the x-axes). The transformed continuity equation has the following form:

$$\begin{aligned}&\frac{\partial}{\partial\xi}\left[\frac{1}{J}\left(u\frac{\partial\xi}{\partial x}+v\frac{\partial\xi}{\partial y}+w\frac{\partial\xi}{\partial z}\right)\right]+\frac{\partial}{\partial\eta}\left[\frac{1}{J}\left(u\frac{\partial\eta}{\partial x}+v\frac{\partial\eta}{\partial y}+w\frac{\partial\eta}{\partial z}\right)\right]\\&+\frac{\partial}{\partial\phi}\left[\frac{1}{J}\left(u\frac{\partial\phi}{\partial x}+v\frac{\partial\phi}{\partial y}+w\frac{\partial\phi}{\partial z}\right)\right]=0\end{aligned} \tag{E.2}$$

Introducing the assumption (as in the spherical case) that the bubble, as it grows, pushes liquid away in a direction perpendicular to the surface, one can reduce the preceding equation to the form:

$$\frac{\partial}{\partial\eta}\left[\frac{1}{J}\left(u\frac{\partial\eta}{\partial x}+v\frac{\partial\eta}{\partial y}+w\frac{\partial\eta}{\partial z}\right)\right]=0 \tag{E.3}$$

The only change of velocity is assumed to occur along the ξ=const line. It is also assumed that velocity does not change with ϕ (axisymmetric).

The equation for the ellipse is given by:

$$\frac{x^2}{\varepsilon^2} + y^2 = b^2 \tag{E.4}$$

where the nonsphericity is defined as $\varepsilon=a/b$.

The equation of a line normal to the elliptical projection of the bubble at a given point $M(x_0,y_0)$ for any particular slice on the plane containing the y-axis is given by:

$$y - y_0 = \varepsilon^2 \frac{y_0}{x_0}(x - x_0) \tag{E.5}$$

Since ϕ does not play any significant role, any plane that passes through y-axis is considered as the x-y plane. In that case, the two equations above will be valid. A simple geometrical analysis leads to the following expressions that relate the original and transformed coordinates:

$$\xi = b_0 \frac{\tan\theta}{\sqrt{\tan^2\theta + \varepsilon^2}} \tag{E.6}$$

where $\xi=y_0$

$$\eta = \sqrt{\frac{1}{\varepsilon^2} \cdot \frac{x^2}{\cos^2\phi} + y^2} \text{ where } \eta=b_i \text{ , } i=0,1,..... \tag{E.7}$$

Once ξ has been determined, the corresponding x_0 can be calculated using the following formula:

$$x_0 = \varepsilon \cdot b_0 \cdot \cos\phi \sqrt{1 - \frac{\xi^2}{b_0^2}} \tag{E.8}$$

The expression (E.8) is derived from the equation for ellipse which represents the projection of a slice at given angle ϕ of the actual ellipsoidal bubble on the x-y plane:

$$\frac{x_0^2}{a_0^2} \cdot \frac{1}{\cos^2\phi} + \frac{\xi^2}{b_0^2} = 1 \tag{E.9}$$

The following is a simple mathematical procedure that gives the explicit expressions for x, y and z as functions of η, ξ and ϕ. The equation (E.5) can be written in the form of:

$$y = \varepsilon^2 \cdot \xi\left(\frac{x}{x_0} - 1\right) + \xi = \xi \cdot \left[\varepsilon^2\left(\frac{x}{x_0} - 1\right) + 1\right]$$

$$\text{or } y = \xi \cdot \left[1 - \varepsilon \cdot \left(\varepsilon - \frac{x}{\cos\phi\sqrt{{b_0}^2 - \xi^2}}\right)\right] \tag{E.10}$$

This latter equation is a combination of equations (E.5) and (E.8).

The supstitution of (E.10) into equation (E.7) leads to:

$$\eta^2 = \frac{1}{\varepsilon^2} \cdot \frac{x^2}{\cos^2\phi} + \xi^2 \cdot \left[\varepsilon^2\left(\frac{x}{x_0} - 1\right) + 1\right]^2 \tag{E.11}$$

After a few simple steps one can obtain:

$$\eta^2 = \left(\frac{1}{\varepsilon^2} + \frac{\varepsilon^2\xi^2}{{b_0}^2 - \xi^2}\right) \cdot \frac{x^2}{\cos^2\phi} + 2\xi^2\varepsilon \frac{1-\varepsilon^2}{\sqrt{{b_0}^2 - \xi^2}} \cdot \frac{x}{\cos\phi} + \xi^2\left(\varepsilon^2 - 1\right)^2 \tag{E.12}$$

One can rearrange (E.12) to obtain the desired explicit form:

$$x = \frac{-\left(\xi^2\varepsilon \frac{1-\varepsilon^2}{\sqrt{{b_0}^2 - \xi^2}}\right) + \sqrt{\left(\xi^2\varepsilon \frac{1-\varepsilon^2}{\sqrt{{b_0}^2 - \xi^2}}\right)^2 - \left(\frac{1}{\varepsilon^2} + \frac{\varepsilon^2\xi^2}{{b_0}^2 - \xi^2}\right) \cdot \left[\xi^2\left(\varepsilon^2 - 1\right)^2 - \eta^2\right]}}{\frac{1}{\varepsilon^2} + \frac{\varepsilon^2\xi^2}{{b_0}^2 - \xi^2}} \cdot \cos\phi \tag{E.13}$$

The substitution of (E.13) into (E.10) leads to:

$$y = \xi \cdot \left[1 - \varepsilon \cdot \left(\varepsilon - \frac{1}{\sqrt{b_0{}^2 - \xi^2}} \cdot \frac{-\left(\xi^2 \varepsilon \frac{1-\varepsilon^2}{\sqrt{b_0{}^2 - \xi^2}} \right) + \sqrt{\left(\xi^2 \varepsilon \frac{1-\varepsilon^2}{\sqrt{b_0{}^2 - \xi^2}} \right)^2 - \left(\frac{1}{\varepsilon^2} + \frac{\varepsilon^2 \xi^2}{b_0{}^2 - \xi^2} \right) \cdot \left[\xi^2 \left(\varepsilon^2 - 1 \right)^2 - \eta^2 \right]}}{\frac{1}{\varepsilon^2} + \frac{\varepsilon^2 \xi^2}{b_0{}^2 - \xi^2}} \right) \right] \tag{E.14}$$

The third variable z, being defined as $z = x \cdot \tan\phi$, can be obtained from (E.13) in its explicit form:

$$z = \frac{-\left(\xi^2 \varepsilon \frac{1-\varepsilon^2}{\sqrt{b_0{}^2 - \xi^2}} \right) + \sqrt{\left(\xi^2 \varepsilon \frac{1-\varepsilon^2}{\sqrt{b_0{}^2 - \xi^2}} \right)^2 - \left(\frac{1}{\varepsilon^2} + \frac{\varepsilon^2 \xi^2}{b_0{}^2 - \xi^2} \right) \cdot \left[\xi^2 \left(\varepsilon^2 - 1 \right)^2 - \eta^2 \right]}}{\frac{1}{\varepsilon^2} + \frac{\varepsilon^2 \xi^2}{b_0{}^2 - \xi^2}} \cdot \sin\phi \tag{E.15}$$

One can determine the partial derivatives:

$$\begin{aligned} &\frac{\partial x}{\partial \xi}, \frac{\partial x}{\partial \eta}, \frac{\partial x}{\partial \phi}; \\ &\frac{\partial y}{\partial \xi}, \frac{\partial y}{\partial \eta}, \frac{\partial y}{\partial \phi} = 0; \\ &\frac{\partial z}{\partial \xi} = \tan\phi \frac{\partial x}{\partial \xi}, \frac{\partial z}{\partial \eta} = \tan\phi \frac{\partial x}{\partial \eta}, \frac{\partial z}{\partial \phi} = \frac{\partial x}{\partial \phi} \left(\frac{-1}{\tan\phi} \right); \end{aligned} \tag{E.16}$$

The assumption is that the liquid adjacent to the bubble interface has the velocity equal to the bubble growth rate (since it is being pushed by the growing bubble). From equations (E.4), (E.5) and (E.8) one can find the coordinates of the intersection between the line ξ=const and the interface of the bubble at t+Δt:

$$\frac{x_1{}^2}{a_1{}^2} + \frac{\left[\varepsilon^2 \xi \left(\frac{x_1}{\varepsilon \cdot \cos\phi \sqrt{b_0{}^2 - \xi^2}} - 1 \right) + \xi \right]^2}{b_1{}^2} = 1 \tag{E.17}$$

and:

$$u\big|_{\eta=b_0} = \frac{dx}{dt} = \frac{(x_1 - x_0)\big|_{\xi=const}}{\Delta t}\cos\phi \tag{E.18}$$

The solution for the Continuity equation:

Having defined the partial derivatives (E.16) and the Jacobian transformations:

$$\begin{aligned}
\frac{\partial\eta}{\partial x} &= J\left(\frac{\partial y}{\partial\phi}\frac{\partial z}{\partial\xi} - \frac{\partial z}{\partial\phi}\frac{\partial y}{\partial\xi}\right)\\
\frac{\partial\eta}{\partial y} &= J\left(\frac{\partial z}{\partial\phi}\frac{\partial x}{\partial\xi} - \frac{\partial x}{\partial\phi}\frac{\partial z}{\partial\xi}\right)\\
\frac{\partial\eta}{\partial z} &= J\left(\frac{\partial x}{\partial\phi}\frac{\partial y}{\partial\xi} - \frac{\partial y}{\partial\phi}\frac{\partial x}{\partial\xi}\right)
\end{aligned} \tag{E.19}$$

the equation (E.3) can be rewritten in the following form:

$$\frac{\partial}{\partial\eta}\left[-u\frac{\partial z}{\partial\phi}\frac{\partial y}{\partial\xi} + v\left(\frac{\partial z}{\partial\phi}\frac{\partial x}{\partial\xi} - \frac{\partial x}{\partial\phi}\frac{\partial z}{\partial\xi}\right) + w\frac{\partial x}{\partial\phi}\frac{\partial y}{\partial\xi}\right] = 0 \tag{E.20}$$

or, again, taken the relations between partial derivatives (E.16):

$$\frac{\partial}{\partial\eta}\left[\frac{\partial x}{\partial\phi}\left(u\frac{\cos\phi}{\sin\phi}\frac{\partial y}{\partial\xi} - v\left(\frac{\cos\phi}{\sin\phi}\frac{\partial x}{\partial\xi} + \frac{\sin\phi}{\cos\phi}\frac{\partial x}{\partial\xi}\right) + w\frac{\partial y}{\partial\xi}\right)\right] = 0 \tag{E.21}$$

Given the relations between u, v and w:

$$\begin{aligned}
v &= u\cdot\tan\theta;\\
w &= \frac{u}{\cos\theta}\tan\phi
\end{aligned} \tag{E.22}$$

one can obtain:

$$\frac{\partial}{\partial\eta}\left[\frac{\partial x}{\partial\phi}\cdot u\left(\frac{\partial y}{\partial\xi}\left(\frac{\cos\phi}{\sin\phi} + \frac{1}{\cos\theta}\frac{\sin\phi}{\cos\phi}\right) - \tan\theta\frac{\partial x}{\partial\xi}\left(\frac{\cos\phi}{\sin\phi} + \frac{\sin\phi}{\cos\phi}\right)\right)\right] = 0 \tag{E.23}$$

or:

$$\frac{\partial x}{\partial \phi}\cdot u\left[\frac{\partial y}{\partial \xi}\left(\frac{\cos\phi}{\sin\phi}+\frac{1}{\cos\theta}\frac{\sin\phi}{\cos\phi}\right)-\tan\theta\frac{\partial x}{\partial \xi}\left(\frac{\cos\phi}{\sin\phi}+\frac{\sin\phi}{\cos\phi}\right)\right]=F(\xi,\phi) \qquad (E.24)$$

The function $F(\xi,\phi)$ in the equation (E.24) can be derived given the boundary conditions at the interface, i.e. from:

$$\left.\frac{\partial x}{\partial \phi}\right|_{\eta=b_0};\left.\frac{\partial y}{\partial \xi}\right|_{\eta=b_0};\left.\frac{\partial x}{\partial \xi}\right|_{\eta=b_0}; \qquad (E.25)$$

and the equation (E.18):

$$F(\xi,\phi)=\left.\frac{\partial x}{\partial \phi}\right|_{\eta=b_0}\cdot\frac{dx_0}{dt}\left[\left.\frac{\partial y}{\partial \xi}\right|_{\eta=b_0}\left(\frac{\cos\phi}{\sin\phi}+\frac{1}{\cos\theta}\frac{\sin\phi}{\cos\phi}\right)-\tan\theta\left.\frac{\partial x}{\partial \xi}\right|_{\eta=b_0}\left(\frac{\cos\phi}{\sin\phi}+\frac{\sin\phi}{\cos\phi}\right)\right] \qquad (E.26)$$

Hence:

$$u=\frac{\left.\frac{\partial x}{\partial \phi}\right|_{\eta=b_0}\cdot\frac{dx_0}{dt}\left[\left.\frac{\partial y}{\partial \xi}\right|_{\eta=b_0}\left(\frac{\cos\phi}{\sin\phi}+\frac{1}{\cos\theta}\frac{\sin\phi}{\cos\phi}\right)-\tan\theta\left.\frac{\partial x}{\partial \xi}\right|_{\eta=b_0}\left(\frac{\cos\phi}{\sin\phi}+\frac{\sin\phi}{\cos\phi}\right)\right]}{\frac{\partial x}{\partial \phi}\left[\frac{\partial y}{\partial \xi}\left(\frac{\cos\phi}{\sin\phi}+\frac{1}{\cos\theta}\frac{\sin\phi}{\cos\phi}\right)-\tan\theta\frac{\partial x}{\partial \xi}\left(\frac{\cos\phi}{\sin\phi}+\frac{\sin\phi}{\cos\phi}\right)\right]} \qquad (E.27)$$